UNIVERSITAT ROVIRA I VIRGILI

NITROGEN-BASED LIGANDS FOR IRON, ZINC AND COBALT CATALYZED SELECTIVE PROCESSES

Elisabet Mercadé Espinosa

ELISABET MERCADÉ ESPINOSA

NITROGEN-BASED LIGANDS FOR IRON, ZINC AND COBALT CATALYZED SELECTIVE PROCESSES

DOCTORAL THESIS

Supervised by

Dr. Cyril Godard and Prof. Carmen Claver Cabrero

Departament de Química Física i Inorgànica

UNIVERSITAT ROVIRA I VIRGILI

Tarragona 2015

UNIVERSITAT ROVIRA I VIRGILI
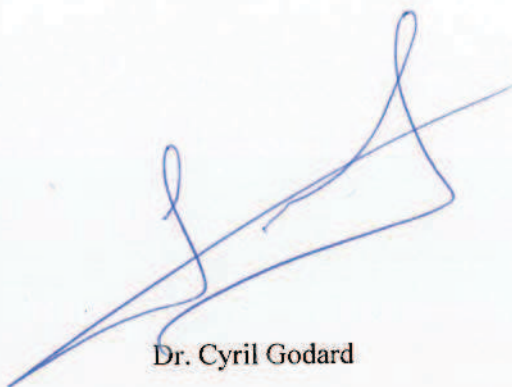
Departament de Química Física i Inorgànica

Facultat de Química

C/Marcel·lí Domingo, s/n

43007, Tarragona
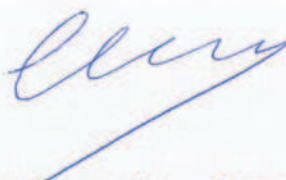
Els sotasignants Cyril Godard Investigador Ramón y Cajal, del Departament de Química Física i Inorgànica de la Universitat Rovira i Virgili, i Carmen Claver Cabrero, Catedràtica d'Universitat, del Departament de Química Física i Inorgànica de la Universitat Rovira i Virgili,

FEM CONSTAR que aquest treball, titulat *"Nitrogen-based ligands for iron, zinc and cobalt catalyzed selective processes"*, que presenta Elisabet Mercadé Espinosa per a l'obtenció del títol de Doctor, ha estat realitzat sota la nostra direcció al Departament de Química Física i Química Inorgànica d'aquesta universitat i que acompleix els requeriments per poder optar a Menció Internacional.

Tarragona, 1 de Setembre de 2015

Dr. Cyril Godard

Prof. Carmen Claver Cabrero

AGRAÏMENTS/AGRACEDIMIENTOS/RINGRAZIAMENTI

Moltes gràcies a tots.

A mis Yayas

Camina hacia el futuro, abriendo nuevas

puertas y probando cosas nuevas, se curioso…

porque nuestra curiosidad siempre nos conduce

por nuevos caminos

Walt Disney

TABLE OF CONTENTS

CHAPTER 4

CHAPTER 5

CHAPTER 6

ABBREVIATIONS AND ACRONYMS

A

ATH	asymmetric transfer hydrogenation
atm	atmosphere

B

br s	broad signal

C

ca	calculated
CIP	Cahn Ingold Prelog
CO	carbon monoxide
CO_2	carbon dioxide
conv.	conversion
Cy	cyclohexyl

D

d	doublet
dd	doublet of doublets
DCM	dichloromethane
DEAD	diethyl azodicarboxylate
deg	degree
DIAD	diisopropyl azodicarboxylate
DMC	dimethyl carbonate
DMAP	4-dimethylaminopyridine
DMSO	dimethyl sulfoxide
DPC	diphenyl carbonate
DPPA	diphenyl phoshphoryl azide

E

EA	elemental analysis
ee	enantioselectivity
EC	ethylene carbonate
Et	ethyl
EPR	electron paramagnetic resonance
ESI-HRMS	electrospray ionization-high mass resolution spectrometry

G

g	grams
GC	gas chromatography
gCOSY	gradient correlation spectroscopy
gHMBC	gradient heteronuclear multiple bond correlation
gHSQC	gradient heteronuclear single quantum coherence

H

h	hour(s)
HPLC	high performance liquid chromatography
Hz	hertz(s)

I

IR	infrared
iPr	isopropyl

J

J	coupling constant

M

m (in NMR)	multiplet
M	multiplicity in NMR spectra

m/z	mass under charge
min	minute(s)
MS	mass spectrometry

N

NHCs	N-heterocyclic carbenes
NMR	nuclear magnetic resonance
n.r.	no reaction
Nu	nucleophile

P

PC	propylene carbonate
Pc	critical pressure
PGMs	platinum-group metals
Ph	phenyl
ppm	parts per million
py	pyridine

Q

q	quadruplet
quint	quintuplet

R

rac	racemic
r.t.	room temperature

S

s	singlet
SET	single electron transfer
SQUID	superconducting quantum interference device

SCF	supercritical fluid

T

t	time
t (in NMR)	triplet
TBABr	tetrabutyl ammonium bromide
TBACl	tetrabutyl ammonium chloride
TBAF	tetrabutyl ammonium fluoride
TBAI	tetrabutyl ammonium iodide
TBP	trigonal bipiramide
Tc	critical temperature
temp.	temperature
THF	tetrahydrofuran
TOF	turnover frequency
TON	turnover number

U

μeff	magnetic effective moment
UV	ultra-violet

SUMMARY

Organometallic compounds have become an established synthetic tool for both fine and bulk chemicals. The reactivity and selectivity of the active catalyst are influenced by the choice of the metal center and the design of the surrounded ligands. Traditionally, second and third-row transition metals have been applied in organometallic chemistry, particularly the platinum-group metals (PGMs) have proven to be efficient for a large number of applications. However, the study of the organometallic chemistry of Earth-abundant metals has increased over the past few years as consequence of their low cost, ready availability, comparable low toxicity and sustainability. The final goal of this thesis is the development of novel families of ligands and their coordination to earth-abundant metals (Fe, Zn and Co) exploring their performance in asymmetric transfer hygrogenation and asymmetric hydrogenation of ketones and the synthesis of cyclic carbonates from CO_2 and epoxides.

Chapter 1 contains a general introduction to the importance of catalysis and the general considerations to be considered when earth-abundant metals are employed in catalysis. Chapter 2 sets out the general objectives of this thesis. The research in Chapter 3 describes the synthesis of chiral PNNP ligands containing a pyrrolidine backbone and their related Fe(II) complexes. The X-Ray structures of some Fe-PNNP complexes were also elucidated. The combination of the $Fe_3(CO)_{12}$ as iron precursor with a chiral PNNP ligand was found to catalyze the asymmetric transfer hydrogenation of a variety of ketones with moderates to high yields and enantioselectivities (Scheme 1). The above mentioned system was found to be heterogeneous rather than homogeneous, having modified iron particles acting as active catalyst.
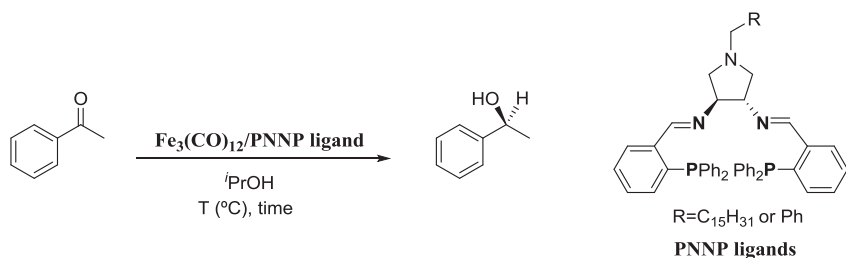
Scheme 1. $Fe_3(CO)_{12}$/PNNP catalytic system for the asymmetric transfer hydrogenation of ketones.

The research in <u>Chapter 4</u> describes the synthesis of a new family of ligands containing a N_2O_2, N_2NH_2, N_4 and $N_4(NH)$ ligand scaffolds with a pyrrolidine backbone. In addition, the corresponding Zn(II) complexes were prepared and fully characterized. The X-Ray structures of a tetranuclear and mononuclear Zn(II) complexes were also elucidated.
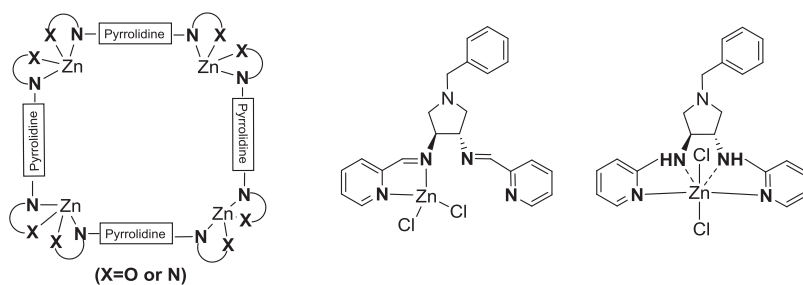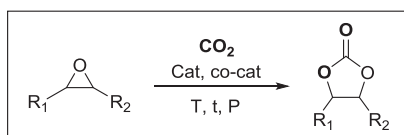
Scheme 2. Zn(II) complexes as catalysts in the coupling of CO_2 with epoxides.

These Zn(II) complexes were tested in the coupling of CO_2 with terminal and internal epoxides and were found to be highly active catalysts for these transformation (Scheme 2). It should be highlighted that excellent activity

and total selectivity to the corresponding cyclic carbonate were obtained. Importantly, one of the Zn(II)/TBAI systems provided the highest conversion obtained for the coupling of CO_2 with the trans-2,3-epoxybutane as substrate using Zn(II) complexes. Additionally, recycling experiments (up to 5 cycles) for one of the catalytic systems were carried out in order to ascertain the robustness of the system.

The research in <u>Chapter 5</u> explores the synthesis of chiral C^N^C type pincer ligands, which were obtained in two steps in moderate to good yields. These ligands were coordinated to cobalt using the $Co(OAc)_2$ as cobalt precursor in good yields (72-78%). The resulting cobalt complexes were characterized by NMR, IR, Magnetic Susceptibility, ICP and EA. With all the collected data in hand, it was proposed the coordination of the $Co(OAc)_2$ moiety to the pyridine of the C^N^C ligand maintaining the imidazole moieties uncoordinated.
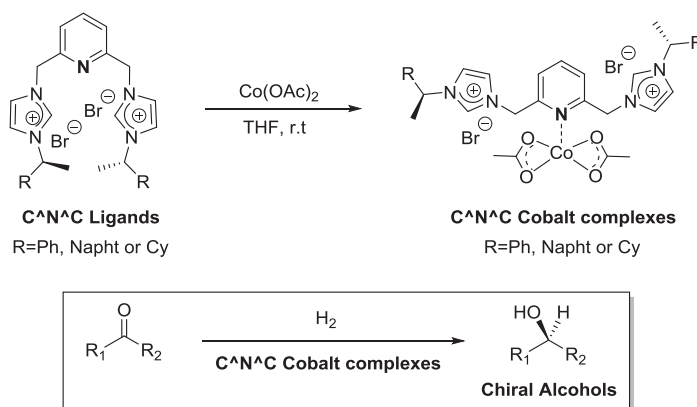
Scheme 3. C^N^C-cobalt complexes as catalysts in the asymmetric hydrogenation of ketones.

These cobalt C^N^C complexes were tested in the asymmetric hydrogenation of ketones with moderate to high yields, although low to moderate ee's were obtained (Scheme 3). Initial attempts to obtain a well

defined Co(II)-pyridine biscarbene complex having both the carbene and the pyridine coordinated to the metal center were accomplished, although still further investigation need to be performed.

CHAPTER 1

GENERAL INTRODUCTION

1.1. INTRODUCTION

1.1.1. IMPORTANCE OF CATALYSIS

The development of sustainable, selective and more efficient organic synthesis is a major goal in chemistry.[1] In this regard, catalysis has a key role since most of the chemical and pharmaceutical products on an industrial scale (above 80%) include at least one catalytic step that assures high conversions and selectivities towards the target product.[2] To put things in perspective, a large scale process can become profitable when compared to competing processes by means of a 1-2% increase in selectivity. In addition, catalysis has some benefits for businesses which include cost reduction, time savings and less waste generation.

Most of the processes in industry (75%) employ a heterogeneous catalyst due to their inherent robustness and the possibility to recover and reuse them.[1,3] Nevertheless, many processes are exclusive of homogeneous catalysts due to their higher activity and selectivity when compared to their heterogeneous counterparts. In particular, organometallic compounds have become a well-established synthetic tool for the synthesis of fine and bulk chemicals. In this regard, a large number of defined pre-catalysts are commercially available for chemists. The choice of the central metal as well as the design of the surrounded ligands plays has an important influence in the reactivity and selectivity of the active catalyst.

The importance of catalysis can be recognized by the examination of the Nobel Prizes for Chemisty in the past 40 years (Table 1.1).[4] These includes the pioneering work of Ziegler and Natta in the chemistry and technology of high polymers (1963), the fundamental work of Fischer and Wilkinson on

organometallic sandwich complexes (1973), the asymmetric hydrogenation and oxidation methodologies of Knowles, Noyori and Sharpless (2001), the award for metathesis given to Chauvin, Grubbs and Schrock (2005), as well as the recognition of Heck, Negishi and Suzuki on palladium-catalyzed cross-coupling reactions (2010).

Table 1.1. Nobel Prizes in chemistry for contribution in homogeneous catalysis.

Year	Laureates	Nobel Prize
1963	Karl Ziegler Giulio Natta	In the chemistry and technology of high polymers
1973	Ernst Otto Fischer Geoffrey Wilkinson	In the field of organometallic sandwich complexes
2001	William S. Knowles Ryoji Noyori K. Barry Sharpless	On chirally catalyzed hydrogenation and oxidation reactions
2005	Yves Chauvin Robert H. Grubbs Richard R. Schrock	On metathesis in organic synthesis
2010	Richard F. Heck Ei-ichi Negishi Akira Suzuki	On palladium-catalyzed cross coupling reactions

The leading scientific advances in catalysis have proved to be instrumental in solving many problems of considerable importance.[5]

1.1.2. EARTH ABUNDANT METALS: GENERAL CONSIDERATIONS

The study of the organometallic chemistry of Earth-abundant metals has increased over the past few years as consequence of their low cost, ready

availability, comparable low toxicity as well as sustainability.[6] Traditionally, second and third-row transition metals have been applied in organometallic chemistry, particularly in catalytic applications where the platinum-group metals (PGMs) play an important role. Nonetheless, there are some issues regarding the use of PGMs:

i)   *Cost and supply*: PGMs are expensive but also their prices can vary depending on the balance between the availability and explotation. In addition, their low natural abundance (Scheme1.1) combined with their production in few regions can also lead to supply and cost issues.
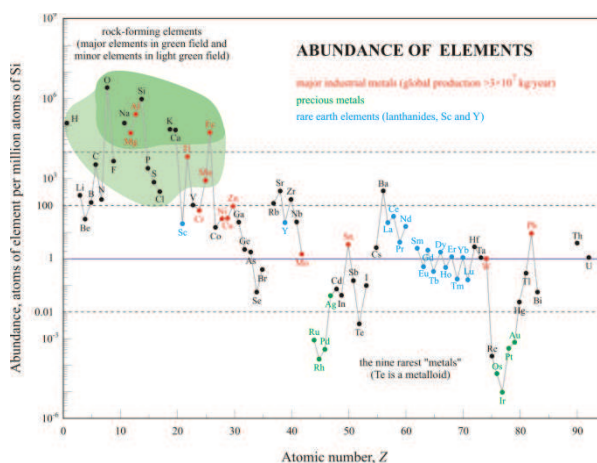
Scheme1.1. Abundance of elements.

It is noteworthy to mention that platinum-group metals are in the "risk list" (Table 1.2) made by the British Geological Survey, which describes the supply risk index for chemical elements or element groups that are of economical value.[7] The position of an element on this list is determined by a number of factors which might impact on supply. In particular, four criteria

are applied: scarcity, production concentration, reserve and distribution and governance.

Table 1.2. Selected Elements from the Risk list 2011 (British Geological Survey).

Element or Element group	Symbol	Relative supply risk index	Leading producer
Antimony	Sb	8.5	China
Platinium group elements	PGE	8.5	South Africa
Zinc	Zn	4.0	China
Nickel	Ni	4.0	Russia
Iron	Fe	3.5	China
Aluminium	Al	3.5	Australia
Titanium	Ti	2.5	Australia

Supply risk list runs from 1 (very low risk) to 10 (very high risk).

ii)   *Relatively high toxicity*: Another issue concerning the use of PGMs is their relatively high toxicity. In addition, many of them have harmful effects on biological systems. Consequently, their use for the preparation of pharmaceutical compounds is hampered by a strict regulatory control in order to minimize the presence of such metals into the final product.

From a mechanistic point of view, first row-transition metals are often significantly more complex than their heavier counterparts. While the latter ones typically undergo two-electron redox processes, first row-transition metals such as Cr, Mn, Fe, Co or Ni are likely to undergo single electron transfer (SET) pathways. The associated radical chemistry often involves electron redistribution between the central atom and the non-innocent ligands which frequently implies open-shell configurations. As consequence, structural analysis and spectroscopic monitoring became affected which make mechanistic elucidations much more challenging.[8]

There are some spectroscopic issues concerning the study of Earth-abundant elements in organometallic chemistry that need to be taken into account. In particular, many of the organometallic starting materials, products and/or intermediates are paramagnetic. For this reason, routine analysis often requires special instrumentation, such as Electron Paramagnetic Resonance (EPR) and Superconducting Quantum Interference Device (SQUID) magnetometry which is not always available in a research laboratory. Additionally, first-row metal complexes are substitutionally more labile than their second and third-row counterparts which makes isomerization or rearrangement reaction more frequent and less controllable than with the more inert precious metals. This lability can lead to a decrease of the stability of their organometallic species when compared with second and third-row counterparts.

All the difficulties related with the study of Earth-abundant elements outline above might be a reason why the organometallic community has concentrated its efforts on the study of precious metals. Nevertheless, the study of Earth-abundant metals is increasing due to the need to develop sustainable synthetic processes that take into account the cost, toxicity and minimize the environmental impact of the employed metals.

1.2. REFERENCES

1. Van Leeuwen, P. W. N. M. *Homogeneous Catalysis: Understanding the Art*; Kluwer, Dordrecht, The Netherlands, **2004**.
2. Behr, A.; Vorholt, A. J. and Seidensticker, T. *ChemBioEng Rev* **2015**, *2*, 6-21.
3. Corma, A. *Catalysis Reviews*, **2004**, *46*, 369-417.
4. Nobel Prize Home Page, http://nobelprize.org/nobel_prizes/chemisty/laureates.
5. Busacca, C. A.; Fandrick, D. R.; Song, J. J. and Senanayake, C. H. *Adv. Synth. Catal.* **2011**, *353*, 1825-1864.
6. Van der Vlugt, J. I. *Eur. J. Inorg. Chem*. **2012**, 363-375.

7. British   Geological   Survey
    http://www.bgs.ac.uk/mineralsuk/statistics/risklist.html.
8. Albrecht, M.; Bedford, R. and Plietker, B. *Organometallics* **2014**, *33*, 5619-
    5621.

CHAPTER 2

OBJECTIVES OF THIS Ph.D. WORK

The final goal of this thesis is the development of novel families of chiral ligands, which upon coordination with first-row transition metals form effective catalysts for asymmetric transfer hydrogenation, asymmetric hydrogenation and coupling of CO_2 with epoxides. In this context, the present work aims to develop new methodologies for the synthesis of polidentate ligands affording efficient catalytic systems for selective transformations.

The research described in <u>Chapter 3</u> aims to develop a synthetic methodology for the preparation of highly active chiral Fe-PNNP-based complexes. In particular, the specific objectives of this chapter are:

- To synthesize a chiral diamine derivatives, based on a pyrrolidine moiety.
- To synthesize a set of new PNNP ligands with a pyrrolidine backbone.
- To prepare and characterize the corresponding iron (II) complexes.
- To study the catalytic behaviour of these complexes and the combination of a iron precursor with the synthesized PNNP ligands in the asymmetric transfer hydrogenation of a wide range of ketones.
- To evaluate whether the system behave as a homogeneous or heterogeneous system.

The research described in <u>Chapter 4</u> aims to develop a methodology for the synthesis of a new family of zinc complexes containing a N_2O_2, N_2NH_2, N_4 and $N_4(NH)$ ligand scaffolds with a pyrrolidine backbone. In particular, the specific objectives of this chapter are:

- To synthesize a novel family of N_2O_2, N_2NH_2, N_4 and $N_4(NH)$ ligands containing a pyrrolidine backbone.

- To prepare and characterize the corresponding zinc (II) complexes.
- To study the catalytic behaviour of the zinc complexes in the synthesis of cyclic carbonates from CO_2 and epoxides.
- To study the robustness of a selected catalytic system upon recycling experiments.

The research described in <u>Chapter 5</u> aims to develop a procedure for the synthesis of C^N^C pincer-based cobalt complexes. In particular, the specific objectives of this chapter are:

- To synthesize a family of C^N^C pincer-based ligands, modifying the substituents in the imidazole moiety.
- To prepare and characterize the corresponding C^N^C pincer-based cobalt complexes.
- To study the catalytic behaviour of these complexes in the asymmetric hydrogenation of ketones.

CHAPTER 3

NOVEL PNNP IRON COMPLEXES FOR THE ASYMMETRIC TRANSFER HYDROGENATION OF KETONES

3.1. INTRODUCTION

The request for novel, efficient chiral transition metal catalysts has been an ongoing effort for the past 40 years. In this context, the development of well designed ligand systems that can be modified in order to tune the properties and provide a sterically-defined binding pocket to the metal center is one of the most important goals in organometallic chemistry and homogeneous catalysis.

Homogeneous catalyst progress has traditionally focused on the more active second- and third-row transition metal in combination with simple ligands.[1] In general, these catalysts provided high turnover frequencies (TOF) and product selectivities which are difficult to achieve by the less active first-row transition metals.[2] However, the limited availability of precious metals as well as their high price and toxicity diminishes their attractiveness and make desirable the search of more sustainable and economically friendly alternatives (Figure 3.1).[3]
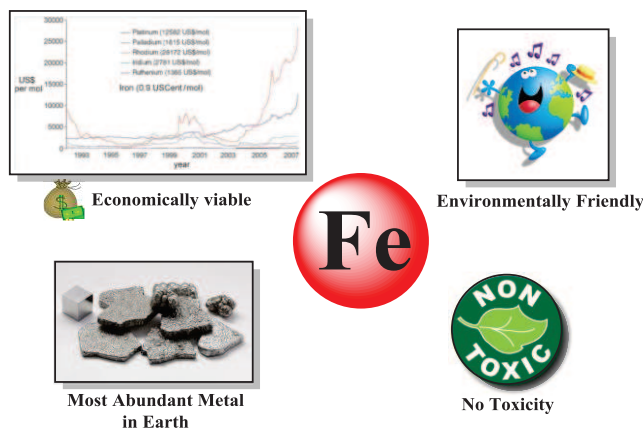
Figure 3.1. Advantages of iron versus precious metals.[4]

Even though iron chemistry has experienced an important breakthrough over the past decade, systems containing multidentate ligands are far more abundant than the well-defined, preferentially diamagnetic iron (II) (pre)catalysts for enantioselective transformations, which are still limited.[5] In this regard, tetradentate ligands, in particular the N_4 donor class, are the most outstanding ones. However, most of them are achiral and provide high-spin complexes.[6] One of the few examples containing a chiral N_4 scaffold was reported by White and co-workers and used in C-H oxidation reactions.[7] Other tetradentate ligands containing P_4 or N_2X_2 (X = P, S, O) scaffolds are scarce and most of them achiral. Concretely, Bianchini and co-workers described the use of tripodal PP_3 in the selective reduction of alkynes to alkenes.[8] In 2009, Le Floch published the use of Fe(II) complexes containing N_2X_2 (X = P, S, O) ligands in the transfer hydrogenation of ketones.[9] Besides the already mentioned tetradentate ligands, the Fe(II) N_2P_2 (pre)catalysts reported by Morris and co-workers are one of the most active and enantioselective (pre)catalysts reported to date in the literature, for asymmetric transfer hydrogenation reactions.[2d,5a,10] In 2012, Gao and co-workers described the use of chiral N_2P_4 type macrocyclic

ligands in the iron-catalyzed enantioselective reduction of ketones as an extended version of the use of N_2P_2 ligands.[11] More recently, Mezzeti and co-workers reported the synthesis of chiral Fe(II) complexes containing N_2P_2 macrocyclic ligands with two stereogenic donor phosphorus atoms (Figure 3.2).[12]

White, 2007   **Bianchini, 1992**   **Le Floch, 2009**

Morris, 2008   **Mezzetti, 2014**
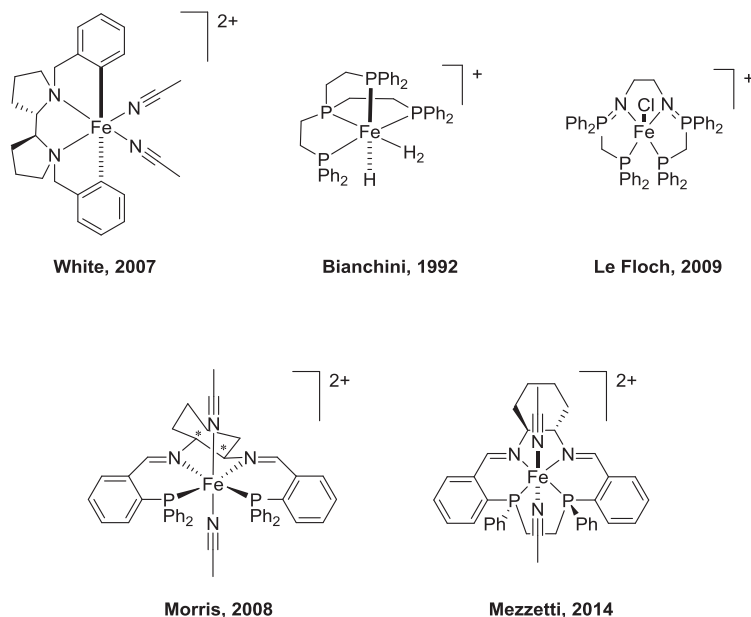
Figure 3.2. Selected Well-Characterized Iron(II) Precatalysts.

3.1.1. TETRADENTATE LIGANDS

Chiral tetradentate ligands offer a great advantage in homogeneous catalysis due to its conformational and configurational rigidity arising from its chelation (Figure 3.3).[13,14] These ligands are expected to hinder the number of possible diastereoisomers as well as to control the stereochemistry at the metal atom and compiling transfer chiral information. However and as previously reported, certain degree of flexibility exists.[12]
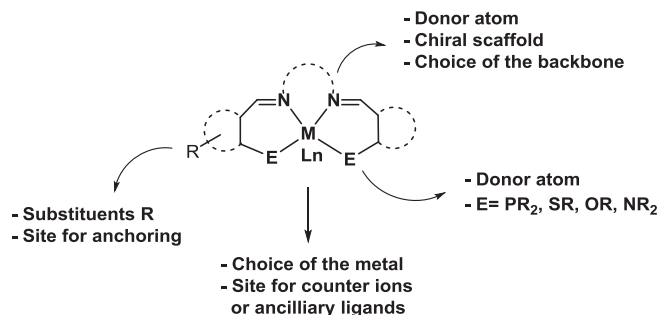
Figure 3.3. General structure of tetradentate-metal complexes.

In order to obtain systems which have considerable catalytic activity, free or potentially free coordination sites are required where the substrate and reagent species may interact in close proximity, besides those occupied by the chiral ligand itself.[15] In this context, tetradentate ligands in combination with metals having coordination number of five or six fulfill these criteria. In particular, this is the case of d^6 metals, which form stable 18e- complexes but also reactive 16e- species.

There are potentially three different classes of tetradentate ligands: linear, tripodal and cyclic (Figure 3.4). Tripodal and cyclic classes may offer a relatively rigid and well-defined coordination cores, but usually they are far more difficult to synthesize. It might be for this reason that the linear class is much more studied.[15] Indeed, the ligands decribed in this chapter will be enrolled in this class.
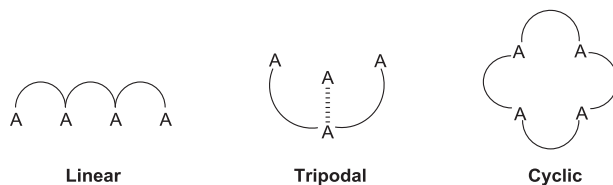
Figure 3.4. Classes of potentially tetradentate ligand systems.

In the case of linear tetradentate ligands in an octahedral coordination environment, three geometrical isomers can be formed (trans, cis-α and cis-β, Figure 3.5).
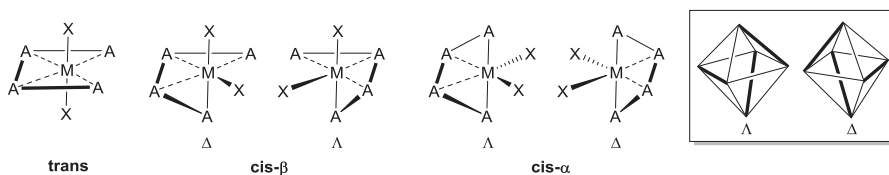
Figure 3.5. Octahedral-based geometrical isomers for tetradentate linear ligands.

The *trans* and the *cis-α* structure have C_2-symmetry whereas the *cis-β* has a C_1-symmetry. In the case of *cis-α* and *cis-β* structures, both have enantiomers with Δ and Λ helicity and cis-oriented co-ligands (X, Figure 3.5), which is of interest for the goal of enantioselective catalysis. When different co-ligands are present in the structure ($X_1 \neq X_2$) additional isomers are possible (Figure 3.6).[15]
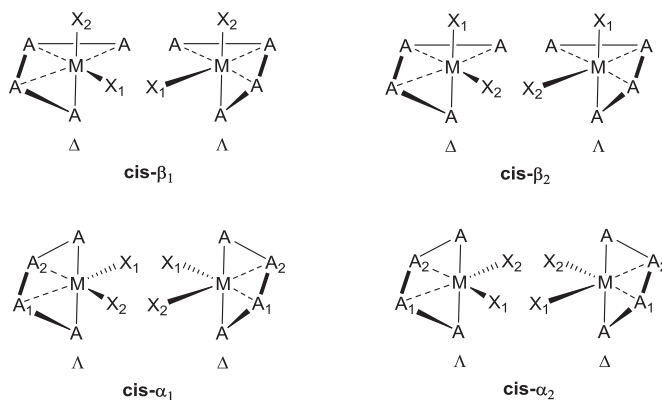
Figure 3.6. Sub-classes of the chiral *cis* geometries.

The configuration of the *cis-β_1* structure is defined where X_1 has a higher cahn ingold prelog (CIP) priority than X_2 (eg: O>N) and is *trans* to the central donor atom of the tetradentate. If we are dealing with an unsymmetrical tetradentate ligand, cis-α_1 and cis-α_2 are also possible. Also in this case, for *cis-α_1*, X_1 is defined so as to have a higher ranking than X_2 and it's, as well, *trans* to the higher central donor (A_1>A_2).[15]

3.1.2. PNNP LIGANDS

The first achiral tetradentate ligand containing a P_2N_2 donor scaffold was described by Rauchfuss and co-workers in 1980.[16] Some years later, in 1984, Pignolet and co-workers reported the chiral version using the 2,2'-dimethyl-6,6'-diaminobiphenyl as chiral framework. This ligand was further coordinated with Rh(I) and Ir(I) and its coordination chemistry was also studied.[14] However, the most important breakthrough was carried out by Noyori, Gao and Ikariya in 1996, effectively applying Ru-PNNP complexes in the asymmetric transfer hydrogenation of ketones (Figure 3.7).[17]
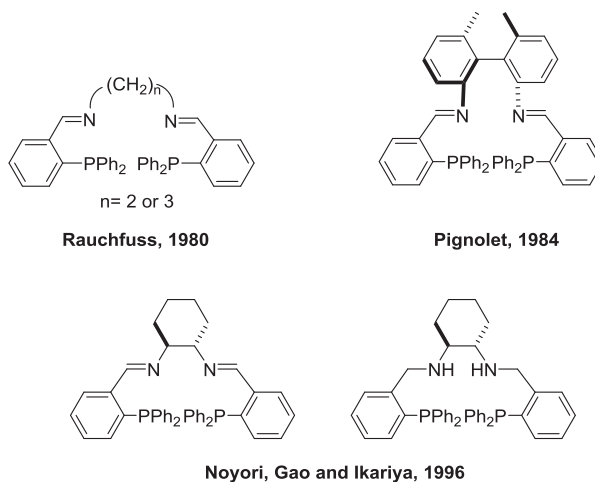
Figure 3.7. Selected PNNP ligands.

Although P_2N_2 ligands have been less investigated than other tetradentate ligands (for instance compared to salen), they offered unexplored potential. Nevertheless, these ligands have been effectively applied in a large number of asymmetric reactions such as, hydrogenation, transfer hydrogenation, hydrosilylation, cyclopropanation, epoxydation or aziridination among others.[5a,10d,18,19]

3.1.2.1. SYNTHESIS OF PNNP LIGANDS AND RELATED FE-COMPLEXES

Two relevant methods are reported for the synthesis of these ligands.[20] One involves a single step procedure with a condensation reaction between the appropriate diamine and the phosphinoaldehyde of choice as reactants (Scheme 3.1 and Figure 3.8). The main drawback of these phosphinoaldehydes is in the air sensitivity.
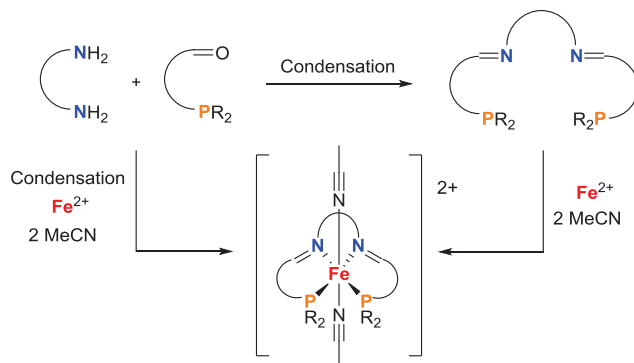
Scheme 3.1. Synthetic route to PNNP ligands and their related Fe (II) complexes.
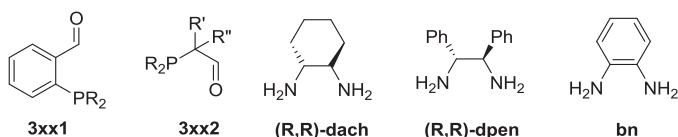
Figure 3.8. Examples of phosphino-aldehyde precursors and diamines that can be used in the synthesis PNNP ligands.

The other method allows a combinatorial synthesis of a wide number of related structures starting from the air-stable phosphonium precursor **3xx3** (Scheme 3.2).
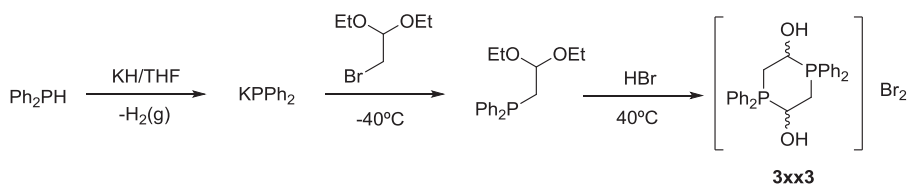
Scheme 3.2. Synthesis of the phosphonium precursor **3xx3**.

The next step involves the reaction between dimer **3xx3**, $Fe(BF_4)_2 \cdot 6H_2O$ as iron precursor and KO^tBu in acetonitrile which yielded the formation of the free monomer of the phosphino-aldehyde and various iron-phosphine

complexes. Then, addition of the desired diamine afforded the formation of *mer*-bis-tridentate complexes **3xx4a-c**, which by reflux allowed the production of the target Fe-PNNP complex **3xx5a-c** in 75-79% yield (Scheme 3.3).
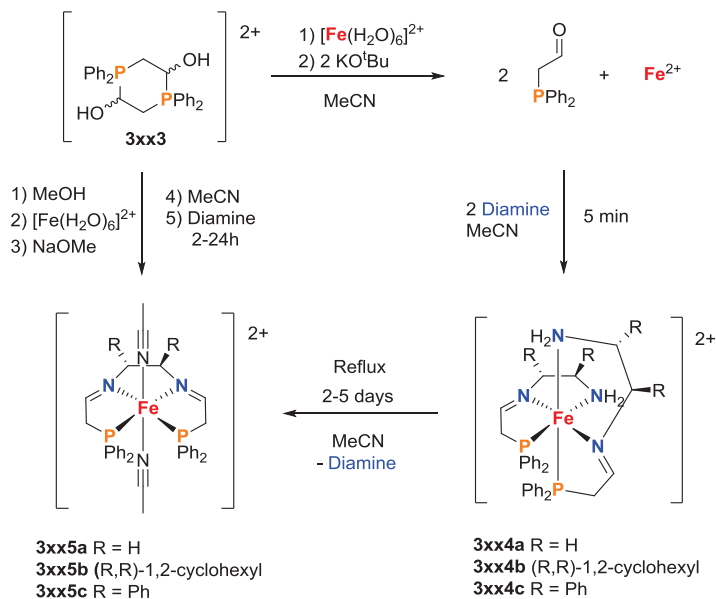
Scheme 3.3. Synthesis of PNNP and PNN Iron complexes.

The main advantage of this methodology is the use of the air stable precursor **3xx3** as starting material. Indeed, it allows an extensive modification of the phosphorous substituents, including both alkyl and aryl groups.[21] However, long reaction times are needed in the final synthetic step.

The group of Morris and co-workers have extensively studied the synthesis of well-defined Fe(II)P$_2$N$_2$ (pre)-catalysts. In this regard, two different families can be distinguished: the so called *first generation*, which form a six membered M-P-N ring generating a 6,5,6 system and the named *second*

generation, with a five membered M-P-N ring generating a smaller chelating ring which is called 5,5,5 system (Figure 3.9).[10b,10c,21,22,23]

6,5,6 system
First generation

5,5,5 system
Second generation
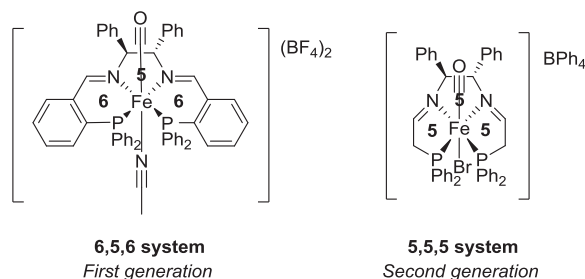
Figure 3.9. Well-defined $Fe(II)P_2N_2$ (pre)-catalysts with 6,5,6 and 5,5,5 M-P-N ring systems.

It has to be noted that the *first generation* can be synthesize by the straightforward method describe above so as the precursors are already commercially available. On the contrary, the *second generation* has to be prepared by the template synthesis, also described above, which provide the advantage of tuning the phosphorous substituents allowing the synthesis of a wide range of $Fe(II)P_2N_2$ (pre)catalysts.

3.1.2.2. MODIFICATIONS IN PNNP LIGANDS

Diamine backbone

The effect of incorporating different diamines into the backbone of the PNNP ligand was investigated by the group of Morris and co-workers.[24] As a general trend, the *second generation* is much more active and provided better enantioselectivitites than the *first generation* of (pre)catalysts (Figure 3.10). For this reason, the study was performed using the second *generation* with a small number of atoms in the ligand-metal ring (5,5,5).
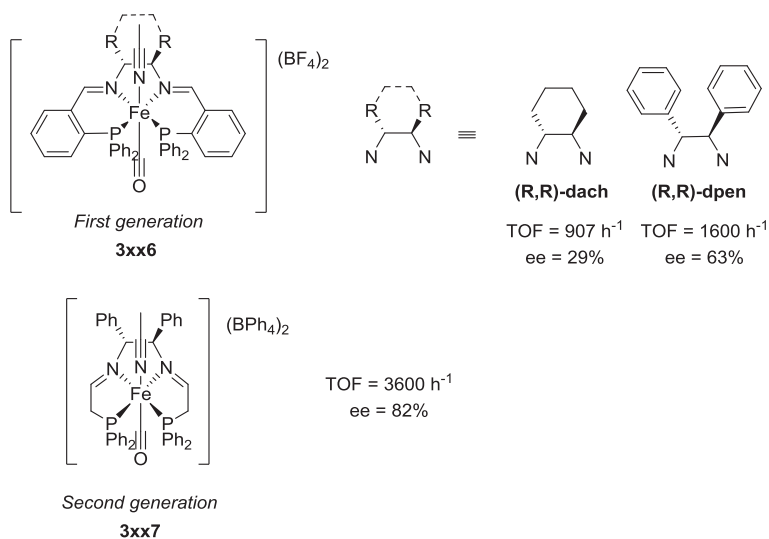
Figure 3.10. Activity and enantioselctivity comparison of the *first generation* vs *second generation* of precatalysts.

The synthesis of the iron(II) precatalysts **3xx7** containing other diamines than the (R,R)-1,2-diphenylethylenediamine (**dpen**) led to the formation of the iron(II) precatalysts **3xx8a-d** containing a bromide *trans* to the carbonyl unit, instead of the acetonitrile moiety (Scheme 3.4).[21a] The Br⁻/CO complexes were thermodynamically more stable than the CH3CN/CO counterparts, since the formation of the iron(II) precatalyst **3xx8a-d** was observed when Br⁻ was present in small quantities in the reaction mixture, containing large excess of acetonitrile. The greater stability of complexes **3xx8** compared to complexes **3xx7** was explained by the strong ionic Fe^{2+}-Br⁻ bond relative to the weaker ion-dipole Fe^{2+}-$N^{\delta-}$ bond of the acetonitrile ligand.[24]
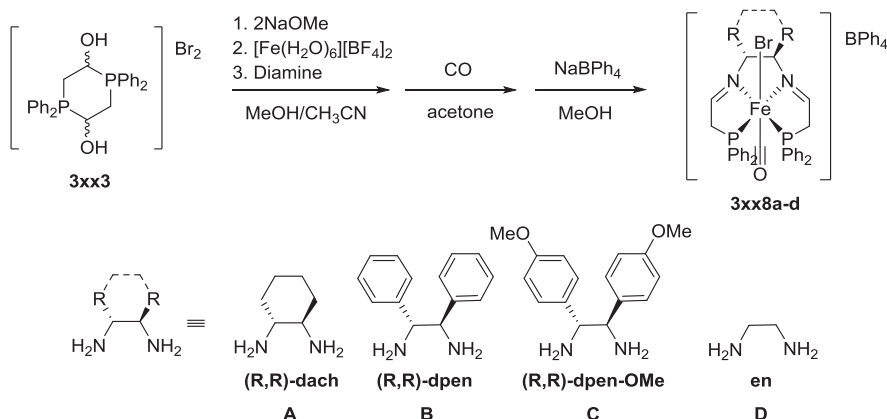
Scheme 3.4. One pot synthesis of iron(II) precatalyst **3xx8a-d** starting from dimer **3xx3**.

Comparable catalytic activities of precatalyst **3xx8b** (having a Br⁻/CO) and precatalyst **3xx7** (having a CH₃CN/CO) were found (Table 3.1). This observation may indicate that dissociation of the ligand *trans* to the carbonyl unit takes places during the activation of the precatalyst and neither the acetonitrile nor the bromide participate in the reduction process of acetophenone to 1-phenylethanol.[24]

The electronic as well as the steric properties of the complexes is affected by the incorporation of the different diamines at the backbone. A correlation between the basicity of the nitrogen donor and the CO stretching wavenumber can be performed: the more basic the donor is, the lower the CO stretching band, as confirmed in Table 3.1 (the basicity of the nitrogen donor increase as follows: **D** < **C**=**B** < **A**). With this information in hand, no correlation between the TOF values and the basicity of the diamines could be extracted. On the other hand, the highest activity and enantioselectivities for the reduction of acetophenone were found when the more bulky diamines (**B** and **C**) were tested. This feature showed that the steric

properties of the diamine backbone had a higher influence on the activity of the catalyst compare to the electronic factors (Table 3.1).

Table 3.1. Transfer hydrogenation of acetophenone catalyzed by complexes **3xx8a-d** in basic 2-propanol.
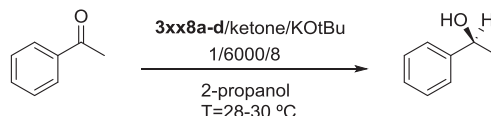
Complex	IR CO stretch (cm^{-1})	TOF (h^{-1})[a]	ee (%)
3xx7	2001	$2.1 \cdot 10^4$	82
3xx8a	1974	$4.9 \cdot 10^3$	60
3xx8b	1975	$2.0 \cdot 10^4$	81
3xx8c	1974	$2.0 \cdot 10^4$	82
3xx8d[b]	1981	$2.1 \cdot 10^3$	

[a] TOF at 15-50% conversion. [b]15% conversion.

Phosphine framework

In 2010 and in a parallel study on the modifications at the diamine backbone, the group of Morris and co-workers investigated the effect of the substituents at the phosphorus atom and their impact in the catalytic activity.[21a]

The substituents at the phosphorus moiety where replace from phenyl group (Ph) to a cyclohexyl (Cy), isopropyl (iPr) and ethyl (Et) groups (Figure 3.11).
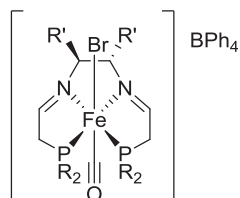
3xx9 R=Cy, R'=H; (S,S)-**3xx10** R=Cy, R'=Ph
3xx11 R=iPr, R'=H; (S,S)-**3xx12** R=iPr, R'=Ph
3xx13 R=Et, R'=H; (S,S)-**3xx14** R=Et, R'=Ph

Figure 3.11. *Trans*-[Fe(CO)(Br)(PNNP)][BPh$_4$] complexes used in this section.

As commented before, when more donor groups are located in the phosphorus moiety, a decrease in the CO stretch wavenumber is observed (the basicity of the phosphorus atom increases as follows: Et < ^{i}Pr < Cy) (Table 3.2). The substituent at the diamine (R'= H or Ph) had a little effect on the electronics at the metal since the CO wavenumber had a modest variation (for example from **3xx9** to **3xx10**).

The complexes containing a Cy (**3xx9** and **3xx10**) or iPr (**3xx11** and **3xx12**) substituents at the phosphorus atom were completely inactive, indicating that there cannot be too much steric bulk at the phosphorus moiety of the ligand. In the case of having Et substituents (**3xx13** and **3xx14**), those complexes were active but much less than complex **3xx7**, containing Ph substituents. Indeed, the poor enantioselectivity exhibited by complex **3xx14** indicate that some degree of steric bulk is required.

Table 3.2. Catalytic transfer hydrogenation of acetophenone using complexes **3xx9-14**.
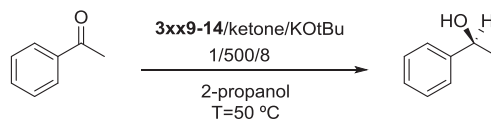
Complex	IR CO stretch (cm^{-1})	Conversion (%)[a]	ee (%)[a]
3xx7	2001	-[b]	82
3xx9	1948	N.R.	-
3xx10	1945	N.R.	-
3xx11	1948	N.R.	-
3xx12	1956	N.R.	-
3xx13	1951	47	-
3xx14	1951	81	26

[a] Conversion and ee's at 60min. N.R.= no reaction. [b] Not given at specified conditions.

Noyori and co-workers described that an increase in activity of their ruthenium bis-chelate direct hydrogenation catalysts was found when changing the phenyl groups on the BINAP by more electron-donating *para*-tolyl groups.[25] Indeed, replacing the phenyl group by meta-xylyl groups afforded more enantiopure products.[25,26] On the contrary, when electron-withdrawing groups where located at the phosphorus moiety, in particular with *para* or 3,5-ditrifluoromethyl-substituted phenyl groups, an increase in activity was observed for rhodium hydroformylation catalysts.[27,28]

In order to separate the steric and the electronic effects, in 2011 also the group of Morris and co-workers prepared a series of complexes with ortho- and para-substituted phenyl groups at the phosphorus atom.[21b] In this manner, the electronics of the systems would be analogous whereas the sterics around the metal would remarkably change.

3xx15a: R = *para*-CH$_3$C$_6$H$_4$
3xx15b: R = *ortho*-CH$_3$C$_6$H$_4$
3xx15c: R = 3,5-(CH$_3$)$_2$C$_6$H$_3$
3xx15d: R = *para*-CF$_3$C$_6$H$_4$
3xx15e: R = 3,5-(CF$_3$)$_2$C$_6$H$_3$
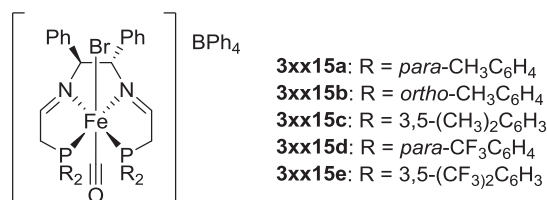
Figure 3.12. *Trans*-[Fe(CO)(Br)(PNNP)][BPh$_4$] complexes used in this section.

When precatalyst **3xx15a** containing a *para*-CH$_3$C$_6$H$_4$ group was tested, high activity and selectivity for the ATH of acetophenone was found, being the most active iron ATH catalyst to date (Table 3.3). However, when the methyl group was located at the *ortho* position of the phenyl group (**3xx15b**), the system was completely inactive. The authors hypothesized that the steric bulk around the phosphorus atom could favor the dissociation of a phosphorus donor which was supported by some peaks in the negative region of the ^{31}P-{1H} NMR spectrum. They conclude that decordination of a phosphorus atom occurred under the catalytic conditions for **3xx15b** and leaded to decomposition products instead of active catalytic species.[21b]

In the case of **3xx15c** with *meta*-xylyl substituents, an improved ee of 90% was achieved for the ATH of acetophenone (compared to **3xx8b**, with Ph substituents, that gave 81% ee) being the most selective iron ATH catalyst reported to date (Table 3.3). On the other hand, precatalysts **3xx15d** and **3xx15e**, containing electron-withdrawing substituents at *para*- and 3,5 positions were completely inactive. The authors hypothesized that if the mechanism would involved transferring a hydride equivalent to an iron intermediate, **3xx15d** and **3xx15e** would favor and stabilized these species as a result of their electron-deficient nature of the metal center however, an increase in activity was not seen.

Table 3.3. Activity and selectivity of complexes **3xx8b**, **3xx15a** and **3xx15c** under the same conditions.[a]

Compound	TOF (h^{-1})	ee (%)
3xx8b	28000	81
3xx15a	30000	84
3xx15c	26000	90

[a] C/B/S = 1:8:6000, T = 28 ºC, [Fe] = 92.4µM.

Although complexes **3xx15a**, **3xx15c** and **3xx8b** were extremely active, there is no significant difference between them. Complex **3xx15a** is more active than **3xx8b** while **3xx15c** is only somewhat slower. This fact is unexpected as both, **3xx15a** and **3xx15c**, should be more electron-donating than **3xx8b** and, as seen in a previous section, electron-rich phosphines inhibited the catalysis (PR$_2$ where R$_2$= Cy or ^{i}Pr). However, the IR spectra showed that those complexes have similar carbonyl stretches indicating that the iron centers have comparable electron densities (Table 3.4).

Table 3.4. IR CO stretches of Iron (II) Carbonyl complexes **3xx8b**, **3xx10**, **3xx12**, **3xx14** and **3xx15a-e**.

Compound	Substituent at the phosphorus	CO stretch (cm^{-1})
3xx8b	Phenyl	1975
3xx10	Cyclohexyl	1945
3xx12	Isopropyl	1956
3xx14	Ethyl	1951
3xx15a	*para*-CH$_3$C$_6$H$_4$	1972
3xx15b	*ortho*-CH$_3$C$_6$H$_4$	1974
3xx15c	3,5-(CH$_3$)$_2$C$_6$H$_3$	1970
3xx15d	*para*-CF$_3$C$_6$H$_4$	1989
3xx15e	3,5-(CF$_3$)$_2$C$_6$H$_3$	1990

In general, a good balance between both sterics and electronics at the phoshorus is required for their activity and selectivity.

3.1.3. PNNP METAL COMPLEXES FOR THE ASYMMETRIC TRANSFER HYDROGENATION REACTION

As previously outlined in section 3.1.2., PNNP ligands have been effectively applied in a large number of asymmetric reactions such as, hydrogenation, transfer hydrogenation, hydrosilylation, cyclopropanation, epoxydation or aziridination among others.[5a,10d,18,19] In this section, selected PNNP-metal complexes will be presented with the aim of showing the development and application of these PNNP-metal complexes in the asymmetric transfer hydrogenation reaction.
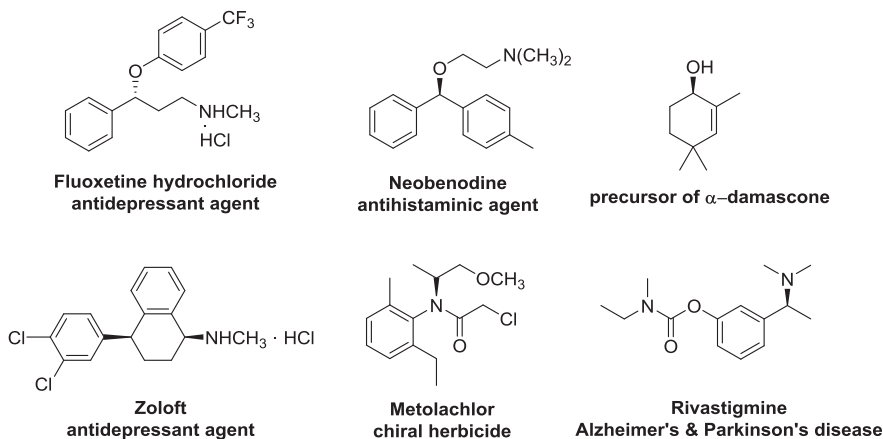
Figure 3.13. Selected chiral alcohols and amines used as pharmaceuticals, precursors for perfumes and agrochemicals.

The asymmetric transfer hydrogenation (ATH) of prochiral ketones and imines is an appealing strategy used in pharmacy, perfume and food

industries for the synthesis of enantiopure alcohols and amines (Figure 3.13).[1,19,29]

This transformation requires a sacrificial reductant, such as isopropanol or formic acid, to provide a hydride and proton equivalent for the hydrogenation of unsaturated substrates (Scheme 3.5). The major benefit of this transformation is that avoids the use of specialized equipment and safety measures needed to work with high pressures of hydrogen gas. Most of the catalysts used for this transformation employed expensive and toxic platinum group metals, such as ruthenium.[30]

X= O, XR
DH_2 = hydrogen donor
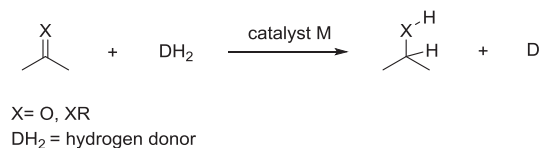
Scheme 3.5. General scheme for the asymmetric transfer hydrogenation reaction.

One of the major breakthroughs in this field was accomplished by Noyori, Gao and Ikariya in 1996, showing that a trans-dichloro(PNNP)ruthenium(II) complex when activated with KO^{i}Pr in isopropanol catalyzed the asymmetric transfer hydrogenation of ketones with moderate to excellent activities and enantioselectivities (Scheme 3.6).[17a]
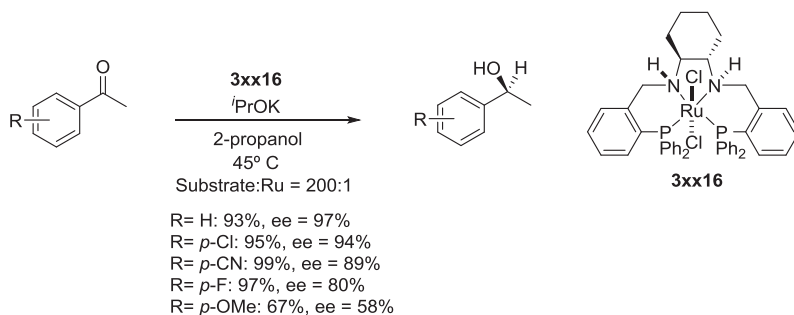
Scheme 3.6. Asymmetric transfer hydrogenation of ketones catalyzed by trans-dichloro(PNNP)ruthenium(II) complex **3xx16**.

In 2000, the group of Gao and co-workers reported an expanded version of the above mentioned trans-dichloro(PNNP)ruthenium(II) complexes, having modifications at the imine/amine backbone for the asymmetric transfer hydrogenation of ketones.[31] Not only the Ru(II) complexes were described but also the related Rh(I) derivatives. It is noteworthy mentioning that independently on the metal used (Ru or Rh), the diamine-metal complexes were far most efficient than their diamine counterparts. In this regard, the authors suggested that the NH linkage possibly can stabilize a six-membered cyclic transition state by forming a hydrogen bond with oxygen atoms of ketones, as previously proposed by Noyori (Figure 3.14).[17b,32]
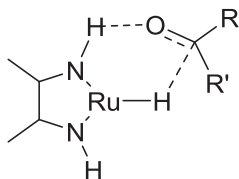
Figure 3.14. A possible six-membered cyclic transition state for activation and reduction of ketones.

In Scheme 3.7 are shown the most successful Ru(II) and Rh(I)-PNNP complexes for the ATH of acetophenone reported by Gao and co-workers.

The trans-dichloro(PNNP)ruthenium(II) complex **3xx16** was the most efficient of the serie, obtaining high activity and enantioselectivity for the asymmetric transfer hydrogenation of acetophenone. Nonetheless, their rhodium counterpart (**3xx18**) exhibited similar results in both, conversion and enantioselectivity, although higher catalyst loading and temperature were required. In the case of the trans-dichloro(PNNP)ruthenium(II) complexe **3xx17**, having a modification at the diamine framework, high activity and enantioselectivity was obtained, although also in this case high catalyst loading and reaction time were needed in comparison with that of the trans-dichloro(PNNP)ruthenium(II) complex **3xx16**.
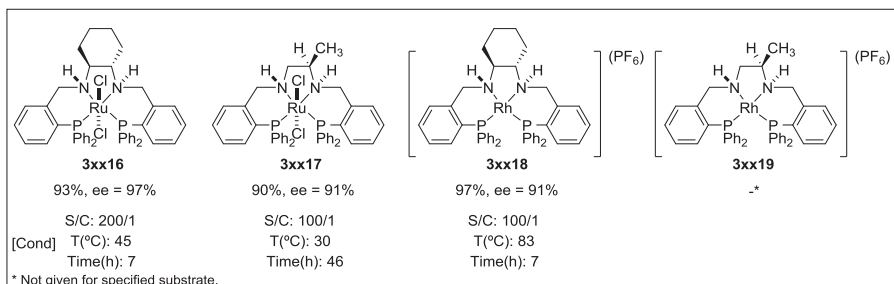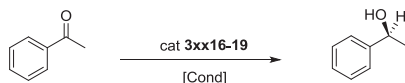
Scheme 3.7. Asymmetric transfer hydrogenation of acetophenone catalyzed by trans-dichloro(PNNP)ruthenium(II) complexes **3xx16** and **3xx17** and (PNNP)rhodium(I) complexes **3xx18** and **3xx19**.

In 2003, Gao and Ikariya reported the first asymmetric transfer hydrogenation of ketones catalyzed by a cluster-based catalyst system generated *in situ* from the commercial available $Ru_3(CO)_{12}$ and chiral PNNP ligands (Scheme 3.8).[33] Contray to the mononuclear ruthenium systems presented above, in these Ru cluster systems, the diiminophosphine ligands were effective for the reduction of ketones obtaining high conversions and

enantioselectivities. The authors suggested that the reaction mode with the cluster system may be different from that proposed for the mononuclear Ru catalyst systems. In addition, the authors proposed that the hydrogen transfer with these cluster-based catalysts proceeded *via* a Meerwein-Ponndorf-Verley (MPV) mechanism.
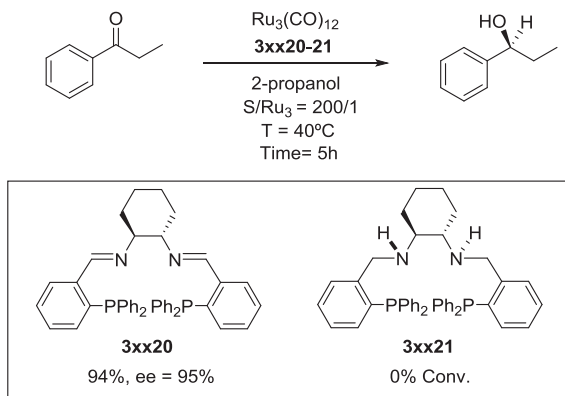
Scheme 3.8. Asymmetric transfer hydrogenation of propiophenone catalyzed *in situ* from $Ru_3(CO)_{12}$ and **3xx20** or **3xx21**.

Other metals have also been used in the asymmetric transfer hydrogenation of ketones catalyzed by PNNP-metal systems. For instance, in 2006, the group of Gao and co-workers developed a water-soluble PNNP ligand systems for the asymmetric transfer hydrogenation of ketones using iridium as metal source.[34] Moderate to high conversions and enantioselectivities were achieved at 0.5mol% of catalyst loading, T = 40ºC and 24h of reaction time (Scheme 3.9).
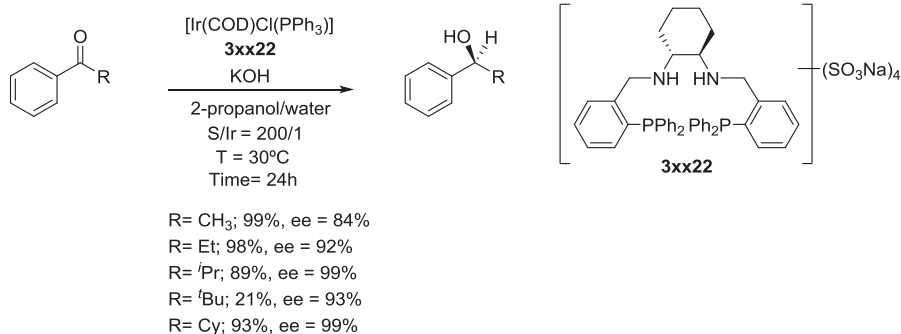
Scheme 3.9. Asymmetric transfer hydrogenation of ketones catalyzed by [Ir(COD)Cl(PPh$_3$)]/**3xx22** catalytic system.

PNNP-rhodium(I) systems have also shown to be effective for the asymmetric transfer hydrogenation of ketones. In particular, the group of Gao and co-workers reported the use of the cationic rhodium(I) complex **3xx23** which catalyzes the asymmetric transfer hydrogenation of alkyl aryl ketones in moderate to good conversions and enantioselectivities (Scheme 3.10).[35]
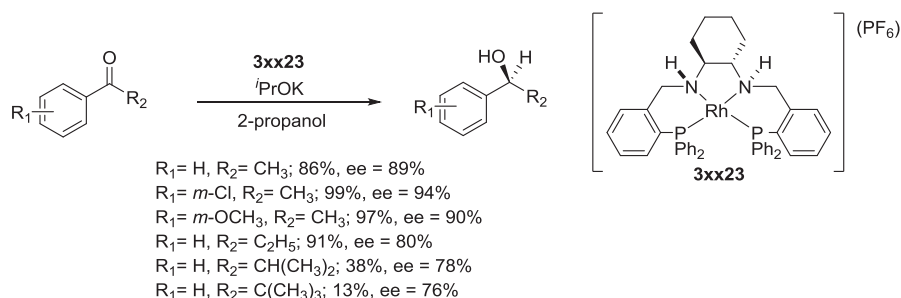
Scheme 3.10. Asymmetric transfer hydrogenation of ketones catalyzed by cationic rhodium(I) complex **3xx23**.

3.1.3.1. FE-PNNP COMPLEXES FOR THE ASYMMETRIC ASYMMETRIC TRANSFER HYDROGENATION REACTION

As a general trend, platinum group metal complexes are expensive due to the cost of the enantiopure ligand and the cost of the metal. The price for platinum group metals continues to increase and its supply is limited. Indeed, ruthenium in its ionic form, for instance, is toxic and as consequence it should be removed from the final product when used as part of a catalytic system.[36] On the other hand, iron is ubiquitous and is thousand times cheaper than ruthenium. In addition, traces of iron in a final product are not as serious problem as with platinum group metals.

The use of less noxious chemicals is an important target for green chemistry. In this sense, many reports have appeared using homogeneous iron complexes for a wide variety of catalytic processes.[8b,22,37,38,39,40,41,42] In this section, selected PNNP-Fe systems for the asymmetric transfer hydrogenation reaction will be presented as part of the objective of this chapter.

In 2004, the group of Gao and co-workers reported the asymmetric transfer hydrogenation of certain ketones using a generated *in situ* system from the iron carbonyl cluster complex $[NHEt_3][Fe_3H(CO)_{11}]$ and PNNP ligands **3xx24** and **3xx25** (Scheme 3.11).[43] The best results were obtained for aryl-alkyl ketones of the type PhCOR (56-93% ee) with variable results in terms of activity (19-92% conv.). The monitoring of the reaction by *in situ* IR spectroscopy revealed peaks thought to be indicative of a trinuclear iron structure.
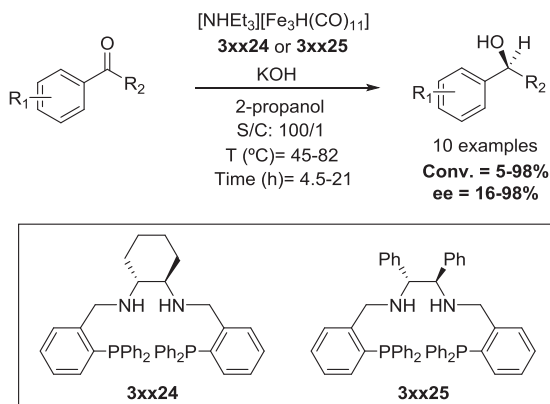
Scheme 3.11. Asymmetric transfer hydrogenation of ketones catalyzed by [NHEt$_3$][Fe$_3$H(CO)$_{11}$]/PNNP ligands **3xx24** and **3xx25**.

Some years later, the group of Morris and co-workers developed a series of well-defined and more active iron-based catalysts of the type trans-[Fe(CO)(MeCN)(PNNP)]$^{2+}$ for the transfer hydrogenation of ketones (Scheme 3.12).[10a,10b,22] It should be pointed out that a crucial point in the development of these catalysts was the comprehension that a CO ligand was needed to activate the iron complexes for this transformation. Previous work reported by the same authors shown that without this ligand the iron catalysts were completely inactive for the ATH of ketones.[5a,10b]
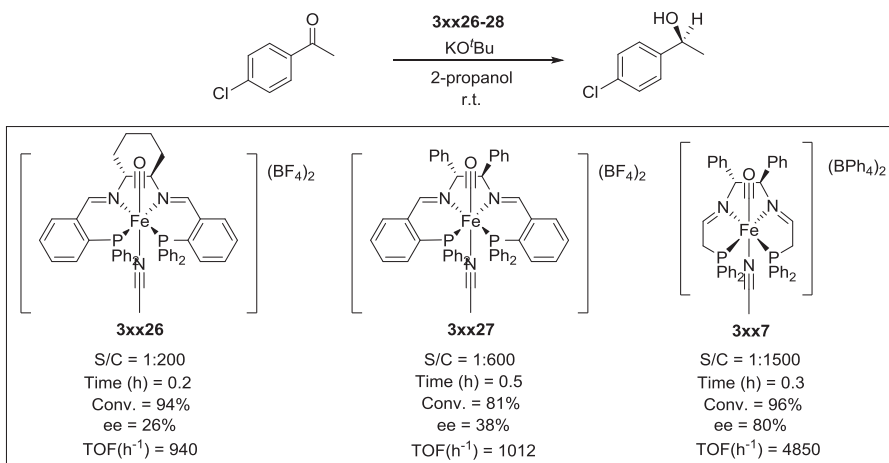
Scheme 3.12. Asymmetric transfer hydrogenation of 4-chloroacetophenone catalyzed by **3xx26-28**.[10a,10b,10c]

The carbonyl complexes **3xx26**-**3xx27** and **3xx7** were highly active catalysts for the asymmetric transfer hydrogenation of ketones at room temperature. Concretely, complexes **3xx26** and **3xx27** showed comparable TOF (above 900h[-1]), whereas complex **3xx7** was four times more active. It has to be pointed out that complex **3xx7** showed comparable activity than that of the best ruthenium-based catalysts used for ATH of ketones at room temperature.

The so called *first generation* of the well-defined Fe(II)P$_2$N$_2$ (pre)-catalysts with a 6,5,6 system (see section 3.1.2.1 for a detailed view of the system) was active for the asymmetric transfer hydrogenation of ketones but the enantioselectivity was only moderate.[10b] In this regard, the authors developed the so called *second generation* with a small metallocyclic ring which would make the ligand more suitable for iron.[2d]

In 2012, the group of Morris and co-workers reported that the active catalytic species for the 6,5,6 systems were iron(0) nanoparticles.[44] The

formation of iron(0) nanoparticles was then explained by the flexibility of the tetradentate PNNP ligand.[45] Upon reaction of the Fe(II)P_2N_2 **3xx28** with base in isopropanol, one of the ligand imines becomes reduce and deprotonated. Then the ligand arm folds upwards to form the ferraziridine species, and eventually, iron nanoparticles (Scheme 3.13).
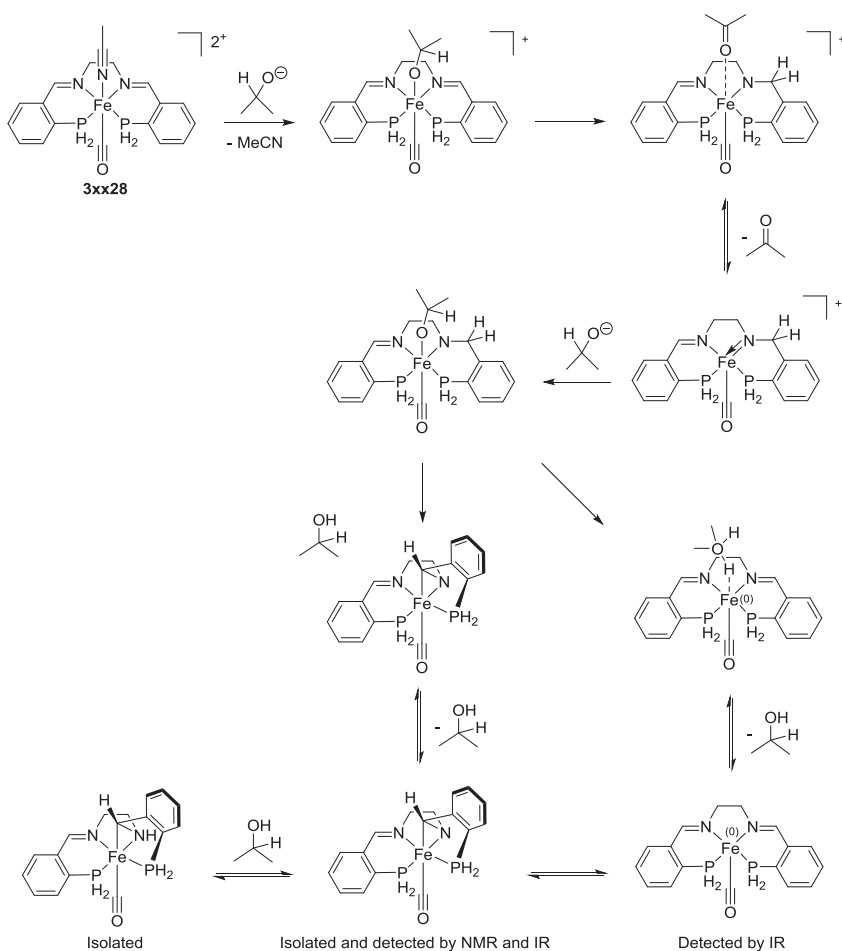
Scheme 3.13. Proposed mechanism for the ferraaziridine species and Fe(0) observed by NMR and or IR spectroscopy.

The development of 5,5,5 systems with a smaller ring were expected to be more rigid and avoid the formation of iron(0) nanoparticles.[2d]

The minor role of the acetonitrile ligand in the catalytic cycle, it acts as a labile ligand and decoordinate during precatalyst activation to generate a vacant site, provided its replacement by a bromide ligand in the 5,5,5 system. Indeed, its replacement did not affect the catalytic activity and enantioselectivity of the resulting catalysts (Scheme 3.14).[21a,24]
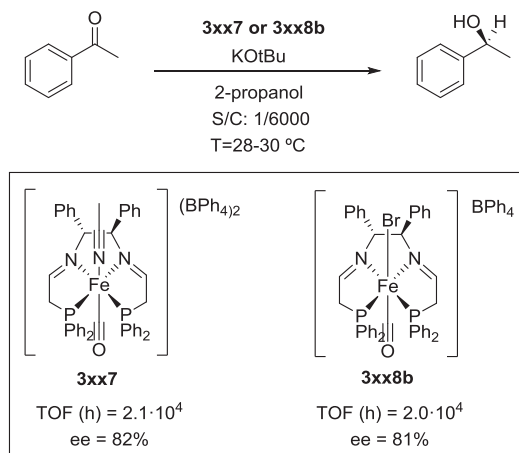
Scheme 3.14. Asymmetric transfer hydrogenation of acetophenone catalyzed by **3xx7** and **3xx8b**.

Role of the base

All the iron carbonyl complexes described in this section are not active by themselves in the ATH of ketones, a strong base in needed to generate the active catalytic species,[10a,10b,10c,21a,22,44] which is quite typical for ATH reactions.[46] The role of the base is not always know but it is thought to deprotonate the amino group on the ligand and then generate an amido intermediate that can enter into the catalytic cycle. However, in 5,5,5 systems there are no acidic amino groups to be deprotonated. In this sense, the group of Morris and co-workers reported that upon addition of the base to the catalytic mixture a colour change from yellow to green was observed. This new green species was identified as the eneamido compound **3xx32-34**

(Scheme 3.15). Deuterium labelling experiments and X-ray diffraction confirmed the formation of **3xx32-34**.[47]

3xx29; R = Cy
3xx30; R = iPr
3xx31; R = Et

MO^{t}Bu

benzene
- MBr
- MBPh$_4$
M = Na, K

3xx32; R = Cy
3xx33; R = iPr
3xx34; R = Et
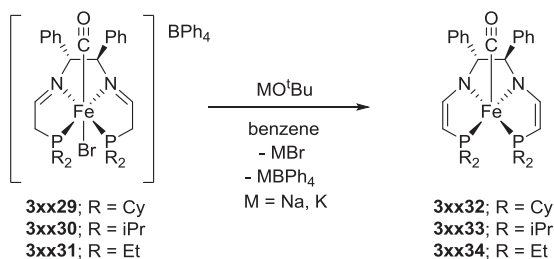
Scheme 3.15. Formation of doubly deprotonated iron(II) complexes **3xx32**-**34**.

Interestingly, when complex **3xx34** was tested in the ATH of acetophenone, similar activity and selectivity to that obtained with complex **3xx31** were obtained, indicating that the base is only needed to deprotonate the PNNP ligand and does not play any further role in the catalysis.

Mechanism for 5,5,5 systems

Regarding the mechanism followed by these 5,5,5 systems, the group of Morris and co-workers make some observations:[48]

- The reaction profile for ATH displayed an induction period, followed by rapid catalysis and then rapid decrease in activity as the system reached a plateau. Although sigmoidal profiles are indicative of heterogeneous catalysis, nanoparticles were excluded via electron microscopy and poisoning experiments. In this case, the induction period was indicative of a high barrier activation process.
- A positive rate dependence on the concentration of substrate was observed, while the induction period was prolonged with increased ketone concentration which indicates that interfered in the activation of the catalyst. The authors attributed this interference to

the formation and coordination of an enolate form of acetophenone. Such hypothesis was confirmed when benzophenone, a non-enolizable ketone, was used as substrate.

- When the bis-enamido complex (**3xx36**) was treated with ^{i}PrOH before the addition of the substrate, the induction period was not seen, but if the bis-enamido complex was treated with the substrate before the addition of the ^{i}PrOH, a more pronounced induction period was observed (which also supports the idea of the enolate inhibition of the activation process).

- The iron carbonyl complexes containing two amino groups were significantly less active than the imino partners, which make negligible the hypothesis that the reduction of the imino functionalities to obtain the amino groups was the activation pathway for these systems.

- An important breakthrough was performed reacting the bis-enamido complex **3xx36** with ^{i}PrOH for 20min, obtaining after quenching with HCl a partially reduced complex (**3xx35**) containing an imino and an amino functionalities. No induction period was seen when precatalyst **3xx35** upon treatment with base was used and the catalysis began immediately (TOF of 55000h^{-1}). The plot of the conversion *vs* time had a similar shape than with **3xx8b**, but without the induction period. The authors suggested that the partially reduced precatalyst **3xx35** reacted with base to produce an amido enamido species (**3xx37**) which can enter to the catalytic cycle.

The scheme of the process is depicted in Scheme 3.16.
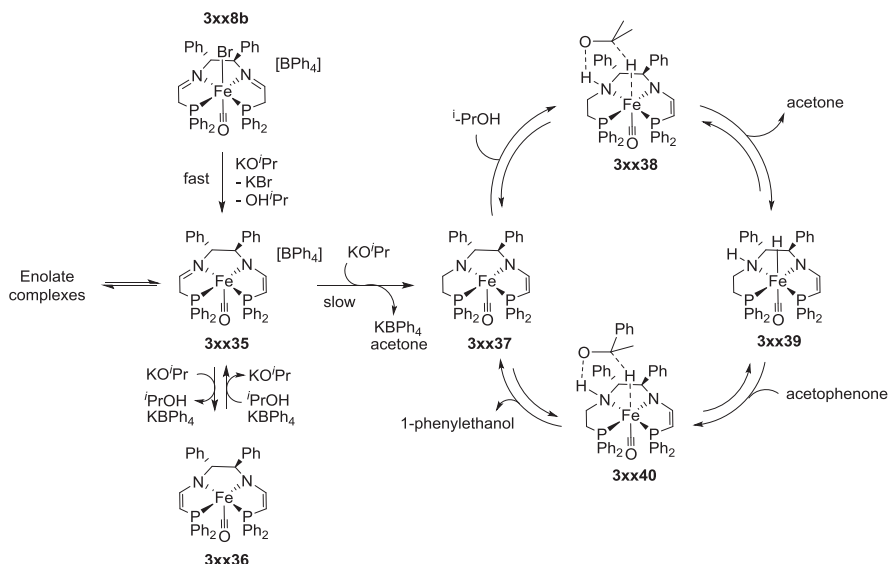
Scheme 3.16. Proposed mechanism for 5,5,5 systems.

The carbonyl precatalyst **3xx8b** reacts with the base to form a set of rapid equilibria between the cationic enamido complex **3xx35** and the neutral bis-enamido complex **3xx36** and two enolate complexes from acetone and the ketone substrate. Only the reaction of **3xx35** with ^{i}PrO$^-$ leads to the formation of **3xx37** which reacts with ^{i}PrOH to borrow a proton and a hydride in an outer sphere step-wise process. Finally, the resulting **3xx39** complex can deliver the hydrogen to the substrate in an outer sphere step-wise process generating the product and regerating **3xx37**.

ATH of N-(diphenylphosphinyl) imines

Not only ketones were substrates of interest in the ATH catalyzed by these and others Fe/PNNP systems. In 2010, the group of Beller and co-workers reported the ATH of activated imines using the iron carbonyl precursor [NHEt$_3$][Fe$_3$H(CO)$_{11}$] and the PNNP ligand **3xx20** of the *first generation* (Scheme 3.17).[19]
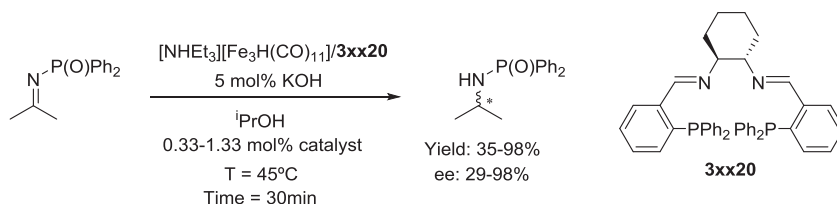
Scheme 3.17. Asymmetric transfer hydrogenation of N-(diphenylphosphinyl) imines catalyzed by [NHEt$_3$][Fe$_3$H(CO)$_{11}$]/**3xx20**.

Good to excellent yields (67-98%) and excellent enantioselectivities (89-95%) were obtained for the asymmetric transfer hydrogenation of aromatic and heteroaromatic N-(diphenylphosphinyl) imines. In the case of aliphatic N-(diphenylphosphinyl) imines, lower yields (35-62%) and enantioselectivies (29-39%) were obtained.

In 2012, the group of Morris and co-workers reported the application of complex **3xx8b**, of the second generation, in the ATH of a variety of N-(diphenylphosphinyl) imines with moderate to high conversions (29-92%) and excellent enantioselectivities (95-99%).[10d]

Third generation amine-imine 5,5,5 systems

When the partially reduced imine-amine complex **3xx35** was treated with base, no induction period was observed in the ATH of ketones and a TOF of 55000h^{-1} was obtained, which is higher than that obtained with the second generation bis(imine)diphosphine iron(II) carbonyl precatalysts. In view of that results, the group of Morris developed a new set of iron(II) complexes containing an imine and amine function (P-N-NH-P) with a 5,5,5 system, the so called *third generation* (Scheme 3.18).[49]

The iron(II) complexes **3xx41-43** were tested in the ATH of ketones and N-(diphenylphosphinyl) imines with moderate to high enantioselectivities (24-

98%). Importantly, TOFs as high as 200s^{-1} were obtained with these P-N-NH-P iron(II) systems. The TOFs obtained with this *third generation* are greater than that of their rival ruthenium-based and osmium-based (R,S)-Josiphos systems, as well as the ruthenium-based P-NH-NH-P complexes which obtained a TOF of 89s^{-1} and 92s^{-1} respectively.[50,51]

R= H, yield: 82%, ee: 78%, TOF: 119s^{-1} (catalyst **3xx41**)
R= H, yield: 83%, ee: 70%, TOF: 152s^{-1} (catalyst **3xx42**)
R= 2,5-CF$_3$, yield: 100%, ee: 98%, TOF: 200s^{-1} (catalyst **3xx43**)

3xx41; R = Ph
3xx42; R = *p*-MeC$_6$H$_4$
3xx43; R = 3,5-Me$_2$C$_6$H$_3$

Yield: 100%
ee: >99%
TOF: 10s^{-1}
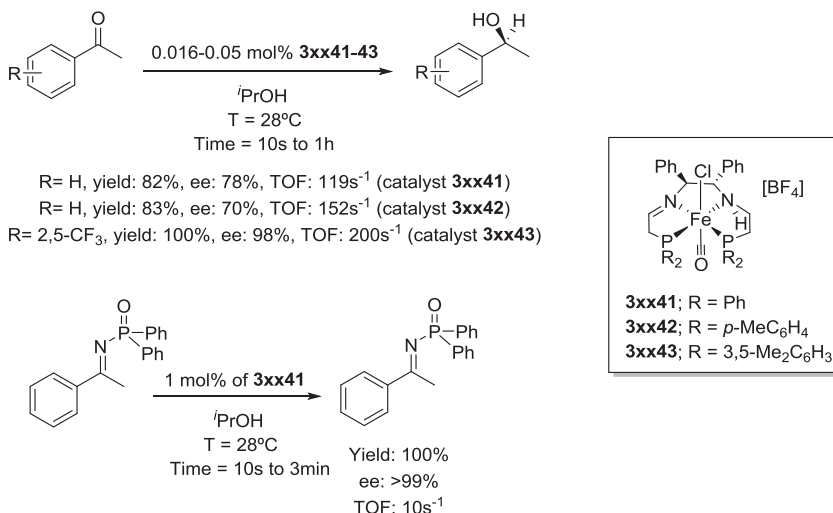
Scheme 3.18. Asymmetric transfer hydrogenation of ketones and N-(diphenylphosphinyl) imines catalyzed by **3xx41-43**.

Macrocyclic PNNP iron (II) complexes

Recently, the group of Mezzetti and co-workers have developed a set of macrocyclic PNNP iron(II) complexes.[12] Such macrocyclic complexes were shown to be highly active for the asymmetric transfer hydrogenation of a wide range of ketones as well as for N-(diphenylphosphinyl) imines. Interestingly, both the diimine[52] and diamine[53] macrocyclic PNNP iron(II) complexes were active in this transformation. More than 20 ketone substrates were transformed into the corresponding chiral alcohols in 62-

99.5% conversion and 86-99% enantioselectivity using **3xx44-45** as catalysts (Scheme 3.19).[53]
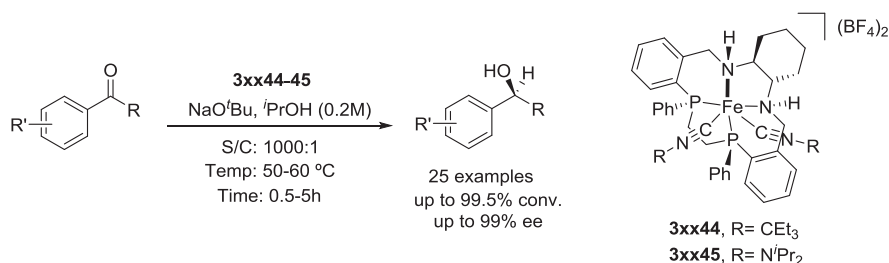
Scheme 3.19. Asymmetric transfer hydrogenation of ketones catalyzed by macrocyclic PNNP iron(II) complexes **3xx44**-**45**.

3.2. OBJECTIVE OF THIS CHAPTER

As previously outlined, iron chemistry has experienced an important breakthrough over the past decade. Nevertheless, systems containing multidentate ligands are far more abundant than the well-defined, preferentially diamagnetic iron (II) (pre)catalysts for enantioselective transformations. In this regard, tetradentate ligands are the most outstanding ones.

Chiral tetradentate ligands offer a great advantage in homogeneous catalysis due to its conformational and configurational rigidity arising from its chelation. These ligands are expected to hinder the number of possible diastereoisomers as well as to control the stereochemistry at the metal atom and compiling transfer chiral information.

In this context, we decided to prepare a novel family of chiral PNNP ligands containing a pyrrolidine backbone. The introduction of a pyrrolidine moiety in PNNP ligands could potentially allow the anchoring of the ligand through the functionalization of the NH group. Moreover, the corresponding Fe (II)

complexes were prepared and fully characterized. Additionally, the catalytic performance of several iron precursors with the synthesized PNNP ligands in the the asymmetric transfer hydrogenation of ketones was studied (Scheme 3.20). Experiments were also conducted in order to ascertain the nature of the catalytic system.
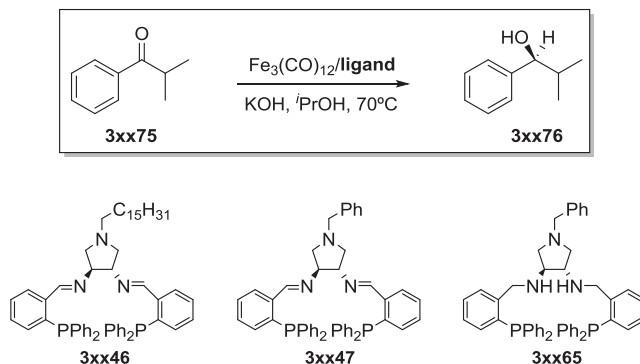
Scheme 3.20. Chiral PNNP ligands and their application in the asymmetric transfer hydrogenation of ketones.

3.3. RESULTS AND DISCUSSION

The analysis of the synthetic pathways of the target chiral PNNP ligands allowed to conclude that the straightforward synthesis of those ligands (**3xx46** and **3xx47**) can be achieved in a single step by condensation of the required diamine (**3xx48** and **3xx49**) and the commercial available 2-diphenylphosphino benzaldehyde **3xx50** (Scheme 3.21).
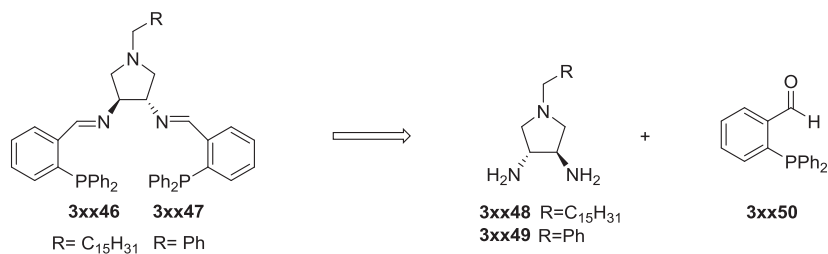
Scheme 3.21. Retrosynthesis for the PNNP ligands **3xx46** and **3xx47**.

The key intermediates for the synthesis of the target chiral ligands **3xx46** and **3xx47** were the chiral diamines **3xx48** and **3xx49**, which can be prepared in four steps from the commercially available L-(+)-Tartaric acid.

3.3.1. SYNTHESIS OF CHIRAL DIAMINE DERIVATIVE

It should be pointed out that the choice of the long chain at the pyrrolidine moiety was selected in order to mimic a possible anchoring of the ligand through the further functionalization of the NH- moiety at that position. The first step in the synthesis of the chiral PNNP ligands involves the reaction between L-(+)-Tartaric acid and the appropiate amine. The reaction proceeds smoothly and the corresponding diols **3xx52** and **3xx53** were obtained in 89% and 90% yield respectively (Scheme 3.22).
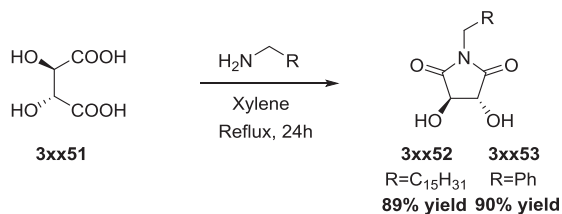
Scheme 3.22. Synthesis of diols **3xx52** and **3xx53**.

Then, reduction of the carbonyl units was performed by reaction with lithium aluminium hydride, to afford the desired diols **3xx54** and **3xx55** in 81% and 52% yield respectively (Scheme 3.23).
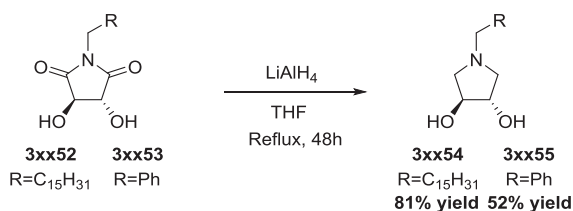
Scheme 3.23. Synthesis of diols **3xx54** and **3xx55**.

Next, diazides **3xx56** and **3xx57** were prepared via Mitsunobu reaction which allows the conversion of primary and secondary alcohols into the corresponding azides by reaction with hydrazoic acid.[54] In Scheme 3.24 the reported mechanism for the Mitsunobu reaction is described.
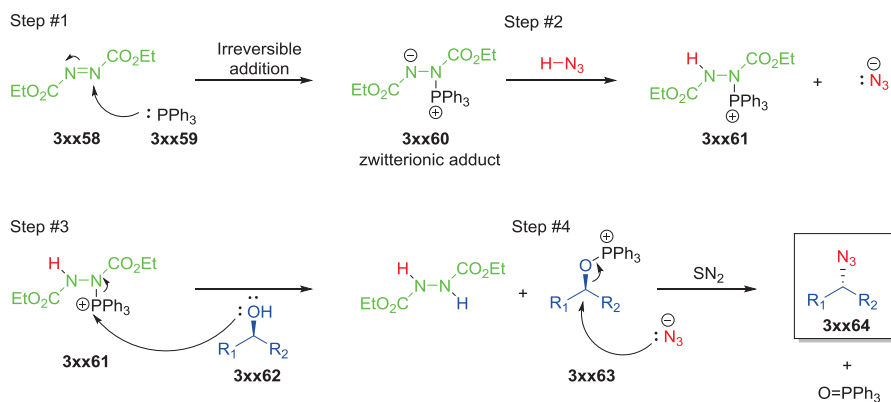
Scheme 3.24. Reported mechanism of the Mitsunobu reaction.

The first step involved the reaction between diethyl azodicarboxylate (DEAD) **3xx58** and triphenylphosphine **3xx59** to form the zwitterionic adduct **3xx60**. In a second step, the reaction with azidoic acid takes place to form the phosphonium intermediate **3xx61** and the nucleophilic azide.

Subsequently, reaction with the desired alcohol forms the phosphonium intermediate **3xx63** that binds to the alcoholic oxygen, thus activating it as a leaving group. Finally, nucleophilic substitution by the azide completes the procedure to form the desired product **3xx64** along with triphenylphosphine oxide as by-product.

The generation of hydrazoic acid was performed by reaction of sodium azide and sulfuric acid. Due to the volatility and flammability of hydrazoic acid, this compound was formed *in situ* and promptly used after its generation.[55]

The Mitsunobu reaction was carried out following a modified procedure reported by Skarzewski and Gupta using 5.2eq of triphenylphosphine and hydrazoic acid and 6eq of diisopropyl azodicarboxylate (DIAD) with toluene as solvent.[56] Under these conditions, diazides **3xx56** and **3xx57** were isolated in 65% and 53% yield respectively after purification by column chromatography (eluent: hexane:ether 100:2.5) (Scheme 3.25).
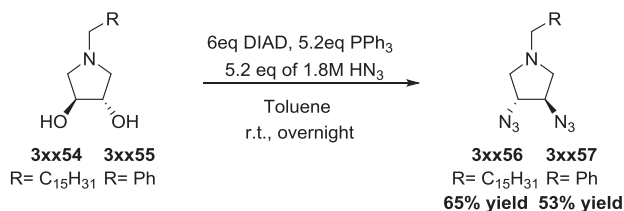
Scheme 3.25. Synthesis of diazides **3xx56** and **3xx57**.

It should be pointed out that the main drawback of this reaction is the generation of the azidoic acid which is highly flammable and toxic. As a consequence, the reaction cannot be scaled up in the laboratory due to the associated hazards.

In the last step, reduction of diazides **3xx56** and **3xx57** was accomplished using Pd/C and ethanol as solvent which led to the formation of diamines **3xx48** and **3xx49** in quantitative yield (Scheme 3.26).
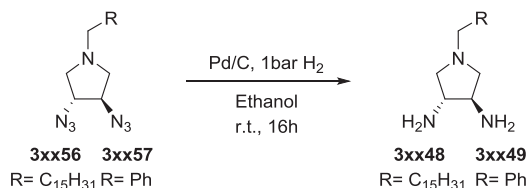
Scheme 3.26. Synthesis of diazides **3xx48** and **3xx49**.

3.3.2. SYNTHESIS OF CHIRAL PNNP LIGANDS

The chiral PNNP ligands **3xx46** and **3xx47** were prepared by condensation of the corresponding diamines **3xx48** and **3xx49** and the commercially available 2-diphenylphosphino benzaldehyde **3xx50** in 42% and 84% yield respectively (Scheme 3.27).
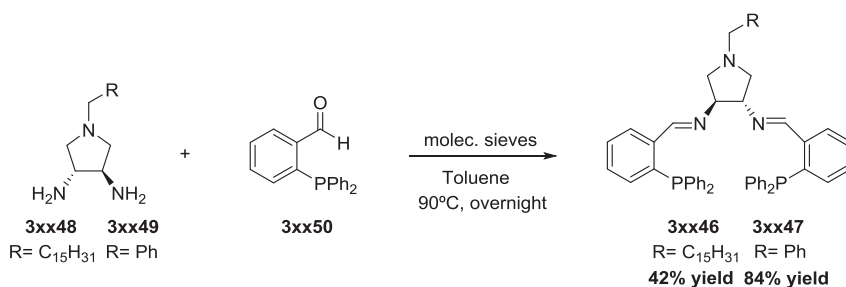
Scheme 3.27. Synthesis of chiral PNNP ligands **3xx46** and **3xx47**.

The formation of both chiral PNNP ligands **3xx46** and **3xx47** were confirmed NMR, ESI-HRMS and EA. Their relevant ^{1}H and ^{31}P{^{1}H} NMR data is summarized in Table 3.5.

Table 3.5. Characterization of **3xx46** and **3xx47** by ^{1}H and ^{31}P{^{1}H} NMR.
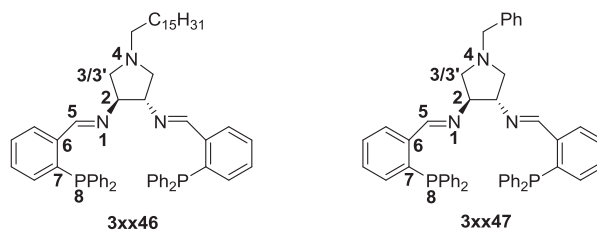
Compound	3xx46			3xx47		
Position	$\delta^{[a]}$	$M^{[b]}$	J (Hz)[c]	$\delta^{[a]}$	$M^{[b]}$	J (Hz)[c]
2	3.47	quint	4	3.49	quint	4
3	2.68	dd	4 / 8	2.71	dd	4 / 8
3'	2.43	dd	4 / 8	2.46	dd	4 / 8
5	8.46	d	4	8.45	d	4
^{31}P-NMR	-12.43	s	-	-12.14	s	-

[a] Chemical shift, in ppm. [b] Multiplicity of the signal. [c] Coupling constant, in Hz. ^{1}H and ^{31}P{^{1}H} NMR were recorded in CD_2Cl_2. For additional characterization of **3xx46** and **3xx47** see Experimental Section.

In the ^{1}H NMR spectrum, the most characteristic signal was the proton located at 5, which appeared as a doublet at 8.46ppm for ligand **3xx46** which indicate the formation of the imine and in consequence the production of the ligand. In the case of ligand **3xx47** the signal also appeared as a doublet at 8.45ppm. In general, no substantial differences in chemical shift are observed between ligand **3xx46** and **3xx47** in the NMR spectrum.

The synthesis of the chiral PNNP ligand **3xx65** was carried out for comparative purposes by reduction of the diamine moiety of ligand **3xx47** with sodium borohydride under refluxing conditions using methanol as solvent in 95% yield (Scheme 3.28).[31]
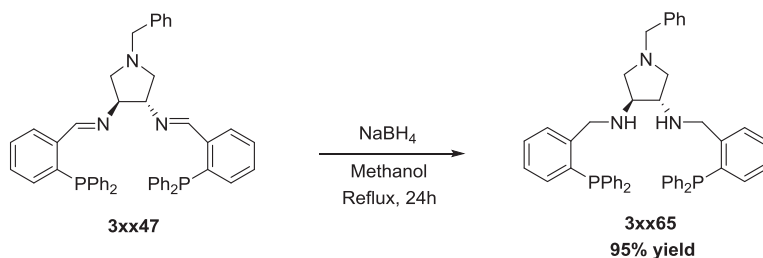
Scheme 3.28. Synthesis of chiral PNNP ligand **3xx65**.

The formation of the chiral PNNP ligand **3xx65** was confirmed by NMR, ESI-HRMS and EA. Their relevant ^{1}H and ^{31}P{^{1}H} NMR data is summarized in Table 3.6 and compared with its diimine counterpart (**3xx47**).

In the ^{1}H NMR spectrum, the most characteristic signals were the diastereotopic protons located at 3/3', which appeared as a doublet of doublets at 2.71ppm and 2.46ppm for ligand **3xx47**. In the case of ligand **3xx65** both sets of protons appeared as doublet of doublets at 2.55ppm and 2.11ppm. It should be pointed out that the benzylic protons located at 5/5' appeared as two doublets at 3.58ppm and 3.55ppm for ligand **3xx47** whereas for ligand **3xx65** a singlet at 3.43ppm was observed. In the ^{31}P NMR spectrum, the phosphorus of the ligand **3xx47** appeared at -12.14ppm, indicative of a less basic phosphine moiety when compared to **3xx65** (δ of -12.14ppm).

Table 3.6. Characterization of **3xx47** and **3xx65** by ^1H and $^{31}P\{^1H\}$ NMR.
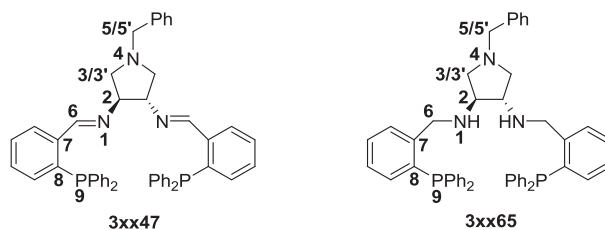
Compound	3xx47			3xx65		
Position	$\delta^{[a]}$	$M^{[b]}$	J (Hz)[c]	δ^a	M^b	J (Hz)[c]
2	3.49	quint	4	2.80	quint	4
3	2.71	dd	4	2.55	dd	4
			8			8
3'	2.46	dd	4	2.11	dd	4
			8			8
5	3.58	d	12	3.43	s	-
5'	3.55	d	12			
6	8.45	d	4	3.84	ddd	4
						12
						32
^{31}P-NMR	-12.14	s	-	-16.21	s	-

[a] Chemical shift, in ppm. [b] Multiplicity of the signal. [c] Coupling constant, in Hz. ^1H and $^{31}P\{^1H\}$ were recorded in CD_2Cl_2. For additional characterization of **3xx47** and **3xx65** see Experimental Section.

3.3.3. SYNTHESIS OF FE-PNNP COMPLEXES

Once the formation of ligands **3xx46** and **3xx47** was accomplished, the synthesis of novel PNNP iron(II) complexes was envisioned from direct reaction between ligands **3xx46** and **3xx47** with $Fe(BF_4)_2 \cdot 6H_2O$, as iron metallic precursor, in acetonitrile at room temperature.

The targeted chiral PNNP iron(II) complexes **3xx66** and **3xx67** were obtained as orange solids, in 79% and 81% yield respectively (Scheme 3.29).
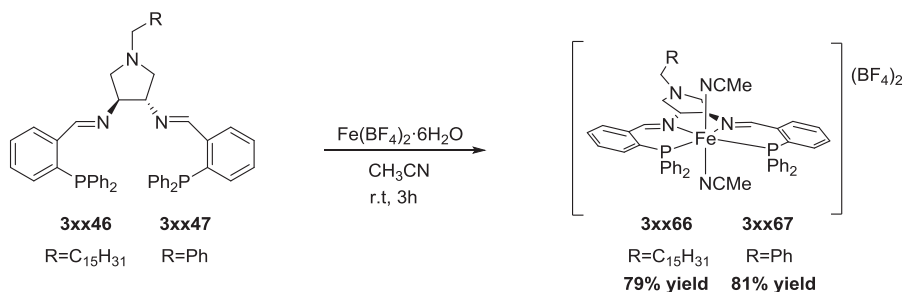
Scheme 3.29. Synthesis of the chiral PNNP iron(II) complexes **3xx66** and **3xx67**.

The formation of both PNNP iron(II) complexes **3xx66** and **3xx67** was confirmed by NMR, ESI-HRMS and EA. The $^{31}P\{^{1}H\}$ NMR spectra of the PNNP iron(II) complex **3xx66** showed a singlet at 52.66ppm, corresponding to a two equivalent phosphorus atoms. On the other hand, the $^{31}P\{^{1}H\}$ NMR spectra of the PNNP iron(II) complex **3xx67** contained two mutually coupled doublet signals at *ca.* δ 51.65 and 52.32ppm ($^{2}J_{P-P'}$ = 42 Hz), indicating the presence of two slightly inequivalent phosphine moieties in the complex. These chemical shifts were similar to those observed by Morris and co-workers for related PNNP iron(II) complexes of the type [Fe(MeCN)$_2$(PNNP)] (BF$_4$)$_2$ (δ: 51.8ppm; when cyclohexyl is used as backbone), although in that case, a singlet signal was reported.[10c]

In order to obtain more information about the symmetry of the complex, a variable temperature study was performed (Figure 3.15).
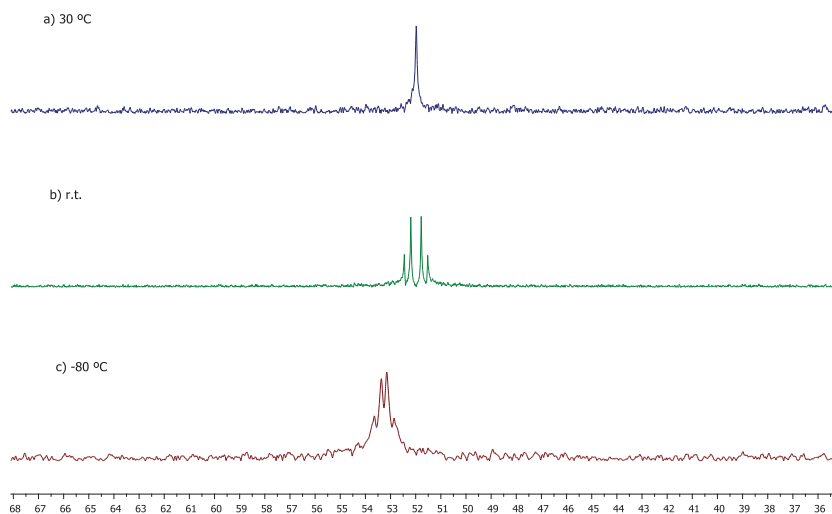
Figure 3.15. ^{31}P{^{1}H} NMR spectrum of **3xx67** at distinct temperatures a) at 30ºC. b) at room temperature. c) at -80ºC.

As previously mentioned, at room temperature two doublets were observed at 52.32ppm and 51.65ppm ($J_{P\text{-}P}$ = 42 Hz) in the ^{31}P{^{1}H} NMR spectrum. Interestingly, upon increasing the temperature to 30ºC only one singlet at 51.98ppm was observed, confirming the C_2-symmetric structure of complex **3xx67**. This feature might indicate that the structure of the chiral PNNP-iron complex at room temperature, as well as at lower temperatures (at -80ºC, see Figure 3.15), is a distorted octahedron and hence the two doublets observed correspond to two slightly different coordinated phosphine moieties.

In order to gain further information about the structure of the chiral PNNP-iron complex, we decided to synthesize complex **3xx68** which contained a PF_6^- instead of a BF_4^- as counter ion (Scheme 3.30). Complex **3xx68** was obtained as an orange solid in 90% yield. The ^{31}P{^{1}H} NMR spectrum showed two doublets at 51.98 and 51.13 ($J_{P\text{-}P}$= 43.7Hz) indicating a distorted octahedron structure with two slightly different coordinating

phosphine moieties as seen previously for complex **3xx67**. As well, the presence of the PF$_6$ anion was confirmed by ^{31}P{^{1}H} NMR (septuplet at -144.3ppm with a $J_{\text{P-F}}$= 712.8Hz) and ^{19}F NMR spectrum (doublet at -71.5ppm with a $J_{\text{F-P}}$= 712.8Hz).
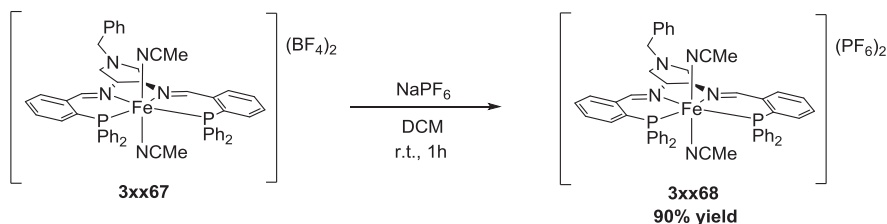
Scheme 3.30. Synthesis of the chiral PNNP iron(II) complex **3xx68**.

Crystals suitable for X-ray diffraction were obtained by vapour diffusion of pentane into a CH$_2$Cl$_2$ solution containing the complex **3xx68**. To our surprise, the structure obtained corresponded to the Fe(III) complex [Fe(NCMe)$_2$(**3xx47**)](PF$_6$)$_3$ where the ligand **3xx47** is coordinated to the iron centre in a tetradentate manner. This fact is attributed to an oxidation process during the course of the crystallization. The molecular structure of this complex is displayed in Figure 3.16.
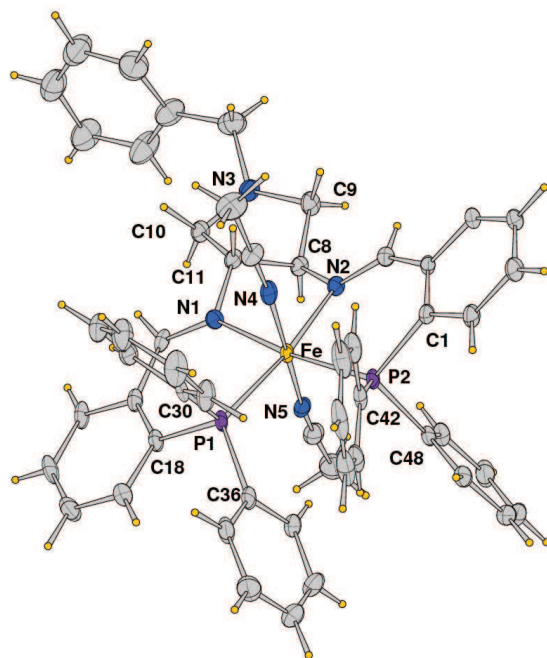
Figure 3.16. ORTEP drawing of the complex [Fe(CH$_3$CN)$_2$(**3xx47**)] (with ellipsoid at 50% probability). Solvent molecules and H atoms are omitted for clarity and only partial labelling scheme is illustrated.

As previously mentioned in the introduction, the bis-acetonitrile iron complexes are not active pre-catalysts in the asymmetric transfer hydrogenation (ATH) reaction.[5a,10b] For this reason, the synthesis of the chiral PNNP-iron carbonyl complex **3xx69** was attempted (Scheme 3.31).
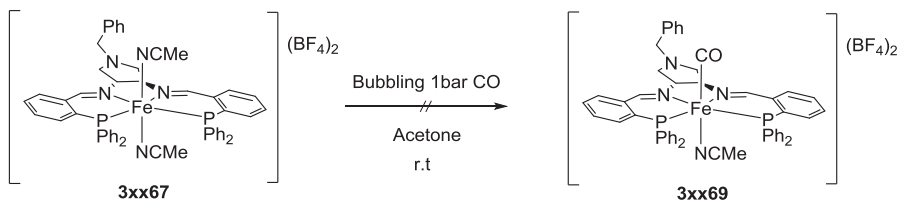
Scheme 3.31. Attempted synthesis of the chiral PNNP iron(II) complex **3xx69**.

Direct reaction of the chiral PNNP-iron complex **3xx67** in acetone under 1bar of carbon monoxide (CO) did not afford the formation of **3xx69**. The $^{31}P\{^{1}H\}$ NMR spectrum revealed the formation of the chiral uncoordinated PNNP ligand **3xx47** but no iron complexes could be detected.

In order to overcome the issues in the reaction, we carried out two experiments in parallel: a) reaction of the chiral PNNP-iron complex **3xx70** reported previously by Morris and co-workers and b) reaction of the chiral PNNP iron complex **3xx67**, using degassed acetone as solvent and under 1bar of CO for 16h (Scheme 3.32).[22] In the case of the chiral PNNP-iron complex **3xx70**, the resulting iron complex **3xx71** was obtained in quantitative yield. Nevertheless, in the case of the chiral PNNP-iron complex **3xx67**, formation of the chiral uncoordinated PNNP ligand **3xx47** was again detected although a colour change from bright orange to orange-yellow was observed as described for **3xx71**.
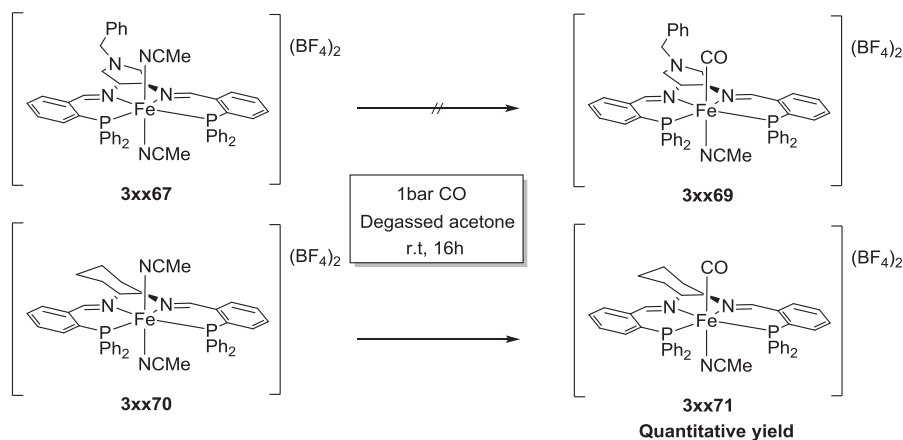
Scheme 3.32. Attempted synthesis of the chiral PNNP iron(II) complex **3xx69**.

Various strategies were employed in order to obtain complex **3xx69**, such as bubbling the CO directly to the solution, using freshly distilled and degassed acetone as solvent, using a fischer porter instead of a schlenk as a

container or increasing the reaction time, however all attempts proved unsuccessful.

In order to gain further structural information, the synthesis of complex **3xx72** was attempted. Direct reaction between ligand **3xx47** and $FeCl_2$ as iron metallic precursor provided a new chiral PNNP-iron complex. In the $^{31}P\{^1H\}$-NMR spectrum a broad signal appeared at -0.65ppm which was in agreement with two equivalent phosphorus atoms. The ^1H NMR spectrum showed paramagnetic shifted resonances in the range of -30ppm to 110ppm. Magnetic measurements (Gouy's method) gave a magnetic effective moment of μ_{eff}= 5.0 which is consistent to a S=2 spin ground state.

As already comment, the $^{31}P\{^1H\}$NMR spectrum showed a broad signal at -0.65ppm which is in the range on the uncoordinated phosphorus atoms. For this reason a low temperature NMR study was performed (Figure 3.17).

As previously mentioned, at room temperature a signal at -0.65ppm was observed. However, upon lowering the temperature to -20 ºC, a new signal at 26.7 ppm was also apparent (Figure 1b). When the temperature was further lowered from -20 ºC to -80 ºC (Figure 1c-e), the signal originally detected at -0.65ppm became broader and was displaced to higher chemical shifts whereas the intensity of the signal at 26.7 ppm increased and was displaced to lower chemical shifts. These observations indicated that at room temperature, complex **3xx72** is involved in a fluxional process resulting in the detection of an average signal at -0.65ppm.
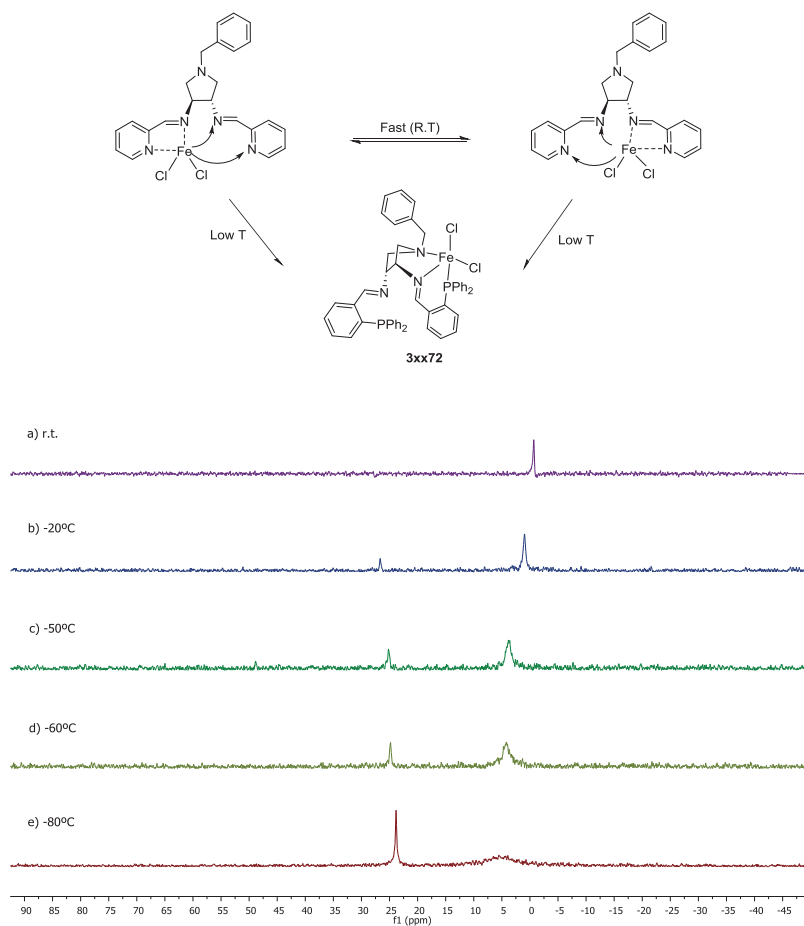
Figure 3.17. $^{31}P\{^{1}H\}$ NMR spectrum of **3xx72** at distinct temperatures a) at room temperature. b) at -20ºC. c) at -50ºC. d) at -60ºC. e) at -80ºC.

Crystals suitable for X-Ray diffraction were grown by vapour diffusion from CH_2Cl_2 in pentane which confirmed the formation of the chiral PNNP-iron complex **3xx72** (Scheme 3.33).
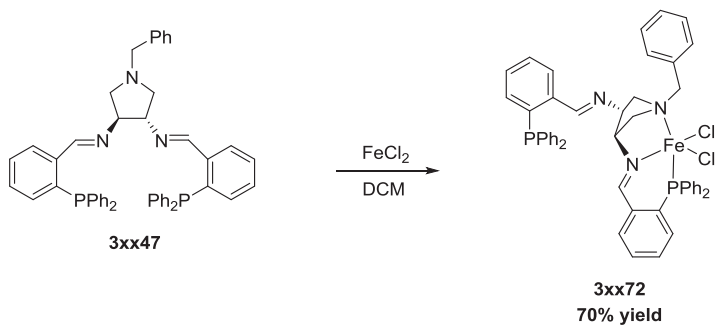
Scheme 3.33. Synthesis of the chiral PNNP iron(II) complex **3xx72**.

Figure 3.18 shows a view (50% probability ellipsoid) of the chiral PNNP-iron complex **3xx72**.
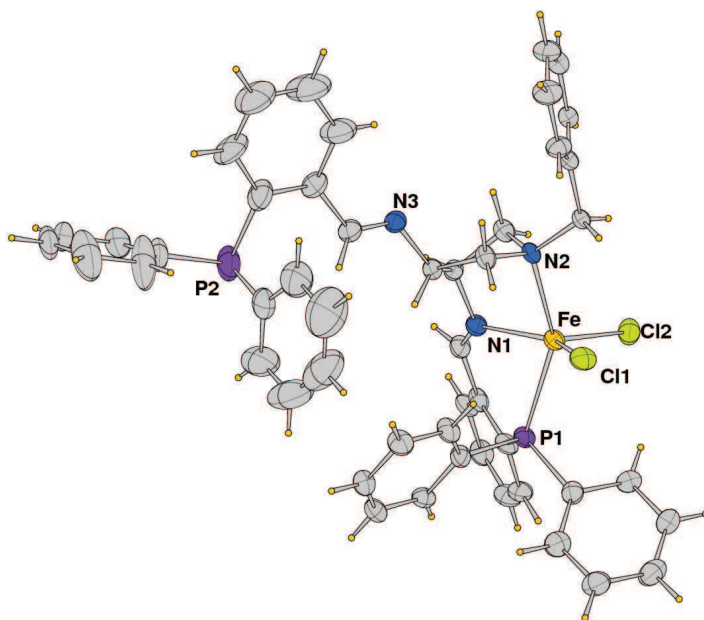
Figure 3.18. ORTEP drawing of the complex [FeCl$_2$(**3xx47**)] (**3xx72**) (with ellipsoids at 50% probability). Solvent molecules and H atoms are omitted for clarity and only partial labeling scheme is illustrated.

The molecular structure of the chiral PNNP-iron complex **3xx72** in the solid state is best described as a strongly distorted trigonal bipyramidal coordination of the iron atom with N2 and P1 occupying the apical positions. Other structurally characterized complexes of the type [(PNN)FeX$_2$] exhibit similar structures (Table 3.7).[57,58] The N2-Fe-P1 angle is 148.56º, strongly deviated of an ideal linear geometry.

It has to be pointed out that the crystal structure of the chiral PNNP-iron complex **3xx72** revealed the unexpected coordination of the pyrrolidine moiety giving rise to [(PNN)FeCl$_2$] complex with a distorted bypiramidal coordination instead of the expected [(PNNP)FeCl$_2$] complex with a octahedral coordination. This feature has to be taken into account as the pyrrolidine moiety may not play a trivial role.

Table 3.7. Selected bond lengths (Å) and angles (deg) of complex **3xx72** and a [(PNN)FeCl₂] complex reported by Milstein and co-workers.
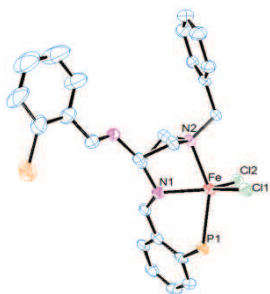
Our work, [(PNN)FeCl₂] **3xx72**   Milstein 2013, [(PNN)FeCl₂]
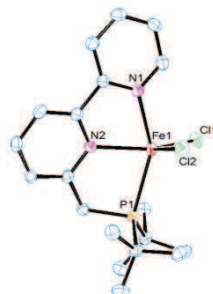
Bond lengths (Å)			
Fe-N(1)	2.212(3)	Fe-N(2)	2.2019(19)
Fe-N(2)	2.212(4)	Fe-N(1)	2.177(2)
Fe-P(1)	2.473(11)	Fe-P(1)	2.5574(7)
Fe-Cl(1)	2.372(12)	Fe-Cl(2)	2.3534(6)
Fe-Cl(2)	2.257(13)	Fe-Cl(1)	2.3082(7)
Bond angles (deg)			
N(1)-Fe-N(2)	75.6(12)	N(1)-Fe-N(2)	73.52(7)
N(1)-Fe-Cl(2)	110.7(11)	N(2)-Fe-Cl(1)	108.81(5)
N(2)-Fe-Cl(2)	104.2(9)	N(1)-Fe-Cl(1)	95.48(6)
N(1)-Fe-Cl(1)	138.9(11)	N(2)-Fe-Cl(2)	142.11(5)
N(2)-Fe-Cl(1)	92.8(9)	N(1)-Fe-Cl(2)	89.44(5)
Cl(2)-Fe-Cl(1)	110.2(5)	Cl(1)-Fe-Cl(2)	107.18(2)
N(1)-Fe-P(1)	79.9(10)	N(2)-Fe-P(1)	78.18(5)
N(2)-Fe-P(1)	148.6(8)	N(1)-Fe-P(1)	151.37(5)
Cl(2)-Fe-P(1)	102.8(5)	Cl(1)-Fe-P(1)	104.31(2)
Cl(1)-Fe-P(1)	92.8(4)	Cl(2)-Fe-P(1)	103.87(2)

In order to make a structural comparison between the chiral PNNP-iron complex **3xx72** and the corresponding chiral PNNP-iron complex **3xx73** containing a cyclohexyl as backbone, the synthesis of **3xx73** was attempted under the same conditions employed for complex **3xx72** (see Experimental Section). The ^{1}H NMR spectrum showed paramagnetic shifted resonances in the range of -10ppm to 90ppm. In the ^{31}P{^{1}H}-NMR spectrum no resonances were observed in the range of -4000ppm to +4000ppm. This feature has also been observed before, for instance in complexes of the type [(PNN)FeX$_2$] were X=Br or Cl reported by Milstein and co-workers.[58] Magnetic measurements (Gouy's method) gave a magnetic effective moment of μ_{eff}= 5.4 which is consistent to a S=2 spin ground state. Crystals suitable for X-Ray diffraction were grown by vapour diffusion from CH_2Cl_2 in pentane which revealed the formation of the chiral PNNP-iron complex **3xx73** (Scheme 3.34).
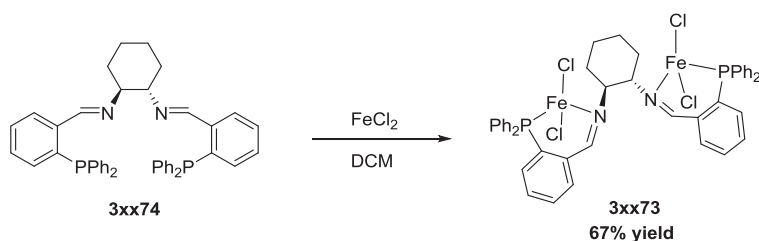
Scheme 3.34. Synthesis of the chiral PNNP iron(II) complex **3xx73**.

Figure 3.19 shows a view (50% probability ellipsoid) of the chiral PNNP-iron complex **3xx73**.
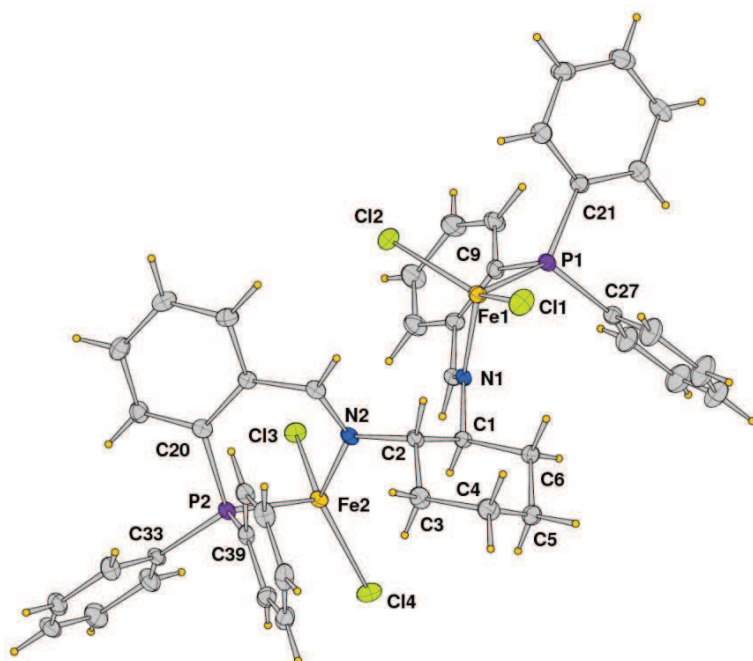
Figure 3.19. ORTEP drawing of the complex [Fe$_2$Cl$_4$(**3xx74**)] (**3xx73**) (with ellipsoids at 50% probability). Solvent molecules and H atoms are omitted for clarity and only partial labeling scheme is illustrated.

The molecular structure of the chiral PNNP-iron dimer **3xx73** is best described as distorted tetrahedral coordination of the iron atoms by one nitrogen and one phosphorus of the ligand with two chloride atoms. The bond lengths are in coherence with other structurally characterized complexes of the type [(PN)FeCl$_2$] which also presented a distorted tetrahedral structure.[59]

In Table 3.8 selected the bond lengths (Å) and angles (deg) of complex **3xx73** are listed.

Table 3.8. Selected bond lengths (Å) and angles (deg) for complex **3xx73**.

Bond lengths (Å)			
Fe(1)-N(1)	2.163(3)	Fe(2)-N(2)	2.106(3)
Fe(1)-Cl(2)	2.2204(9)	Fe(2)-Cl(3)	2.2389(8)
Fe(1)-Cl(1)	2.2225(9)	Fe(2)-Cl(4)	2.2462(9)
Fe(1)-P(1)	2.3970(9)	Fe(2)-P(2)	2.3848(9)
Bond angles (deg)			
N(1)-Fe(1)-Cl(2)	106.27(7)	N(2)-Fe(2)-Cl(3)	101.61(7)
N(1)-Fe(1)-Cl(1)	120.68(7)	N(2)-Fe(2)-Cl(4)	116.15(8)
Cl(2)-Fe(1)-Cl(1)	116.55(4)	Cl(3)-Fe(2)-Cl(4)	129.07(4)
N(1)-Fe(1)-P(1)	83.86(7)	N(2)-Fe(2)-P(2)	84.93(7)
Cl(2)-Fe(1)-P(1)	109.21(4)	Cl(3)-Fe(2)-P(2)	107.79(3)
Cl(1)-Fe(1)-P(1)	115.55(4)	Cl(4)-Fe(2)-P(2)	108.38(3)

3.3.4. DFT STUDIES

This section has been performed by Dr. Anna Clotet at the University Rovira i Virgili.

To further investigate the stability of related structures for complex **3xx72**, DFT calculations were carried out considering: a) a tdp structure (tbp-N1N2) with one imine and the pyrrolidine nitrogen coordinated to the iron center, b) a symmetric tdp structure (tbp-N1N3) where both imines are coordinated to the iron center, c) the octoahedral (oct-N1N3) and d) the tetrahedral (td-N1N3) geometries (Figure 3.20). Calculations were carried out using B3LYP functional, dichloromethane as solvent and for each geometry, various multiplicities were considered. To reduce computational cost, the phenyl substituents on phosphorus atoms were first replaced with hydrogen atoms (**3xx72**$_H$).
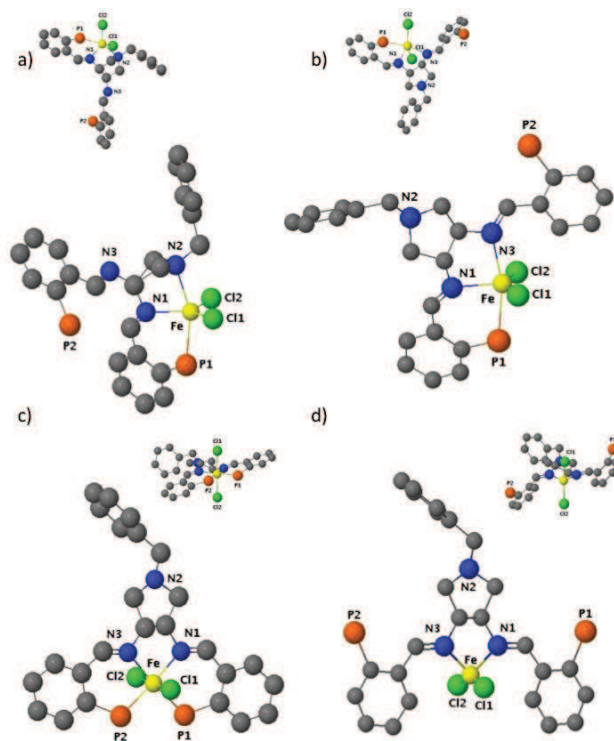
Figure 3.20. Atom labels for [FeCl$_2$(**3xx47**$_H$)] (**3xx72**$_H$) a) tbp-N1N2, b) tbp-N1N3, c) oct-N1N3 and d) td-N1N3 structures. Hydrogen atoms are omitted for clarity. Phenyl groups attached to P are not displayed.

In agreement with the experimental results, the most stable structure was the quintuplet **tbp-N1N2** complex. Quintuplet (2S+1=5) is also the lowest energy state for the other structures. The **tbp-N1N3**, **oct-N1N3** and **td-N1N3** structures are in a narrow energy range (5-7 kcal mol^{-1}) (Table 3.9). When the phenyl substituents at the phosphorus atoms were included in the computed structure for the singlet and quintuplet states (Table 3.9), the quintuplet state of **tbp-N1N2** structure remained the most stable isomer while the oct-like **oct-N1N3** structure was 4.7 kcal mol^{-1} above in energy and in this case, the singlet state was preferred. With these parameters, the energetic difference between the quintuplet state of **tbp-N1N3** structure and

that of the **tbp-N1N2** increases up to 13 kcal mol^{-1}. Interestingly, only a singlet structure very high in energy converged for the td-like structure, indicating that this type of structure could be discarded.

Table 3.9. Computed relative energies (kcal mol^{-1}) of complexes [FeCl$_2$(**3xx47**$_H$)] (**3xx72**$_H$) and [FeCl$_2$(**3xx47**)] (**3xx72**) with different multiplicities (2S+1).

Complex	2S+1	Tbp-N1N2	Oct-N1N3	Tbp-N1N3	Td-N1N3
3xx72$_H$	1	29.7	14.8	33.3	48.1
	3	14.0	19.3	22.8	38.4
	5	0.0	7.1	7.2	5.1
	7	42.5	56.0	53.2	57.0
3xx72	1	19.8	4.7	28.5	44.1
	5	0.0	7.2	13.0	-

DFT calculations were also performed, using B3LYP functional and acetone as solvent, for different structures and multiplicities of complexes [Fe(CH$_3$CN)$_2$(**3xx47**$_H$)]$^{2+}$ (**3xx67**$_H$) and [Fe(CH$_3$CN)(CO)(**3xx47**$_H$)]$^{2+}$ (**3xx69**$_H$) with the aim to clarify whether the problems encountered during the synthetic procedure (for complex **3xx69**; having an acetonitrile and a CO in its structure) were due to thermodynamic or kinetic issues.

For [Fe(CH$_3$CN)$_2$(**4xx47**$_H$)]$^{2+}$ (**3xx67**$_H$) we considered singlet and quintuplet multiplicities for oct- and tbp-N1N2 structures, but also two singlet oct-structures with both acetonitrile ligands coordinated in cis. For [Fe(CH$_3$CN)(CO)(**4xx47**$_H$)]$^{2+}$ (**3xx69**$_H$) we determined the structure of singlet-oct and quintuplet-tbpN1N2 structures. The most stable structure is the low spin (singlet) oct- structure for both complexes ([Fe(CH$_3$CN)(L)(**4xx47**$_H$)]$^{2+}$ L=CH$_3$CN or CO), in agreement with experimental results for bis(acetonitrile) complex **3xx67**. The quintuplet-tbpN1N2 structure is only at 5.8 kcal mol^{-1} for [Fe(CH$_3$CN)$_2$(**4xx47**$_H$)]$^{2+}$ (**3xx67**$_H$) but is higher in energy (20.0 kcal mol^{-1}) in the case of complex [Fe(CH$_3$CN)$_2$(CO)(

4xx47$_H$)]$^{2+}$ (**3xx69**$_H$). Other computed structures of [Fe(CH$_3$CN)$_2$(**4xx47**$_H$)]$^{2+}$ (**3xx67**$_H$) are in the range 9-19 kcal mol^{-1}. In (Table 3.10) are shown the theoretical geometrical parameters for these complexes.

Table 3.10. Selected bond distances (Å) and angles (deg) for experimental (Exp) structure of [Fe(CH$_3$CN)$_2$(**4xx47**)](PF$_6$)$_2$ (**3xx68**) and theoretical (B3LYP) oct structures of complexes [Fe(CH$_3$CN)L(**4xx47**$_H$)]$^{2+}$ (L=CH$_3$CN, CO) (**3xx67**$_H$ and (**3xx69**$_H$). See Figure 3.21 for atomic labels; X=N5 or C1.

	L=MeCN		L=CO
	Exp	B3LYP	B3LYP
d(Å)	**3xx68**	**3xx67**$_H$	**3xx69**$_H$
Fe-N(1)	2.039	2.047	2.047
Fe-N(2)	4.991	4.981	4.924
Fe-N(3)	2.043	2.050	2.047
Fe-N(4)	1.923	1.949	1.981
Fe-X	1.906	1.950	1.810
Fe-P(1)	2.280	2.272	2.277
Fe-P(2)	2.257	2.273	2.273
θ(°)			
N(1)-Fe-N(3)	84.0	85.4	85.4
P(1)-Fe-P(2)	97.5	94.6	94.9
N(1)-Fe-P(1)	89.7	89.6	88.3
N(3)-Fe-P(2)	88.6	90.3	91.3
N(4)-Fe-X	173.3	179.6	178.6
N(1)-Fe-N(4)	89.1	89.7	89.3
N(1)-Fe-X	86.6	90.0	92.0
P(2)-Fe-N(4)	92.5	89.6	87.5
P(2)-Fe-X	91.1	90.7	91.1
P(1)-Fe-N(4)	96.7	90.7	89.2
P(1)-Fe-X	88.4	89.5	91.2
N(3)-Fe-N(4)	86.5	90.2	88.6
N(3)-Fe-X	87.9	89.5	91.2

Experimental and theoretical results are in agreement for the [Fe(CH₃CN)L(**3xx47**_H)]²⁺ (**3xx67**_H) (L=CH₃CN), taking into account the absence of couteranions and phenyl groups on theoretical calculations. The calculated octahedral structure is slightly less distorted than the experimental one. No important structural differences appears on [Fe(CH₃CN)L(**3xx47**_H)]²⁺ depending on the identity of L (acetronitrile or CO).
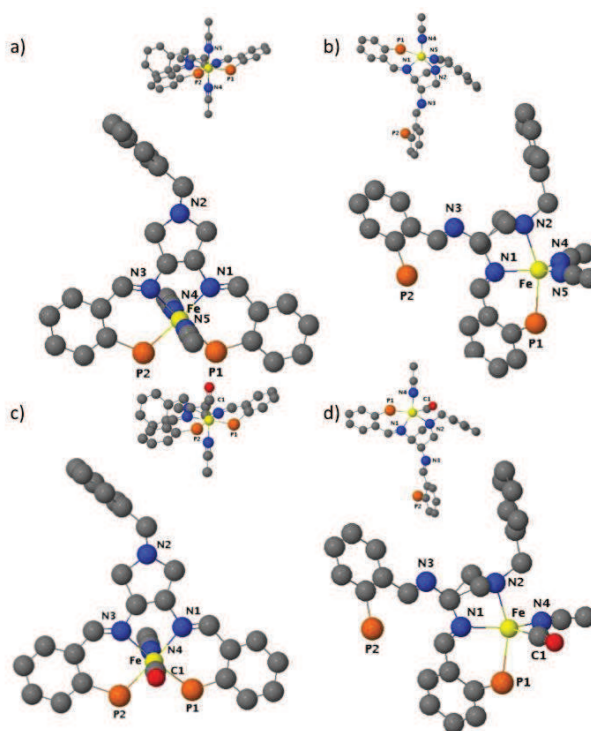
Figure 3.21. Atom labels for a) oct-[Fe(CH₃CN)₂(**3xx47**_H)], b) tbp-N1N2-[Fe(CH₃CN)₂(**3xx47**_H)], c) oct-[Fe(CH₃CN)(CO)(**3xx47**_H)] and d) tbp-[Fe(CH₃CN)(CO)(**3xx47**_H)]. Hydrogen atoms are omitted for clarity. Aromatic bonds of phenyl groups are not displayed.

Finally, the computed energy for substitution reaction shown in Scheme 3.35 is of -3.2 kcal mol^{-1}. Consequently, from a thermodynamic point of view, [Fe(CH$_3$CN)(CO)(**3xx47$_H$**)]$^{2+}$ could be obtained. Therefore, kinetics arguments should explain the impossibility to obtain this complex from the bis(acetonitrile) complex **3xx67**. Unraveling kinetic aspects is out of the scope of the present work.
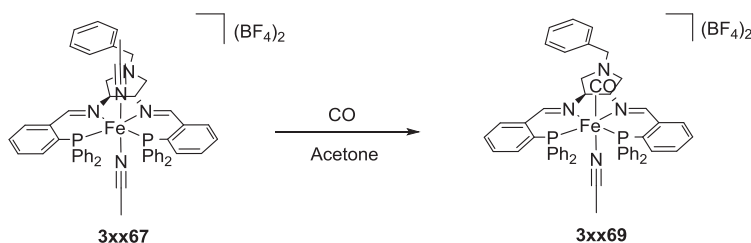
Scheme 3.35. Reaction pathway for the synthesis of the PNNP iron(II) complex **3xx69** from **3xx67**.

3.3.5. CATALYTIC ASYMMETRIC TRANSFER HYDROGENATION OF KETONES

We decided to test our novel PNNP ligands **3xx46**, **3xx47** and **3xx65** in the iron catalyzed asymmetric transfer hydrogenation of ketones. For these initial tests, *iso*-butyrophenone was chosen as a benchmark substrate together with a catalyst loading of 5mol% using KOH as base and Fe$_3$(CO)$_{12}$ as iron source. The ratio between ligand:Fe$_3$(CO)$_{12}$:base was 1:1:8. First results are summarized in Table 3.11.

The chiral PNNP ligand **3xx47** effectively catalyzed the asymmetric transfer hydrogenation of **3xx75** with 97% conversion and 96% enantiomeric excess (entry 2). In the case of the chiral PNNP ligand **3xx65** the reaction proceeded slowly although maintenance of the enantioselectivity was observed (entry 3). Nevertheless, very low conversion was observed when ligand **3xx46** was tested as well as the enantiomeric excess decreased

drastically. This feature can be attributed to the presence of the long alkyl chain at the pyrrolidine moiety which may interfere during the catalytic performance due to their inherent flexibility.

Table 3.11. Asymmetric transfer hydrogenation of *iso*-butyrophenone catalyzed by **3xx46**, **3xx47** and **3xx65**.[a]
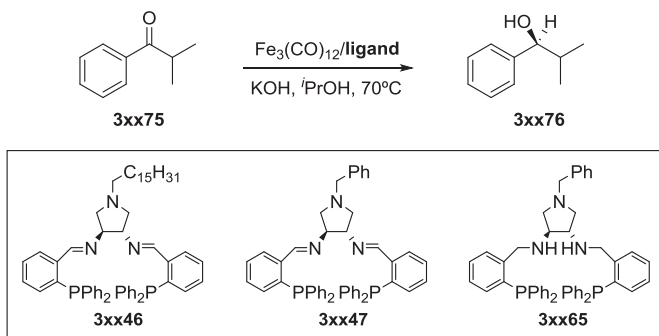
Entry	Ligand	Conv. (%)[b]	ee (%)[c]
1	**3xx46**	5	29
2	**3xx47**	97	96
3	**3xx65**	58	97

[a] General conditions: $Fe_3(CO)_{12}$/Ligand/KOH= 1:1:8; 0.0068mmol of $Fe_3(CO)_{12}$, 0.0068mmol of ligand, 0.054mmol of KOH, 3ml of *^{i}PrOH*, time = 16h, temperature = 70 ºC. [b] Conversion was calculated by ^{1}H NMR. [c] Enantiomeric excess was calculated by GC using a ChirasilDex CB column.

Having found ligand **3xx47** as efficient ligand, we next examined the effect of the catalyst loading in the reaction (Table 3.12). When the catalyst loading was decreased from 20mol% to 5mol% (entry 1-3), conversions and enantioselectivities were retained. However, diminishing the catalyst loading down to 1mol% (entry 5) led to a strong decrease in conversion, although the enantioselectivity remained high.

Table 3.12. Asymmetric transfer hydrogenation of *iso*-butyrophenone catalyzed by **3xx47** at various catalyst loadings.[a]
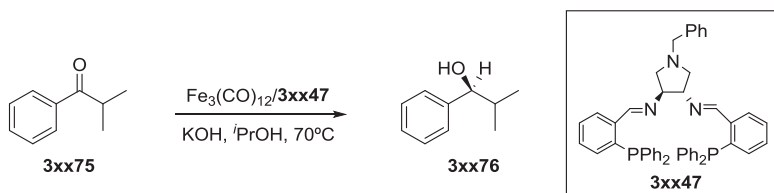
Entry	Cat. loading (mol%)	Conv. (%)[b]	ee (%)[c]
1	20	100	95
2	10	92	97
3	5	97	96
4	2.5	58	89
5	1	41	89

[a] General conditions: $Fe_3(CO)_{12}$/**3xx47**/KOH= 1:1:8; 0.0068mmol of $Fe_3(CO)_{12}$, 0.0068mmol of **3xx47**, 0.054mmol of KOH, 3ml of ^{i}PrOH, time = 16h, temperature = 70 °C. [b] Conversion was calculated by ^{1}H NMR. [c] Enantiomeric excess was calculated by GC using a ChirasilDex CB column.

The study of the temperature was also conducted at 5mol% of catalyst loading using KOH as base and $Fe_3(CO)_{12}$ as iron source. Nevertheless, decreasing the temperature from 70 °C to 50 °C a drastic decreased in conversion was observed from 97% to 6% whereas the enantiomeric excess was preserved.

We next examined a series of iron precursors with different oxidation states (0, +2) (Table 3.13). Using the monometallic $Fe(BF_4)_2 \cdot 6H_2O$ (entry 1) as precursor, no conversion was observed. However, the application of the iron carbonyl cluster $Fe_3(CO)_{12}$ achieved high conversion and excellent enantioselectivity for this transformation (entry 2). It is important to note that without the ligand (entry 3) or the iron source (entry 9), no reaction was observed. We also tested the iron hydride carbonyl cluster complex $[Et_3NH][HFe_3(CO)_{11}]$ which converted *iso*-butyrophenone in 98%

conversion and 97% enantiomeric excess (entry 8). This feature might suggest that a similar active catalyst is formed either using the iron carbonyl cluster $Fe_3(CO)_{12}$ or the iron hydride carbonyl cluster $[Et_3NH][HFe_3(CO)_{11}]$. In view of the results obtained with the iron carbonyl clusters, other iron (0) carbonyl precursors were tested (entries 4-6). Nevertheless, either using $Fe_2(CO)_9$ or $Fe(CO)_5$ as iron souce did not proved to be effective for this transformation. It is worth mentioning that Gao and co-workers also observed the same feature using the iron carbonyl cluster $Fe_2(CO)_9$ compared to the use of $Fe_3(CO)_{12}$ as iron source in the asymmetric transfer hydrogenation of ketones catalyzed by P-NH-NH-P ligands.[43] We also tried the use of $Fe(CO)_5$ in a ratio of 1:3 ligand/Fe in order construct a similar catalytic system that using the iron carbonyl cluster $Fe_3(CO)_{12}$, however no conversion was observed (entry 6). A combination of $Fe(CO)_5/ Fe_2(CO)_9$ was also tested and as well in this case the conversion was very low. As very similar results were obtain using either $Fe_3(CO)_{12}$ or $[Et_3NH][HFe_3(CO)_{11}]$ as iron source, we decided to continue the optimization using the iron carbonyl cluster $Fe_3(CO)_{12}$ due to its commercial availability.

It should be pointed out the importance of the carbonyl unit in the structure of the iron precursor as it can be related to the fact that the use of, for instance, the chiral PNNP-iron complex **3xx67** (which contained a bis-acetonitrile moiety) was inactive for this transformation. However, the complexes of the type [(PNNP)(CH₃CN)(CO)] were highly active not only in the asymmetric transfer hydrogenation of ketones but also of imines.[10b,10d]

Table 3.13. Asymmetric transfer hydrogenation of *iso*-butyrophenone catalyzed by **3xx47** using a series of iron precursors.[a]
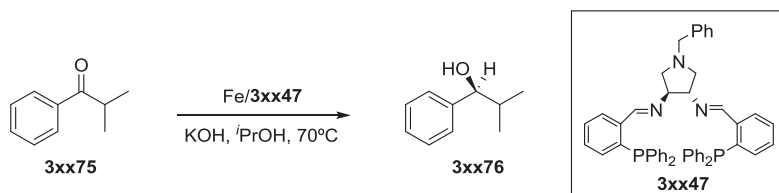
Entry	Iron precursor	Conv. (%)[b]	ee (%)[c]
1	$Fe(BF_4)_2 \cdot 6H_2O$	0	-
2	$Fe_3(CO)_{12}$	97	96
3	$Fe_3(CO)_{12}$[d]	0	-
4	$Fe_2(CO)_9$	<5	85
5	$Fe(CO)_5$[e]	8	50
6	$Fe(CO)_5$[f]	0	-
7	$Fe_2(CO)_9/Fe(CO)_5$	<5	10
8	$[Et_3NH][HFe_3(CO)_{11}]$	98	97
9	-	0	-

[a] General conditions: Fe/**3xx47**/KOH= 1:1:8; 0.0068mmol of Fe, 0.0068mmol of **3xx47**, 0.054mmol of KOH, 3ml of ^{i}PrOH, time = 16h, temperature = 70 ºC. [b] Conversion was calculated by ^{1}H NMR. [c] Enantiomeric excess was calculated by GC using a ChirasilDex CB column. [d] No ligand used. [e] Ligand/Fe 1:3. [f] Ligand/Fe 1:1.

The study of different bases was performed as well as the equivalents employed (Table 3.14). The best results were obtained when KOH was used as base, with 97% conversion and 96% of enantioselectivity (entry 2). Using NaOH instead of KOH lowered the conversion considerably whereas the enantioselectivity was maintained (entry 1). When the basicity of the base applied was increased, lower conversions were also observed although again the enantiomeric ratio remained high (entry 3). However, when NaO^{i}Pr was used, the reaction did not take place (entry 4).

Having found KOH as optimal base, we next examined the effect of the amount of base used. Decreasing the amount of base from a ligand/Fe ratio of 1:8 to 1:4 did a strong impact in the activity whereas the enantioselectivity remained high (entry 7). Consequently, at lower ligand/Fe ratios the conversion remained low (entries 8 and 9).

Table 3.14. Asymmetric transfer hydrogenation of *iso*-butyrophenone catalyzed by **3xx47** using a series of bases and different equivalents.[a]
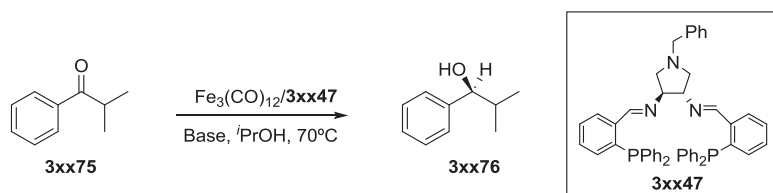
Entry	Base	pka	L/Base	Conv. (%)[b]	ee (%)[c]
1	NaOH	13.8	1:8	46	91
2	KOH	13.5	1:8	97	96
3	KO^{t}Bu	17	1:8	70	86
4	NaO^{i}Pr	16.5	1:8	0	-
5	-	-	-	0	-
6	KOH	13.5	1:10	98	97
7	KOH	13.5	1:4	38	89
8	KOH	13.5	1:2	32	86
9	KOH	13.5	1:1	25	83

[a] General conditions: Fe$_3$(CO)$_{12}$/**3xx47**/Base= 1:1:X; 0.0068mmol of Fe, 0.0068mmol of **3xx47**, 3ml of ^{i}PrOH, time = 16h, temperature = 70 °C. [b] Conversion was calculated by ^{1}H NMR.[c] Enantiomeric excess was calculated by GC using a ChirasilDex CB column.

The ligand/Fe$_3$(CO)$_{12}$ ratio was also studied (Table 3.15). When the ligand/Fe$_3$(CO)$_{12}$ used was 0.5:1 almost no conversion was observed (entry1). Increasing the ligand/Fe$_3$(CO)$_{12}$ ratio to 0.75:1, provided moderate conversion together with high enantioselectivity (entry 2). However,

excellent conversions and enantiomeric ratios were achieved when a ligand/Fe$_3$(CO)$_{12}$ of 1:1 was applied (entry 3). Higher ligand/Fe$_3$(CO)$_{12}$ ratios showed a decrease in conversion as well as in the enantioselectivity of the process which might be attributed to an agglomeration of ligands around the metal precursor (entries 4 and 5). As the optimum ratio between ligand/Fe$_3$(CO)$_{12}$ seemed to be a 1:1 ratio , we speculated that at least one ligand is coordinated to the cluster in order to generate the active species responsible for the catalysis.

Table 3.15. Asymmetric transfer hydrogenation of *iso*-butyrophenone catalyzed by **3xx47** using a different ligand/Fe$_3$(CO)$_{12}$ ratios.[a]
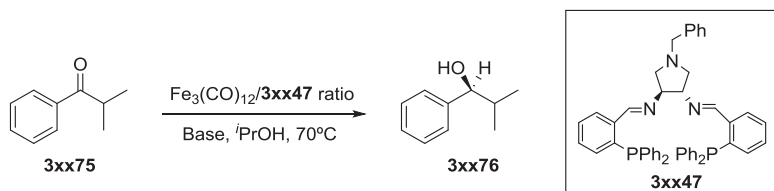
Entry	Ligand (eq)	Fe$_3$(CO)$_{12}$ (eq)	Conv (%)[b]	ee (%)[c]
1	0.5	1	<5	70
2	0.75	1	71	97
3	1	1	97	96
4	2	1	92	85
5	3	1	72	82

[a] General conditions: Fe$_3$(CO)$_{12}$/**3xx47**/KOH= 1:1:8; 0.0068mmol of Fe, 0.054mmol of KOH, 3ml of *i*PrOH, time = 16h, temperature = 70 °C. [b] Conversion was calculated by ^{1}H NMR. [c] Enantiomeric excess was calculated by GC using a ChirasilDex CB column.

The analysis of the reaction time was also analyzed using the iron carbonyl cluster Fe$_3$(CO)$_{12}$ and the iron hydride carbonyl cluster [Et$_3$NH][HFe$_3$(CO)$_{11}$] (Figure 3.22). Both precursors provided similar results being the optimal reaction time of the two at 5h. However, slightly

higher TOF (h^{-1}) (calculated at 2h) were obtained for the iron hydride carbonyl cluster $[Et_3NH][HFe_3(CO)_{11}]$ than for $Fe_3(CO)_{12}$, $7.6(h^{-1})$ and $6.4(h^{-1})$ respectively.
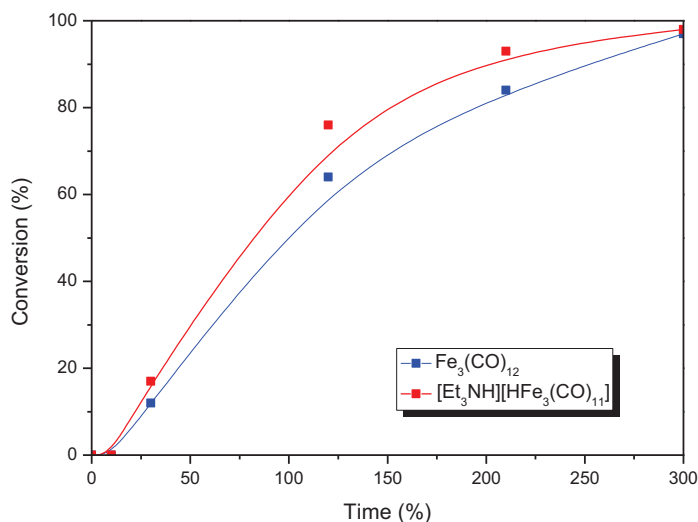
Figure 3.22. Graphic conversion *vs* time in the asymmetric hydrogenation of *iso*-butyrophenone catalyzed by **3xx47** using $Fe_3(CO)_{12}$ or $[Et_3NH][HFe_3(CO)_{11}]$.

Based on the reaction conditions, the scope and limitations of the **3xx47**/$Fe_3(CO)_{12}$ catalytic system were explored with a wide range of ketones (Table 3.16). First of all, the hydrogenation of acetophenone provided high conversions whereas the enantioselectivity was modest. Then, the reduction of more hindered ketones was investigated. When the methyl group of acetophenone was replaced by an ethyl, the enantiomeric excess increased significantly (**3xx78**). Following the same trend, *iso*-butyrophenone (**3xx76**), *iso*-valerophenone (**3xx79**) and *tert*-butyl diphenyl ketone (**3xx80**) showed the better enantioselectivities of the serie. This tendency was also observed by Morris and co-workers using a [(PNNP)(CH₃CN)(CO)] complex.[10b] Replacing the phenyl group of the

acetophenone by the naphthalene ring gave similar results in terms of conversion and enantioselectivity (**3xx77** and **3xx81**). However, in the case of methyl 2,4,6-trimetrylphenyl ketone no reaction was observed, even at longer reaction times (**3xx82**). Replacing the methyl group of the acetophenone by a trifluoromethyl group provided full conversion while the racemic alcohol was obtained (**3xx77** and **3xx83**). Finally, both electron withdrawing and electron donating substituent patterns on the aromatic ring provided similar conversions and enantioselectivities, compared to those of the acetophenone (**3xx84**, **3xx85** and **3xx77**).

Table 3.16. Scope of the asymmetric transfer hydrogenation of ketones catalyzed by **3xx47**.[a]
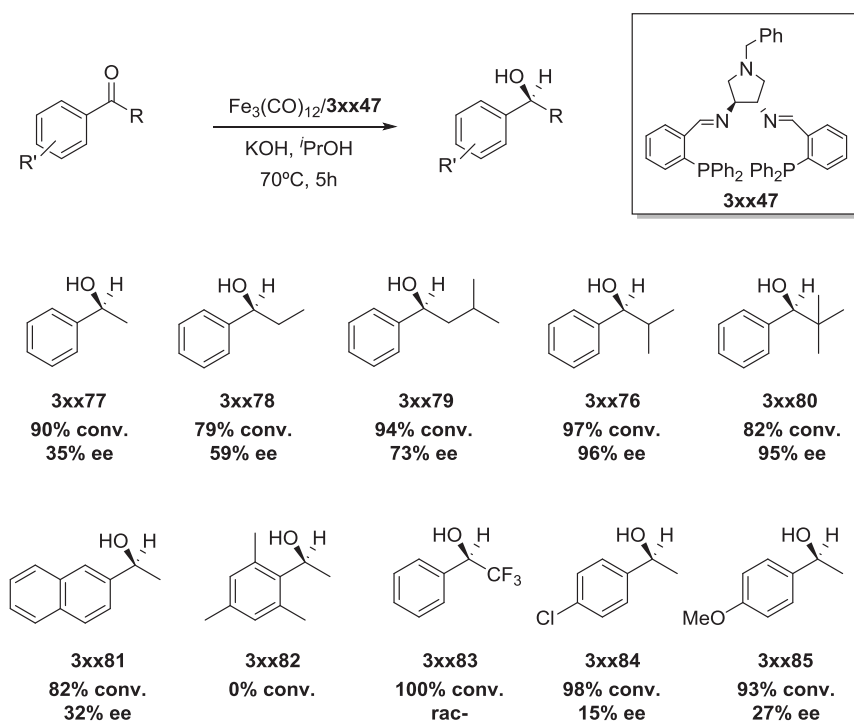
[a] General conditions: $Fe_3(CO)_{12}$/**3xx47**/KOH= 1:1:8; 0.0068mmol of Fe, 0.0068mmol of **3xx47**, 0.054mmol of KOH, 3ml of ^{i}PrOH, time = 5h, temperature = 70 °C. Conversion was calculated by ^{1}H NMR. Enantiomeric excess was calculated by GC using a ChirasilDex CB column.

Then, the reduction of cyclic phenyl ketones and ketones containing annulated-rings was carried out (Table 3.17). When the rigid cyclopropyl phenyl ketone was tested, only 8% conversion towards **3xx86** was obtained in moderate enantiomeric excess. On the contrary, when more flexible rings were located in the α-position of the ketone, high conversions and enantiomeric ratios were obtained (**3xx87**, **3xx88** and **3xx89**). When ketones containing annulated-rings were tested, low conversions were obtained with moderate enantioselectivities (**3xx90** and **3xx91**).

Table 3.17. Scope of the asymmetric transfer hydrogenation of ketones catalyzed by **3xx47**.[a]

[a] General conditions: $Fe_3(CO)_{12}$/**3xx47**/KOH= 1:1:8; 0.0068mmol of Fe, 0.0068mmol of **3xx47**, 0.054mmol of KOH, 3ml of ^{i}PrOH, time = 5h, temperature = 70 ºC. Conversion was calculated by ^{1}H NMR. Enantiomeric excess was calculated by GC using a ChirasilDex CB column. [b] Time=16h.

Turning to heteroaromatic methyl ketones, low conversions were observed in all cases (**3xx92**, **3xx93** and **3xx94**) whereas the enantioselectivity is comparable to the obtained for 1-phenylethanol **3xx77**. In the case of phenyl-2-pyridyl ketone, complete conversion towards the corresponding alcohol (**3xx95**) was obtained although as a racemic product.

Table 3.18. Scope of the asymmetric transfer hydrogenation of ketones catalyzed by **3xx47**.[a]

[a] General conditions: $Fe_3(CO)_{12}$/**3xx47**/KOH= 1:1:8; 0.0068mmol of Fe, 0.0068mmol of **3xx47**, 0.054mmol of KOH, 3ml of ^{i}PrOH, time = 5h, temperature = 70 ºC. Conversion was calculated by ^{1}H NMR. Enantiomeric excess was calculated by GC using a ChirasilDex CB column.

Finally, we investigated other substrates (Table 3.19) such as 3-phenylpropan-2-ol **3xx96** and 4-phenylbutan-2-ol **3xx97**. Low conversions were obtained when increasing the chain lengths between the phenyl ring and the ketone moiety (**3xx77**, **3xx96** and **3xx97**) as well as the enantioselectivity was affected. We also tried the hydrogenation of methyl benzoylformate, observing very low conversion and enantioselectivity although chemioselective reduction of the ketone moiety was detected (**3xx98**). Finally, we also test an imine and a 1,1-disubstituted olefin but no

conversion was detected, and the starting material was recovered unreacted (**3xx99** and **3xx100**). In contrast, (diphenylphosphinyl)(1-phenylethylidene) imine was converted into the corresponding amine **3xx101** in moderate conversion and enantioselectivity. Beller and co-workers also reported the efficiency of a PNNP/[Et$_3$NH][HFe$_3$(CO)$_{11}$] system that catalyzed the asymmetric transfer hydrogenation of diphenylphosphinyl imines but completely inactive for the asymmetric transfer hydrogenation of imines.[19]

Table 3.19. Scope of the asymmetric transfer hydrogenation of ketones catalyzed by **3xx2**.[a]
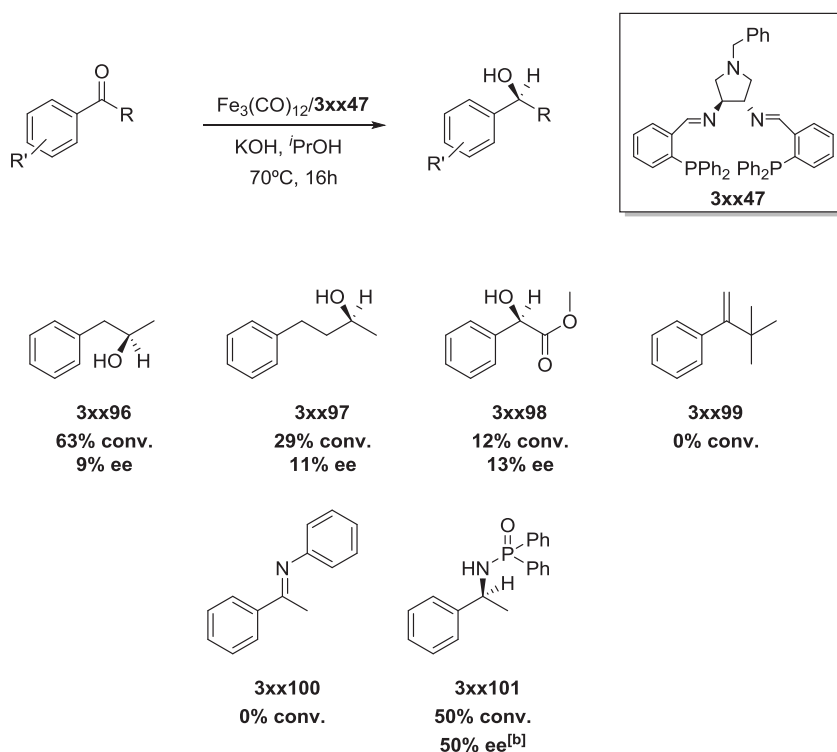
[a] General conditions: Fe$_3$(CO)$_{12}$/**3xx47**/KOH= 1:1:8; 0.0068mmol of Fe, 0.0068mmol of **3xx47**, 0.054mmol of KOH, 3ml of ^{i}PrOH, time = 16h, temperature = 70 ºC. Conversion was calculated by ^{1}H NMR. Enantiomeric excess was calculated by GC using a ChirasilDex CB column. [b] Enantiomeric excess calculated by HPLC.

3.3.6. MECHANISTIC CONSIDERATIONS

In 2012 the group of Morris and co-workers reported the use of Fe(II) PNNP complexes having a 6,5,6 system that catalyzes the asymmetric transfer hydrogenation of ketones *via* formation of iron nanoparticles.[44] The authors reported several methods for determining whether the catalyst was heterogeneous or homogeneous such as the mercury poisoning test. Nevertheless, the addition of Hg(0) is not always a reliable method due to the fact that iron does not form an stable amalgam with mercury.[60] Other well known methods involves the use of substoichiometric amounts of small phosphines and sulphides such as PPh_3 and CS_2 as poisoning agents, X-ray Photoelectron Spectroscopy (XPS), Scanning Transmission Electron Microscopy (STEM) or Superconducting Quantum Interference Device (SQUID).[61,62,63,64,65]

After a methodical analysis by STEM, SQUID and XPS, the authors postulated that Fe(0) NPs were being formed during catalysis when a Fe(II)-PNNP complex was used (Figure 3.23). The STEM showed NPs around 4.5 nm in diameter, the SQUID showed that the catalytic mixture contained primarily a superparamagnetic species and the XPS analysis confirmed the formation of Fe(0) species. In addition, several poisoning agents were tested, being the PMe3 the most effective, stopping the reaction with only a 10% loading of poison relative to the catalyst.

Following the same trend, in 2014 the group of Gao and co-workers reported the use of a macrocyclic ligand $(NH)_4P_2$ in combination with $Fe_3(CO)_{12}$ as iron source for the asymmetric hydrogenation of ketones which also involves the formation of iron NPs as active catalytic species (Figure 3.23).[11b] The authors confirmed the existence of particles *via*

Dynamic Light Scattering (DLS) and *via* distinct poisoning agents such as phosphines (PPh₃) or mercury which immediately stopped the reaction.
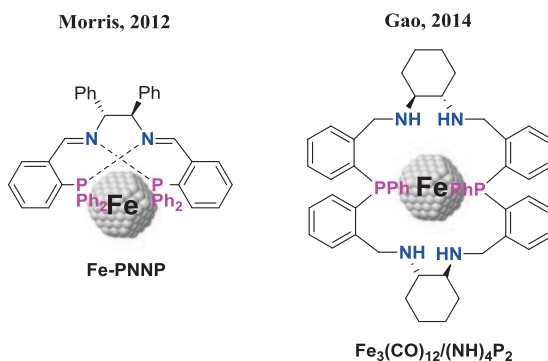
Figure 3.23. Previous heterogeneous Fe-PNNP and $Fe_3(CO)_{12}/(NH)_4P_2$ systems reported by Morris and Gao respectively.

With all these antecedents in hand, we decided to run a simple poisoning test using Hg(0) as poisoning agent in order to ascertain whether our **3xx47**/ $Fe_3(CO)_{12}$ catalytic system is homogeneous or heterogeneous.

In our case, the use of 3eq of Hg was sufficient to stop the ATH completely. This result is in agreement with the previous work reported by Gao and co-workers with similar *in situ* systems.[11b] Consequently, it is suggested that the ATH catalyzed by **3xx47**/$Fe_3(CO)_{12}$ is probably heterogeneous, having **3xx47**-modified iron particles acting as active catalyst.

3.4. CONCLUSIONS

From the study described in this chapter, the following conclusions can be extracted:

i)   Two chiral diamine derivatives, **3xx48** and **3xx49**, based on a pyrrolidine moiety were synthesized in four steps from L-(+)-Tartaric acid.

ii)   The PNNP ligands **3xx46**, **3xx47** and **3xx63** were synthesized and characterized obtaining moderate to excellent yields.

iii)   The corresponding chiral PNNP iron(II) complexes were synthesized and fully characterized by NMR, ESI-HRMS and EA. The X-ray structures of complexes **3xx68**, **3xx72** and **3xx73** were also obtained.

iv)   The new set of PNNP ligands **3xx46**, **3xx47** and **3xx63** in combination with $Fe_3(CO)_{12}$ as iron source efficiently catalyzes the asymmetric transfer hydrogenation of a wide range of substrates being the **3xx47**/ $Fe_3(CO)_{12}$ the most active of the series.

v)   The **3xx47**/ $Fe_3(CO)_{12}$ catalytic system catalyzes the asymmetric transfer hydrogenation of *iso*-butyrophenone, *iso*-valerophenone and *tert*-butyl diphenyl ketone having bulky groups at the alkylic position with high conversions (82-97%) and enantiomeric excesses (73-96%) towards the corresponding chiral alcohol at 5mol% of catalyst loading, T = 70º C and 5h of reaction.

vi)   The **3xx47**/ $Fe_3(CO)_{12}$ catalytic system catalyzes the asymmetric transfer hydrogenation of cyclic phenyl ketones and ketones containing annulated-rings with moderate to high conversions (21-91%) whereas high enantiomeric ratios were obtained in all cases (61-97%) towards the corresponding chiral alcohol at 5mol% of catalyst loading, T = 70º C and 5h of reaction.

vii)   Heteroaromatic methyl ketones were also hydrogenated but in this case with low conversions although the enantioselectivity was comparable to that obtained for 1-phenylethanol.

viii) The initial poisoning tests performed using Hg as poisoning agent, suggested that the asymmetric transfer hydrogenation catalyzed by

3xx47/Fe$_3$(CO)$_{12}$ is probably heterogeneous, having **3xx47**-modified iron particles acting as active catalyst.

3.5. EXPERIMENTAL PART

<u>GENERAL EXPERIMENTAL CONDITIONS</u>

All preparations and manipulations were carried out under an oxygen-free nitrogen atmosphere using conventional Schlenk techniques or inside a glovebox. Solvents were purified by the system Braun MB SPS-800 and stored under nitrogen atmosphere. CH$_3$CN, ^{i}PrOH and MeOH were dried, distilled and degassed using standard procedure.[66] Deuterated solvents were degassed via three freeze-pump-thaw cycles and kept in the glovebox over 4Å molecular sieves. Reagents were purchased from Aldrich, Alfa-Aesar and Strem and were used as received.

^{1}H, ^{13}C, ^{31}P, ^{11}B and ^{19}F-NMR spectra were recorded on a Varian® Mercury VX 400 (400 MHz, 100.6 MHz, 162 MHz, 128.5 MHz and 376.8 MHz respectively). Chemical shift values for ^{1}H and ^{13}C were referred to internal SiMe$_4$ (0.0 ppm) and for ^{31}P was referred to H$_3$PO$_4$ (85% solution in D$_2$O, 0 ppm). 2D correlation spectra (gCOSY, gHSQC and gHMBC) were visualized using VNMR program (Varian®). ESI-HMRS were run on an Agilent® 1100 Series LC/MSD instrument. ESI-HRMS of the complexes and EA were performed at the Serveis Tècnics de Recerca from the Universitat de Girona (Spain).

Reactions were monitored by TLC carried out on 0.25 mm E. Merck® silica gel 60 F$_{254}$ glass or aluminum plates. Developed TLC plates were visualized under a short-wave UV lamp (254 nm) and by heating plates that were dipped in potassium permanganate. Flash column chromatography was

carried out using forced flow of the indicated solvent on Merck® silica gel 60 (230-400 mesh).

The enantiomeric ratios were determined by GC or HPLC analysis. Gas chromatography analyses were carried out in a Hewlett-Packard HP 6890 gas chromatograph, using the appropriate chiral column (CP Chirasil-Dex CB or β-ciclodex 120). HPLC analyses were carried out in a Merck-Hitachi L-6200A liquid chromatograph, using the appropriate chiral column (Chiralpack AD-H or Chiralpack OD-H).

Synthesis of diols 3xx52 and 3xx53
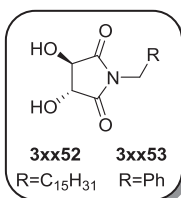
L(+) tartaric acid (10g, 0.066mol) and benzylamine (7.20ml, 0.066mol) or hexadecylamine (15.93g, 0.066mol) were azeotropically dehydrated with boiling xylene in a Dean-Stark apparatus for 24h. After cooling at room temperature, white precipitate was observed. The product was filtered off and washed with hexane (when R=$C_{15}H_{31}$) or acetone (R=Ph) until white crystals were obtained. Evaporation under reduced pressure of the remaining acetone affords **3xx52** and **3xx53** as white cristalls in 89% and 90% yield respectively.

For **3xx52**:

^{1}H-NMR (CDCl$_3$, 400 MHz, δ in ppm): δ = 4.08 (s, 2H, -CH-), 3.24-3.11 (m, 2H, =N-CH$_2$-), 1.26-1.22 (m, 2H, =N-CH$_2$-CH$_2$), 0.95-0.93 (m, 26H), 0.56 (t, 3H, J=6.8Hz). **^{13}C{^{1}H}-NMR** (CDCl$_3$, 100.6 MHz, δ in ppm): δ = 174.60 (2C, -C=O), 74.63 (2C, -CH-), 38.42 (=N-CH$_2$-), 31.62 (=N-CH$_2$-CH$_2$-), 29.36-29.24 (m, 10C,-CH$_2$-), 29.14 (-CH$_2$-), 29.04 (-CH$_2$-), 28.80 (-CH$_2$-), 13.47 (-CH$_3$). **ESI-HRMS:** Calculated for **$C_{20}H_{37}NO_4$**: Exact: (M: 355.2723; [M+Na]$^+$: 378.2620); Experimental ([M+Na]$^+$: 378.2608).

For **3xx53**:

¹H-NMR (MeOH-d4, 400 MHz, δ in ppm): δ = 7.32-7.27 (m, 5H, Ar-), 4.27 (s, 2H, -CH-), 3.98 (s, 2H, -CH₂-). **¹³C{¹H}-NMR** (MeOH-d4, 100.6 MHz, δ in ppm): δ = 177.08 (2C, -C=O), 134.76 (Ar-, -C-), 130.04 (Ar-, -CH-), 129.94 (Ar-, -CH-), 129.86 (Ar-, -CH-), 74.21 (-CH-), 44.45 (-CH₂-). **ESI-HRMS:** Calculated for **C₁₁H₁₁NO₄**: Exact: (M: 221.0688; [M+H]⁺: 222.0688); Experimental ([M+H]⁺: 222.0766).

Synthesis of diols 3xx54 and 3xx55
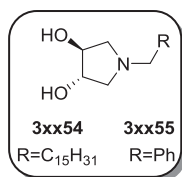
A solution of **3xx52** or **3xx53** (0.072mol) in dry THF (500ml) was cooled to 0ºC, and lithium tetrahydroaluminate (0.216 mol) was added dropwise. The resulting grey solution was heated at reflux for 48h and then cooled to 0ºC. Water was added carefully into the reaction mixture until effervescence was no longer observed. The white gel was filtered off and the resulting colourless solution was washed with ethyl ether (100ml x 3). The organic layer was washed with water, dried with anhydrous MgSO₄ and filtered, and the solvent evaporated under reduced pressure to give **3xx54** as a white solid in 81% yield or **3xx55** as a beige solid in 52% yield. In the case of **3xx55**, repeatedly co-evaporation with ether is needed for the solidification of the product. (Exposure to air and trituration of the product with small amounts of ether helps in the solidification).

For **3xx54**:

¹H-NMR (CDCl₃, 400 MHz, δ in ppm): δ = 4.13-4.11 (bs, 2H, -CH-), 2.97 (dd, 2H, *J*=10 & 5.2Hz), 2.89-2.74 (bs, 2H, -OH), 2.50 (dd, 2H, *J*=7.2 & 3.6Hz), 2.47-2.40 (m, 2H, =N-CH₂), 1.48-1.43 (m, 2H, =N-CH₂-CH₂), 1.28-1.23 (m, 26H, -CH₂-), 0.87 (t, 3H, *J*=6.8). **¹³C{¹H}-NMR** (CDCl₃, 100.6

MHz, δ in ppm): δ = 78.65 (2C, -CH-), 60.76 (2C, -CH$_2$-), 56.62 (=N-CH$_2$-), 32.22 (=N-CH$_2$-CH$_2$-), 30.01-29.98 (m, 4C,-CH$_2$-), 29.97 (-CH$_2$-), 29.96 (-CH$_2$-), 29.93 (-CH$_2$-), 29.92 (-CH$_2$-), 29.91(-CH$_2$-), 29.82 (-CH$_2$-), 29.66 (-CH$_2$-), 27.78 (-CH$_2$-), 22.99 (-CH$_2$-), 14.44 (-CH$_3$). **ESI-HRMS:** Calculated for **C$_{20}$H$_{41}$NO$_2$**: Exact: (M: 327.3137; [M+H]$^+$: 328.3137); Experimental ([M+H]$^+$: 328.3213).

For **3xx55**:

^{1}H-NMR (DMSO, 400 MHz, δ in ppm): δ = 7.30-7.20 (m, 5H, Ar-), 3.86 (t, 2H, J=4.4Hz, -CH-), 3.56 (d, 1H, J=12.8Hz, -CH$_2$-Ph, -CH$_2$-), 3.44 (d, 1H, J=12.8Hz, -CH$_2$-Ph, -CH$_2$-), 2.74 (dd, 2H, J=5.6 & 9.6Hz, -CH$_2$-), 2.30 (dd, 2H, J=4.4 & 9.6Hz, -CH$_2$-). **^{13}C{^{1}H}-NMR** (DMSO, 100.6 MHz, δ in ppm): δ = 139.45 (Ar-, -C-), 128.95 (Ar-, -CH-), 128.53 (Ar-, -CH-), 127.17 (Ar-, -CH-), 78.03 (2C, -CH-), 61.22 (2C, -CH$_2$-), 60.38 (=N-CH$_2$-). **ESI-HRMS:** Calculated for **C$_{11}$H$_{15}$NO$_2$**: Exact: (M: 193.1103; [M+H]$^+$: 194.1103); Experimental ([M+H]$^+$: 194.1181).

Generation of HN$_3$

In a three-necked flask fitted with an efficient stirrer, a thermometer and a gas-exit tube was added sodium azide (8.19g, 0.126mmol), 8.2ml of warm water and 70ml of dry toluene. The mixture was cooled to 0ºC, and sulphuric acid (3.5ml, 0.063mmol) was added dropwise with control of the temperature to 0-5ºC. Then, the organic layer was separated and dried over sodium sulphate. The concentration of the solution of hydrazoic acid was determined by transferring a 3ml sample of azidoic acid in an erlenmeyer, shaking with distilled water and by titration with a 0.38M solution of sodium hydroxide. The generated hydrazoic acid was kept below 0ºC until its use.

Synthesis of diazides 3xx56 and 3xx57
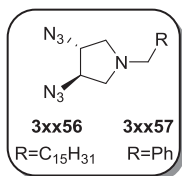
To a magnetically stirred solution of triphenylphosphine (3.54g, 0.014mol) in 3ml of dry toluene was added dropwise diisopropyl azodicarboxylate (DIAD) (3.05ml, 0.016mol) with control of temperature around 0 ºC. Then a solution of 1.8M of azidoic acid (7.5ml, 0.014mol) was added dropwise during 15 minutes. Formation of an orange-pink solid was observed and allowed to stir until complete dissolution. Then, diol **3xx54** or **3xx55** (0.0027mol) in dry toluene (2ml) was added carefully. The reaction was allowed to stir overnight at room temperature. The solution was concentrated *in vacuo* and the residue was purified by column chromatography (100:2.5, hexane:ether) to give **3xx56** as a white solid in 65% yield or **3xx57** as an incolor liquid in 53% yield.

For **3xx56**:

¹H-NMR (CDCl₃, 400 MHz, δ in ppm): δ = 3.87 (t, 2H, *J*=4Hz, -CH-), 2.95 (dd, 2H, *J*=10 & 6.4Hz, -CH₂-), 2.57 (dd, 2H, *J*=10 & 4.8Hz, -CH₂-), 2.48-2.38 (m, 2H, =N-CH₂), 1.48-1.42 (m, 2H, =N-CH₂-CH₂), 1.30-1.24 (m, 26H, -CH₂-), 0.88 (t, 3H, *J*=6.8). **¹³C{¹H}-NMR** (CDCl₃, 100.6 MHz, δ in ppm): δ = 66.07 (2C, -CH-), 58.27 (2C, -CH₂-), 55.91 (=N-CH₂-), 32.30 (=N-CH₂-CH₂-), 31.28 (-CH₂-), 30.08-30.05 (m, 4C,-CH₂-), 30.03 (-CH₂-), 29.98 (-CH₂-), 29.94 (-CH₂-), 29.86 (-CH₂-), 29.73 (-CH₂-), 28.66 (-CH₂-), 27.69 (-CH₂-), 23.06 (-CH₂-), 14.49 (-CH₃). **ESI-HRMS:** Calculated for **C₂₀H₃₉N₇**: Exact: (M: 377.3267; [M+H]⁺: 378.3267); Experimental ([M+H]⁺: 378.3342).

For **3xx57**:

¹H-NMR (CDCl₃, 400 MHz, δ in ppm): δ = 7.31-7.20 (m, 5H, Ar-), 3.82 (t, 2H, J=4.8Hz, -CH-), 3.62 (d, 1H, J=12.8Hz, -CH₂-Ph, -CH₂-), 3.57 (d, 1H, J=13.2Hz, -CH₂-Ph, -CH₂-), 2.94 (dd, 2H, J=6.4 & 10Hz, -CH₂-), 2.55 (dd, 2H, J=4.8 & 10Hz, -CH₂-). **¹³C{¹H}-NMR** (CDCl₃, 100.6 MHz, δ in ppm): δ = 137.95 (-C-), 128.83 (Ar-, -CH-), 128.67 (Ar-, -CH-), 127.61 (Ar-, -CH-), 65.97 (-CH-), 59.58 (-CH₂-), 57.89 (-CH₂-). **ESI-HRMS:** Calculated for **C₁₁H₁₃N₇**: Exact: (M: 243.1232; [M+H]⁺: 244.1232); Experimental ([M+H]⁺: 244.1304).

Synthesis of diamines 3xx48 and 3xx49
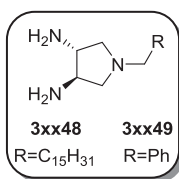
To a stirred solution of **3xx56** or **3xx57** (1.67mmol) in ethanol (15ml), 10%Pd on charcoal (0.167mmol) was added and the mixture was hydrogenated at 1bars of pressure at room temperature for 16h. The catalyst was filtered off through a pad of celite and washed with ethyl alcohol. Ethyl alcohol was evaporated under reduced pressure to give **3xx48** or **3xx49** in quantitative yield. In the case of **3xx49** repeatedly co-evaporations with ether are needed for the solidification of the product. (Trituration of the product with small amounts of ether helps in the solidification).

For **3xx48**:

¹H-NMR (CDCl₃, 400 MHz, δ in ppm): δ = 3.09-3-01 (m, 2H, -CH-), 2.98-2.90 (m, 2H, -CH₂-), 2.48-2.29 (m, 6H, =N-CH₂, -CH₂-, -NH₂), 1.53-1.41 (m, 2H, =N-CH₂-CH₂), 1.30-1.24 (m, 26H, -CH₂-), 0.89(t, 3H, J=6.4). **¹³C{¹H}-NMR** (CDCl₃, 100.6 MHz, δ in ppm): δ = 62.59 (2C, -CH₂-), 61.12 (2C, -CH-), 56.88 (=N-CH₂-), 32.15 (=N-CH₂-CH₂-), 30.00-29.76 (m, 8C,-CH₂-), 30.03 (-CH₂-), 29.59 (-CH₂-), 28.63 (-CH₂-), 27.77 (-CH₂-),

22.92 (-CH$_2$-), 14.37 (-CH$_3$). **ESI-HRMS:** Calculated for **C$_{20}$H$_{43}$N$_3$**: Exact: (M: 325.3457; [M+H]$^+$: 326.3457); Experimental ([M+H]$^+$: 326.3554).

For **3xx49**:

^{1}H-NMR (CDCl$_3$, 400 MHz, δ in ppm): δ = 7.28-7.20 (m, 5H, Ar-), 3.61 (d, 1H, *J*=12.8Hz, -CH$_2$-Ph, -CH$_2$-), 3.54 (d, 1H, *J*=12.8Hz, -CH$_2$-Ph, -CH$_2$-), 3.01 (t, 2H, *J*=4.8Hz, -CH-), 2.90 (dd, 2H, *J*=6 & 9.2Hz, -CH$_2$-), 2.27 (dd, 2H, *J*=4.8 & 9.2Hz, -CH$_2$-), 1.58 (s, 4H, -NH$_2$) **^{13}C{^{1}H}-NMR** (CDCl$_3$, 100.6 MHz, δ in ppm): δ = 138.93 (-C-), 128.94 (Ar-, -CH-), 128.43 (Ar-, -CH-), 127.18 (Ar-, -CH-), 62.39 (-CH-), 61.23 (-CH$_2$-), 60.49 (-CH$_2$-). **ESI-HRMS:** Calculated for **C$_{11}$H$_{17}$N$_3$**: Exact: (M: 191.1422; [M+H]$^+$: 192.1422); Experimental ([M+H]$^+$: 192.1508).

Synthesis of chiral PNNP ligands 3xx46 and 3xx47
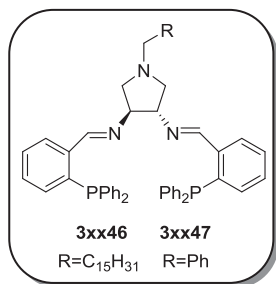
2-(diphenylphosphino)benzaldehyde (0.155 g, 0.53 mmol) was added to 4ml of dry and degassed toluene provided with molecular sieves. Then, **3xx48** or **3xx49** (0.26mmol) was added to the mixture. This solution was allowed to stir overnight at 90ºC. The reaction mixture was filtrated under nitrogen atmosphere and collected by vacuum filtration. Recrystalization with cool MeOH in a glovebox afforded **3xx46** as a thick yellow liquid in 42% yield and **3xx47** as a yellow solid in 84% yield.

For **3xx46**:

^{1}H-NMR (CDCl$_3$, 400 MHz, δ in ppm): δ = 8.46 (d, 2H, *J*= 4, -CH=N), 7.77 (dd, 2H, *J*= 4 & 8Hz, -CH-), 7.38 (t, 2H, *J*=8Hz, -CH-), 7.29-7.12 (m, 22H, -CH-), 6.75 (dd, 2H, , *J*= 4 & 8Hz, -CH-), 3.49 (t, 2H, *J*= 4, -CH-), 2.68 (dd, 2H, , *J*= 4 & 8Hz, -CH$_2$-), 2.43 (dd, 2H, *J*= 4 & 8Hz, -CH$_2$-), 2.36-

2.20 (m, 2H, -CH$_2$-), 1.37-1.32 (m, 2H, -CH$_2$-), 1.26-1.13 (m, 26H, -CH$_2$-), 0.80 (t, 3H, *J*= 8, -CH$_3$) . **^{13}C{^{1}H}-NMR** (CDCl$_3$, 100.6 MHz, δ in ppm): δ = 159.1 (d, 2C, J$_{C-P}$=17.1Hz, CH=N), 139.4 (d, 2C, J$_{C-P}$=27.5Hz, -C-), 137.7 (d, 2C, J$_{C-P}$=17.8Hz, -C-), 137.3 (d, 2C, J$_{C-P}$=17.8Hz, -C-), 134.2, 134.0, 133.8, 133.4, 129.9, 129.0, 128.65, 128.6, 128.56, 128.5, 128.4, 128.2, 125.3, overlapped signals, 75.57 (2C, -CH=N), 60.49 (2C, -CH$_2$-), 56.19 (=N-CH$_2$-), 31.80 (=N-CH$_2$-CH$_2$-), 19.58 (bs, 9C,-CH$_2$-), 29.24 (-CH$_2$-), 28.64 (-CH$_2$-), 27.45 (-CH$_2$-), 22.58 (-CH$_2$-), 13.78 (-CH$_3$). **^{31}P{^{1}H}-NMR** (CDCl$_3$, 161MHz, δ in ppm): -12.45. **ESI-HRMS:** Calculated for **C$_{58}$H$_{69}$N$_3$P$_2$**: Exact: (M: 869.4967; [M+H]$^+$: 870.4967); Experimental ([M+H]$^+$: 870.5097).

For **3xx47**:

^{1}H-NMR (CD$_2$Cl$_2$, 400 MHz, δ in ppm): δ = 8.45 (d, 2H, *J*=4Hz, HC=N), 7.80 (dd, 2H, *J*=4 & 8Hz, Ar-), 7.39-7.19 (m, 29H, Ar-), 6.85 (dd, 2H, *J*=4 & 8Hz, Ar-), 3.56 (d, 2H, *J*=4, -CH$_2$-Ph, -CH$_2$-), 3.48 (quint, 2H, *J*=4Hz, -CH-), 2.70 (dd, 2H, *J*=4 & 8Hz, -CH$_2$-), 2.46 (dd, 2H, *J*=4 & 8Hz, -CH$_2$-). **^{13}C{^{1}H}-NMR** (CD$_2$Cl$_2$, 100.6 MHz, δ in ppm): δ 159.4 (d, *J$_{C-P}$*=16Hz, HC=N), 134.2, 134.0, 133.8, 133.5, 129.9, 128.8, 128.7, 128.5, 128.4, 128.3, 128.1, 126.8, overlapped signals, 75.8 (-CH-), 60.4 (-CH$_2$-), 60.2 (-CH$_2$Ph). **^{31}P{^{1}H}-NMR** (CD$_2$Cl$_2$, 161MHz, δ in ppm): -12.14. **ESI-HRMS:** Calculated for **C$_{49}$H$_{43}$N$_3$P$_2$**: Exact: (M: 735.2932; [M+H]$^+$: 736.2932); Experimental ([M+H]$^+$: 736.2997). **Elemental Analysis:** Calculated for **C$_{49}$H$_{43}$N$_3$P$_2$**: C, 79.98; H, 5.89; N, 5.71; Found: C, 79.09; H, 5.73; N, 5.37.

Synthesis of chiral PNNP ligand 3xx65
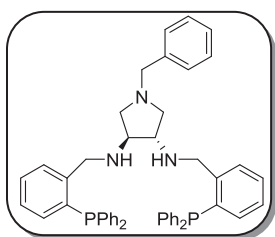
3xx47 (90mg, 0.12mmol) was dissolved in 5ml of dry methanol. Then, $NaBH_4$ (28mg, 0.73mmol) was added under nitrogen atmosphere. The reaction was refluxed with stirring under nitrogen for 24h. The solution was cooled to room temperature and H_2O (desoxigenated for 3h) 3ml was added to destroy the excess of $NaBH_4$. The mixture solution was extracted with CH_2Cl_2 (desoxigenated 2h) (3ml×3). The organic layer was dried over anhydrous $MgSO_4$ and evaporation under vacuum affords **3xx65** in 95% yield.

^{1}H-NMR (CD$_2$Cl$_2$, 400 MHz, δ in ppm): δ = 7.45-7.42 (m, 3H, Ar-), 7.32-7.19 (m, 26H, Ar-), 7.16-7.12 (m, 2H, Ar-), 6.87-6.84 (m, 2H, Ar-), 3.86 (qd, 4H, -CH$_2$-, *J*=12 & 4Hz, CH$_2$-NH), 3.43 (s, 2H, -CH$_2$-Ph, -CH$_2$-), 2.80 (t, 2H, *J*=4Hz, -CH-), 2.55 (dd, 2H, *J*=4 & 12Hz, -CH$_2$-), 2.11 (dd, 2H, *J*=4 & 12Hz, -CH$_2$-). **^{13}C{^{1}H}-NMR** (CD$_2$Cl$_2$, 100.6 MHz, δ in ppm): δ = 145.0 (d, $^2J_{C-P}$= 24.1Hz, Ar-, -C-), 139.4 (CH$_2$Ph, Ar-, -C-), 137.2 (d, $^1J_{C-P}$=11.1Hz, PPh$_2$, Ar-, -C-), 137.1 (d, $^1J_{C-P}$=11.1Hz, PPh$_2$, Ar-, -C-), 135.9 (d, $^1J_{C-P}$=11.1Hz, Ar-, -C-), 133.9 (d, *J*= 2Hz, Ar-, -CH-), 133.8 (d, *J*= 2Hz, Ar-, -CH-), 133.5 (Ar-, -CH-), 129.3 (d, *J*= 5Hz, Ar-, -CH-), 128.9 (Ar-, -CH-), 128.8 (Ar-, -CH-), 128.7 (d, *J*= 3Hz, Ar-, -CH-), 128.6 (d, *J*= 3Hz, , Ar-, -CH-), 128.5 (d, *J*= 3Hz, Ar-,-CH-), 128.1 (Ar-, -CH-), 127.1 (Ar-, -CH-), 126.7 (Ar-, -CH-), overlapped signals, 64.3 (CH-NH, -CH-), 60.2 (CH$_2$-Ph, -CH$_2$,), 59.7 (CH$_2$-CH-NH, -CH$_2$,), 50.8 (d, $^3J_{C-P}$=21.1Hz, CH$_2$-NH, -CH$_2$-). **^{31}P{^{1}H}NMR** (CD$_2$Cl$_2$, 161MHz, δ in ppm): -16.21. **ESI-HRMS:** Calculated for **C$_{49}$H$_{45}$N$_3$P$_2$**: Exact: (M: 739.3245; [M+H]$^+$: 740.3245); Experimental ([M+H]$^+$: 740.3717).

Synthesis of chiral PNNP iron(II) complexes 3xx66 and 3xx67
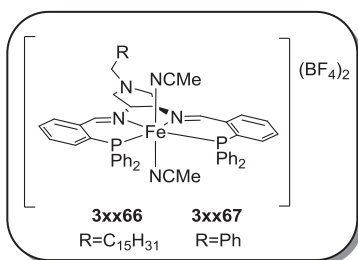
3xx46 or **3xx47** (0.135mmol) in 4ml of MeCN was added to a solution of Fe(BF$_4$)$_2$·6H$_2$O (0.133mmol) in 1ml of MeCN. After stirring for 3h, the red solution was evaporated to dryness. Then, 1ml of CH$_2$Cl$_2$ was added to re-dissolve the deep red powder. Hexane (4ml) was added to the solution and a precipitate started to form. The solid was filtered under nitrogen via *canula* and washed repeatedly with hexane to afford **3xx66** or **3xx67** as a deep red solid in 79% yield and 81% of yield respectively.

For **3xx66**:

^{1}H-NMR (CDCl$_3$, 400 MHz, δ in ppm): δ = 8.88 (br s, 1H, CH=CN), 8.82 (br s, 1H, CH=CN), 8.63 (br s, 2H, Ar-), 8.05 (br s, 2H, Ar-), 7.76-7.41 (m, 9H, Ar-), 7.24 (br s, 6H, Ar-), 6.99-6.51 (m, 9H, Ar-), 4.97-4.90 (m, 2H, -CH-), 4.42 (br s, 2H, -CH$_2$-), 3.94 (br s, 2H, -CH$_2$-), 3.62 (br s, 2H, -CH$_2$-), 1.90 (br s, 2H, -CH$_2$-), 1.83 (s, 3H, -CH$_3$, CH$_3$CN), 1.80 (s, 3H, -CH$_3$, CH$_3$CN), 1.45-1.29 (m, 26H, -CH$_2$-), 0.88 (br s, 3H, -CH$_3$) all signals are broad. **^{31}P{^{1}H}-NMR** (CDCl$_3$, 161MHz, δ in ppm): 52.66. **^{11}B{^{1}H}-NMR** (CD$_2$Cl$_2$, 128.51MHz, δ in ppm): -1.10. **^{19}F{^{1}H}-NMR** (CD$_2$Cl$_2$, 376.8MHz, δ in ppm): -150.24. **ESI-HRMS:** Calculated for **C$_{62}$H$_{75}$B$_2$F$_8$FeN$_5$P$_2$**: Exact: (M: 1181.4905, M-(CH$_3$CN)$_2$(BF$_4$)$_2$/Z: 462.7153); Experimental (M-(CH$_3$CN)$_2$(BF$_4$)$_2$:/Z: 462.7153).

For **3xx67**:

^{1}H-NMR (CD$_2$Cl$_2$, 400 MHz, δ in ppm): δ = 8.82 (br s, 1H, CH=CN), 8.77 (br s, 1H, CH=CN), 8.06-7.96 (m, 3H, Ar-), 7.75-7.21 (m, 20H, Ar-), 6.99-

6.68 (m, 8H, Ar-), 6.43 (br s, 2H, Ar-), 5.34 (s, 2H, CH$_2$-Ph, -CH$_2$-), 4.95 (br s, 1H, -CH-), 4.80-4.71 (m, 2H, -CH$_2$-), 4.55 (br s, 1H, -CH$_2$-), 4.19-4.07 (m, 2H, -CH$_2$-) all signals are broad. **^{31}P{^{1}H}-NMR** (CD$_2$Cl$_2$, 161MHz, δ in ppm): 52.32 (d, J_{P-P}= 42Hz) and 51.65 (J_{P-P}= 42Hz). **^{11}B{^{1}H}-NMR** (CD$_2$Cl$_2$, 128.51MHz, δ in ppm): -1.03. **^{19}F{^{1}H}-NMR** (CD$_2$Cl$_2$, 376.8MHz, δ in ppm): -150.05. **ESI-HRMS:** Calculated for **C$_{53}$H$_{49}$B$_2$F$_8$FeN$_5$P$_2$**: Exact: (M: 1047.2871, M-(CH$_3$CN)$_2$(BF$_4$)$_2$/Z: 395.6136); Experimental (M-(CH$_3$CN)$_2$(BF$_4$)$_2$:/Z: 395.6146). **Elemental Analysis:** Calculated for **C$_{53}$H$_{49}$B$_2$F$_8$FeN$_5$P$_2$** · **3CH$_2$Cl$_2$**: C, 51.65; H, 4.26; N, 5.38; Found **C$_{53}$H$_{49}$B$_2$F$_8$FeN$_5$P$_2$** · **3CH$_2$Cl$_2$**: C, 51.62; H, 4.49; N, 5.61.

Synthesis of chiral PNNP iron(II) complex 3xx68
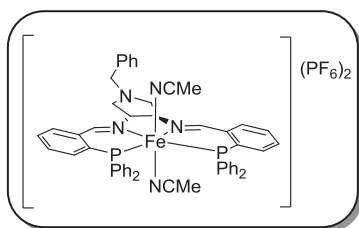
NaPF$_6$ (16mg, 0.095mmol) was added to a solution of **3xx67** (50mg, 0.047mmol) in dichloromethane (4ml). After stirring for 1h the resulting orange mixture was filtered through a small pad of Celite and evaporated to dryness to give **3xx68** as an orange solid in 90% yield.

^{1}H-NMR (CD$_2$Cl$_2$, 400 MHz, δ in ppm): δ = 8.80 (br s, 1H, CH=CN), 8.71 (br s, 1H, CH=CN), 8.04-7.97 (m, 3H, Ar-), 7.78-7.20 (m, 22H, Ar-), 7.02-6.71 (m, 7H, Ar-), 6.36 (br s, 1H, Ar-), 5.16 (br s, 1H, -CH-), 4.85 (br s, 2H, -CH$_2$-), 4.76 (s, 2H, CH$_2$Ph, -CH$_2$-), 4.52 (br s, 1H, -CH-), 4.13 (br s, 2H, -CH$_2$-) all signals are broad. **^{31}P{^{1}H}-NMR** (CD$_2$Cl$_2$, 161MHz, δ in ppm): 51.98 (d, J_{P-P}= 43.7Hz), 51.13(d, J_{P-P}= 43.7Hz), -144.3 (sept, J_{P-F}= 712.8Hz, PF$_6$). **^{19}F{^{1}H}-NMR** (CD$_2$Cl$_2$, 376.8MHz, δ in ppm): δ = -71.5 (d, 6F, J_{F-P}= 712.8Hz, PF$_6$). **ESI-HRMS:** Calculated for **C$_{53}$H$_{49}$F$_{12}$FeN$_5$P$_4$**: Exact: (M: 1163.2096, M-(CH$_3$CN)$_2$(PF$_6$)$_2$/Z: 395.6136); Experimental (M-(CH$_3$CN)$_2$(PF$_6$)$_2$:/Z: 395.6130). **Elemental Analysis:** Calculated for

C₅₃H₄₉F₁₂FeN₅P₄ · **3CH₂Cl₂**: C, 47.42; H, 3.91; N, 4.94; Found
C₅₃H₄₉F₁₂FeN₅P₄ · 3CH₂Cl₂: C, 47.32; H, 3.21; N, 4.81.
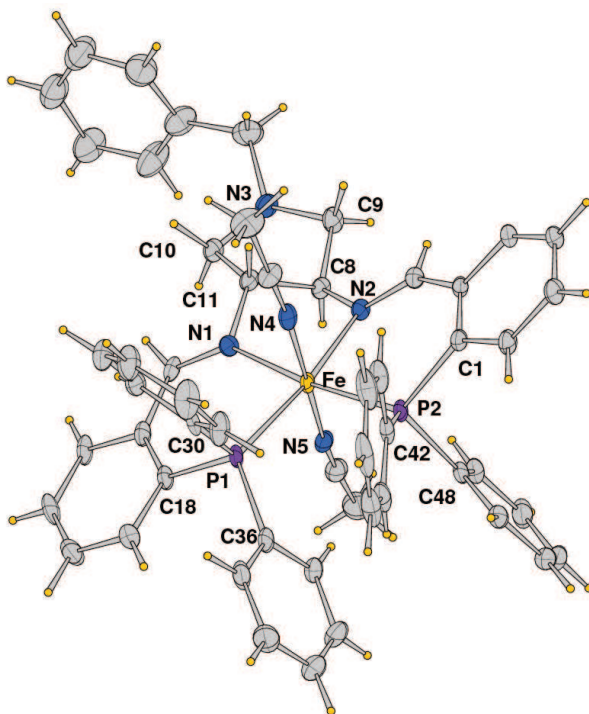
Figure 3.24. Molecular structure of **3xx68**.

Table 3.20. Crystal data and details of refinement for **3xx68**.

Empirical formula	$C_{58}H_{63}F_{18}FeN_5OP_5$ $[C_{53}H_{49}F_{18}FeN_5P_5, \cdot C_5H_{12} \cdot H_2O]$
Formula weight	1397.83
Temperature (K)	100(2)
Wavelength (Å)	0.800
Crystal system	Monoclínic
Space group	$P\,2_1$
Unit cell dimensions (Å / º)	$a = 11.9220(11)$, $\alpha = 90.00$ $b = 14.7690(13)$, $\beta = 98.505(10).$ $c = 18.0630(19)$, $\gamma = 90.00$
Volume ($Å^3$)	3145.5(5)
Z	2
Calculated Density (Mg/m^3)	1.476
Absorption coefficient (mm^{-1})	0.588
F(000)	1432
Theta range (º) for data collection	1.28 - 29.99
Index ranges	-14<=h<14=,-18<=k<=18,-22<=l<=22
Reflections collected	12028
Data [$I > 2\sigma(I)$]	11346
Parameters	816
Goodness-of-fit on F^2	1.025
Final R indices [$I>2\sigma(I)$]	R1 = 0.0649, wR2 = 0.1800
R indices (all data)	R1 = 0.0678, wR2 = 0.1835
Largest diff. peak and hole ($e/Å^3$)	0.937, -0.910

Synthesis of chiral PNNP iron(II) complex 3xx72
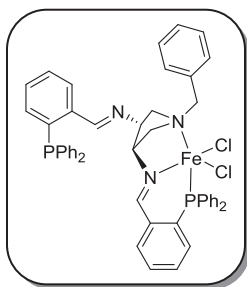
Iron dichloride anhydrous (12mg, excess) dissolved in 1ml of CH_2Cl_2 was added to a solution of **3xx47** (50mg, 0.068mmol) in 3ml of CH_2Cl_2. The mixture was allowed to stir at room temperature for 48h to which a change of color was appreciated from pale yellow to pink-red. The mixture was filtered *via canula* under nitrogen atmosphere and, ether was added to the pink-red solution to force the product precipitation. **3xx72** was isolated as a pink-red solid in 70% of yield. Crystals suitable for X-Ray diffraction were ground by vapor diffusion of pentane into CH_2Cl_2 solution of the complex.

^{1}H-NMR (CD_2Cl_2, 400 MHz, δ in ppm): δ = 105.08, 85.55, 72.60, 60.50, 16.48, 15.43, 12.66, 10.33, 9.94, 8.04, 7.56, 7.32, 7.22, 6.87, 6.72, 6.54, 6.17, 6.02, -1.01, -7.17, -30.37.**^{31}P{^{1}H}-NMR at r.t.** (CD_2Cl_2, 161MHz, δ in ppm): δ = -0.694. **^{31}P{^{1}H}NMR at -80°C** (CD_2Cl_2, 161MHz, δ in ppm): δ = 23.83 & 5.32 (bs). **ESI-HRMS:** Calculated for **$C_{49}H_{43}FeN_3P_2Cl_2$**: Exact: (M: 861.1659, M-Cl: 826.1970); Experimental (M-Cl: 826.1986). **Elemental Analysis:** Calculated for **$C_{49}H_{43}FeN_3P_2Cl_2 \cdot 0.5CH_2Cl_2$**: C, 65.69; H, 4.90; N, 4.64; Found **$C_{49}H_{43}FeN_3P_2Cl_2 \cdot 0.5CH_2Cl_2$**: C, 65.89; H, 4.66; N, 4.16.
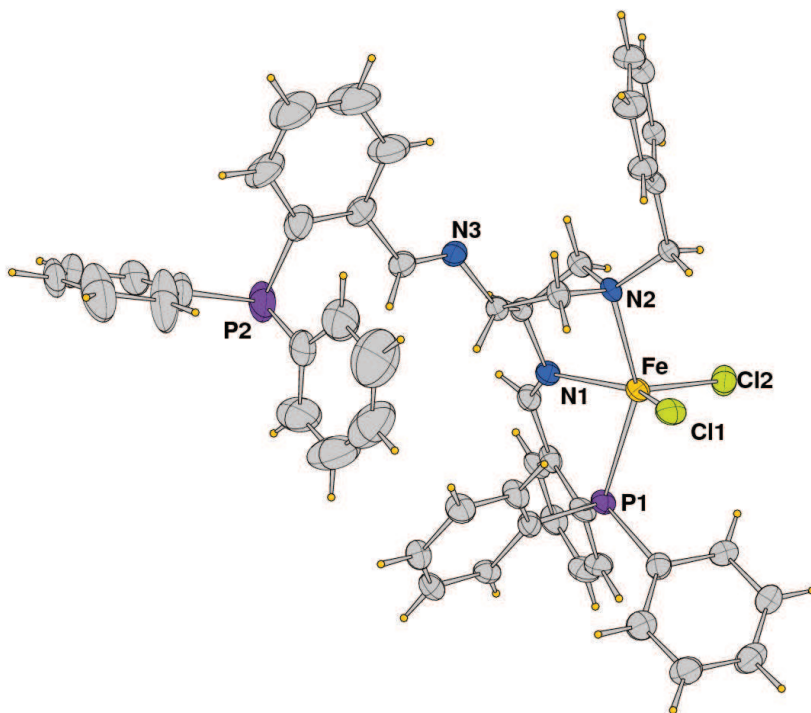
Figure 3.25. Molecular structure of **3xx72**.

Table 3.21. Crystal data and details of refinement for **3xx72**.

Empirical formula	$C_{49.5}H_{44}Cl_3FeN_3P_2$ [$C_{49}H_{43}Cl_2FeN_3P_2$, $0.5CH_2Cl_2$]
Formula weight	905.02
Temperature (K)	293(2)
Wavelength (Å)	0.7000
Crystal system	Monoclinic
Space group	$P\,2_1$
Unit cell dimensions (Å / º)	a = 9.3211(9), α = 90.00. b = 16.0716(11), β = 98.180(11). c = 15.8320(12), γ = 90.00.
Volume ($Å^3$)	2347.6(3)
Z	2
Calculated Density (Mg/m^3)	1.280
Absorption coefficient (mm^{-1})	0.526
F(000)	938
Crystal size (mm^3)	0.38 x 0.35 x 0.12
Theta range (º) for data collection	6.72 - 27.41
Index ranges	-12<=h<=12, -20<=k<=19, 0<=l<=20
Reflections collected	10182
Parameters	529
Goodness-of-fit on F^2	1.035
Final R indices [I>2σ(I)]	R1 = 0.0298, wR2 = 0.1906
R indices (all data)	R1 = 0.0809, wR2 = 0.1992
Largest diff. peak and hole ($e/Å^3$)	0.944, -0.848

Synthesis of chiral PNNP iron(II) complex 3xx73
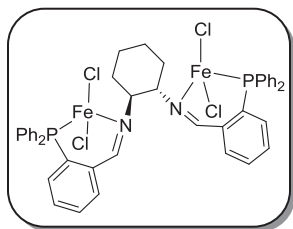
Iron dichloride anhydrous (15mg, excess) dissolved in 1ml of CH_2Cl_2 was added to a solution of **3xx74** (70mg, 0.10mmol) in 4ml of CH_2Cl_2. The mixture was allowed to stir at room temperature for 48h to which a change of color was appreciated from pale yellow to pink-red. The mixture was filtered *via canula* under nitrogen atmosphere and, ether was added to the pink-red solution to force the product precipitation. **3xx73** was isolated as a pink-red solid in 67% of yield. Crystals suitable for X-Ray diffraction were ground by vapor diffusion of pentane into CH_2Cl_2 solution of the complex.

^{1}H-NMR (CD_2Cl_2, 400 MHz, δ in ppm): δ = **^{31}P{^{1}H}-NMR** (CD_2Cl_2, 161MHz, δ in ppm): No phosphorus found in the range of -4000ppm to +4000ppm. **ESI-HRMS:** Calculated for **$C_{44}H_{40}Fe_2N_2P_2Cl_4$**: Exact: (M: 910.0120, M-FeCl$_3$: 749.1705); Experimental (M: 749.1719).
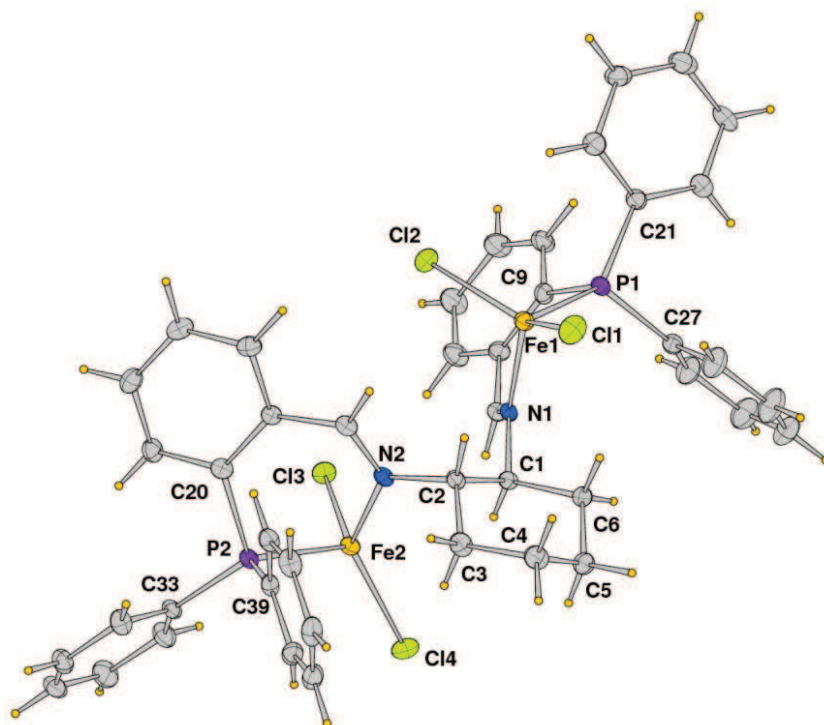
Figure 3.26. Molecular structure of **3xx73**.

Table 3.22. Crystal data and details of refinement for **3xx73**.

Empirical formula	$C_{45}H_{42}Cl_6Fe_2N_2P_2$ $[C_{44}H_{40}Cl_4Fe_2N_2P_2, 1CH_2Cl_2]$
Formula weight	997.15
Temperature (K)	100(2)
Wavelength (Å)	0.7000
Crystal system	Monoclinic
Space group	$P\,2_1$
Unit cell dimensions (Å / º)	a = 11.9550(7), α = 90.00. b = 7.4830(4), β = 92.509(10). c = 25.6260(12), γ = 90.00°.
Volume ($Å^3$)	2290.3(2)
Z	2
Calculated Density (Mg/m^3)	1.446
Absorption coefficient (mm^{-1})	1.087
F(000)	1020
Theta range (º) for data collection	1.57 - 27.82
Index ranges	-15<=h<=15, 0<=k<=9, 0<=l<=34
Reflections collected	5941
Parameters	533
Goodness-of-fit on F^2	1.035
Final R indices [I>2σ(I)]	R1 = 0.0298, wR2 = 0.0764
R indices (all data)	R1 = 0.0319, wR2 = 0.0777
Largest diff. peak and hole ($e/Å^3$)	0.544, -0.761

General procedure for the asymmetric transfer hydrogenation reaction

In a typical experiment, inside the glovebox $Fe_3(CO)_{12}$ (3.4 mg, 0.0068 mmol), **3xx47** (5 mg, 0.0068 mmol) were placed in a tube equipped with a Teflon-coated magnetic stirring bar. Isopropyl alcohol (3ml) was then added and the mixture was stirred at 70 ºC for 30 min. An appropriate amount of KOH was then added, and the mixture was continually stirred for another 15

min. Ketone was then introduced and the mixture was stirred at 70 ºC for the required reaction time. Conversion was calculated by ^{1}H-NMR and enantiomeric ratios by GC or HPLC.

Method 1: Gas chromatography. CP Chirasil-Dex CB, 25 m column, internal diameter: 0.25 mm, film thickness: 0.25 μm, carrier gas: 120 kPa He, temperature: 130 ºC for 10min, rate 10 ºC/min to 180 ºC and hold for 3min.

Method 2: Gas chromatography. CP Chirasil-Dex CB, 25 m column, internal diameter: 0.25 mm, film thickness: 0.25 μm, carrier gas: 120 kPa He, temperature: 90 ºC, rate 0.5 ºC/min to 120 ºC and hold for 3min.

Method 3: Gas chromatography. β-cyclodex 120, 30 m column, internal diameter: 0.25 mm, film thickness: 0.25 μm, carrier gas: 120 kPa He, temperature: 90 ºC, rate 0.5 ºC/min to 120 ºC and hold for 3min.

Method 4: HPLC. Chiralpack AD-H column, hexanes:iPrOH = 95:5, flow: 1 mL/min, λ: 245 nm.

Method 5: HPLC. Chiralpack OD-H column, hexanes:iPrOH = 99:1, flow: 1 mL/min, λ: 245 nm.

Product	Method	Ret. Time (min)	Product	Method	Ret. Time (min)
3xx76	2	35.73, 36.22	**3xx88**	1	14.00, 14.10
3xx77	1	3.18, 3.33	**3xx89**	1	15.71, 15.90
3xx78	1	4.75, 4.87	**3xx90**	1	28.69, 29.45
3xx79	1	8.14, 8.70	**3xx91**	1	10.08, 10.37
3xx80	1	8.22, 8.86	**3xx92**	3	19.42, 20.03
3xx81	1	16.19, 16.36	**3xx93**	1	4.29, 4.46
3xx82	1	-	**3xx94**	1	2.62, 2.75
3xx83	1	4.96, 5.17	**3xx95**	4	-
3xx84	1	3.49, 3.78	**3xx96**	2	7.30, 7.58
3xx85	1	9.26, 9.83	**3xx97**	2	5.24, 5.41
3xx86	1	7.30, 7.56	**3xx98**	2	34.44, 38.15
3xx87	2	56.18, 56.48	**3xx101**	5	-

X-ray crystallography

Data collections of structures reported were carried out at the X-ray diffraction beamline of the Elettra Synchrotron, Trieste (Italy), using the rotating crystal method with a monochromatic wavelength of 0.7000 Å, on a Pilatus detector. Measurements were performed at 100(2) K using a nitrogen stream cryo-cooler. Cell refinement, indexing and scaling of the data set were performed using the CCP4 package,[67] and programs Denzo and Scalepack.[68] The structure was solved by direct methods and Fourier analyses and refined by the full-matrix least-squares method based on F^2 with all observed reflections.[69] All the calculations were performed using the WINGX SYSTEM, Ver 2013.3.[70]

3.6. References

1. Ikariya, T. and Blacker, A. J. *Acc. Chem. Res.* **2007**, *40*, 1300-1308.
2. (a) Doucet. H.; Ohkuma, T.; Murata, K.; Yokozawa, T.; Kozawa, M.; Katayama, E.; England, A. F; Ikariya, T. and Noyori, R. *Angew. Chem. Int. Ed.* **1998**, *37*, 1703-1707. (b) Junge, K.; Schroder, K. and Beller, M. *Chem. Commun.* **2011**, *47*, 4849-4859. (c) Bullock, R. M. *Science* **2013**, *342*, 1054-1055. (d) Sues, P. E.; Demmans, K. Z. and Morris, R. H. *Dalton Trans.* **2014**, *43*, 7650-7667. (e) Bullock, R. M. Molybdenum and Tungsten Catalysts for Hydrogenation, Hydrosilylation and Hydrolysis, in *Catalysis without Precious Metals*, Wiley-VCH Verlag GmbH & Co., 2010, pp 51-81.
3. (a) Enthaler, S.; Junge, K. and Beller, M. *Angew. Chem. Int. Ed.* **2008**, *47*, 3317-3321. (b) Bauer, G. and Kirchner, K. A. *Angew. Chem. Int. Ed.* **2011**, *50*, 5798-5800.
4. Values based on www.platinum.matthey.com. Stated values are the average of the last three month period. In the case of iron the price based on scrap iron (www.metalprices.com).
5. (a) Morris, R. H. *Chem. Soc. Rev.* **2009**, *38*, 2282-2291. (b) Chakraborty, S. and Guan, H. *Dalton Trans.* **2010**, *39*, 7427-7436. (c) Nakazawa, H. and Itazaki, M. *Top. Organomet. Chem.* **2011**, *33*, 27-81. (d) Le Bailly, B. A. F. and Thomas, S. P. RSC *Adv.* **2011**, *1*, 1435-1445. (e) Darwish, M. and Wills, M. *Catal. Sci. Technol.* **2012**, *2*, 243-255.
6. For selected examples, see (a) Chen, K. and Que, L. *J. Am. Chem. Soc.* **2001**, *123*, 6327-6337. (b) Costas, M.; Tipton, A. K.; Chen, K.; Jo, D.-H. and Que, L. *J. Am. Chem. Soc.* **2001**, *123*, 6722-6723. (c) White, M. C.; Doyle, A. G. and Jacobsen, E. N. *J. Am. Chem. Soc.* **2001**, *123*, 7194-7195. Costas, M. and Que, L. *Angew. Chem. Int. Ed.* **2002**, *41*, 2179-2181.
7. (a) Chen, M. S. and White, M. C. *Science* **2007**, *318*, 783-787. (b) Chen, M. S. and White, M. C. *Science* **2010**, *327*, 566-571. (c) Bigi, M. A.; Reed, S. A. and White, M. C. Nat. Chem. 2011, 3, 216-222. (d) Bigi, M. A.; Liu, P.; Zou, L; Houk, K. N. and White, M. C. *J. Am. Chem. Soc.* **2012**, *134*, 9721-9726.
8. (a) Bianchini, C.; Peruzzini, M. and Zanobini, F. *Organomet. Chem.* **1988**, *354*, C19-C22. (b) Bianchini, M.; Meli, A.; Peruzzini, M.; Frediani, P.; Bohanna, C.; Esteruelas, M. A. and Oro, L. *Organometallics* **1992**, *11*, 138-145.
9. Buchard, A.; Heuclin, H.; Auffrant, A.; Le Goff, X. F. and Le Floch, P. *Dalton Trans*, **2009**, 1659-1667.
10. For selected examples, see: (a) Mikhailine, A.; Lough, A. J. and Morris, R. H. *J. Am. Chem. Soc.* **2009**, *131*, 1394-1395. (b) Meyer, N.; Lough, A. J. and Morris, R. H. *Chem. Eur. J.* **2009**, *15*, 5605-5610. (c) Sui-Seng, C.; Haque, F. N.; Hadzovic, A.; PÜtz, A-M.; Reuss, V.; Meyer, N.; Lough, A. J.; Zimmer-

De Iuliis, M. and Morris, R. H. *Inorg. Chem.* **2009**, *48*, 735-743. (d) Mikhailine, A. A.; Maishan, M. I. and Morris, R. H. *Org. Lett.* **2012**, *14*, 4638-4641.

11. (a) Yu, S.; Shen, W.; Li, Y.; Dong, Z.; Xu, Y.; Li, Q.; Zhang, J. and Gao, J. *Adv. Synth. Catal.* **2012**, *354*, 818-822. (b) Li, Y.; Yu, S.; Wu, X.; Xiao, J.; Shen, W.; Dong, Z. and Gao, J. *J. Am. Chem. Soc*, **2014**, *136*, 4031-4039.

12. Bigler, R.; Otth, E. and Mezzetti, A. *Organometallics*, **2014**, *33*, 4086-4099.

13. For a review on structural aspects of tri- and tetradentate P- and P,N donor ligands, see: Hierso, J. C.; Amardeil, R.; Bentabet, E.; Broussier, R.; Gautheron, B.; Meunier, P. and Kalck, P. *Coord. Chem. Rev*. **2003**, *236*, 143-206.

14. Marxen, T. L.; Johnson, B. J.; Nilsson, P. V. and Pignolet, L. H. *Inorg. Chem.* **1984**, *23*, 4663-4670.

15. Knight, P. D. and Scott, P. *Coord. Chem. Rev.* **2003**, *242*, 125-143.

16. Jeffery, J. C.; Tucker, P. A. and Rauchfuss, T. B. *Inorg. Chem*. **1980**, *19*, 3306-3316.

17. (a) Gao, J. X.; Ikariya, T. and Noyori, R. *Organometallics*, **1996**, *15*, 1087-1089. (b) Noyori, R and Hashiguchi, S. *Acc. Chem. Res.* **1997**, *30*, 97-102.

18. Mezzetti, A. *Dalton Trans*. **2010**, *39*, 7851-7869.

19. Zhou, S.; Fleischer, S.; Junge, K.; Das, S.; Addis, D. and Beller, M. *Angew. Chem. Int. Ed.* **2010**, *49*, 8121-8125.

20. Mikhailine, A. A.; Kim, E.; Dingels, C.; Lough, A. J. and Morris, R. H. *Inorg. Chem.* **2008**, *47*, 6587-6589.

21. (a) Lagaditis, P. O.; Lough, A. J. and Morris, R. H. *Inorg. Chem.* **2010**, *49*, 10057-10066. (b) Sues, P. E.; Lough, A. J. and Morris, R. H. *Organometallics*, **2011**, *30*, 4418-4431.

22. Sui-seng, C.; Freutel, F.; Lough, A. J. and Morris, R. H. *Angew. Chem. Int. Ed.* **2008**, *47*, 940-943.

23. For a comparison between 6,5,6 and 5,5,5 M-P-N ring systems, see: Sonnenberg, J. F. and Morris, R. H. Catal. *Sci. Technol.* **2014**, *4*, 3426-3438.

24. Mikhailine, A. A. and Morris, R. H. *Inorg. Chem*. **2010**, *49*, 11039-11044.

25. Noyori, R. Ohkuma, T. *Angew. Chem. Int. Ed.* **2001**, *40*, 40-73.

26. Guo, R.; Chen, X.; Espelt, C.; Song, D. and Morris, R. H. *Org. Lett.* **2005**, *7*, 1757-1759.

27. Moser, W. R.; Papile, C. J.; Brannon, D. A.; Duwell, R. A. and Weininger, S. J. *J. Mol. Catal.* **1987**, *41*, 271-282.

28. Palo, D. R. and Erkey, C. *Organometallics*, **1999**, *19*, 81-86.

29. Noyori, R. *Angew. Chem. Int. Ed*. **2002**, *41*, 2008-2022.

30. Chapham, S. E.; Hadzovic, A. and Morris, R. H. *Coord. Chem. Rev*. **2004**, *248*, 2201-2237.

31. Gao, J. X.; Zhang, H.; Yi, X. D.; Xu, P. P.; Tang, C. L.; Wan, H. L. Tsai, K. R. and Ikariya, T. *Chirality* **2000**, *12*, 383-388.

32. Haack, K. J.; Hashiguchi, S.; Fujii, A.; Ikariya, T. and Noyori, R. *Angew. Chem. Int. Ed. Engl.* **1997**, *36*, 285-287.

33. Zhang, H.; Yang, C. B.; Li, Y. Y.; Donga, Z. R.; Gao, J. X.; Nakamura, H.; Murata, K. and Ikariya, T. *Chem. Commun.* **2003**, 142-143.

34. Li, B. Z.; Chen, J. S.; Dong, Z. R.; Li, Y. Y.; Biao, Q. and Gao, J. J. *J. Molec. Catal. A. Chem*. **2006**, *258*, 113-117.

35. Gao, J. J.; Yi, Z. D.; Xu, P. P.; Tang, C. L.; Wan, H. L. and Ikariya, T. *J. Molec. Chem*. **1999**, *592*, 290-2295.

36. Naud, F.; Spindler, F.; Rueggeberg, C. J.; Schmidt, A. T. and Blaser, H. U. *Org Process Res. Dev.* **2007**, *11*, 519-523.

37. Correa, A.; Mancheno, O. G. and Bolm, C. *Chem. Soc. Rev*. **2008**, *37*, 1108-1117.

38. Casey, C. P. and Guan, H. *J. Am. Chem. Soc.* **2007**, *129*, 5816-5817.

39 . Shaikh, N. S.; Enthaler, S.; Junge, K. and Beller, M. *Angew. Chem. Int. Ed.* **2008**, *47*, 2497-2501.

40. Trovitch, R. J.; Lobkovsky, E.; Bill, E. and Chirik, P. J. *Organometallics* **2008**, *27*, 1470-1478.

41. Suzuki, K.; Oldenburg, P. D. and Que Jr, L. *Angew. Chem. Int. Ed*. **2008**, *47*, 1887-1889.

42. Bohr, M. D.; Bhanushali, M. J.; Nandurkar, N. S. and Bhanage, B. M. *Tetrahedron Lett*. **2008**, *49*, 965–969.

43. Chen, J. S.; Chen, L. L.; Xing, Y.; Chen, G.; Shen, W. Y.; Dong, Z. R.; Li, Y. Y. and Gao, J. X. *Acta Chim. Sin*. (Huaxue Xuebao), **2004**, *62*, 1745-1750.

44. Sonnenberg, J.; Coombs, N.; Dube, P. A. and Morris, R. H. *J. Am. Chem. Soc.* **2012**, *134*, 5893-5899.

45. Prokopchuk, D. E.; Sonnenberg, J. F.; Meyer, N.; Zimmer-De Iuliis, M.; Lough, A. J. and Morris, R. H. *Organometallics* **2012**, *31*, 3056-3064.

46. Gladiali, S. and Alberico, E. *Chem. Soc. Rev*. **2006**, *35*, 226-236.

47. Lagaditis, P. O.; Lough, A. J. and Morris, R. H. *J. Am. Chem. Soc.* **2011**, *133*, 9662-9665.

48. Mikhailine, A. A.; Maishan, M. I.; Lough, A. J. and Morris, R. H. *J. Am. Chem. Soc*. **2012**, *134*, 12266-12280.

49. Zuo, W.; Lough, A. J.; Li, Y. F. and Morris, R. H. *Science* **2013**, *342*, 1080-1083.

50. Rautenstrauch, V.; Hoang-Cong, X.; Churlaud, R.; Abdur-Rashid, K. and Morris, R. H. *Chem. Eur. J.* **2003**, *9*, 4954-4967.

51. Baratta, W.; Benedetti, F.; Del, Z. A.; Fanfoni, L.; Felluga, F.; Magnolia, S.; Putignano, E. and Rigo, P. *Organometallics* **2010**, *29*, 3563-3570.

52. Biegler, R. and Mezzetti, A. *Org. Lett*. **2014**, *16*, 6460-6463.

53. Biegler, R.; Huber, R. and Mezzetti, A. *Angew. Chem. Int. Ed.* **2015**, *54*, 5171-5174.

54. Kürti, L. and Czakó, B., *Strategic application of named reactions in organic synthesis,* Elsevier, **2005**, p. 294.

55. Fieser, L.F. and Fieser, M. *Reagents for Organic Synthesis,* vol.1; John Wiley and Sons, Inc.: New York, **1967**; p.446.

56. Skarzewski, J. and Gupta, A. *Tetrahedron: Asymmetry* **1997**, *8*, 1861-1867.

57. (a) Zhang, J.; Gandelman, M.; Herrman, D.; Leitus, G.; Shimon, L. J. W.; Ben-David, Y. and Milstein, D. *Inorg. Chim. Acta* **2006**, *359*, 1955-1960. (b) Schmiege, B. M.; Carney, M. J.; Small, B. L.; Gerlach, D. L. and Halfen, J. A. *Dalton Trans*. **2007**, 2547-2562.

58. Zell, T.; Langer, R.; Iron, M. A.; Konstantinovski, L.; Shimon, L. J. W.; Diskin-Posner, Y.; Leitus, G.; Balaraman, E.; Ben-David, Y. and Milstein, D. *Inorg. Chem*. **2013**, *52*, 9636-9649.

59. Son, K., Pearson, D.M; Jeon, S. and Waymouth, R. M. *Eur. J. Inorg. Chem.* **2011**, 4256-4261.

60. Lihl, F. *Z. Metallkd.* **1953**, *44*, 160-166.

61. Widegren, J. A. and Finke, R. G. *J. Mol. Catal. A: Chem.* **2003**, *198*, 317−341.

62. Crabtree, R. H. *Chem. Rev.* **2012**, *112*, 1536−1554.

63. Rangheard, C.; de Julian Fernandez, C.; Phua, P. H.; Hoorn, J.; Lefort, L. and de Vries, J. G. *Dalton Trans.* **2010**, *39*, 8464−8471.

64. Clark, T. J.; Jaska, C. A.; Turak, A.; Lough, A. J.; Lu, Z. H. and Manners, I. *Inorg. Chem.* **2007**, *46*, 7394−7402.

65. Jaska, C. A.; Temple, K.; Lough, A. J.; Manners, I. *J. Am. Chem. Soc.* **2003**, *125*, 9424−9434.

66. Perrin, D. D.; Armarego, W. L. F. *Purification of Laboratory Chemicals*, 3rd ed., Pergamon Press, Oxford, **1989**.

67. Collaborative Computational Project, Number 4. *Acta Crystallogr.* **1994**, *Sect. D 50*, 760-763.

68. Otwinowski, Z. Minor, W, Processing of X-ray Difraction Data Collected in Oscillation Mode, Methods in Enzymology, vol 276: Macromolecular Crystallograpy, part A, 307-326 (Eds.; C. W. Carter Jr. R. M. Sweet), Academic Press, New York, 1997.

69. Sheldrich, G. M. *Acta Cryst*. **2008**, *A64*, 112-122.

70. Farrugia, L. J. *J. Appl. Crystallogr.* **1999**, *32*, 837-838.

CHAPTER 4

NOVEL ZINC COMPLEXES FOR THE SYNTHESIS OF CYCLIC CARBONATES FROM CO_2 AND EPOXIDES

4.1. INTRODUCTION

During the last century, the concentration of carbon dioxide (CO_2) in the atmosphere has been increasing continuously. This fact is clearly demonstrated by the current CO_2 concentration of 386 ppm which is far from the pre-industrial levels of 280 ppm.[1] Such drastic increase in CO_2 concentration has been considered the main responsible for the augment in earth's temperature. Therefore, the reduction, capture, or utilization of CO_2 release from industrial processes is one of the greatest scientific and technological challenges of the 21st century (Figure 4.1).[2]

Atmosphere

Generation

Capture

CO_2

Storage

Utilization

Extraction   Reaction

Tecnological uses
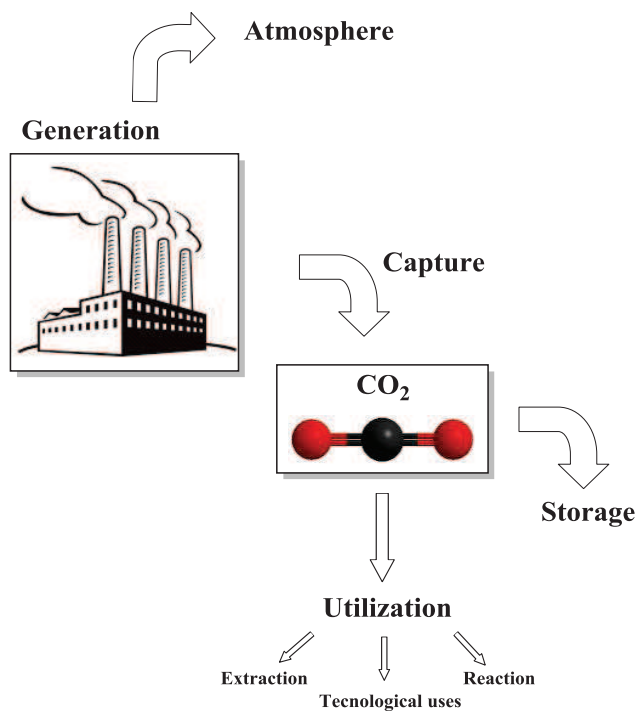
Figure 4.1. Generation, capture and utilization of industrial CO_2.

4.1.1. USES OF CO_2

CO_2 is an abundant, inexpensive, non-toxic and widely available renewable carbon source. However, its use for the production of valuable chemicals is often hampered due to its thermodynamic stability.[3,4] The development of chemical processes that can convert CO_2 into high added-value products is thus an important goal for scientists.[5]

The reduction of CO_2 into carbon containing products requires significant amounts of energy.[6] This energy can be economically produced by renewable energy, such as solar power. In this regard, the group of Traynor and Jensen have demonstrated the reduction of CO_2 using direct sunlight for the production of CO and O_2. Although this work is promising, further work is required in this field.[7]

CO_2 can also be used as solvent, as alternative to organic solvents. A supercritical fluid (SCF) is any substance above its critical temperature (T_c) and pressure (P_c) (Figure 4.2).
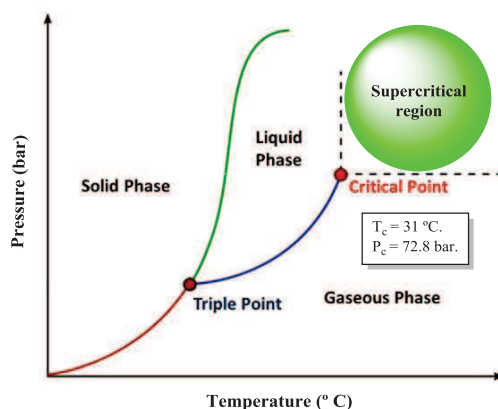
Figure 4.2. Qualitative representation of the CO_2 phase diagram.

The T_c for CO_2 is 304 K (31 ºC) and P_c is 72.8 bar (7.3 MPa) making the supercritical region easily accessible.[8] The properties of a SCF have been described as intermediate between gas and liquid having the advantages of both phases: high diffusivity and low viscosity. $ScCO_2$ can be employed as solvent for extraction and reactions. Interestingly, the solvent can be recycled resulting in a nearly zero waste. Its inherent properties: nontoxic, non-flammable, colourless makes $scCO_2$ an ideal extraction solvent for natural products.

CO_2 can be used for the synthesis of organic products such as esters, lactones, carbonates, methanol and urea among many others (Scheme 4.1).
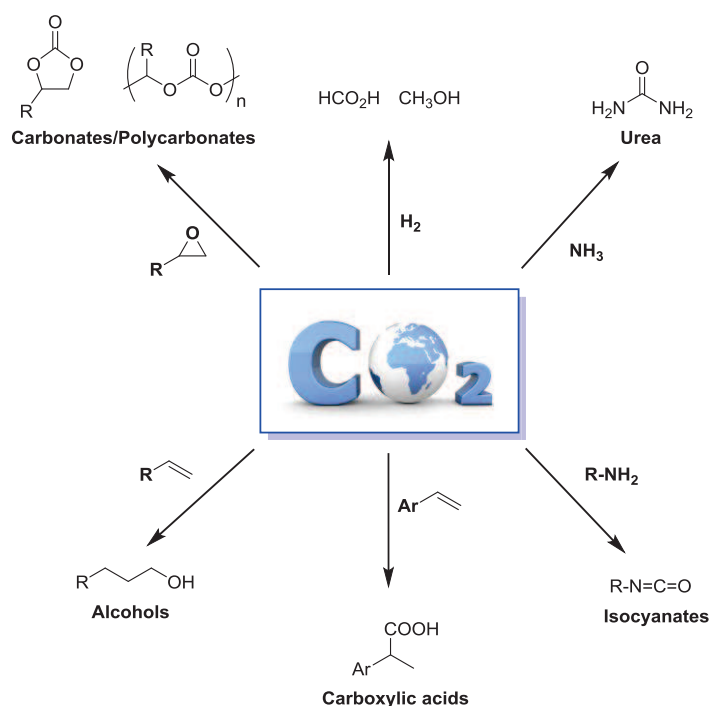
Scheme 4.1. Some examples of organic compounds produced from CO_2 utilization.

Approximately 90 Mt a^{-1} of CO_2 are used for such chemical syntheses; nevertheless, CO_2 is also manufacture of urea and methanol. In consequence, these processes might result in a net increase of CO_2 emissions.

4.1.1.1. REACTIONS USING CO_2

CO_2 is miscible with all gases in all proportion at above 304 K. Such properties are highly useful for reactions involving gases such as hydrogenation, hydroformylation and oxidation.[9]

The solubility of catalyst and reagent in the scCO_2 phase is an important factor in homogeneous catalysis with scCO_2, which frequently hamper their commercial developments.[10] A small number of industrial patents have been registered in this area.

In the case of hydrogenation reaction, Poliakoff and co-workers investigated the hydrogenation of a variety of aliphatic and aromatic substances in scCO_2 which lead to the construction of a pilot plant for the Thomas Swan Company in Durham (UK) by Chematur Engineering.[11] This company is also able to carry out Friedel-Craft acylation and alkylations.

scCO_2 has also been used in hydroformylation, for the production of aldehydes from alkenes involving CO and H_2.[12] Also in this case the reaction is restricted by the solubility and transport of the gases. The use of CO_2 as solvent had some beneficial effects such as reduction of the required pressure and temperature, waste by-products and improved selectivity.[9] Some patents can also be found in this field by the Thomas Swan Company[13] and Mitsubishi Chemical Co.[14]

As previously mentioned, CO_2 cannot be oxidized in presence of oxygen and catalysts; therefore it can be used in oxidation reaction to eliminate the solvent by-product waste. As example, CO_2 has been used in the conversion of propylene into propylene oxide using a silver catalyst and O_2 which is patented by the Lyondell Chemical Co.

CO_2 can also be employed in polymerization reactions. Polymers were produced in around 50 Mt in the USA in 2001.[15] In this reaction CO_2 can be employed as solvent, monomer and as nonsolvent. Nonetheless, it should be pointed out that the use of CO_2 as solvent in polymerization reactions is problematic, as the dissolution of polymers is very low due to its weak solvating power.[9]

$scCO_2$ is an alternative solvent in biocatalysis when non-aquous media is required. In particular, the stability of enzymes in $scCO_2$ and reaction rates are similar to those observed when *n*-hexane or cyclohexane are used as solvents.[16]

From an industrial and environmental point of view, the production of synthesis gas from the CO_2 reforming of CH_4 is considered an important reaction. This reaction involves the use of the two most abundant greenhouse gases to synthesis gas that is high in CO content which is highly valuable for the synthesis of oxygenated products.[17]

The use of CO_2 generated from industrial processes and power production can help into the CO_2 mitigation. However, large-scale applications are required in order to further reduce the impact of this greenhouse gas.

4.1.2. COUPLING OF CO_2 WITH EPOXIDES

One of the most successful processes for the use of CO_2 is the coupling with epoxides to produce polycarbonates and/or cyclic carbonates (Scheme 4.1).
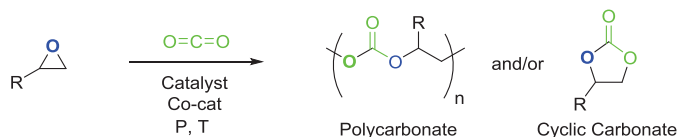
Scheme 4.1. Synthesis of polycarbonates and/or cyclic carbonates from CO_2 and epoxides.

Organic carbonates are important synthetic targets as a result of:

a) Thermodynamics: synthetic targets should be chosen taking into account the energy difference between the product and CO_2. In this regard, organic carbonates fulfil these criteria.

b) Environmental demand: phosgene is a reactive and available reagent for the synthesis of organic carbonates and isocyanates. However phosgene is highly toxic and corrosive which makes desirable to avoid its use as a reagent. As consequence, the use of CO_2 makes this process environmentally benign and 100% atom economical.[18]

c) Market size: organic carbonates are industrially useful products. In particular, the world annual production of aromatic polycarbonates is about two million tons. As example, four industrial organic carbonates are: dimethyl carbonate (DMC), diphenyl carbonate (DPC), ethylene carbonate (EC) and propylene carbonate (PC). DMC and DPC have open chain structure while EC and PC are cyclic.

4.1.2.1. APPLICATION OF ORGANIC CARBONATES

Polycarbonates, have various applications such as thermoplastics, packaging materials, etc. due to their inherent properties which include durability, heat resistance, strength, high transparency, electrical insulation and compatibility with other polymers.[19,20,21] Cyclic carbonates can also be used for numerous applications such as polar aprotic solvents, additives, plasticizers, electrolyte solvents for lithium-ion batteries, precursors for poly(carbonate) synthesis and more recently as useful intermediates in organic synthesis (Figure 4.3).[19,22,23,24]

Lithium Bateries

Aprotic Solvents

Additives

Plasticizers

Intermediates in organic synthesis

Figure 4.3. Applications of cyclic carbonate products.

4.1.2.2. INDUSTRIAL APPLICATIONS OF CYCLIC CARBONATES

The aim of this chapter is to synthesize cyclic carbonates, for this reason in this section some industrial application of cyclic carbonates will be presented.

Ethylene glycol (**4xx1**) is an important industrial chemical which has been traditionally synthesized by hydrolysis of ethylene oxide (Scheme 4.2, pathway A).[25] Nonetheless, the high reactivity of ethylene oxide has impeded the isolation of ethylene glycol without being contaminated by oligomers (**4xx2**), such as diethylene glycol and triethylene glycol. As consequence, expensive purification of the crude product was needed. In this regard, a process was developed by Mitsubishi Chemicals and Shell in which ethylene oxide is first converted to ethylene carbonate (**4xx3**) and then hydrolysis takes place to obtained the target ethylene glycol (Scheme 4.2, pathway B).[26] Although this is a two-step process, it has some advantages compared to pathway A such as lower reactivity of the ethylene carbonate (**4xx3**) when compared to the ethylene oxide which assures no oligomers as by-products and makes the purification procedure for ethylene glycol more convenient. Importantly, Shell has commercialized this process (also called OMEGA process) making 750 kt per year.
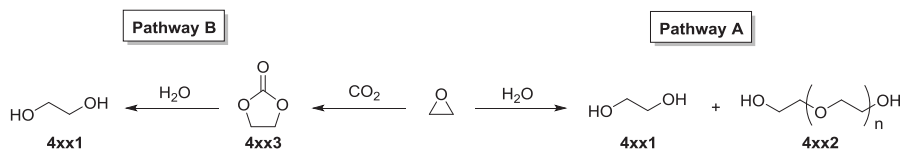
Scheme 4.2. Synthetic pathways for the production of ethylene glycol (**4xx1**).

Aromatic polycarbonate **4xx4** can be prepared by reaction of bisphenol A (**4xx5**) with phosgene. Nevertheless, as previously mentioned in section 4.1.2., phosgene is highly toxic and corrosive making desirable to find

alternatives for its use. In this regard, the Asahi Kasei corporation developed an alternative synthesis for polycarbonate **4xx4** avoiding the use of phosgene (Scheme 4.3).[27] This synthesis involves the use of diphenyl carbonate (**4xx6**) as phosgene replacement which is produced by transesterification of dimethyl carbonate (**4xx7**), which itself is produced from ethylene carbonate (**4xx3**) which come from the reaction of CO_2 with ethylene oxide. This process is used to prepare 50 kt of polycarbonate **4xx4** per year and also involves the production of ethylene glycol **4xx1** as co-product.
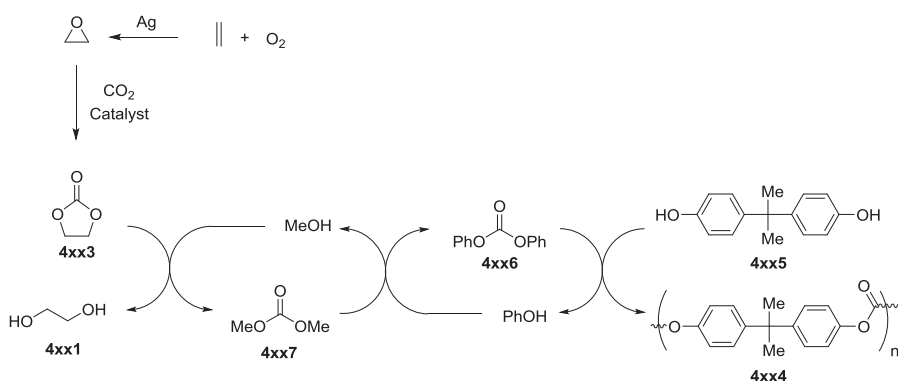
Scheme 4.3. Synthesis of aromatic polycarbonate **4xx4** developed by Asahi Kasei corporation.

4.1.2.3. MECHANISTIC CONSIDERATIONS

As previously mentioned in section 4.1.2, the coupling of CO_2 and epoxides can generate two types of products: polycarbonates and cyclic carbonates. The selective formation of the polymer or the carbonate product can be modulated by the catalytic system, substrate and reaction conditions employed. In all cases, the activation of the epoxide requires a nucleophile, which is the common feature of all catalytic systems employed for this

transformation. In addition, all mechanisms involve an intermediate containing a carbonate precursor, which can either react further through consecutive additions of other epoxide and CO_2 molecules (propagation) to generate the polycarbonate, or undergo back-biting reaction leading to ring closure with formation of the cyclic carbonate (Scheme 4.4).[28,29]
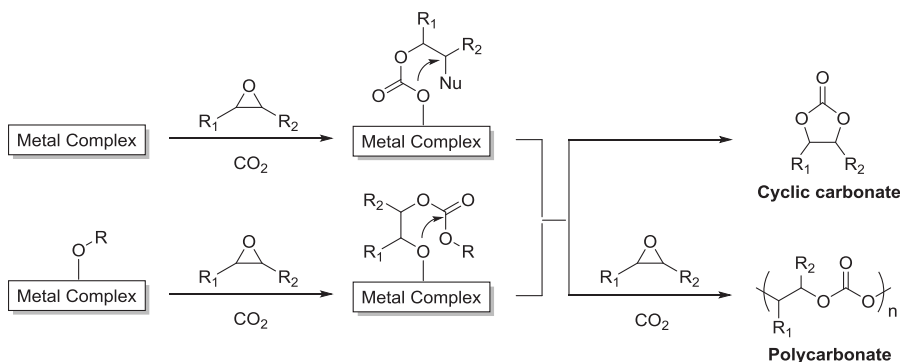
Scheme 4.4. Possible intermediates for the coupling of CO_2 with epoxides catalyzed by metal complexes. Nu is referred to nucleophile (from the metal complex or the co-catalyst). O-R is referred to alkoxide or aryloxide that can act as nucleophile. The arrows indicate possible back-biting reaction leading to the formation of cyclic carbonate product.

Catalysts for the coupling of CO_2 and epoxides include halides, quaternary alkyl ammonium or phosphonium salts, ionic liquids and metal complexes.[18] The use of halides, quaternary alkyl ammonium or phosphonium salts or ionic liquids (non-metallic catalysts), generally requires high temperatures (>80 ºC) to achieve high product yields which favours the formation of the thermodynamically more stable cyclic carbonate as product.[29] Nevertheless, the most studied type of catalysts for the coupling of CO_2 and epoxides are homogeneous metal complexes, which can be employed alone if they contain a ligand that can act as nucleophile, or in combination with a co-catalyst providing the nucleophilic

species. It has to be mentioned that heterogeneous catalysts have also been applied in the coupling of CO_2 and epoxides being zinc glutarate the most widely applied. Heterogeneous catalysts are considered to follow similar pathways than their homogeneous counterparts.[30]

Two main pathways have been described when homogeneous metal complexes are employed as catalyst for the coupling of CO_2 with epoxides:

Monometallic pathways:

a) The common monometallic mechanism is depicted in Scheme 4.5. First the epoxide coordinates to the Lewis acidic metal and gets activated towards the attack by the nucleophile. Then, nucleophilic attack takes place and ring opens the epoxide leading to the formation of a metal-bound alkoxide. This alkoxide can act as a nucleophile leading to the CO_2 insertion to the metal alkoxide bond, generating the carbonate intermediate which can led to the formation of the cyclic carbonate product or propagate by further addition of epoxide and CO_2 for the formation of the polycarbonate product.
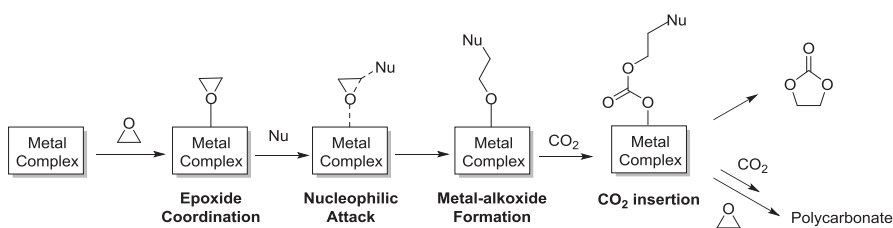
Scheme 4.5. Monometallic pathway involving one nucleophile.

b) Monometallic mechanism involving two nucleophiles. In this case one of the two nucleophiles involves in the mechanism is part of the metal complex as axial ligand (Nu_a) while the second nucleophile

(Nu$_b$) is added to the system and coordinates to the metal center in the remaining *trans* axial position, generating a six-coordinated intermediate (tetradentate ligand used). The coordination of the second nucleophile (Nu$_b$) serves to labilize the other metal-nucleophile bond which favours the coordination and nucleophilic attack of the epoxide generating the alkoxide species. The formed alkoxide species acts as nucleophile that attacks CO_2 to form a metal carbonate species (Scheme 4.6). It has been reported that the presence of a nucleophile in the *trans* position to this carbonate favour the further nucleophilic attack and ring opening of a new epoxide, meaning that the preferred path for this mechanism leads to the formation of polycarbonates.[31]
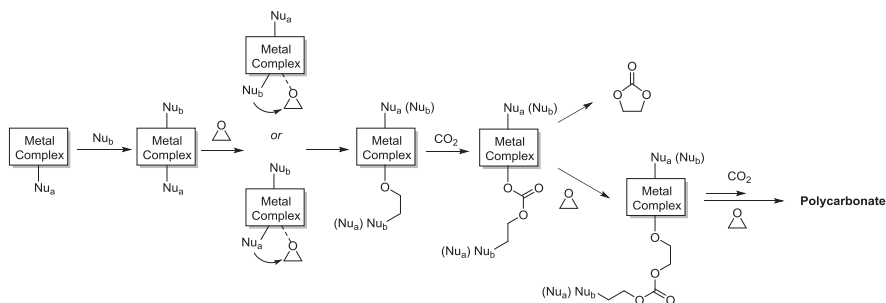
Scheme 4.6. Monometallic pathway involving two nucleophiles.

Bimetallic pathways: in this case the catalyst contains two metal centres or two monometallic catalysts act in collaboration.

a) Bimetallic mechanism involving two separate metal complexes. This mechanism is similar to the one reported for the monometallic mechanism (a) with the difference that the nucleophile that attacks the epoxide activated by the metal center is coordinated to a second metal (Scheme 4.7). This bimetallic initiation is followed by a monometallic pathway which leads to the formation of either the

cyclic carbonate by cyclization or the polycarbonate by propagation. This pathway is expected to occur when low ratios of epoxide/catalyst are used.[35] It is worth mentioning that the group of Darensbourg and co-workers has suggested that this mechanism is likely to be followed when a weaker Lewis base is used as co-catalyst, while the monometallic mechanism (b) is more likely to take place in presence of stronger Lewis base which are able to weaken the metal-nucleophile bond and allow concerted opening of the epoxide ring.[32]
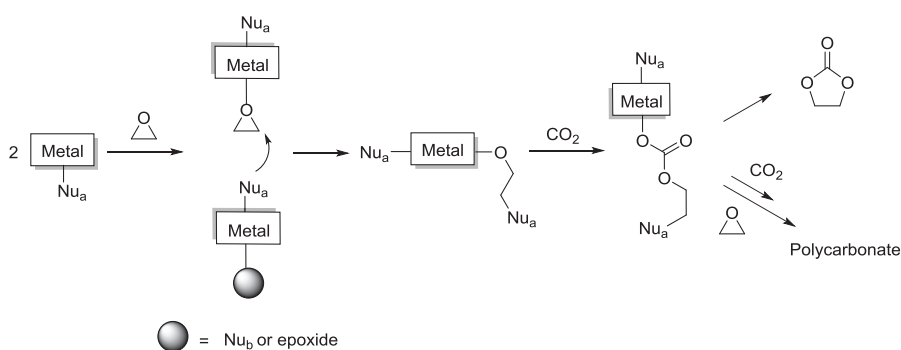
Scheme 4.7. Bimetallic pathway involving two metal complexes.

b) Metal complexes containing two neighbouring metal centers. In this case, the epoxide and the CO_2 might be activated simultaneously (Scheme 4.8). This promotes the intramolecular nucleophilic attack of the alkoxide to the carbon atom of the activated CO_2 molecule. It has been proposed that in this case the co-catalyst used plays a second role besides the ring opening of the epoxide. For instance, tetrabutylammonium bromide can decompose to tributylamine that can form a carbamate salt with CO_2 (Bu_3N^+-CO_2^-) and this salt coordinate more easily to the second metal center compared to CO_2 alone.
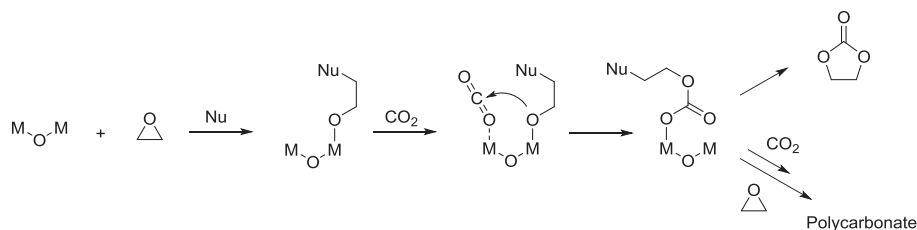
Scheme 4.8. Bimetallic pathway involving a metal complex with two neighbouring metal centers.

4.1.3. SYNTHESIS OF CYCLIC CARBONATES FROM CO_2 AND EPOXIDES

Cyclic carbonates are the thermodynamic products of the reaction and can be obtained from the coupling of CO_2 with epoxides, or by depolymerization of an initially formed aliphatic-polycarbonate. The formation of cyclic carbonates from CO_2 and epoxides is a highly exothermic reaction due to the reduction of ring-strain on converting the three-membered epoxide ring into a five-membered ring within the cyclic carbonate. As example, the synthesis of ethylene carbonate from ethylene oxide and CO_2 has a calculated $\Delta H = -140 kJmol^{-1}$.[33]

Since the pioneering work of Inoue and co-workers for the copolymerization of CO_2 with epoxides,[34] an increasing number of homogeneous and heterogeneous catalysts have emerged in this area.[24,35] In this section, highlighted homogeneous metal complexes for the coupling of CO_2 with epoxides and oxetanes will be presented.

The most common ligands reported for this process are based on Salen/Salphen and related ligands (N_2O_2),[36,37,38,39] tetraarylporphyrins (N_4),[40,41,42] Schiff bases (N_4),[43] β-diiminates[44] or substituted phenols and related ligands (N_2O/N_4O_2)[45].

Among all different homogeneous catalytic systems for the synthesis of cyclic carbonate products, salen and salphen metal complexes have been extensively studied. These ligands provided complexes with a preferred planar geometry with tetradentate coordination around the metal center. Depending on the nature of the metal center, these complexes can accommodate two labile ligands in two axial positions. Furthermore, the nucleophile can be embedded or weakly coordinated to the catalyst, resulting in a dual effect: it can act as a nucleophile and ring open the epoxide or favour the coordination of the epoxide to the metal center by a *trans* ligand effect.[29]

In 2007, the group of North and co-workers reported the use of a dinuclear μ-oxo-bridged Al(salen) complex which were active at room temperature and atmospheric pressure for the coupling of CO_2 with terminal and aromatic epoxides (Figure 4.4, **4xx8**).[46] Nonetheless, high catalyst loading (2.5 mol%) and long reaction times (24h) were required for the formation of cyclic carbonates in high yields. It is important to note that the bimetallic system showed higher activities than their monometallic counterpart.[47] This fact was attributed to the presence of two neighbouring metal centers able to activate simultaneously the epoxide and the CO_2 by promoting an intramolecular nucleophilic attack of the alkoxide to the carbon atom of the activated CO_2 molecule.[28,29]

In 2010, the group of Kleij and co-workers described the use of a highly active mononuclear Zn(salphen) complex (Figure 4.4, **4xx9**) for the coupling of CO_2 with terminal epoxides. Moderate CO_2 pressures ($p(CO_2)$ = 2-10 bar) and temperatures (25-45 ºC) were employed although high catalyst loadings (2.5 mol%) and limited scope of substrates was reported.[37]

A year later, the group of Williams and co-workers reported the use of a dinuclear, macrocyclic Fe(III) complex (Figure 4.4, **4xx10**) which is able to

form cyclic carbonates or polycarbonates depending on the co-catalyst used.[48] This system was able to work at temperatures between 25-80 ºC and low CO_2 pressures (1-10bar) although high reaction times were needed (24-120h).

Aminotriphenolate ligands have also been applied for the synthesis of cyclic carbonates from CO_2 and epoxides. In particular, the group of Kleij and co-workers have developed a family of Al(III)amino(triphenolate) complexes (Figure 4.4, **4xx11**) which shown to be highly active for this transformation.[49] Furthermore, a wide substrate scope and functional group tolerance was described. In terms of coordination, the aminotriphenolate ligands have trigonal bipyramidal coordination geometry around the metal center. In addition, the presence of fewer donor atoms in the plane of the metal would be beneficial for the coordination/activation of more sterically demanding substrates (such as internal epoxides) and might facilitate the approach of the nucleophile to the substrate and entering the coordination sphere of the metal.
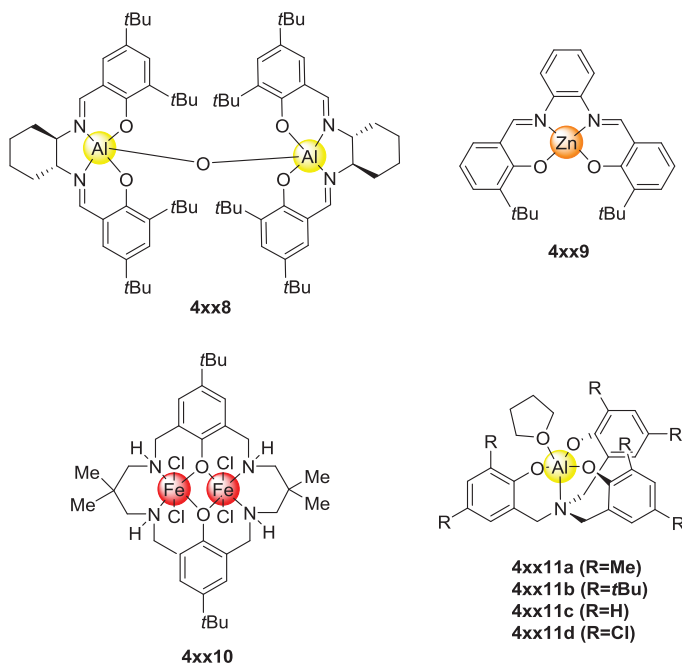
Figure 4.4. Sketch of homogeneous complexes for the synthesis of cyclic carbonates from CO_2 and epoxides.

Taking into account the activity of a catalyst through turnover numbers (TONs) and initial turnover frequencies (TOFs), some examples in the literature should be considered.

Porphyrin-based catalysts are powerful catalytic systems for the coupling of CO_2 with epoxides. These catalysts have planar geometry, which is beneficial for the coordination of terminal epoxides. In this sense, the group of Ema and co-workers reported the use of bifunctional metalloporphyrins complexes containing both, a Lewis acid center and nucleophilic pendant groups in the molecular structure.[40,41,42] Such catalysts provided one of the highest TONs reported for homogeneous metal-based systems without the use of a co-catalyst. Concretely, the use the Mg(II) porphyrin **4xx12** (Figure 4.5) gave a TON = 103.000 after 24h of reaction with an initial TOF =

12.000h^{-1}.[40] The authors suggested a cooperative effect of embedding the nucleophile moiety (Br) and the Lewis acidic metal center in a tight coordination sphere which lead to a simultaneous epoxide activation/ nucleophile attack.

In 2013, the group of Ghosh and co-workers reported the use of a Co(III) catalyst containing a bisamido-bisamine ligand with electron-withdrawing groups at the ligand framework that increase the Lewis acidity of the metal center. This binary catalyst **4xx13** exhibited an average TOF of 662 h^{-1} for the coupling of CO_2 with propylene oxide using a 0.05 mol% of catalyst loading, DMAP as co-catalyst (0.1 mol%), a CO_2 pressure of 20bar and a temperature of 130 ºC (Figure 4.5).[50] Importantly, not only terminal epoxides were converted to the corresponding cyclic carbonates but also cyclohexene oxide, although in this case higher temperatures were required (150 º C).

In the same year, the group of Kleij and co-workers reported the use of Al(III) catalysts containing aminotriphenolate ligands, also in this case with electron-withdrawing groups at the ligand framework. Concretely, catalyst **4xx11d** displayed an initial TOF of 36.000 h^{-1} and a TON>100.000 after 18h which is the higher reported for Al(III)-based catalysts (Figure 4.5).[49,51]

Recently, the group of Capacchione and co-workers reported the use of a dinuclear Fe(III) complex containing a dithioether-triphenolate ligand. The soft donor properties of sulphur ligands increase the Lewis acidity of the metal center, in comparison with nitrogen or oxigen ligands. The combination of the binuclear Fe(III) catalyst **4xx14** with TBAB provided a TON = 3480 and a TOF = 580 h^{-1} for the coupling of CO_2 with propylene oxide (Figure 4.5).[52]
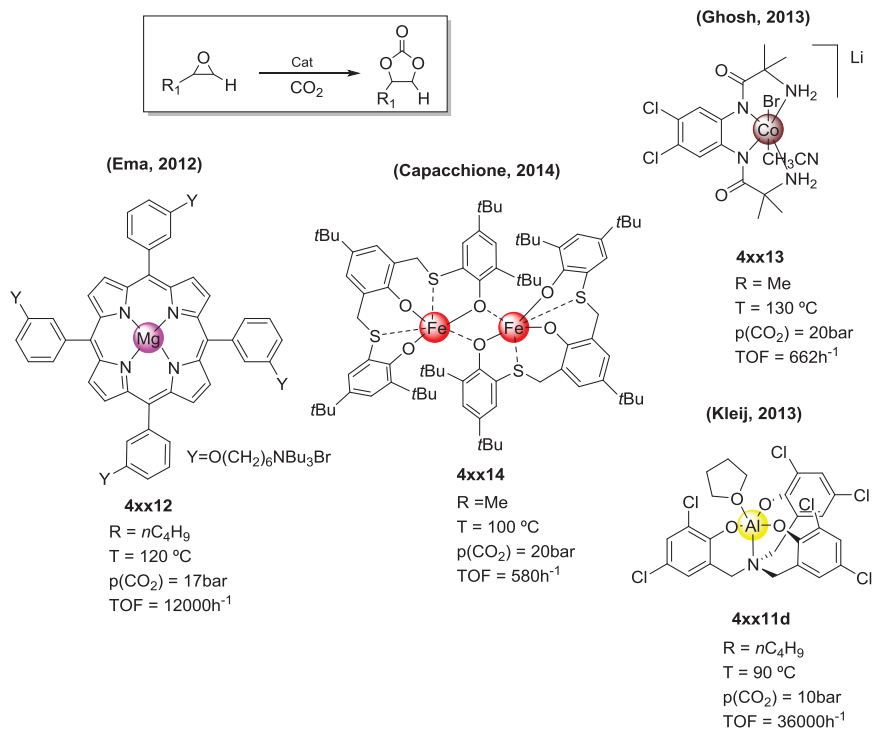
Figure 4.5. Homogeneous complexes exhibiting high catalytic activity for cyclic carbonate synthesis.

Internal epoxides have shown to be far less reactive than terminal or aromatic epoxides. Nonetheless, some catalytic systems can be found in the literature for the coupling of CO_2 with internal epoxides.

As previously mentioned, the group of North and co-workers reported the use of a µ-oxo-bridged Al(salen) **4xx8** for the coupling of CO_2 with terminal and internal epoxides. This catalyst exhibited moderate conversion towards the corresponding cyclic carbonates starting from 1,2-diphenyloxirane and 1,2-dimethyloxirane (Table 4.1, entries 1 & 2). It should be mentioned that complete conversion, in both cases, could be reached after 72h of reaction.[46]

Amino(trisphenolate)-based systems also shown to be highly active for the coupling of CO_2 with internal epoxides. In particular the group of Kleij and co-workers applied the above mentioned Al(III)amino(trisphenolate) catalyst **4xx11d** with very high conversion for 1,2-dimethyloxirane and 1,2-diphenyloxirane (Table 4.1, entries 3 & 4), with low catalyst loading, although high reaction times and temperature were required.[49] The same group also reported different substituted Fe(III)amino(trisphenolate) catalysts (**4xx15**, **4xx16a** and **4xx16b**) for the coupling of CO_2 with internal epoxides (Table 4.1, entries 5-7). In this case, lower reaction times were required to achieve conversion towards the cyclic carbonate from moderate to high (69-83%).[53,54]

In 2013, the group of Muralidharan and co-workers reported the use of Zn(II) and Cu(II) complexes containing 2,5-bis{*N*-(2,6-diidopropylphenyl)-iminomethyl}-pyrrole ligands (**4xx17a** and **4xx17b**) for the conversion of internal epoxides into the corresponding cyclic carbonates. Both catalysts exhibited moderate conversions towards the corresponding cyclic carbonates (36-42%), but they are active at room temperature and low CO_2 pressure.[55]

Table 4.1. Metal-catalyzed conversion of internal epoxides into the corresponding cyclic carbonates *via* coupling with CO_2.
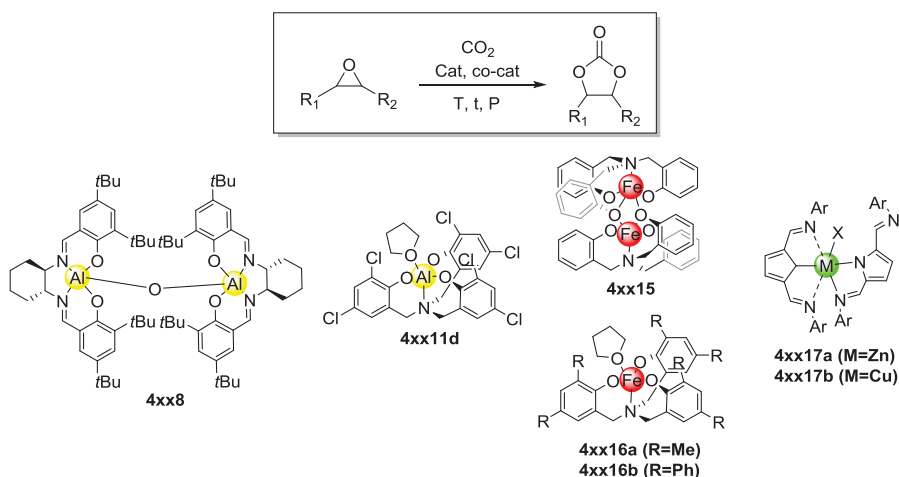
Entry	R_1	R_2	Cat (mol%)	Cocat (mol%)	T (ºC)	t (h)	$p(CO_2)$ (bar)	Conv. (%)
1[46]	Ph	Ph	**4xx8** (2.5)	TBAB 2.5	60	24	10	32
2[46]	Me	Me (cis)	**4xx8** (2.5)	TBAB 2.5	60	24	10	49
3[49]	Me	Me (trans)	**4xx11d** (0.5)	TBAB 5.0	90	42	10	99
4[49]	Ph	Ph	**4xx11d** (0.5)	TBAB 5.0	90	42	10	84
5[53]	Me	Me (trans)	**4xx15** (0.5)	TBAB 5.0	85	18	10	83
6[53]	Me	Me (trans)	**4xx16a** (0.5)	TBAI 5.0	85	18	2	69
7[53]	Me	Me (trans)	**4xx16b** (0.5)	TBAB 5.0	85	18	10	82
8[55]	Me	Me (cis)	**4xx17a** (2.5)	TBAB 5.0	25	24	1	42
9[55]	Me	Me (cis)	**4xx17b** (2.5)	TBAB 5.0	25	24	1	36

4.1.4. ZINC COMPLEXES FOR CYCLIC CARBONATE SYNTHESIS

The most efficient catalysts involve aluminium,[46,49] cobalt,[50] iron,[43,53] chromium[56,57] and zinc as the most suitable metals. Among those, Zn based complexes exhibit some advantages such as low toxicity, lower price and higher stability towards oxidation. In this section, an overview of the most important zinc complexes for the synthesis of cyclic carbonates will be presented.

Among all catalytic systems for the synthesis of cyclic carbonate products involving Zn as metal center, salphen ligands have been widely studied. In particular, the group of Kleij and co-workers have developed a series of mononuclear,[37,58] multinuclear[59,60,61] and bifunctional[62] Zn based complexes (Figure 4.6) for the coupling of CO_2 with epoxides. As previously outlined, the mononuclear Zn(salphen) complex **4xx9** exhibited moderate to high conversions for terminal and aromatic epoxides at low temperatures (25-45 ºC) and pressures (10bar) although high catalyst loadings (2.5 mol%) and time (18h) were required.[37] The same group reported the use of Zn(salphen) complex **4xx9** under scCO$_2$ conditions which allowed the coupling of CO_2 with epoxides in low reaction times (5h) although still high catalyst loadings (2.5 mol%). Importantly, moredate yields for cyclohexene carbonate were also achieved (38%).[58] The use of multinuclear complexes was also described by Kleij and co-workers. Concretely, the octanuclear Zn complex **4xx18** showed similar activity than that of the mononuclear complex **4xx9** for the coupling of CO_2 with propylene oxide at 0.24 mol% of catalyst loading, $p(CO_2) = 10$ bar, T = 45 ºC and 66h of reaction time.[61]

There is a growing interest for the development of bifunctional catalysts, as a result of their powerful catalytic performance and the possibility to recover and reuse them. Nonetheless, bifunctional catalysts have been less

developed than binary catalysts as a probable result of their synthetically demanding preparation. In this regard, the group of Kleij and co-workers reported the use of bifunctional Zn based complexes for the coupling of CO_2 with epoxides. Concretely, the bifunctional Zn complex **4xx19** exhibited high conversions for a wide range of terminal epoxides at 0.5 mol% of catalyst loading, $p(CO_2) = 10$ bar, T = 80º C and 18h of reaction. It is important to note that the bifunctional catalyst **4xx19** showed increase activity that the Zn(salpyr) **4xx20** alone. However, low conversion were achieved by the bifunctional catalyst **4xx19** (67%) compared to the binary system **4xx20**/TBAI (92%).[62]
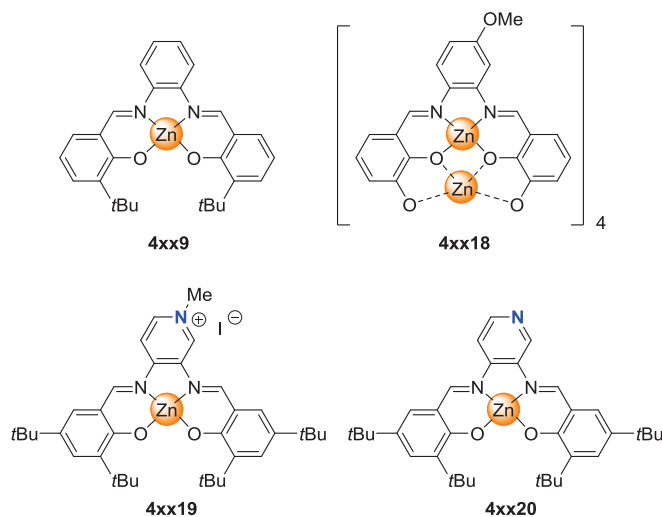
Figure 4.6. Selected Zn-based complexes reported by Kleij and co-workers.

In 2014, the group of Ji and co-workers reported the use of 2,2-bipyridine Zn(II) complexes bearing ionic liquids (IL) in the ligand structure. The Zn(II) complex **4xx21** (Figure 4.7) displayed moderate to high conversion (25-99%) for terminal and aromatic epoxides at 0.5 mol% catalyst loading, $p(CO_2) = 10$ bar, T = 100º C and 5h of reaction. It is important to note that the Zn(II) complex **4xx21** exhibited higher activity than that of the 2,2-

bipyridine Zn(II) complex without the IL in the structure or the IL alone. Furthermore, this bifunctional system could be recycled up to four times without appreciable lost of activity.[63]

In the same year, the group of Zevaco and co-workers reported the use of Zn(II) complexes displaying chelating N_2O_2 ligands with ancially nitrilo and/or ester groups for the coupling of CO_2 with epoxides. Catalyst **4xx22a** and **4xx22b** (Figure 4.7) exhibited a maximum TON = 7700 for the coupling of CO_2 with propylene oxide at 0.01 mol% of catalyst loading, $p(CO_2)$ = 50 bar, T = 80º C and 20h of reaction.[39,64]

In 2015, the same group published the use of Zn(II) complexes containing N_4-chelating ligands for the synthesis of cyclic carbonates from CO_2 and epoxides. Among the different Zn(II) complexes prepared, catalyst **4xx23** (Figure 4.7) bearing two chloride atoms at the phenyl moiety of the backbone showed the best results for the coupling of CO_2 with terminal and aromatic epoxides. Moderate to high conversions were achieved (27-84%) at 0.2 mol% of catalyst loading, $p(CO_2)$ = 50 bar, T = 80º C and 20h of reaction. In the case of cyclohexene oxide, low conversion towards the corresponding cyclic carbonate was accomplished (10%).[65]
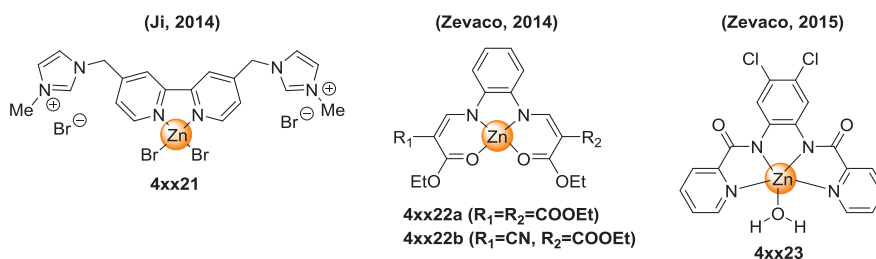
Figure 4.7. Selected Zn-based complexes reported for the synthesis of cyclic carbonates from CO_2 and epoxides.

Porphyrin-based catalysts are powerful catalytic systems for the coupling of CO_2 with epoxides. In this regard, the group of Ema and co-workers reported the use of bifunctional Zn catalysts bearing *m*-phenylene-bridged porphyrins dimer and trimer platforms for the synthesis of cyclic carbonates from CO_2 and epoxides. Concretely, the bifunctional trimer **4xx24** (Figure 4.8) showed a TON = 310.000 and a TOF = 40.000h^{-1} which are the highest values reported for the synthesis of cyclic carbonates from CO_2 and epoxides.[42]
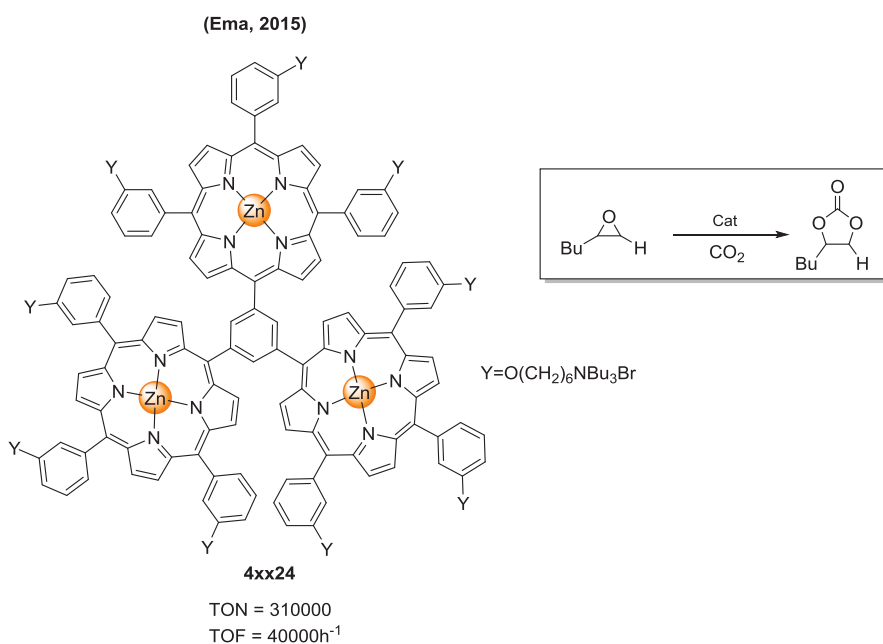
Figure 4.8. Bifunctional trimer **4xx24** reported by Ema and co-workers for the synthesis of cyclic carbonates CO_2 and epoxides.

It has to be mentioned that there is a small number of publications related to the use of Zn-based systems for the coupling of CO_2 with internal epoxides which are far less reactive than internal and aromatic epoxides. In this regard, the maximum conversion for the cyclohexene oxide (38%) was reported by the group of Kleij and co-workers using the above mentioned

Zn(salphen) **4xx9** at 2.5 mol% catalyst loading, $p(CO_2)$ = 80 bar, T = 80º C and 5h of reaction.[58] In the case of 2,3-dimethyloxirane, the group of Muralidharan reported the use of a Zn(II) complexs containing 2,5-bis{*N*-(2,6-diidopropylphenyl)-iminomethyl}-pyrrole ligand (**4xx17a**) also described above which obtained a 42% conversion towards the corresponding cyclic carbonate at 2.5 mol% catalyst loading, $p(CO_2)$ = 10 bar, T = 25º C and 24h of reaction.[55]

It should be pointed out that in all cases, high catalyst loadings are needed for the coupling of CO_2 with internal epoxides. Other internal epoxides or oxetanes have been converted in very low conversions (<5%) or no conversion has been achieved using Zn-based systems up to date.

4.2. OBJECTIVE OF THIS CHAPTER

As previously outlined, the concentration of carbon dioxide (CO_2) in the atmosphere has been increasing continuously. In this sense, the reduction, capture, or utilization of CO_2 release from industrial processes is one of the greatest scientific and technological challenges of the 21st century.

One of the most successful processes for the use of CO_2 is the coupling with epoxides to produce polycarbonates and/or cyclic carbonates. A large number of homogeneous and heterogeneous catalysts have been described for this transformation up to date.

The most efficient catalysts involved aluminium, cobalt, iron, chromium and zinc as the most suitable metals. However, Zn-based complexes exhibit some advantages such as low toxicity, lower price and higher stability towards oxidation.

In this context, we decided to prepare a family of chiral ligands containing a N_2O_2, N_2NH_2, N_4 and $N_4(NH)$ ligand scaffolds with a pyrrolidine backbone. Moreover, the corresponding Zn(II) complexes were prepared and fully characterized, and their catalytic performance in the coupling of CO_2 with epoxides was studied (Scheme 4.9). Additionally, recycling experiments for one of the catalytic systems were carried out in order to ascertain the robustness of the system.
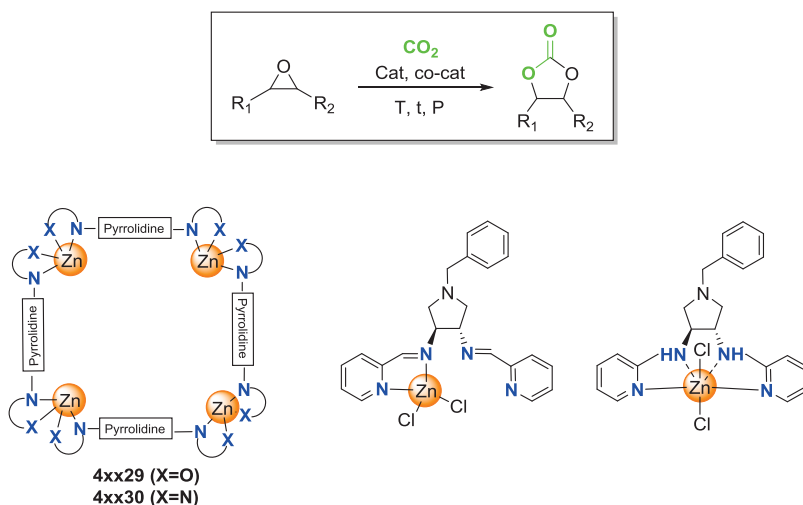
Scheme 4.9. Chiral Zn(II) complexes and their application in the coupling of CO_2 with epoxides.

4.3. RESULTS AND DISCUSSION

4.3.1. SYNTHESIS OF N_2O_2, N_2NH_2, N_4 AND $N_4(NH)$ LIGANDS AND RELATED ZINC COMPLEXES

The synthesis of the ligands N_2O_2 (**4xx25**), $N_2(NH)_2$ (**4xx26**), N_4 (**4xx27**) and N_4-NH (**4xx28**) was carried out by condensation of (*3R,4R*)-3,4-diamino-1-benzylpyrrolidine with two equivalents of the appropriate

aldehyde to yield the corresponding compounds in moderate to good yields (Scheme 4.10). It has to be mentioned that the chiral salen N_2O_2(pyrrolidine) **4xx25** has been synthesized by modifying a previously described procedure.[66] The ligands **4xx25-4xx28** were characterized using NMR spectroscopy, IR spectroscopy, HRMS and Elemental Analysis (see experimental part).
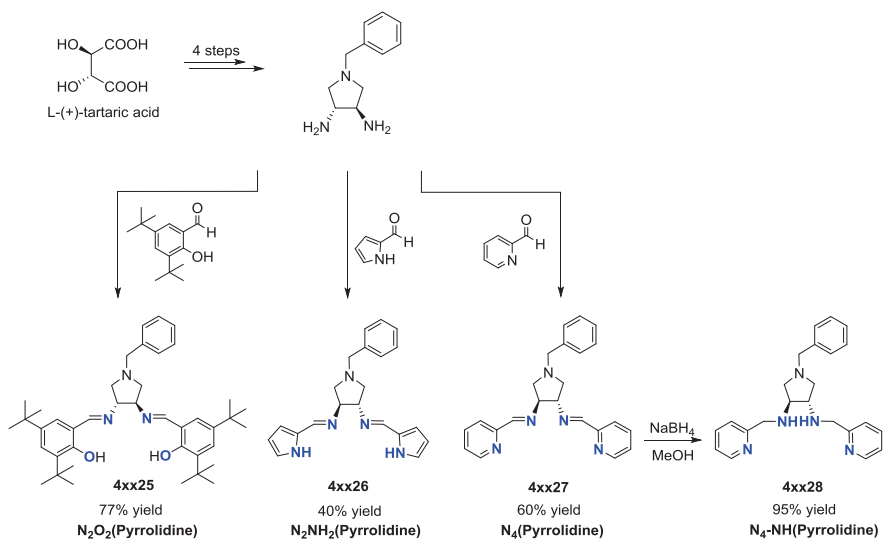
Scheme 4.10. Synthesis of chiral ligands (**4xx25**-**4xx28**).

The corresponding air stable Zn(II) complexes were synthesized by reaction with Et₂Zn (for **4xx29** and **4xx30** complexes) or with ZnCl₂/THF (for **4xx31** and **4xx32** complexes) (Scheme 4.11).
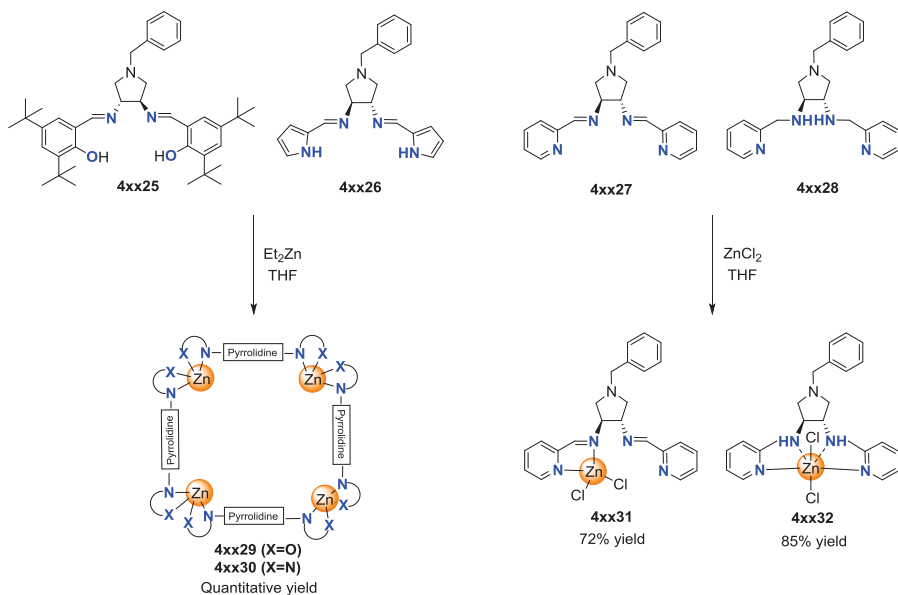
Scheme 4.11. Synthesis of Zn(II) complexes **4xx29**-**4xx32**.

In the ^{1}H NMR spectra of the complexes **4xx29** and **4xx30**, the detected resonances indicated the formation of symmetric species. Compared to the spectra of the ligands, the higher chemical shift observed for the CH=N moiety and the absence of broad OH/NH signals suggested the coordination of the ligands through the imine and phenoxo groups. Similarly, in the corresponding IR spectra, the absence of a strong absorption band in the ν(O-H) region (ca 3600 cm^{-1} for **4xx29** complex) and ν(N-H) region (ca 3400 cm^{-1} for **4xx30** complex), and the shift to lower frequencies of the ν(C=N) stretching band (ν(C=N)free ligand = 1625 cm^{-1} ν(C=N)complex = 1598 cm^{-1} for **4xx29** complex) and (ν(C=N)free ligand = 1633 cm^{-1} ν(C=N)complex = 1579 cm^{-1} for **4xx30**) confirmed a tetradentate coordination mode for both ligands. Importantly, the mass spectra (HRMS) of these complexes revealed the formation of tetrameric species of formula [Zn$_4$(L)$_4$]. This result was confirmed when crystals of **4xx29** suitable for X-

ray diffraction were obtained by vapor diffusion from EtOH in hexane at room temperature (Figure 4.9).
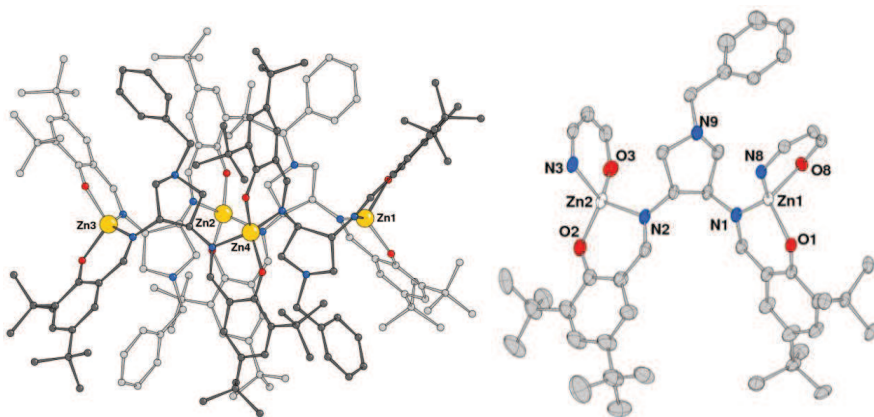
Figure 4.9. a) Crystal structure of the tetranuclear complex $[Zn_4(\mathbf{4xx25})_4]$ (only disordered groups at higher occupancy are shown); b) Detail of $[Zn_4(\mathbf{4xx25})_4]$ showing the ligand coordinated to zinc atoms Zn1 and Zn2 (probability ellipsoids at 40%; solvent molecules and H atoms are omitted for clarity and only a partial labelling scheme is illustrated).

The complex $[Zn_4(\mathbf{4xx25})_4]$ forms a cyclic tetrameric aggregate where the two N,O moieties of each ligand coordinate to two Zn atoms. The metals, located at a mean distance of 6.75 Å, afford a rhomboid arrangement with intermetallic angles of *ca.* 70 and 110°. The ligands are arranged in such a way that the benzyl-pyrrolidine moieties are located alternatively above and below the mean plane through the metal atoms, so that the complex presents a pseudo S_2-symmetry. Each Zn(II) atom, chelated by two salicylaldimine N,O donors from different ligands, exhibits a slightly distorted tetrahedral geometry with close comparable Zn-O and Zn-N bond distances (Table 4.2) that vary in the range 1.893(4)-1.921(3) and 2.000(3)-2.034(3) Å, respectively. The chelating O-Zn-N bond angles average at *ca.* 97.0°. All these data are within the range detected in other salicylaldimine tetranuclear

zinc complexes reported in the literature.[67,68] Nevertheless, few examples can be found in which two zinc metal atoms are bound to one ligand,[68] which is indeed our case scenario. This fact was attributed by Harder and co-workers to the rigidity of the backbone used.

Table 4.2. Selected Bond distances (Å) and Angles (deg) for [Zn$_4$(**4xx25**)$_4$].

Bond lenghts			
Zn(1)-O(1)	1.918(3)	Zn(2)-O(2)	1.903(3)
Zn(1)-O(8)	1.921(3)	Zn(2)-O(3)	1.900(3)
Zn(1)-N(1)	2.000(3)	Zn(2)-N(2)	2.021(3)
Zn(1)-N(8)	2.008(3)	Zn(2)-N(3)	2.030(3)
Bond angles			
O(1)-Zn(1)-N(1)	96.50(11)	O(2)-Zn(2)-N(2)	96.75(13)
O(8)-Zn(1)-N(8)	95.09(12)	O(3)-Zn(2)-N(3)	96.24(14)
O(1)-Zn(1)-O(8)	111.87(12)	O(2)-Zn(2)-O(3)	123.85(14)
O(1)-Zn(1)-N(8)	111.39(11)	O(2)-Zn(2)-N(3)	115.31(15)
O(8)-Zn(1)-N(1)	106.17(12)	O(3)-Zn(2)-N(2)	116.77(14)
N(1)-Zn(1)-N(8)	135.46(12)	N(2)-Zn(2)-N(3)	108.14(13)

In order to test the stability of such tetrameric structure, a sample of **4xx29** was dissolved in pyridine-d$_5$ and a ^{1}H-NMR spectrum was recorded. Two sets of signals were detected in a 1:10 ratio, indicating that two species were present under these conditions. The major product was characterized by NMR and MS (ESI-TOF) (see supporting information) and identified as the mononuclear complex **4xx33** (Scheme 4.12) containing a pyridine ligand coordinated to the zinc atom. Similar species were previously detected by Kleij and co-workers for a Zn(II) complex containing salphen ligands.[69] The minor product was attributed to unreacted **4xx29** tetranuclear complex.
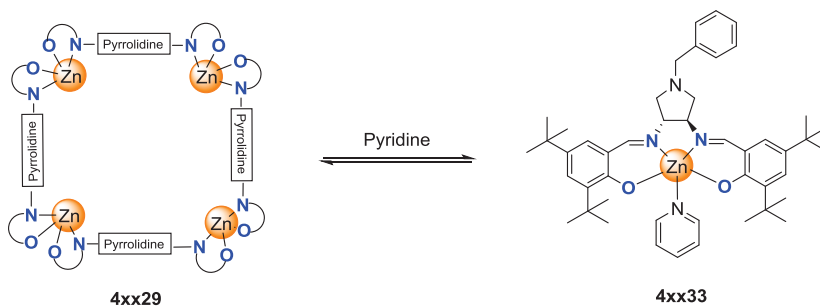
Scheme 4.12. Reactivity of the tetrameric **4xx29** complex in pyridine.

The zinc complexes **4xx31** and **4xx32** were synthesized in THF by reaction of the ligands **4xx27** and **4xx28** in the presence of $ZnCl_2$ at room temperature and isolated as orange powders in yields over 70%. Interestingly, 12 signals were detected in the ^{1}H NMR spectrum of complex **4xx31** at room temperature, indicating the formation of a C_2-symmetric complex. Furthermore, 7 of these resonances in both the aromatic and the aliphatic regions were broad, suggesting a fluxional behavior for this complex. These signals were attributed to the pyridine moiety at 8.70, 7.89 and 7.52 ppm, the C=N fragment (8.40 ppm), and three signals at 4.10, 3.42, 2.92 ppm corresponding to the CH- and CH_2- protons of the pyrrolidine backbone (Figure 4.10).

To clarify the structure of the complex, NMR spectra was recorded at low temperature (-66 °C) where new signals were detected (Figure 4.10). The 7 broad set of signals that appeared at room temperature were split into two sets of signals in all cases, indicating that the ligand was not symmetrically coordinating to the Zn centre.
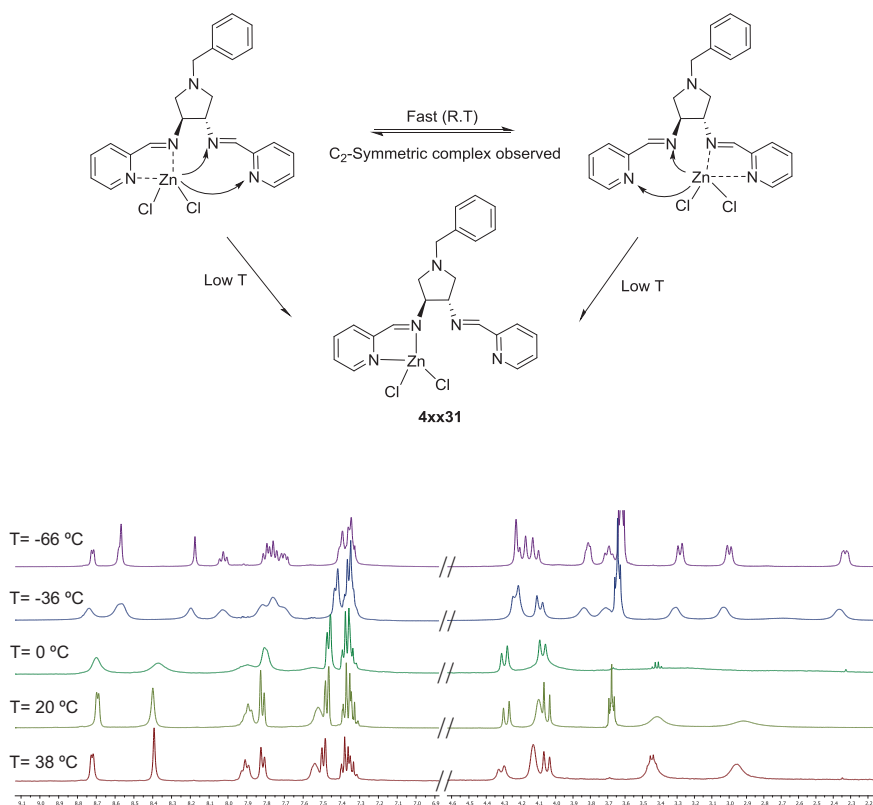
Figure 4.10. ^{1}H-NMR spectra of complex **4xx31** in CD_2Cl_2 at various temperatures (ºC).

In the IR spectrum of complex **4xx31**, two bands were detected in the $\nu(C=N)$ region at 1644 and 1597 cm^{-1}. The band at 1644 cm^{-1} was attributed to an uncoordinated imino group whereas the band at 1597 cm^{-1} was assigned to an imine moiety coordinated to Zn. This result was thus in agreement with the NMR observations. To gain information on the coordination of the chloride atoms in this complex, the molar conductivity of **4xx31** was recorded (0.001 M in THF) and the obtained value ($\Lambda_M = 0.062$ $\Omega^{-1} \cdot cm^2 \cdot mol^{-1}$) indicating the coordination of the chloride atoms to the zinc centre.

In view of these results, it can be concluded that a rapid exchange between the two "arms" of the ligand (one coordinated to Zn and one uncoordinated) occurs at room temperature, leading to the detection of a C_2-symmetric complex. At low temperature, this exchange process is slowed down and resonances for both the coordinated and uncoordinated arms were detected (Figure 4.10). X-ray diffraction of the mononuclear Zn (II) complex [Zn(**4xx27**)Cl$_2$] confirmed this hypothesis where the metal presents a distorted trigonal bipyramidal coordination geometry. An Ortep view of the complex is shown on Figure 4.11 and relevant bond lengths and angles are listed in Table 4.3.

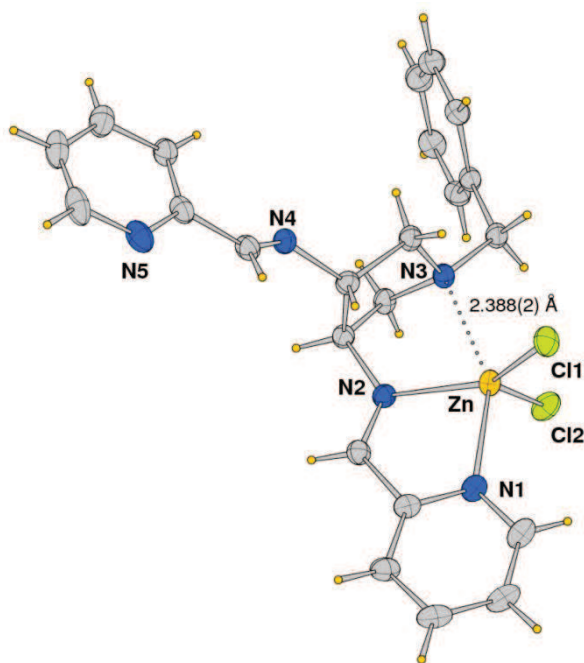**Figure 4.11.** Crystal structure for [Zn(**4xx27**)Cl$_2$] with probability ellipsoids drawn at the 50% level. Only a partial labelling scheme is illustrated for clarity.

The ligand acts as a tridentate species with pyridine N(1) and amine nitrogen N(3) occupying the axial positions in the TBP geometry, and the

two chlorides and the imine nitrogen N(2) are located in the equatorial plane. Remarkably, the imine nitrogen donor appears to be bound more strongly to Zn than the pyridine (Zn-N(2) of 2.0619(19) *vs* Zn-N(1) of 2.202(2) Å), while the pyrrolidine nitrogen N(3) has a significantly weaker interaction with the zinc atom (Zn-N(3) of 2.388(2) Å), nevertheless providing a stabilizing effect around the metal centre (Figure 4.11).

The N(1)-Zn-N(3) bond angle of 150.11(7)° and data of Table 4.3 give indication of the distortions from the ideal values around the coordination sphere due to the requirements to accomplish the formation of two five-membered rings.

Table 4.3. Selected Bond distances (Å) and Angles (deg) for [Zn(**4xx27**)Cl$_2$].

Bond lengths			
Zn-N(1)	2.202(2)	Zn-Cl(1)	2.229(7)
Zn-N(2)	2.062(19)	Zn-Cl(2)	2.247(7)
Zn-N(3)	2.388(2)		
Bond angles			
N(1)-Zn-N(2)	76.00(8)	N(2)-Zn-Cl(1)	123.30(6)
N(2)-Zn-N(3)	74.18(7)	N(2)-Zn-Cl(2)	116.01(6)
N(1)-Zn-N(3)	150.11(7)	N(3)-Zn-Cl(1)	97.21(5)
N(1)-Zn-Cl(1)	97.31(6)	N(3)-Zn-Cl(2)	94.68(5)
N(1)-Zn-Cl(2)	100.15(6)	Cl(1)-Zn-Cl(2)	120.55(3)

Recently, Yang and co-workers reported a series of Zn(II) complexes containing similar N$_4$ ligands and showed that the rigidity of the diamine backbone played a crucial role in the structure of the resulting complexes.[70] With flexible or semi-flexible backbones such as 1,4-diaminobutane or 1,2-cyclohexanediamine, the formation of dinuclear Zn(II) complexes of type [Zn$_2$(**L**)Cl$_4$] was observed, whereas with more rigid backbones such as 1,2-

phenylenediamine, mononuclear complexes of type [Zn(**L**)Cl$_2$], with only one imino and pyridine nitrogen bound to the metal center, were obtained. This suggests that our pyrrolidine backbone acts as a rigid backbone, leading to the formation of the mononuclear complex [Zn(**4xx27**)Cl$_2$] with only one imine and pyridine nitrogen atoms bound to the metal centre.

The ^{1}H-NMR spectrum of complex **4xx32** showed the expected signals when both the pyridine and the NH- groups are coordinated to the zinc atom. Mass spectrum (HRMS) exhibited a molecular peak at m/z = 472.1262 corresponding to the mononuclear species [ZnCl$_2$(**4xx28**)] (*calc* for C$_{23}$H$_{27}$N$_5$ClZn m/z = 472.1241 [M-Cl]$^+$). In addition, the molar conductivity of **4xx32** (0.001M in DMSO, Λ_M= 16.05 $\Omega^{-1} \cdot cm^2 \cdot mol^{-1}$) confirmed the coordination of the chloride atoms to the zinc metal. This complex was therefore identified as [Zn(*N,N*-**4xx28**)(Cl)$_2$] (Scheme 4.11).

4.3.2. COUPLING OF CO$_2$ WITH EPOXIDES

Complexes **4xx29**-**4xx32** were tested as catalysts in the coupling of CO$_2$ with 1,2-epoxyhexane as model substrate. The effect of the nature of the co-catalyst, catalyst/co-catalyst ratio, pressure and temperature were particularly looked at. Based on reported data, the initial conditions were 0.2 mol% catalyst loading (**4xx29** as catalyst), p(CO$_2$) = 30 bar, T= 80 °C in neat substrate for 16h. First, the effect of the co-catalyst was examined. These results are summarized in Table 4.4 .

Table 4.4. Screening of co-catalyst for the coupling of CO_2 with epoxides catalyzed by **4xx29**.[a]
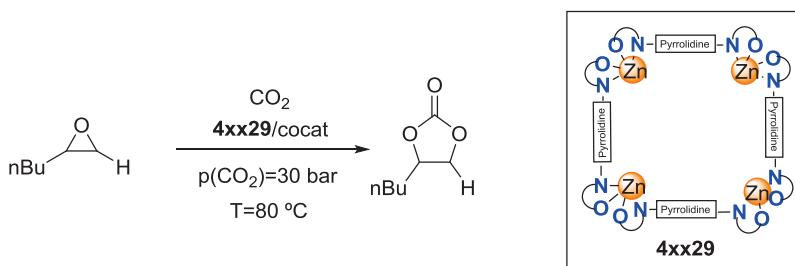
Entry	Cocat	Cat/Cocat ratio	Conv (%)[b]	TON[c]
1	-	-	0	-
2	TBAF	1/1	24	120
3	TBACl	1/1	12	60
4	TBABr	1/1	50	250
5	TBAI	1/1	73	365
6	DMAP	1/1	0	-
7	TBAI	1/2	83	415
8	TBAI	1/5	85	425

[a] General conditions: **4xx29**=0.2 mol%, T=80 ºC, PCO_2=30 bar, time=16h, 1,2-epoxyhexane=24.89 mmols (3ml); [b] measured by ^{1}H-NMR; [c] mol of substrate converted/mol of catalyst.

Under these conditions, no catalytic activity was observed using **4xx29** alone (Entry 1). With the addition of TBAF or TBACl, low conversions were obtained (Entries 2 and 3). However, using TBABr or TBAI as co-catalysts (Entries 4 and 5), an increase in conversion up to 73% was observed. The observed activity trend: iodide (73%) > bromide (50%) > chloride (12%) can be explained by the increased nucleophilicity of the anion, as previously reported.[3] Nonetheless, the use of 4-dimethyl-aminopyridine (DMAP) as co-catalyst did not provide any conversion (Entry 6). This could be due to the formation of a stable N_2O_2-Zn-DMAP

complex, as previously suggested by the groups of Rieger[71] and Zhang[72] for similar systems. Optimization of the cat/cocat ratio (Entries 5, 7 and 8) showed that a cat/cocat ratio of 1/2 provided the most active catalytic system with a conversion of 83% (Entry 7) into the corresponding cyclic carbonate. Importantly, low conversion towards the cyclic carbonate product was achieved using 0.4 mol% of TBAI alone (39%).

The effect of the temperature and pressure was also examined and revealed that the initial conditions (30 bar of CO_2 pressure and 80 °C of temperature) were the optimal values.

Then, the catalytic performance of complexes **4xx30**, **4xx31** and **4xx32** was investigated and compared to that of **4xx29** under the optimized conditions: T=80 °C, PCO_2=30 bar, ratio cat/cocat= 0.2/0.4 mol% and time=16h (Table 4.5).

Table 4.5. Coupling of CO_2 with epoxides catalyzed by **4xx29-4xx32**.[a]

Entry	Catalyst	Conv. (%)[b]	TON[c]
1	**4xx29**	83	415
2	**4xx30**	83	415
3	**4xx31**	>99(83)[d]	495(1660)
4	**4xx32**	>99(75)[d]	495(1500)

[a] General conditions: T=80 °C, PCO_2=30 bar, ratio cat/cocat= 0.2/0.4 mol% respect to the substrate, cocat= TBAI, time=16h, 1,2-epoxyhexane=24.89 mmols (3ml); [b] measured by ^{1}H-NMR; [c] mol of substrate converted/mol of catalyst. [d] at 0.05 mol% catalyst loading.
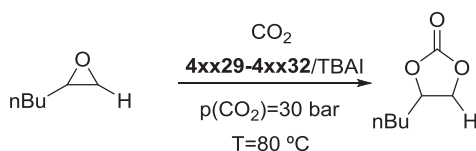
Interestingly, both systems containing a tetranuclear complex (Entry 1 and 2) behaved identically, providing 83% conversion to the corresponding cyclic carbonate while the **4xx31**/TBAI system displayed the highest activity of the series.

In order to exploit the potential of the complex **4xx31**, an optimization of the catalyst loading, amount of co-catalyst used, time and pressure was performed (Table 4.6). Reducing the catalyst loading up to 0.025 mol% a maximum TON of 2359 was achieved (Figure 4.12). It is also important to note that increasing the reaction time up to 60h, a TON of 4500 was reached at 0.01mol% of catalyst loading which indicates that the **4xx31** complex is highly robust. A maximum TOF of 480 h^{-1} was obtained at 0.05 mol% of catalyst loading (value calculated at 24% conversion).
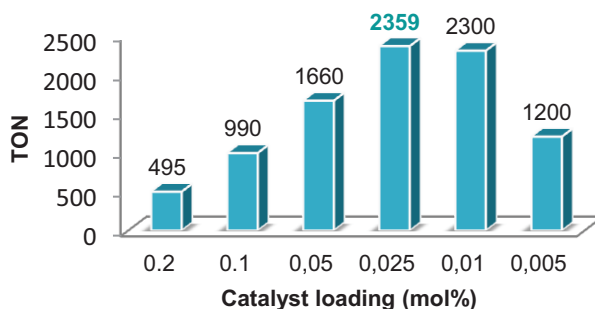
Figure 4.12. Optimization of TON using **4xx31**/TBAI catalytic system. Reaction conditions: ratio cat/cocat 1:2 in all cases, T= 80 ºC, PCO$_2$=30 bar, time=16h.

The optimal catalyst/co-catalyst ratio revealed to be 1:2 (Entry 2) as no improvement was achieved when the ratio was increased up to 1:5 (Entry 3). Increasing the temperature from 80 to 100 °C provided a slightly higher conversion (92%, Entry 4) whereas at 60 °C, a clear decrease of activity was observed (16%, Entry 6). Performing the reaction at 50 bar of CO$_2$

pressure (Entry 7) did not improve the activity of the catalyst while a decrease in activity was observed using 20 or 10 bar (Entries 8 and 9). Importantly, low conversion was observed using 0.1 mol% of TBAI alone (32%).

Table 4.6. Optimization of the amount of co-catalyst, temperature and pressure for the coupling of CO_2 and epoxides catalyzed by **4xx31**/TBAI.[a]
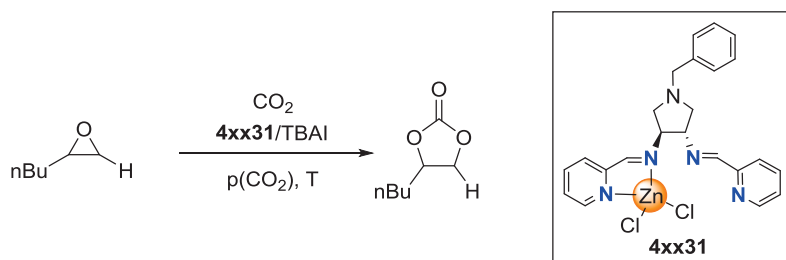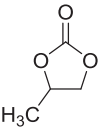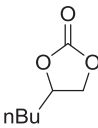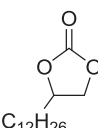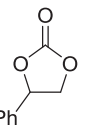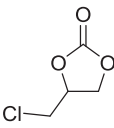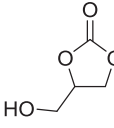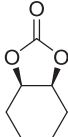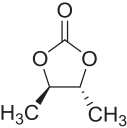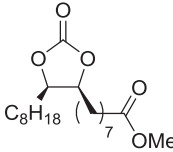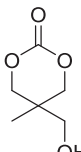
Entry	Cat/Cocat (mol%)[b]	Temp (°C)	PCO$_2$ (bar)	Conv. (%)[c]	TON[d]
1	0.025/0.025	80	30	34	1359
2	0.025/0.05	80	30	59	2359
3	0.025/0.125	80	30	60	2399
4	0.05/0.1	100	30	92	1840
5	0.05/0.1	80	30	83	1660
6	0.05/0.1	60	30	26	520
7	0.05/0.1	80	50	83	1660
8	0.05/0.1	80	20	70	1400
9	0.05/0.1	80	10	68	1360

[a] General conditions: Catalyst: **4xx31**, cocat= TBAI, time=16h, 1,2-epoxyhexane=24.89 mmols (3ml); [b] mol% respect to the substrate; [c] measured by ^{1}H-NMR; [d] mol of substrate converted/mol of catalyst.

In order to investigate the scope and limitations of these new zinc complexes, the **4xx31**/TBAI system was tested as catalyst for a variety of terminal and internal epoxides/oxetanes, including challenging substrates

such as styrene oxide, cyclohexene oxide, trans-2,3-epoxybutane and methyl epoxioleate (Table 4.7).[24] Exclusive formation of the cyclic carbonate product was observed by NMR spectroscopy for all substrates.

Table 4.7. Scope of the coupling of CO_2 with epoxides catalyzed by **4xx31**.

Yield: 89%
[Zn] = 0.05 mol%

Yield: 80%
[Zn] = 0.05 mol%

Yield: 67%
[Zn] = 0.1 mol%

Yield: 78%
[Zn] = 0.05 mol%

Yield: 72%
[Zn] = 0.1 mol%

Yield: 61%
[Zn] = 0.05 mol%

Yield: 34% (66%)[b],[c]
[Zn] = 0.3 mol%

Yield: 72%[b],[d]
[Zn] = 0.5 mol%

Yield: 46%[b],[c]
[Zn] = 0.5 mol%

Conv: 0%
[Zn] = 2 mol%

[a] General conditions: Catalyst: **4xx31**, cocat= TBAI, ratio cat/cocat= 1:2, T=80 ºC, PCO_2=30 bar, time=16 h. Selectivity towards the cyclic carbonate product was >99% in all cases, determined by ^{1}H-NMR in $CDCl_3$ except for glycidol (determined in DMSO-d_6). Yield determined using mesitylene as internal stardard. [b] Using TBABr as co-catalyst. [c] Selectivity towards the cis-product was observed. [d] Selectivity towards the trans-product was observed.

For terminal epoxides, the **4xx31**/TBAI catalytic system exhibited moderate to high activity with yields (67-89%). For alkyl substituted epoxides, the activity depended on the steric hindrance induced by the substituents (Me >

nBu > $C_{12}H_{26}$). The **4xx31**/TBAI catalytic system also provided high yield for styrene oxide (78%), which is higher than that obtained with the recently reported Zn-N_4/TBABr systems.[65] In addition, high TON was obtained when propylene oxide (1840) was the substrate. Good yields were also obtained using epichlorohydrin (72% using 0.1 mol% catalyst) and glycidol (61% using 0.05 mol% catalyst) as substrates.

Then, internal epoxides were tested as substrates. Cyclohexene oxide was converted into the corresponding cyclic carbonate in 66% yield using the **4xx31**/TBABr catalytic system. Compared to the Zn-salphen/TBAI system reported by Kleij[58] and co-workers (37% CHC, at 80 °C, 80 bar, 2.5 mol% catalyst loading and 3h), the **4xx31**/TBABr catalytic system operates at lower CO_2-pressure (30 bar) and lower catalyst loading (0.3 mol%), although longer reaction times are needed (16h). Regarding the tetrabutylammonium halides (TBAI and TBABr) tested for cyclohexene oxide, TBABr showed in this case higher conversion towards the cyclic carbonate. This can be explained due to the fact that bulky epoxides (such as cyclohexene oxide), once activated by the metal center, can be easily opened by the co-catalyst (halide) which need to fulfill these criteria: high nucleophilicity, good leaving group ability and small size. In this respect, bromide showed the best compromise for all these statements and thus displayed a higher activity. This trend has also been observed before.[54] For more challenging substrates such as trans-2,3-epoxybutane, a 72% yield towards the corresponding cyclic carbonate product was achieved at 0.5 mol% of catalyst loading. It has to be also highlighted the 46% yield (at 0.5mol% of catalyst loading) obtained for the methyl epoxioleate, which derives from a natural product. Nonetheless, no conversion was obtained for the more challenging substrate 3-methyl-2-oxetanemethanol.

To evaluate the robustness of the catalytic system, a typical recycling experiment was carried out with propylene oxide as substrate using the **4xx31**/TBAI catalytic system (reaction conditions: 3ml of epoxide, catalyst loading = 0.1 mol%, at 80 °C, 30 bar of CO_2, 16h, five consecutive runs). After the catalytic experiment, the catalyst was recovered by distillation to dryness of the volatiles and reused for a new batch reaction under identical conditions. The minimal loss of the catalyst observed during the recycling experiments was compensated by adjusting the amount of propylene oxide used in order to uphold the epoxide:catalyst ratio unchanged (1000:1). Practically full conversion was maintained for the first two cycles after which a small decrease was observed (92%) but also preserved up to the fifth cycle (Figure 4.13).
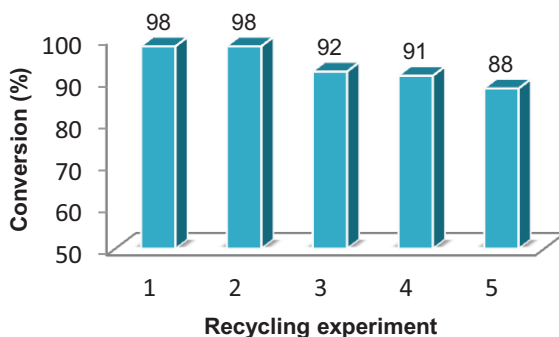
Figure 4.13. Recycling experiment using the **4xx31**/TBAI catalytic system. Reaction conditions: 3ml of propylene oxide, 0.1 mol% catalyst, T=80 °C, PCO_2=30 bar, time=16 h.

These promising results indicate the robustness and reusability of this catalytic system without relevant loss of neither activity nor selectivity for the coupling of carbon dioxide with epoxides.

4.3.3. MECHANISTIC CONSIDERATIONS

The proposed mechanistic cycle for the **4xx31** complex is shown in Figure 4.14. We proposed an initial coordination of the epoxide to the **4xx31** forming the penta-coordinated **4xx31-**substrate. Next, the ring-opening of the epoxide by the nucleophile (iodide) takes places producing a zinc-alkoxide intermediate which reacts with CO_2 to form a carbonate complex through insertion of CO_2 into the Zn-O bond. Finally, ring-closing and regeneration of the catalyst by coordination of another molecule of epoxide takes place.
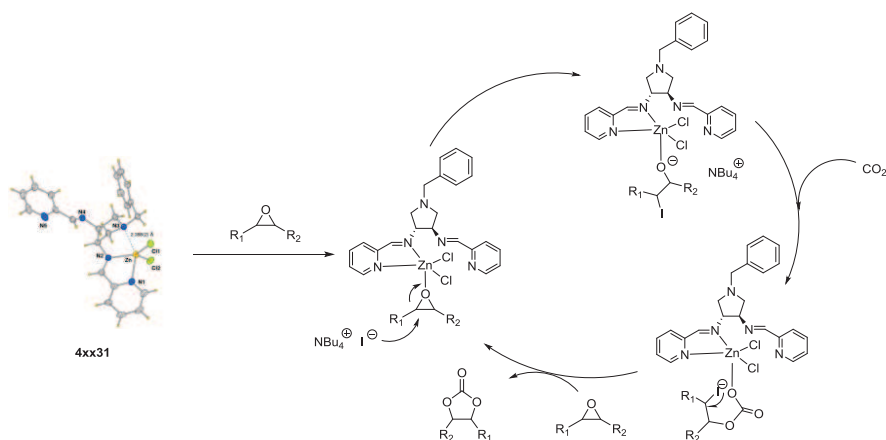
Figure 4.14. Proposed mechanism for the formation of the cyclic carbonate from the mononuclear comlex **4xx31**.

4.4. CONCLUSIONS

From the study described in this chapter, the following conclusions can be extracted:

i) Ligands N_2O_2(pyrrolidine) **(4xx25)**, N_2NH_2(pyrrolidine) **(4xx26**), N_4(pyrrolidine) **(4xx27)** and N_4(NH)(pyrrolidine) **(4xx28)** were

synthesized and fully characterized obtaining moderate to high yields (40-95%).

ii) The corresponding chiral Zn(II) complexes **4xx29-4xx32** were synthesized and fully characterized by NMR, IR, HRMS and EA. The X-ray structures of complexes **4xx29** and **4xx31** were also obtained.

iii) The Zn(II) complexes **4xx29-4xx32** efficiently catalyzes the coupling of CO_2 with 1,2-epoxihexane as substrat, being the **4xx31**/TBAI catalytic system the most active of the series.

iv) The **4xx31**/TBAI catalytic system catalyzes the coupling of CO_2 with a variety of terminal and aromatic epoxides with good to high conversions (61-89%) towards the corresponding cyclic carbonate at 0.05-0.1mol% of catalyst loading, $p(CO_2)$ = 30 bar, T = 80º C and 16h of reaction. Furthermore, internal epoxides such as cyclohexene oxide and 2,3-epoxybutane were efficiently converted to the corresponding cyclic carbonate (Conv.= 66% and 72% respectively) at 0.3-0.5mol% catalyst loading, $p(CO_2)$ = 30 bar, T = 80º C and 16h of reaction. Methyl epoxioleate that derives from a natural product was also converted in a 46% conversion using 0.5mol% catalyst loading, $p(CO_2)$ = 30 bar, T = 80º C and 16h of reaction.

v) The **4xx31**/TBAI catalytic system was recycled up to 5 times without appreciable lost of activity for the coupling of CO_2 with propylene oxide which demonstrated the robustness of the catalytic system.

4.5. EXPERIMENTAL PART

All preparations and manipulations were carried out under an oxygen-free nitrogen atmosphere using conventional Schlenk techniques. Solvents were purified by the system Braun MB SPS-800 and stored under nitrogen atmosphere. Reagents were purchased from Sigma-Aldrich and used as received. Carbon dioxide (SCF Grade, 99.999 %, Air Products) was used introducing an oxygen/moisture trap in the line (Agilent).

[1]H and ^{13}C spectra were recorded on a Varian Mercury VX 400 (400 MHz, 100.6 MHz, respectively). Chemical shift values for ^{1}H and ^{13}C were referred to internal $SiMe_4$ (0.0 ppm). 2D correlation spectra (gCOSY, gHSQC and gHMBC) were visualized using VNMR program (Varian®). IR spectra were recorded on a Midac Grams/386 spectrometr in KBr range (4000-600 cm^{-1}). ESI-HMRS and Elemental analysis were performed at the Serveis Tècnics de Recerca from the Universitat de Girona (Spain).

Synthesis of N_2O_2(pyrrolidine) (4xx25)
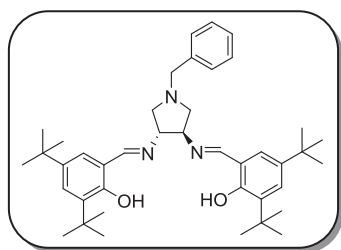
3,5-di-tert-butyl-2-hydroxybenzaldehyde (0.245g, mmol) was added to 4ml of toluene containing activated molecular sieves. Then, (3S,4S)-3,4-diamino-1-benzylpyrrolidine (0.1g, mmol) was added to the mixture. This solution was allowed to stir overnight at 90 ºC. The reaction was filtered through a pad of celite and evaporated to dryness. To this crude solid, methanol was added and the product precipitates. Then, the product was filtered and washed further with methanol. Evaporation to dryness afforded a yellow solid in 77% yield.

¹H-NMR (CDCl₃, 400 MHz, δ in ppm): δ = 13.42 (s, 2H, -OH), 8.17 (s, 2H, -HC=N), 7.29-7.14 (m, 7H, Ar-), 6.92 (d, 2H, J=4Hz, Ar-), 3.87 (quint, 2H, J=4Hz, -CH-), 3.62 (s, 2H, -CH₂-Ph), 3.01 (dd, 2H, J=4 & 8Hz, -CH₂), 2.82 (dd, 2H, J=4 & 8Hz, -CH₂), 1.34 (s, 18H, ᵗBu, -CH₃), 1.16 (s, 18H, ᵗBu, -CH₃). **¹³C-NMR** (CDCl₃, 100.6 MHz, δ in ppm): δ = 166.3 (C=N), 157.9 (C-OH), 140.2 (-C-), 138.4 (-C-), 136.6 (-C-), 128.8 (Ar-), 128.3 (Ar-), 127.2 (Ar-), 127.1 (Ar-), 126.2 (Ar-), 117.6 (-C-), 75.4 (-CH-), 60.3 (-CH₂), 60.1 (CH₂-Ph, -CH₂), 35.0 (-C-), 34.1(-C-), 31.4 (-CH₃) 29.4 (-CH₃). **IR** (KBr pellet): ν$_{C=N}$= 1625cm⁻¹. **ESI-HRMS:** Calculated for **C₄₁H₅₇N₃O₂**: Exact: (M: 623.4524, [M+H]⁺: 624.4524); Experimental ([M+H]⁺: 624.4509). **Elemental Analysis:** Calculated for **C₄₁H₆₁N₃O₂**: C, 78.93; H, 9.21; N, 6.73; Found: C, 78.26; H, 9.16; N, 6.41.

Synthesis of N₂NH₂(pyrrolidine) (4xx26)
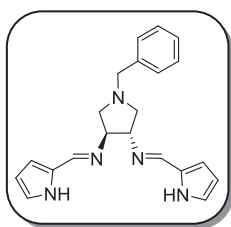
Pyrrole-2-carboxyaldehyde (197.8mg, 2.08 mmol) was added to 8ml of dry and degassed toluene containing activated molecular sieves. Then, (3R,4R)-3,4-diamino-1-benzylpyrrolidine (0.2g, 1.04mmol) was added to the mixture. Finally, few drops of acetic acid were added to the reaction mixture and the solution was allowed to stir overnight at 90ºC. The reaction was filtered through a pad of celite and evaporated to dryness to obtain a brown syrup. This syrup was triturated repeatedly with diethylether. After filtration, the organic solution was concentrated to dryness in order to afford the product as a bright orange-red powder in 40% yield.

¹H-NMR (CDCl₃, 400 MHz, δ in ppm): δ = 7.92 (s, 2H, -HC=N), 7.38-7.24 (m, 5H, Ar-), 7.01 (s, 2H, Pyrrole), 6.55 (d, 2H, J=4Hz, Pyrrole), 6.23 (t, 2H, J=4Hz, Pyrrole), 3.92 (quint., 2H, J=4Hz, -CH-), 3.77 (d, 1H, J=12Hz, -CH₂-Ph), 3.69 (d, 1H, J=12Hz, -CH₂-Ph), 3.08 (dd, 2H, J=4& 8Hz, -CH₂),

2.83 (dd, 2H, J=4 & 8Hz, -CH$_2$). **^{13}C-NMR** (CDCl$_3$, 100.6 MHz, δ in ppm): δ = 151.63 (C=N), 138.04 (-C-), 128.99 (Ar-), 128.88 (-C-), 128.26 (Ar-), 127.14 (Ar-), 123.51 (Pyrrole, -CH-), 116.49 (Pyrrole, -CH-), 110.29 (Pyrrole, -CH-), 74.81 (-CH-), 60.09 (-CH$_2$), 60.00 (-CH$_2$). **IR** (KBr pellet): v_{NH}= 3170cm^{-1} $v_{C=N}$= 1633cm^{-1}. **ESI-HRMS:** Calculated for **C$_{21}$H$_{23}$N$_5$**: Exact: (M: 345.2014; [M+H]$^+$: 346.2014); Experimental ([M+H]$^+$: 346.2026). **Elemental Analysis:** Calculated for **C$_{21}$H$_{23}$N$_5$·5CH$_2$Cl$_2$**: C, 40.55; H, 4.32; N, 9.09; Found: C, 40.48; H, 3.98; N, 9.59.
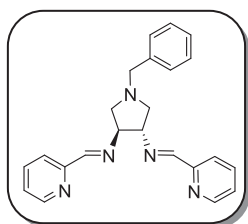
Synthesis of N$_4$(pyrrolidine) (4xx27)

2-Pyridinecarboxyaldehyde (0.198ml, 2.08 mmol) was added to 7ml of dry and degassed toluene containing activated molecular sieves. Then, (3R,4R)-3,4-diamino-1-benzylpyrrolidine (0.2g, 1.04mmol) was added to the mixture which was allowed to stir overnight at 90ºC. The reaction was filtered through a pad of celite and evaporated to dryness. To this crude solid, diethylether (2ml) was added and a white solid precipitate. The solution was filtered and evaporated. The residue was washed with hexane until the washings were colourless. The solid was dried to afford the product as a pale orange powder in 60% yield.

^{1}H-NMR (CD$_2$Cl$_2$, 400 MHz, δ in ppm): δ = 8.57 (d, 2H, J=4Hz, o-Py), 8.25 (s, 2H, -HC=N), 8.03 (d, 2H, J=4Hz, m-Py), 7.74 (t, 2H, J=8Hz, m-Py), 7.41-7.24 (m, 7H, Ar-), 4.09 (quint., 2H, J=4Hz, -CH-), 3.77 (d, 1H, J=12Hz, -CH$_2$-Ph), 3.74 (d, 1H, J=12Hz, -CH$_2$-Ph), 3.12 (dd, 2H, J=4& 8Hz, -CH$_2$), 2.90 (dd, 2H, J=4 & 8Hz, -CH$_2$). **^{13}C-NMR** (CD$_2$Cl$_2$, 100.6 MHz, δ in ppm): δ = 162.96 (C=N), 155.07 (Py, -C-), 149.86 (o-Py, CH-), 136.57 (-C-), 136.89 (m-Py, CH-), 129.39 (Ar-), 128.76 (Ar-), 127.50 (Ar-), 125.27 (p-Py, -CH-), 121.56 (m-Py, -CH-), 76.38 (-CH-), 60.79 (-CH$_2$), 60.74 (-CH$_2$). **IR** (KBr pellet): $v_{C=N}$= 1644cm^{-1}. **ESI-HRMS:** Calculated for

$C_{23}H_{23}N_5$: Exact: (M: 369.2026; $[M+H]^+$: 370.2026); Experimental ($[M+H]^+$: 370.2026). **Elemental Analysis:** Calculated for $C_{23}H_{23}N_5$: C, 74.77; H, 6.27; N, 18.96; Found: C, 74.41; H, 5.82; N, 18.56.

Synthesis of N₄-NH(pyrrolidine) (4xx28)
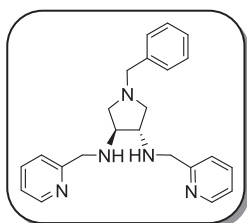
4xx27 (50mg, 0.135mmol) was dissolved in 5ml of dry methanol and placed in an ice bath (0ºC). Then, $NaBH_4$ (25.5mg, 0.675mmol) was added dropwise. The reaction was stirred at room temperature for 16h and H_2O (0.5ml) was added. The mixture was extracted with CH_2Cl_2 (3ml×3). The combined organic layers were dried over anhydrous $MgSO_4$ and evaporation under vacuum afforded the product as a pale yellow viscous liquid in 95% yield.

^{1}H-NMR (CD_2Cl_2, 400 MHz, δ in ppm): δ = 8.51 (d, 2H, J=8Hz, o-Py), 7.63 (t, 2H, J=8Hz, m-Py), 7.33-7.30 (m, 5H, Ar-), 7.28-7.21 (m, 2H, Ar-), 7.15 (dd, 2H, J=4 & 8Hz, Ar-), 3.86 (d, 2H, J=12Hz, CH_2-NH), 3.82 (d, 2H, J=12Hz, CH_2-NH), 3.58 (s, 2H, CH_2-Ph), 3.06 (quint, 2H, J=4Hz, -CH-), 2.84 (dd, 2H, J=4 & 8Hz, -CH_2), 2.41 (dd, 2H, J=4 & 8Hz, -CH_2), 2.10 (sh, 2H, NH-). **^{13}C-NMR** (CD_2Cl_2, 100.6 MHz, δ in ppm): δ = 160.67 (Py, -C-), 149.59 (o-Py, -CH-), 139.79 (-C-), 136.77 (m-Py, -CH-), 129.23 (Ar-), 128.66 (Ar-), 127.32 (Ar-), 122.68 (Ar-), 122.30 (Ar-), 64.96 (-CH-), 60.82 (-CH_2), 60.46 (-CH_2), 54.08 (CH_2-NH, -CH_2). **IR** (KBr pellet): ν_{NH}= 3311cm^{-1} $\nu_{C=N}$= 1593cm^{-1}. **ESI-HRMS:** Calculated for $C_{23}H_{27}N_5$: Exact: (M: 373.2333, $[M+H]^+$: 374.2333); Experimental ($[M+H]^+$: 374.2339).

Synthesis of Zn(II) complex 4xx29
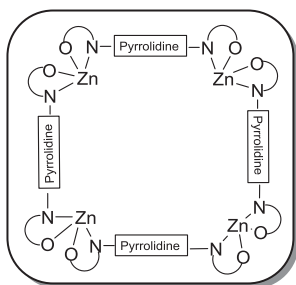
Diethyl zinc (1M in hexane) (0.32ml, 0.32mmol) was added to a solution of **4xx25** (0.2g, 0.32mmol) in 6ml of THF. The solution was allowed to stir at room temperature for 16h and a colour change from yellow to bright yellow was observed. The product was isolated after evaporation to dryness in quantitative yield.

^{1}H-NMR (CD$_2$Cl$_2$, 400 MHz, δ in ppm): δ = 7.60 (s, 2H, -HC=N), 7.48 (d, 2H, J=4Hz, Ar-), 7.26-7.18 (m, 5H, Ar-), 6.55 (d, 2H, J=4Hz, Ar-), 4.39 (quint, 2H, J=8Hz, -CH-), 3.60 (d, 1H, J=12Hz, CH$_2$-Ph), 3.48 (d, 1H, J=12Hz, CH$_2$-Ph), 2.93 (t, 2H, J=8Hz, -CH$_2$), 2.72 (t, 2H, J=8Hz, -CH$_2$), 1.46 (s, 18H, -CH$_3$), 1.27 (s, 18H, -CH$_3$). **^{13}C-NMR** (CD$_2$Cl$_2$, 100.6 MHz, δ in ppm): δ = 173.86 (C=N), 168.85 (C-O), 142.15 (-C-), 139.44 (-C-), 136.38 (-C-), 131.42 (Ar-), 129.82 (Ar-), 128.76 (Ar-), 128.72 (Ar-), 127.46 (Ar-), 117.62 (-C-), 69.27 (N-CH), 60.83 (CH$_2$-Ph, -CH$_2$), 59.49 (-CH$_2$), 35.97 (-C-^{t}Bu, -C-), 34.39 (-C-^{t}Bu, -C-), 31.72 (-CH$_3$), 29.83 (-CH$_3$). **IR** (KBr pellet): $v_{C=N}$= 1598cm^{-1}. **ESI-HRMS:** Calculated for **(C$_{41}$H$_{55}$N$_3$O$_2$)$_4$Zn$_4$**: Exact: (M: 2741.4343; [M+Na]$^{+}$: 2764.4241); Experimental ([M+Na]$^{+}$: 2764.4218). **Elemental Analysis:** Calculated for **(C$_{41}$H$_{55}$N$_3$O$_2$)$_4$Zn$_4$·0,5CH$_2$Cl$_2$**: C, 68.30; H, 7.74; N, 5.76; Found: C, 68.87; H, 7.68; N, 5.62.
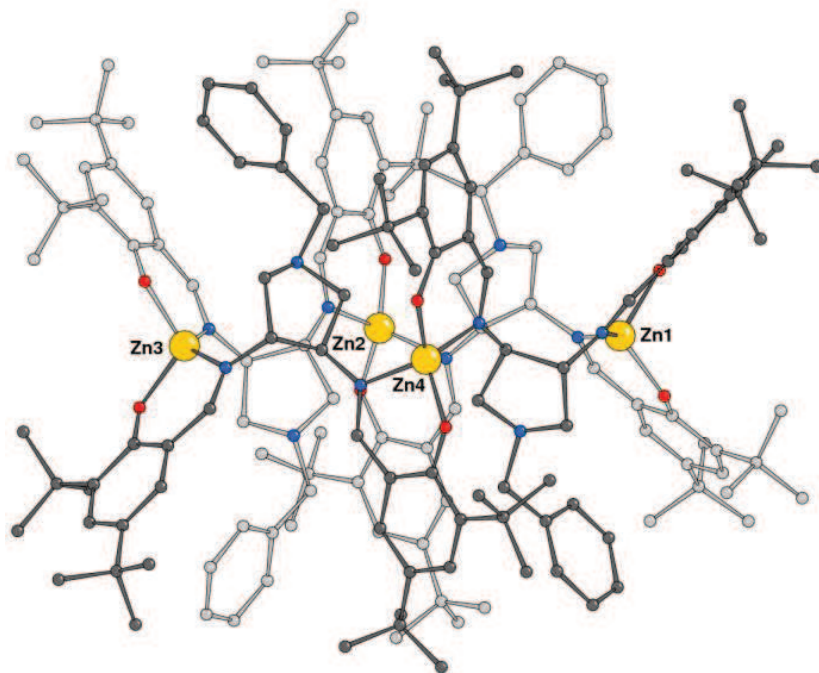
Figure 4.15. Molecular structure of **4xx29**.

Table 4.8. Crystal data and details of refinement for **4xx29**.

Empirical formula	$C_{164}H_{220}N_{12}O_8Zn_4 \cdot 2(C_6H_{14})$
Formula weight	2921.33
Temperature (K)	100(2)
Wavelength (Å)	0.7000
Crystal system	Monoclinic
Space group	$P 2_1$
Unit cell dimensions (Å / º)	$a = 18.0440(8)$, $\alpha = 90.00$. $b = 28.0230(11)$, $\beta = 95.027(5)$. $c = 17.8910(7)$, $\gamma = 90.00$.
Volume (Å^3)	9011.7(6)
Z	2
Calculated Density (Mg/m^3)	1.077
Absorption coefficient (mm^{-1})	0.580
F(000)	3144
Crystal size (mm^3)	0.38 x 0.30 x 0.12
Theta range (º) for data collection	1.12 – 27.82
Index ranges	-24<=h<=24,-37<=k<=37,-23<=l<=23
Reflections collected	138260
Independent reflections	44180 [R(int) = 0.0291]
Data [$I>2\sigma(I)$]	6641
Parameters	1897
Goodness-of-fit on F^2	1.048
Final R indices [$I>2\sigma(I)$]	R1 = 0.0532, wR2 = 0.1519
R indices (all data)	R1 = 0.0550, wR2 = 0.1542
Largest diff. peak and hole (e/Å^3)	1.001, -1.836

Synthesis of Zn(II) complex 4xx33
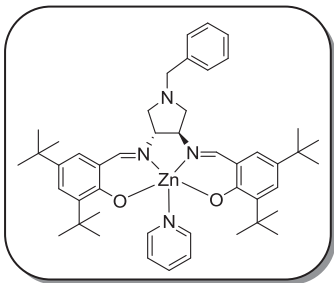
0.7ml of pyridine-d$_5$ was added to a 20mg of the **4xx29** complex which was shake it for 2 h at room temperature.

^{1}H-NMR (Py-d$_5$, 400 MHz, δ in ppm): δ = 8.26 (s, 2H, -HC=N), 7.81 (d, 2H, *J*=4Hz, Ar-), 7.35-7.24 (m, 5H, Ar-), 7.10 (d, 2H, *J*=4Hz, Ar-), 4.68 (quint, 2H, *J*=8Hz, -CH-), 3.58 (d, 1H, *J*=12Hz, CH$_2$-Ph), 3.29 (d, 1H, *J*=12Hz, CH$_2$-Ph), 2.88 (t, 2H, *J*=8Hz, -CH$_2$), 2.71 (t, 2H, *J*=8Hz, -CH$_2$), 1.77 (s, 18H, -CH$_3$), 1.38 (s, 18H, -CH$_3$). **^{13}C-NMR** (Py-d$_5$, 100.6 MHz, δ in ppm): δ = 175.26 (C=N), 169.18 (C-O), 141.98 (Ar-, -C-), 139.64 (Ar-, -C-), 136.53 (Ar-, -C-), 131.34 (Ar-), 131.28 (Ar-), 129.18 (Ar-), 129.10 (Ar-), 127.82 (Ar-), 199.0 (Ar-, -C-), 69.64 (N-CH), 61.06 (CH$_2$-Ph, -CH$_2$), 59.93 (-CH$_2$), 36.39 (-C-^{t}Bu, -C-), 34.68 (-C-^{t}Bu, -C-), 32.15 (-CH$_3$), 30.36 (-CH$_3$). **ESI-HRMS:** Calculated for **C$_{46}$H$_{55}$D$_5$N$_4$O$_2$Zn**: Exact: (M: 769.4322; [M+O+H]$^+$: 786.4427); Experimental ([M+O+H]$^+$ 786.4357:).

Synthesis of Zn(II) complex 4xx30
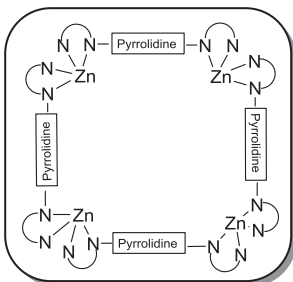
Diethyl zinc (1M in hexane) (0.29ml, 0.29mmol) was added to a solution of **4xx26** (0.1g, 0.29mmol) in 6ml of THF. The solution was stirred at room temperature for 16h and a colour change from yellow to bright yellow was observed. The product was isolated in quantitative yield after evaporation to dryness.

¹H-NMR (CD$_2$Cl$_2$, 400 MHz, δ in ppm): δ = 7.31-7.17 (m, 7H, Ar- & C=N), 7.07 (s, 2H, *o*-Pyrrole), 6.70 (d, 2H, *J*=4Hz, *p*-Pyrrole), 6.37 (dd, 2H, *J*=4 & 8Hz, *m*-Pyrrole), 3.76 (t, 2H, *J*=4Hz, -CH-), 3.62 (d, 1H, *J*=12Hz, CH$_2$-Ph), 3.43 (d, 1H, *J*=12Hz, CH$_2$-Ph), 2.91 (t, 2H, *J*=8Hz, -CH$_2$), 2.58 (t, 2H, *J*=8Hz, -CH$_2$). **¹³C-NMR** (CD$_2$Cl$_2$, 100.6 MHz, δ in ppm): δ = 160.67 (C=N), 139.20 (-C-), 137.36 (-C-), 135.91 (*o*-Pyrrole, -CH-), 128.90 (Ar-), 128.75 (Ar-), 127.50 (Ar-), 119.40 (*p*-Pyrrole, -CH-), 113.69 (*m*-Pyrrole, -CH-), 68.49 (-CH-), 60.78 (CH$_2$-Ph), 58.36 (-CH$_2$). **IR** (KBr pellet): ν$_{C=N}$= 1579cm^{-1}. **ESI-HRMS:** Calculated for **(C$_{21}$H$_{21}$N$_5$)$_4$Zn$_4$**: Exact: (M: 1628.4354; [M+H]$^+$: 1629.4499); Experimental ([M+H]$^+$: 1629.4426). **Elemental Analysis:** Calculated for **(C$_{21}$H$_{21}$N$_5$)$_4$Zn$_4$·4CH$_2$Cl$_2$·C$_4$H$_8$O**: C, 42.45; H, 4.54; N, 8.53; Found: C, 43.20; H, 3.87; N, 8.72.

Synthesis of Zn(II) complex 4xx31
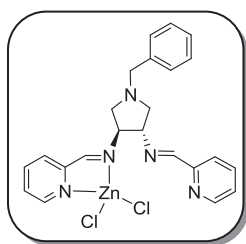
Zinc dichloride (73.8mg, 0.54mmol) in THF (4ml) was added to a solution of **4xx27** (0.2g, 0.54mmol) in THF. The reaction mixture was stirred at room temperature for 16h and evaporated under vacuum. Then, the residue was re-dissolved in DCM (2ml) and diethylether (4ml) was added to the mixture in order to precipitate the product. The obtained orange solid was filtered and further washed with diethylether (3x3ml). The product was isolated in 72% yield after drying under vacuum.

¹H-NMR (CD$_2$Cl$_2$, 400 MHz, δ in ppm, at -65°C): δ = 8.73 (d, 1H, *J*=4Hz, coordinated *o*-Py), 8.58 (bs, 2H, uncoordinated *o*-Py & coordinated C=N), 8.18 (s, 1H, uncoordinated C=N), 8.05 (t, 1H, *J*=8Hz, *p*-Py), 7.81-7.69 (m, 4H, -Py), 7.39-7.35 (m, 6H, Ar-), 4.23 (s, 1H, -CH-), 4.20 (d, 1H, *J*=12Hz, CH$_2$-Ph), 4.12 (d, 1H, *J*=12Hz, CH$_2$-Ph), 3.81 (s, 1H, -CH-), 3.69 (t, 1H, *J*=8Hz, -CH$_2$), 3.29 (d, 1H, *J*=8Hz, -CH$_2$), 3.00 (d, 1H, *J*=12Hz, -CH$_2$), 2.33

(d, 1H, *J*=8Hz, -CH$_2$). ^{13}**C-NMR** (CD$_2$Cl$_2$, 100.6 MHz, δ in ppm, at -65ºC): δ = 162.82 (uncoordinated C=N), 158.27 (coordinated C=N), 152.94 (-C-), 149.52 (uncoordinated *o*-Py), 149.30 (coordinated *o*-Py), 144.98 (-C-), 140.00 (*p*-Py, -CH-), 136.79 (-Py,-CH-), 132.97 (-C-), 131.44 (Ar-), 129.21 (Py-), 127.95 (Ar-), 127.65 (Ar-), 126.98 (Py, -CH-), 125.34 (Py, -CH-), 121.33 (Py, -CH-), 73.82 (-CH-), 69.86 (-CH-), 55.77 (-CH$_2$), 55.12 (-CH$_2$-Ph), 54.47 (-CH$_2$). **IR** (KBr pellet): ν$_{C=N}$= 1644cm^{-1} (uncoordinated C=N) & 1597cm^{-1} (coordinated C=N). **Conductivity** (0.001M in THF)= 0.062Ω^{-1}·cm·mol^{-1}. **ESI-HRMS:** Calculated for **C$_{23}$H$_{23}$N$_5$Cl$_2$Zn**: Exact: (M: 503.0622; [M-Cl]$^+$: 468.0933); Experimental ([M-Cl]$^+$: 468.0928). **Elemental Analysis:** Calculated for **C$_{23}$H$_{23}$N$_5$Cl$_2$Zn·0,5CH$_2$Cl$_2$**: C, 51.49; H, 4.41; N, 12.78; Found: C, 52.36; H, 4.27; N, 12.98.
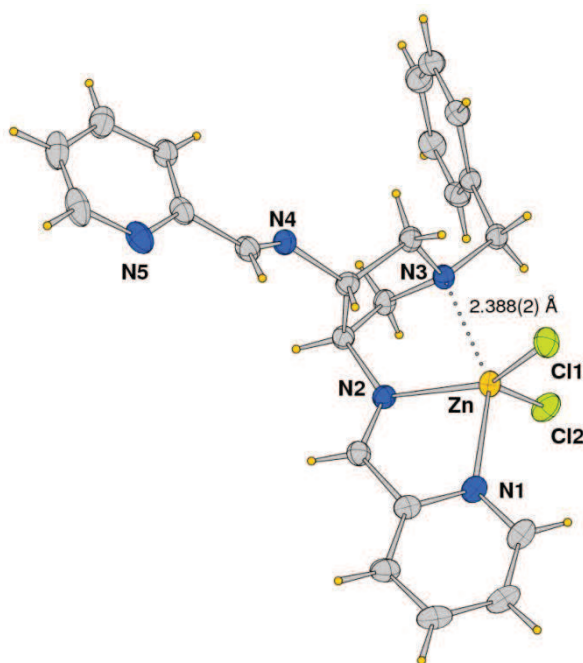
Figure 4.16. Molecular structure of **4xx31**.

Table 4.9. Crystal data and details of refinement for **4xx31**.

Empirical formula	$C_{23}H_{23}Cl_2N_5Zn$
Formula weight	505.73
Temperature (K)	100(2)
Wavelength (Å)	0.7000
Crystal system	Orthorombic
Space group	P $2_12_12_1$
Unit cell dimensions (Å / º)	a = 8.6890(17) , α = 90.00. b = 10.718(2), β = 90.00. c = 24.973(5), γ = 90.00.
Volume ($Å^3$)	2325.7(8)
Z	4
Calculated Density (Mg/m^3)	1.444
Absorption coefficient (mm^{-1})	1.306
F(000)	1040
Crystal size (mm^3)	0.39 x 0.18 x 0.15
Theta range (º) for data collection	1.61 – 29.97
Index ranges	-12<=h<=12,-15<=k<=14,-35<=l<=35
Reflections collected	20755
Independent reflections	7014 [R(int) = 0.0285]
Data [$I>2\sigma(I)$]	6641
Parameters	280
Goodness-of-fit on F^2	1.110
Final R indices [$I>2\sigma(I)$]	R1 = 0.0254, wR2 = 0.0668
R indices (all data)	R1 = 0.0283, wR2 = 0.0682
Largest diff. peak and hole ($e/Å^3$)	0.241, -0.544

Synthesis of Zn(II) complex 4xx32
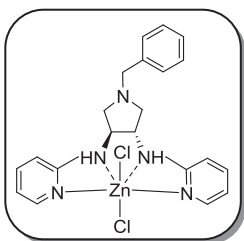
Triethylamine (1ml, exces) was added to a solution of **4xx28** (0.1g, 0.27mmol) in 4ml of THF. Then, zinc dichloride (36.9mg, 0.27mmol) in THF (2ml) was added to the solution. The reaction was stirred at room temperature for 16h during which an orange solid precipitated. The obtained solid was filtered and washed with THF (3x3ml). The product was isolated in 85% yield after drying under vacuum.

^{1}H-NMR (DMSO-d$_6$, 400 MHz, δ in ppm): δ = 8.94 (d, 2H, *J*=4Hz, *o*-Py), 8.04 (t, 2H, *J*=8Hz, *p*-Py), 7.57 (t, 2H, *J*=8Hz, *m*-Py), 7.52 (d, 2H, *J*=8Hz, *m*-Py), 7.29-7.19 (m, 5H, -Ar), 4.48 (bs, 2H, -NH), 4.26 (dd, 2H, *J*=4&16Hz, -CH$_2$), 3.95 (d, 2H, *J*=16Hz, -CH$_2$), 3.65 (d, 1H, *J*=12Hz, CH$_2$-Ph), 3.50 (d, 1H, *J*=12Hz, CH$_2$-Ph), 2.83 (s, 2H, -CH$_2$NH), 2.43 (bs, 4H, -CH$_2$NH & -CH-). **^{13}C-NMR** (DMSO-d$_6$, 100.6 MHz, δ in ppm): δ = 155.49 (Py, -C-), 148.38 (*o*-Py, -CH-), 139.63 (*p*-Py, -CH-), 139.04 (-C-), 128.71 (Ar-), 128.41 (Ar-), 127.12 (Ar-), 124.52 (*m*-Py, -CH-), 123.72 (*m*-Py, -CH-), 60.25 (-CH$_2$-Ph), 59.48 (-CH-), 53.08 (-CH$_2$NH), 48.34 (-CH$_2$-). **IR** (KBr pellet): ν_{NH}= 3221cm^{-1}, $\nu_{C=N}$= 1607cm^{-1}. **Conductivity** (0.001M in DMSO)= 16.05 $\Omega^{-1} \cdot$cm$\cdot$mol^{-1}. **ESI-HRMS:** Calculated for **C$_{23}$H$_{27}$N$_5$Cl$_2$Zn**: Exact: (M: 507.0935; [M-Cl]$^+$: 472.1241); Experimental ([M-Cl]$^+$: 472.1262). **Elemental Analysis:** Calculated for **C$_{23}$H$_{25}$N$_5$Zn·1,5CH$_2$Cl$_2$**: C, 46.18; H, 4.75; N, 10.99; Found: C, 45.98; H, 5.02; N, 10.55.

General catalytic procedure

The catalytic tests were carried out in a 100 mL Berghoff or 25 mL Parr reactor, which were previously kept under vacuum for 2 h (in the case of **4xx31**, the catalyst was placed into the autoclave prior to vacuum). Then, a solution containing the catalyst, the epoxide substrate and the co-catalyst

were injected into the reactor under inert atmosphere. The autoclave was then pressurized with CO_2 and heated at the appropriate temperature. After the reaction, the system was cooled down with an ice bath and slowly depressurized through a dichloromethane trap.

General procedure for recycling experiments

The recycling experiments were carried out in a 100 mL Berghoff reactor containing the catalyst (**4xx31**), which was previously kept under vacuum 2 h at room temperature. Then, the substrate (propylene oxide) and the co-catalyst (TBAI) were injected into the reactor under inert atmosphere. The autoclave was then pressurized with CO_2 and heated to reach the desired pressure (reaction conditions: 3ml of epoxide, catalyst loading = 0.1 mol%, ratio cat:cocat 1:2, at 80ºC, 30bar of CO_2, 16h). Once the reaction was finished, the reactor was cooled down with an ice bath and slowly depressurized through a dichloromethane trap. After each catalytic experiment, the propylene carbonate was separated by vacuum distillation and the catalyst was directly used for the next catalytic cycle (five consecutive runs).

X-Ray crystallography

Data collections of structures reported were carried out at the X-ray diffraction beamline of the Elettra Synchrotron, Trieste (Italy), using the rotating crystal method with a monochromatic wavelength of 0.7000 Å, on a Pilatus detector. Measurements were performed at 100(2) K using a nitrogen stream cryo-cooler. Cell refinement, indexing and scaling of the data set were performed using the CCP4 package,[73] and programs Denzo and Scalepack.[74] The structure was solved by direct methods and Fourier analyses and refined by the full-matrix least-squares method based on F^2 with all observed reflections.[75] The electron density map of **Zn-1** shows

four disordered n-C_6H_{14} molecules, the atoms of which were fixed at half occupancy (for a total of 2 molecules) and isotropically refined with restrained bond distances. Some positionally disorder groups were detected in the tetranuclear **Zn-1** complex: a benzyl group (attached to a pyrrolidine) and a phenyl ring with one *t*-butyl group were found disordered over two positions (refined occupancies of 0.61/0.39 and 0.56/0.44, respectively). Finally another *t*-butyl group was split over two positions with half occupancy each. All the calculations were performed using the WINGX SYSTEM, Ver 2013.3.[76]

4.6. REFERENCES

1. Nurhanna, S. and Zhang, Y. *Dalton Trans.* **2010**, *39*, 2247-3357.
2. Hunt, A. J.; Sin, E. H. K.; Marriott, R. and Clark, J. H. *ChemSusChem* **2010**, *3*, 306-322.
3. Arakawa, H.; Aresta, M.; Armor, J. N.; Barteau, M. A.; Beckman, E. J.; Bell, A. T.; Bercaw, J. E.; Creutz, C.; Dinjus, E.; Dixon, D. A.; Domen, K.; Dubois, D. L.; Eckert, J.; Fujita, E.; Gibson, D. H.; Goddard, W. A.; Goddman, D. W.; Keller, J.; Kubas, G. J.; Kung, H. H.; Lyons, J. E.; Manzer, L. E.; Marks, T. J.; Morokuma, K.; Nicholas, K. M.; Periana, R. L.; Rostrup-Nielson, I. J.; Sachtler, W. M. H.; Schmidt, L. D.; Sen, A.; Somorjai, G. A.; Stair, P. C.; Stults, B. R. and Tumas, W. *Chem. Rev.* **2001**, *101*, 953-996.
4. Centi, G.; Quadrelli, E. A. and Perathoner, S. *Energy Environ. Sci*. **2013**, *6*, 1711-1731.
5. Aresta, M.; Dibenedetto, A. and Angelini, A. *Chem. Rev.* **2014**, *114*, 1709-1742.
6. Halmann, M. M. *Chemical Fixation of Carbon Dioxide: Methods for Recycling CO_2 into Useful Products*, CRC Press, New York, USA, **1993**.
7. Traynor, A. J. and Jensen, R. J. *Ind. Eng. Chem. Res.* **2002**, *41*, 1935-1939.
8. (a) Jessop, P. G. and Leitner, W. *Chemical Synthesis using Supercritical Fluids*, Wiley-VCH, Weinheim, Germany, **1999**, pp. 1-5. (b) Kearton, F. M. *Alternative Solvents for Green Chemistry*; RSC Publishing, Cambridge, UK, **2009**, pp. 60-70.
9. Beckman, E. J. *J. Supercrit. Fluids* **2004**, *28*, 121-191.
10. Chouchi, D.; Gourgouillon, D.; Courel, M.; Vital, J. and da Ponte, M. N. *Ind. Eng. Chem. Res.* **2001**, *40*, 2551-2554.
11. (a) Poliakoff, M.; Swan, T. M.; Tacke, T.; Hitzler, M. G.; Ross, S, K. and Wieland, S. US Patent No. 6156933, **2000**. (b) Licence, P.; Ke, J.; Sokolova, M.; Ross, S. K. and Poliakoff, M. *Green Chem.* **2003**, *5*, 99-104.
12. Weissermel, K. and Arpe, H. J. *Industrial Organic Chemistry*, 3rd Ed.; Wiley-VCH, Weinheim, Germany, **1997**, pp. 127-128.
13. Poliakoff, M.; Meehan, N. J.; Ross, S. K.; Wieland, S. and Roeder, S. US Patent No. 6566558, **2003**.
14. Ojima, I. and Urata, H. US Patent No. 5962744, **1999**.
15. Odian, G. *Principles of Polymerization*, 4th Ed., Wiley, New York, USA **2004**, p. 300.
16. Miller, D. A.; Blanch, H. M. and Prausnitz, J. M. *Ind. Eng. Chem. Res*. **1991**, *30*, 939-946.
17. Burch, R. and Petch, M. I. *Appl. Catal. A: Gen.* **1992**, *88*, 39-60.
18. Darensbourg, D. J. and Holtcamp, M. W. *Coord. Chem. Rev.* **1996**, *153*, 155-174.

19. Coates, G. W. and Moore, D. R. *Angew. Chem. Int. Ed.* **2004**, *43*, 6618-6639.

20. Darensbourg, D. J. *Chem. Rev.* **2007**, *107*, 2388-2410.

21. Luinstra, G. A. and Borchardt, E. *Adv. Polym. Sci.* **2012**, *245*, 29-48.

22. Shaikh, A-A. G. *Chem. Rev.* **1996**, 951-976.

23. Martin, C.; Fiorani, G. and Kleij, A. W. *ACS Catal.* **2015**, *5*, 1353-1370.

24. North, M.; Pasquale, R. and Young, C. *Green Chem.* **2010**, *12*, 1514-1539.

25. Rebsdat, S. and Mayer, D. *Ethylene Glycol Ullmann's Encyclopedia of Industrial Chemistry*, Wiley, **2000**.

26. (a) Harmsen, G. J.; van der Heide, E. and Vrouwenvelder, C. L. Process for preparation of alkanediol Shell internation research, WO2004089866(A1). (b) Evans, W. E.; Hess, M. L.; Matusz, M. and van Kruchten, E. M. G. A. Process for the preparation of an alkylene carbonate and a alkylene glycol Shell international research, WO2009140318(A1).

27. Fukuoka, S.; Kawamura, M.; Komiya, K.; Tojo, M.; Hachiya, H.; Hasegawa, K.; Aminaka, M.; Okamoto, H.; Fukawa, I. and Konno, S. *Green Chem.* **2003**, *5*, 497-507.

28. North, M. and Pasquale, R. *Angew. Chem. Int. Ed.* **2009**, *48*, 2946-2958.

29. Pescarmona, P. P. and Taherimehr, M. *Catal. Sci. Technol.* **2012**, *2*, 2169-2187.

30. Klaus, S.; Lehenmeier, M. W.; Herdtweck, E.; Deglmann, P.; Ott, A. K. and Rieger, B. *J. Am. Chem. Soc.* **2011**, *133*, 13151-13161.

31. Chisholm, M. H. and Zhou, Z. *J. Am. Chem. Soc.* **2004**, *126*, 11030-11039.

32. Darensbourg, D. J.; Mackiewicz, R. M.; Rodgers, J. L. and Phelps, A. L. *Inorg. Chem.* **2004**, *43*, 1831-1833.

33. North, M. *New and future developments in catalysis*, **2013**, 379-413.

34. Inoue, S.; Koinuma, H. and Tsuruta, T. *J. Polym. Sci. B: Polym. Letters* **1969**, *7*, 287-292.

35. Klaus, S.; Lehenmeier, M. W.; Anderson, C. E. and Rieger, B. *Coord. Chem. Rev.* **2011**, *255*, 1460-1479.

36. Cohen, C. T.; Chu, T. and Coates, G. W. *J. Am. Chem. Soc.* **2005**, *127*, 10869-10878.

37. Decortes, A.; Martinez Belmonte, M.; Benet-Buchholz, J. and Kleij, A. W. *Chem. Commun.* **2010**, *46*, 4580-4582.

38. Decortes, A. and Kleij, A. W. *ChemCatChem.* **2011**, *3*, 831-834.

39. Fuchs, M. A.; Staudt, S.; Altesleben, C.; Walter, O.; Zebaco, T. A. and Dinjus, E. *Dalton Trans.* **2014**, *43*, 2344-2347.

40. Ema, T.; Miyazaki, Y.; Koyama, S.; Yano, Y. and Sakai, T. *Chem. Commun.* **2012**, *48*, 4489-4491.

41. Ema, T.; Miyazaki, Y.; Shimonishi, J.; Maeda, C. and Hasegawa, J.-Y. *J. Am. Chem. Soc.* **2014**, *136*, 15270-15279.

42. Maeda, C.; Taniguchi, T.; Ogawa, K. and Ema, T. *Angew. Chem. Int. Ed.* **2015**, *54*, 134-138.

43. Dengler, J. E.; Lehenmeier, M. W.; Klaus, S.; Anderson, C. W.; Herdtweck, E. and Rieger, B. *Eur. J. Inorg. Chem*. **2011**, 336-343.

44. (a) Cheng, M.; Moore, D. R.; Reczek, J. J.; Chamberlain, B. M.; Lobkovsky, E. B. and Coates, G. W. *J. Am. Chem. Soc.* **2001**, *123*, 8738-8749. (b) Moore, D. R.; Cheng, M.; Lobkovsky, E. B. and Coates, G. W. *J. Am. Chem. Soc.* **2003**, *125*, 11911-11924.

45. (a) Darensbourg, D. J.; Wildeson, J. R.; Yarbrough, J. C. and Reibenspies, J. H. *J. Am. Chem. Soc.* **2000**, *122*, 12487-12496. (b) Kember, M. R.; Knight, P. D.; Reung, P. T. R. and Williams, C. K. *Angew. Chem. Int. Ed.* **2009**, *48*, 931-933.

46. Meléndez, J.; North, M. and Pasquale, R. *Eur. J. Inorg. Chem.* **2007**, 3323-3326.

47. Clegg, W.; Harrington, R. W.; North, M. and Pasquale, R. *Chem. Eur. J.* **2010**, *16*, 6828-6843.

48. Buchard, A.; Kember, M. R.; Sandeman, K. G. and Williams, C. K. *Chem. Comm.* **2011**, *47*, 212-214.

49. Whiteoak, C. J.; Kielland, N.; Laserna, V.; Escudero-Adán, E. C.; Martin, E. and Kleij, A. W. *J. Am. Chem. Soc.* **2013**, *135*, 1228-1231.

50. Ramidi, P.; Gerasimchuk, N.; Gartia, Y.; Felton, C. M. and Ghosh, A. *Dalton Trans.* **2013**, *42*, 13151-13160.

51. Whiteoak, C. J.; Kielland, N.; Laserna, V.; Catro-Gómez, F.; Martin, E. Escudero-Adán, E. C. Bo, C. and Kleij, A. W. *Chem. Eur. J.* **2014**, *20*, 2264-2275.

52. Buonerba, A.; De Nisi, A.; Grassi, A.; Milione, S.; Capacchione, C.; Vagin, S. and Rieger, B. *Catal. Sci. Technol*. **2015**, *5*, 118-123.

53. Whiteoak, C. J.; Gjoka, B.; Martin, E.; Belmonte, M. M.; Escudero-Adán, E. C.; Zonta, C.; Licini, G. and Kleij, A. W. *Inorg. Chem*. **2012**, *51*, 10639-10649.

54. Whiteoak, C. J.; Martin, E.; Belmonte, M. M.; Benet-Buchholz, J. and Kleij, A. W. *Adv. Synth. Catal*. **2012**, *354*, 469-476.

55. Vignesh Babu, H. and Muralidharan, K. *Dalton Trans.* **2013**, *42*, 1238-1248.

56. Darensbourg, D. J. and Moncada, A. I. *Macromolecules* **2010**, *43*, 5996-6003.

57. Darensborg, D. J.; Moncada, A. I. and Wei, S.-H. *Macromolecules* **2011**, *44*, 2568-2576.

58. Taherimehr, M.; Descortes, A.; Al-Amsyar, S. M.; Lueangchaichaweng, W.; Whiteoak, C. J.; Escudero-Adán, E. C.; Kleij, A. W. and Pescarmona, P. P. *Catal. Sci. Technol*. **2012**, *2*, 2231-2237.

59. Escárcega-Bobadilla, M. V.; Martínez Belmonte, M.; Martin, E.; Escudero-Adán, E. C. and Kleij, A. W. *Chem. Eur. J.* **2013**, *19*, 2641-2648.

60. Haak, R. M.; Decortes, A.; Escudero-Adán, E. C.; Martínez Belmonte, M.; Martin, E.; Benet Buchholz, J. and Kleij, A. W. *Inorg. Chem.* **2011**, *50*, 7934-7936.

61. Kielland, N.; Escudero-Adán, E. C.; Martínez Belmonte, M. and Kleij, A. W. *Dalton Trans.* **2013**, *42*, 1427-1436.

62. Martín, C.; Whiteoak, C. J.; Martin, E.; Martínez Belmonte, M.; Escudero-Adán, E. C. and Kleij, A. W. *Catal. Sci. Technol.* **2014**, *4*, 1615-1621.

63. Luo, R.; Zhou, X.; Zhang, W.; Liang, Z.; Jiang, J. and Ji, H. *Green Chem*. **2014**, *16*, 4179-4189.

64. Fuchs, M. A.; Altesleben, C.; Staudt, S. C.; Zevaco, T. A. and Dinjus, E. *Catal. Sci. Technol.* **2014**, *4*, 1658-1673.

65. Adolph, M.; Zevaco, T. A. Altesleben, C.; Staudt, S. C. and Dinjus, E. *J. Molec. Catal.* **2015**, *400*, 104-110.

66. (a) Reddy, D. R. and Thornton, E. R. *J. Chem. Soc., Chem. Commun.* **1992**, 172-173; (b) Konsler, R. G.; Karl, R. and Jacobsen, E. N. *J. Am. Chem. Soc.* **1998**, *120*, 10780-10781; (c) Cheng, Y.; Wang, M.; Jin, K.; Wang, D.; Na, Y. and Sun, L. *Inorg. Chem. Commun*. **2005**, 606-609; (d) Wang, D.; Wang, M.; Wang, X.; Chen, Y.; Gao, A. and Sun, L. *J. Catal.* **2006**, *237*, 248-254; (e) Lv, W.; Cheng, Q.; Xu, D.; Wang, S.; Xia, C. and Sun, W. *Eur. J. Org. Chem*. **2011**, 3407-3411.

67. (a) Kleij, A. W.; Kuil, M.; Tooke, D. M.; Lutz, M.; Spek, A. L. and Reek, J. N. H. *Chem. Eur. J.* **2005**, *11*, 4743-4750; (b) Kleij, A. W.; Kuil, M.; Tooke, D. M.; Spek, A. L. and Reek, J. N. H. *Inorg. Chem.* **2007**, *46*, 5829-5831.

68. Range, S.; Piesik, D. F.-J. and Harder, S. *Eur. J. Inorg. Chem*. **2008**, 3442-3451.

69. Escudero-Adán, E. C.; Benet-Buchholz, J. and Kleij, A. W. *Eur. J. Inorg. Chem.* **2009**, 3562-3568.

70. Wang, X.-M.; Chen, S.; Fan, R.-Q.; Zhang, F.-Q. and Yang, Y.-L. *Dalton Trans.* **2015**, *44*, 8107-8125.

71. Klaus, S.; Vagin, S. I.; Lehenmeier, M. W.; Deglmann, P.; Brym, A. K. and Rieger, B. *Macromolecules* **2011**, *44*, 9508-9516.

72. Rao, D.-Y.; Li, B.; Zhang, R.; Wang, H. and Lu, X.-B. *Inorg. Chem.* **2009**, *48*, 2830-2836.

73. Collaborative Computational Project, Number 4. *Acta Crystallogr.* **1994**, *Sect. D 50*, 760-763.

74. Otwinowski, Z. Minor, W, Processing of X-ray Difraction Data Collected in Oscillation Mode, Methods in Enzymology, vol 276: Macromolecular Crystallograpy, part A, 307-326 (Eds.; C. W. Carter Jr. R. M. Sweet), Academic Press, New York, 1997.

75. Sheldrich, G. M. *Acta Cryst*. **2008**, *A64*, 112-122.

76. Farrugia, L. J. *J. Appl. Crystallogr.* **1999**, *32*, 837-838.

CHAPTER 5

PRELIMINARY STUDY OF COBALT
COMPLEXES FOR THE ASYMMETRIC
HYDROGENATION OF KETONES

5.1. INTRODUCTION

Over the last decades, N-heterocyclic carbenes (NHCs), which are cyclic carbenes bearing at least one R-amino substituent, have become universal ligands in coordination chemistry and were shown to be highly efficient ligands in several catalytic processes.[1,2] Heterocyclic electron-rich carbenes such as imidazol-2-ylidines and their saturated analogues imidazolydin-2-ylidines are of high interest due to their ability to stabilize metals in low oxidation states to form robust complexes. Carbenes have also been widely used in organic synthesis as a type of highly active and short-lived species, although the isolation and characterization of free stable carbenes remains an appreciable task.[3]

Since the pioneering work of Öfele[4] and Wanzlick[5] in 1968 reporting the first N-heterocyclic carbenes (NHCs) metal complexes **5xx1** and **5xx2** (Scheme 5.1), several NHC metal complexes have been synthesized and characterized to date. Despite this early discovery, the isolation of the first stable free NHC **5xx3** (Scheme 5.1), was not reported until 1991 by Arduengo and co-workers which was characterized by X-Ray diffraction. In this report, Arduengo claimed that the stability of carbenes rely on a combination of steric and electronic factors.[6]
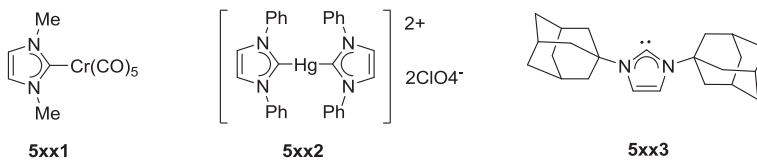
Scheme 5.1. First reported examples of NHC-complexes (**5xx1** and **5xx2**) and first stable NHC ligand **5xx3** reported by Arduengo.

Regarding the effect of the N-substituents in the NHCs, the presence of bulky groups such as the adamantly substituent in the **5xx3** ligand, were reported to increase the stability of the free carbene by hindering the reaction with external reagents.

In terms of electronic properties, NHCs are aromatic compounds with 6 electrons, with σ-donor and π-acceptor properties that can be modulated through the introduction of appropriate N-substituents. The two components of the M-NHC bonding are represented in Figure 5.1. On one hand, the inductive effect of the N-substituents directly affects the σ-donating capacity of the carbonic carbon atom. The presence of electro-withdrawing substituents thus reduces the nucleophile character of the free carbene an as consequence, increases its stability. On the other hand, the presence of π-donor or π-acceptor substituents mainly influences the π-accepting properties of the ligand. The presence of π-acceptor substituents enhances the π-accepting properties of the NHC and in consequence, favors the stabilization of low oxidation state metals. In addition, this type of carbenes can also act as π-donor ligands when bounded to electronically deficient metal centers in high oxidation states.
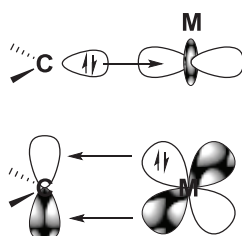
Figure 5.1. Schematic representation of the M-NHC bonding components.

Comparison between phosphines and NHCs

As strong σ-donors and in general poor π-acceptors ligands, NHCs have often been compared to phosphines. Nevertheless, although both types of ligands are electronically and sterically tuneable and efficient ligands in a large number of catalytic reactions, NHCs differ from PR_3 in several aspects.

For instance, the thermodynamic instability of free NHCs strongly disfavours their dissociation from the metal centres which in turn increases the stability of their corresponding catalysts.

From a steric point of view, phosphines and NHC occupy in a very distinct manner the space around the metal centre. Compared with the cone shape of the phosphine ligands where the substituents are pointing away from the metal centre, the substituents of a N-heterocyclic carbine are oriented towards the metallic center and can therefore transmit higher steric hindrance to the metal environment (Figure 5.2).

| Metal-phosphine complexes | Metal-NHC complexes |

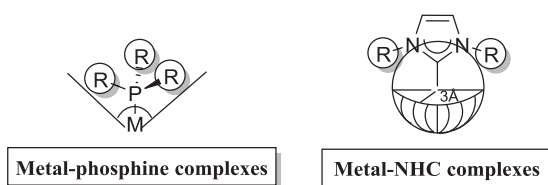**Figure 5.2.** Spartial arrangement of phosphines and NHC substituents.

The steric properties of NHCs have been studied following a similar model to the Tolman's conical angle used for phosphines.[7] Due to the symmetry of these NHCs, the steric factor is analyzed through the $\%V_{Bur}$ or buried volume parameter that measures the volume occupied by the carbene ligand inside a 3Å sphere centered on the metal atom.

Several experimental and computational studies have been performed in order to compare the σ-donating abilities of NHCs and terciary phosphines for a variety of transition metal complexes.[8,9,10,11,12,13,14,15,16,17] The Tolman electronic parameter (TEP) is a measure of the electron donating or withdrawing ability of a ligand and it is determined by measuring the frequency of the M-C-O vibrational mode of a complex. As illustrative examples, a series of complexes of the type $[Ni(L)(CO)_3]$ and $[Ir(L)(CO)_3]$ revealed that NHC complexes have lower $\nu(CO)$ stretching frequencies than their related phosphines (Figure 5.3).[18]
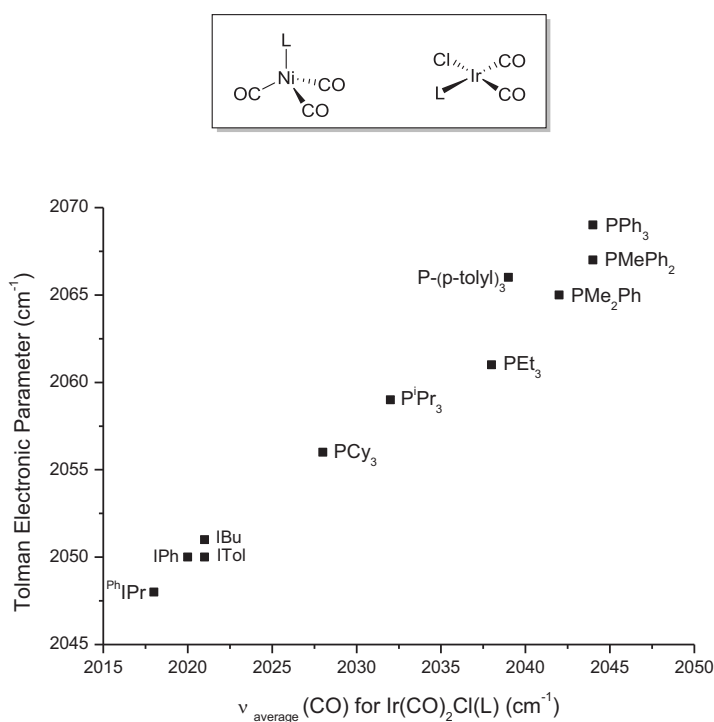

Figure 5.3. Relationship between the Tolman electronic parameters and IR stretching frequencies for the $[Ir(L)(CO)_3]$ complex.[12,16]

These data suggests that NHCs are more σ-donors than even the most basic terciary phosphines. The computational studies performed have suggested

that the M-C of the NHC complexes has mainly a σ-bond character, which little contribution from π-backbonding.[1] The strong σ-donating ability of NHC underlines the ability of these ligands to stabilize high oxidation state metal complexes.

In terms of substituent effects, the presence of ring substituents has the greatest effect on the electronic properties of NHCs. In contrast, the nature of the R groups directly bonded to the nitrogens does not affect strongly the electronics of the NHC but have an impact on the steric properties of these ligands.

These features have made NHCs an interesting alternative ligand to phosphines in several catalytic processes.

Synthetic routes to M-NHC complexes

The preparation of a large number of imidazolium precursors have been described via distinct routes.[19,20] The corresponding NHC ligands are formed by deprotonation of the corresponding imidazolium precursor in presence of a base.

Generally, M-NHC complexes can be prepared from nucleophilic reaction of the free carbene and the appropriate metal precursor (Scheme 5.2, method A[6,21]). Nevertheless, this method requires the generation of the free carbene which implies the use of strong bases as well as the handling of the unstable free carbene. A convenient route involves reaction of the imidazolium salt with basic metal acetates, alkoxides, amides, etc (Scheme 5.2, method B[4,5,22]). The main limitation of this method arises from the moisture sensitivity of the metals precursors as well as their availability. Another well established method is the *in situ* deprotonation of the imidazolium salt with a transition-metal precursor in presence of a base

(Scheme 5.2, method C[23]). Another method for the synthesis of M-NHC complexes is the thermal decomposition of carbene adducts of alcohol[24], chloroform[25], CO_2[26] or cyanide[27] among others, in presence of the appropriate metal precursor (Scheme 5.2, method D). The main disadvantage of this methos is the availability of the carbene precursors and the use of strong bases and toxic reagents. A convenient procedure involves a NHC transfer from one metal center to another which is advantageous due to the broad tolerance toward imidazolium salts having various N-substituents (Scheme 5.2, method E). The AgX-NHC complexes are the most commonly used NHC transfer reagent.[28] The main drawback of this method is the light-sensitivity of such complexes and the fact that silver occasionally induces degradation of the imidazolium precursors.[29] Other carbene sorces involving W, Mn, Cu, Au or Ni as metal-NHC have been far less employed.[30] Method F (Scheme 5.2) shows the synthesis of M-NHCs by reaction of the imidazolium salt and metal powders.[31]
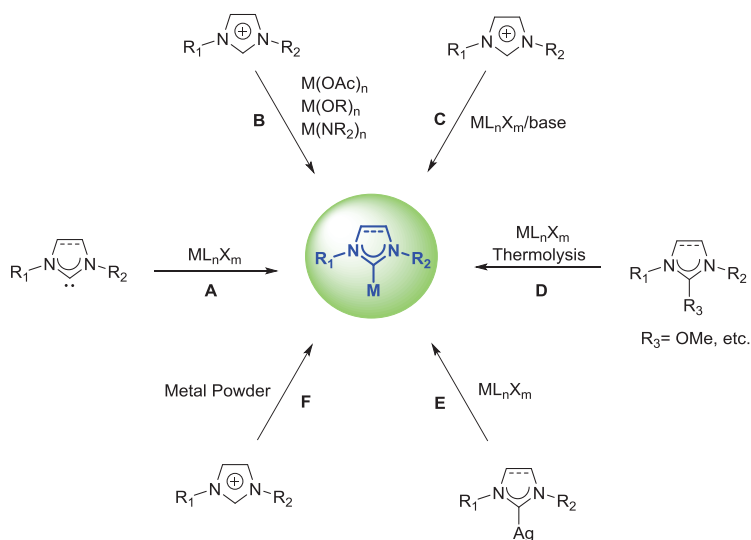
Scheme 5.2. Synthetic routes to M-NHCs complexes.

Chiral NHC ligands

Since the pioneering work developed by Enders[32] and Herrmann[33] in 1996, a huge number of chiral NHCs have been developed although only few successful applications have been reported in asymmetric catalysis so far. It is fair to say that only few efficient chiral NHC catalysts were known until 2001, with the disclosure of Burgess'[34] and Grubbs'[35] catalysts, amongst others. The limitation of NHC structural properties as well as the lack of systematic NHC-design methods might be responsible for their sluggish growth.

Looking at the structure of a generic NHC-metal complex (Figure 5.4), the flat heterocyclic structure is generally described as fan-shaped, with free rotation around the R_1-N and R_2-N bonds and C-M bond, depending on the π-component of the bond. These internal rotations make the active chiral space around the metal poorly defined which affects the enantioinduction in catalysis.
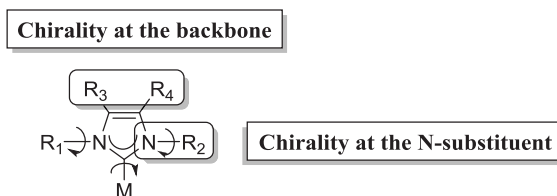

Figure 5.4. Structural modification for the introduction of chirality in a generic NHC-metal complex.

Two general strategies are commonly used for the insertion of chiral elements into the structure:[3]

 - *Introduction of a chiral backbone* (a): by this strategy, the presence of bulky N-substituents is localized away from the metal centre, which makes this technique not often employed to induce enantioselectivity in catalysis.

- *Introduction of chiral substituents at the nitrogen atom* of the ligand (b): this strategy conveys chiral information to the catalytic active site, affecting the enantioinduction in catalysis.

5.1.1. PINCER LIGANDS

Among the different ligand systems that can be found in the chemical literature, pincer-type ligands and their complexes have received increasing attention as a result of their high activity, variability and stability.[36] In 1970 the first pincer ligands and complexes were synthesized, although this area remained unexplored until the late 1990's were several application of pincer complexes were disclosed (Figure 5.5). For instance, pincer complexes have been used in organic synthesis, bond activation, supramolecular chemistry, polymer chemistry and photochemistry.[37]
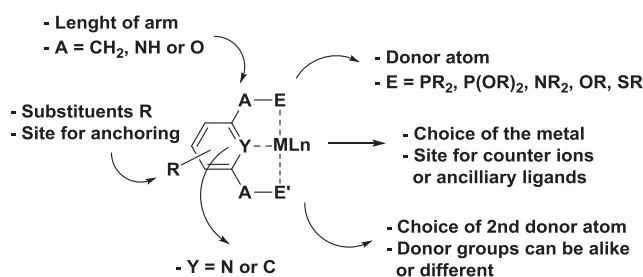

Figure 5.5. General structure of pincer-metal complexes.

Pincer ligands named after their particular coordination mode to metal centers, are tridentate ligands usually having a central aromatic ring that is *ortho-ortho* disubstituted with two electron donor substitutents. The

substituents E are connected to the central aromatic backbone by different spacers (A), such as methylene groups, nitrogen or oxygen atoms. Generally, the aromatic ring can be a pyridine ring (Y = N) or a benzene (Y = CH), obtaining neutral or anionic pincer ligands. Donors E are tipically amines, phosphines, phosphites, ethers or thioethers an even N-Heterocyclic carbenes (NHC),[38] arsines (AsR$_2$)[39] or selenoethers (SeR). It has to be mentioned that the donor groups E do not need to be identical and indeed systems with different donor groups have been reported.

Pincer ligands coordinate to the metal center in *meridional*-fashion via the two electron-donor groups (E) and metal-carbon (benzene-based pincer complexes) or metal-nitrogen (pyridine-based pincer complexes) σ-bonds. Hence, the modifications of one or more parameters in the general structure lead to a wide range of different EYE pincer ligands.

Regarding the nomenclature of the pincer ligands, the general agreement for symmetrically-substituted ligands with methylene linking groups is [R]EYE (Figure 5.6), where E is the donor group, R its substitutent and Y the central aromatic ring.
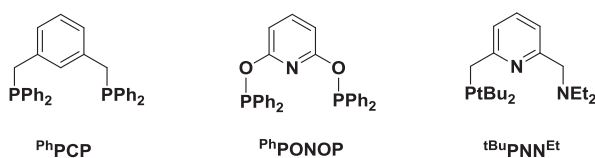
Figure 5.6. Pincer ligands and their abbreviations.

5.1.2. PINCER-NHC LIGANDS

Among the polydentate ligand structure with carbene donors, tripodal[40,41] and pincer[42,43,44] type systems have attracted much of attention (Figure 5.7).

The rigid linear tridentate and pincer type ligands support meridional (in octahedral geometries) or pseudo-meridional (in trigonal bipyramidal, square pyramidal or square planar geometries) coordination.
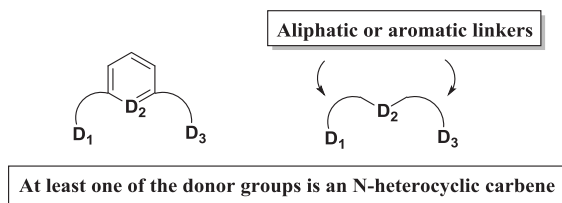
Figure 5.7. Generic structure for tripodal and pincer type ligands.

In the majority of the cases, the ligands shown in Figure 5.8 adopt meridional coordination with most of the transition metals, except for metals of group 11. Nevertheless, complexes with less rigid, long aliphatic linkers may adopt distorted facial coordination modes.[45]
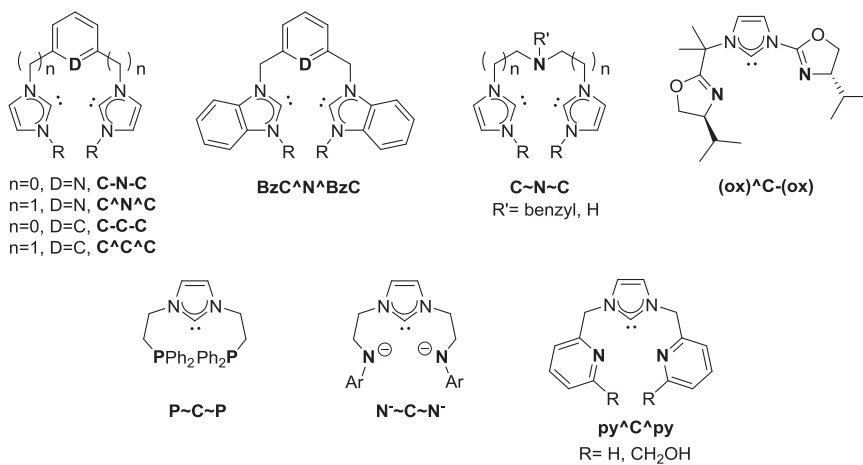
Figure 5.8. Representative structures of tripodal and pincer type ligands.

5.1.2.1. SYNTHESIS OF PYRIDINE-BISCARBENE LIGANDS

The synthesis of the pyridine-biscarbene ligands can be accomplished by reaction of the 2,6-bis(bromomethyl)pyridine with 2 equivalent of the desired imidazole (Scheme 5.3), which can be prepared via distinct routes.[19,20] It shoud be pointed out that no synthetic differences are found when the spacer is a methylene group or no linker is present between the aromatic ring and the donor atom.
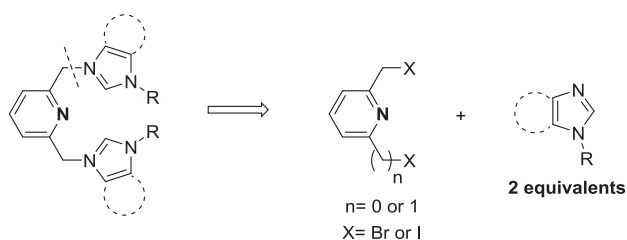


Scheme 5.3. Retrosynthesis for pyridine-biscarbene ligands.

Among all the synthetic possibilities for the synthesis of imidazoles, a straight forward method arises from the one-pot condensation between the desired amine, glyoxal, formaldehyde and an ammonium salt (Scheme 5.4, method A).[46] This procedure works well for aliphatic amines and a limited number of aromatic ones. For unhindered aromatic amines, another one-step route can be applied (Scheme 5.4, method B),[47] which consisted in a N-arylation reaction. Nevertheless, this method is inconvenient for scale-up so as 1eq of 1,10-phenanthroline is used, and this basic heterocycle can be difficult to separate from the imidazole product. In the case of aromatic amines, a multi-step route is required (Scheme 5.4, method C).[48] This method allows scale-up purposes because no chromatographic separations are required. It is worth it mentioning that 2,6-bis(bromomethyl)pyridine and 2,6-dibromopyridine are commercially available, whereas their iodo

derivates can be synthesized in one step from their commercially available bromo derivates.[49]
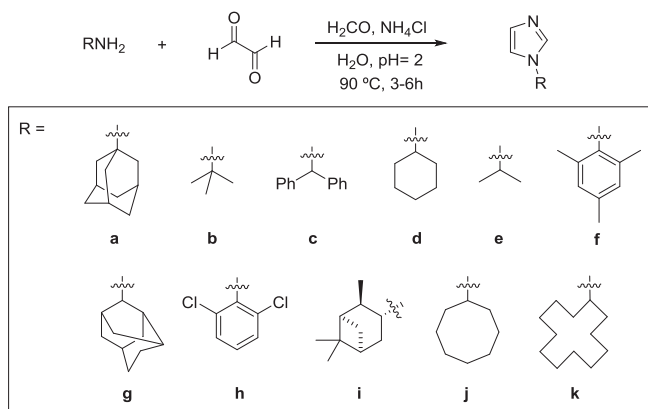
Method A

Method B
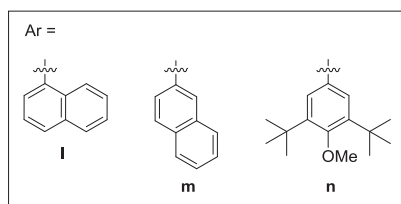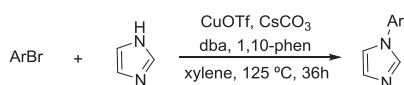
Method C
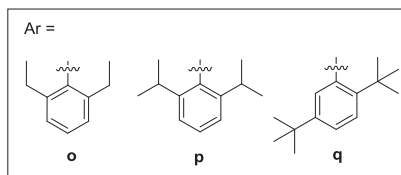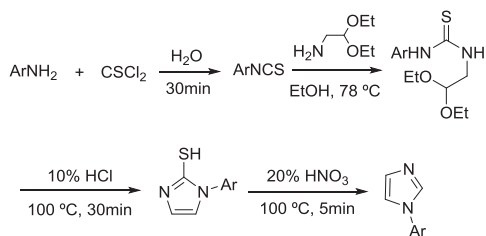
Scheme 5.4. Selected methods for the synthesis of imidazoles depending on the amine used.

5.1.2.2. SYNTHESIS OF PYRIDINE-BISCARBENE COBALT-COMPLEXES

Only two reports have been published for the synthesis of Co-pincer complexes containing an NHC moiety, which corresponds to a C-N-C ligand system.[50,51] On one hand, the synthesis of the Co(II)-pyridine biscarbene complex was carried by aminolysis of Co(HMDS)$_2$ with the imidazolium salt **5xx4**, resulting in the formation of a five coordinate paramagnetic Co(II) complex **5xx5**. The authors explained that no characterization was possible for this Co(II) complex, although reactivity towards substitution, oxidation and reduction was presented (Scheme 5.5).[51]
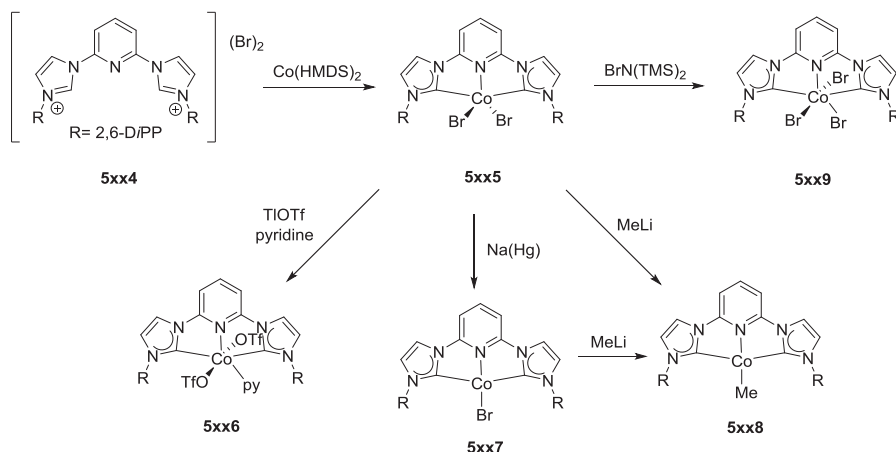
Scheme 5.5. Synthesis and reactivity of Co(II)-pyridine biscarbene complex **5xx5**.

The authors reported the alkylation of **5xx5** with 4eq. of MeLi which yield the Co(I) methyl complex **5xx8** rather than the expected Co(II) alkyl complex. Complex **5xx8** was also synthesized from reduction of **5xx5** with Na/Hg and further alkylation with MeLi. The Co(I)-pyridine biscarbene complexes **5xx7** and **5xx8** are diamagnetic square planar complexes. Furthermore, the oxidation of **5xx5** with BrN(TMS)$_2$ resulted in the formation of the six coordinate octahedral Co(III) complex **5xx9**.

Gibson and co-workers also in 2004, reported the synthesis of the related Co(II)-pyridine biscarbene complex **5xx11** by deprotonation of the corresponding imidazolium salt **5xx4** with KN(SiMe$_3$)$_2$ as base and CoCl$_2$ as metal precursor (Scheme 5.6).[50]
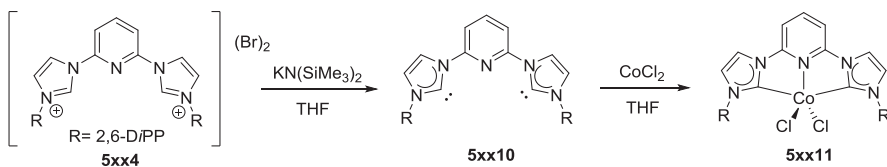
Scheme 5.6. Synthesis of the Co(II)-pyridine biscarbene complex **5xx11**.

It has to be highlighted that the isolation of both Co(II)-pyridine biscarbene complexes **5xx5** and **5xx11** is limited to carbenes with the sterically demanding 2,6-diisopropyl phenyl groups, less bulky aromatic or aliphatic groups gave complexes that have not been characterized to date.[51]

5.1.3. ASYMMETRIC COBALT-CATALYZED REACTIONS

In the field of asymmetric cobalt-catalyzed reactions, an impressive amount of novel methodologies has been developed on the basis of the extraordinary ability of cobalt catalysts to adopt unexpected reaction patways to new chiral cyclic as well as acyclic products under relatively mild conditions.

Cobalt has affinity to carbon-carbon π-bonds, carbon-nitrogent π-bonds, and carbonyl groups which has been used to develop the Pauson-Khand reaction, [2+2+2] cycloadditions among many others. These pioneering works have been followed by the development of a large number of new cobalt promoted transformations (Figure 5.9).
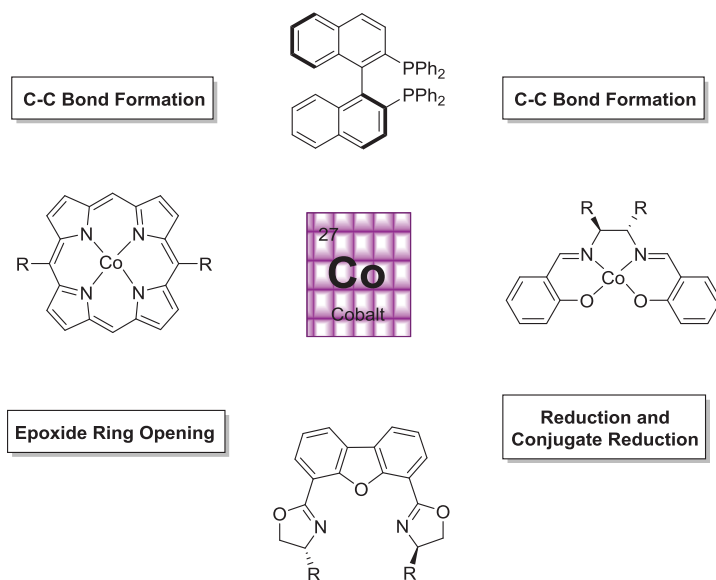
Figure 5.9. Selected catalysts used for asymmetric cobalt catalyzed transformations.

In this section, selected asymmetric cobalt catalyzed transformation will be presented with the aim of showing the development and application of cobalt catalysts in this field.[52]

The formation of multiple bonds, rings and stereocenteres is an important tool for the efficient assembly of complex molecular structures.[53] In this regard, the cyclopropanation reaction is an important synthetic method and indeed, many advances have been made in this trasformation.[54] Cobalt, is a competent metal to promote enantioselectively the formation of carbo- and heterocycles of various ring sizes.

The cyclopropanation of olefins by transition-metal-catalyzed decomposition of diazoalkanes is a well studied reaction in organic synthesis.[55] In 1966, Nozaki and co-workers reported the first enantioselective copper catalyzed cyclopropanation.[56] Since then, many

groups have tried to search for more efficient catalysts with remarkable advances performed by the group of Aratani and co-workers who discovered a (salicylaldiminato)copper(II) complex, which allowed enantioselectivities up to 95% ee.[57]

Although these early discoveries established that chiral cobalt(II) complexes were catalytically active, the low levels of diastereo- and enantiocontrol hampered their use in synthesis for a long time.[58] In 1978, Nakamura and co-workers reported on of the first successes in enantioselective intramolecular cobalt-catalyzed cyclopropanation reactions using a chiral dioximatocobalt(II) complex derived from camphor, which provided ee's up to 88%. However, additional studies were frustrated due to difficulties in the catalyst homogeneity of such dioximato ligands.[59] Some years later, in 1995, Katsuki and co-workers found a chiral salen cobalt(III) complex (**5xx12**) to induce *trans*-selective cyclopropanation reaction (Scheme 5.7).[60]

Ar = Ph: 80%, de = 92%, ee (trans) = 93%, ee (cis) = 91%
Ar = *p*-ClC$_6$H$_4$: 86%, de = 94%, ee (trans) = 96%
Ar = 2-Naph: 87%, de = 90%, ee (trans) = 92%
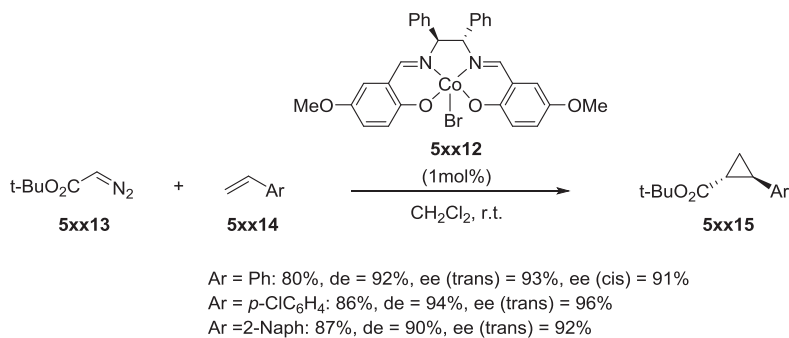
Scheme 5.7. *Trans*-selective cyclopropanation of aromatic alkenes catalyzed by chiral salen cobalt (III) complex **5xx12**.

The decomposition of *tert*-butyl diazoacetate **5xx13** in presence of styrene derivatives **5xx14** generates the corresponding *trans*-cyclopropanes **5xx15** with excellent diastereoselectivities (up to 94%) and enantiomeric excesses (up to 96%).

Other interesting intermediates in organic synthesis are aziridines, which acts as precursors for many complex molecules due to the strain incorporated in their skeletons. Aziridines are far less used in synthesis compared to their oxygen counterparts as a result of the fewer efficient methods for aziridination relative to epoxidation. This fact is pronounced when asymmetric methods are considered.

An interesting strategy for the synthesis of aziridines is the nitrogen-atom transfer to alkenes, as result of the availability of the starting materials as well as the direct nature of the process. In 2008, Zhang and co-workers reported a cobalt asymmetric aziridination of olefins in presence of a D_2-symmetric chiral porphyrins and using diphenylphosphoryl azide (DPPA) as nitrogen source, affording the corresponding N-phosphorylated aziridines in moderate to good yields (52-88%) and ee's up to 53%.[61] A year later, the same authors were able to improve the enantiomeric excess up to 94% with a range of aromatic and aliphatic monosubstituted alkenes, using trichloroethoxysulfonyl azide **5xx18** and the cobalt(II) chiral and polar porphyrin **5xx16** (Scheme 5.8).[62]
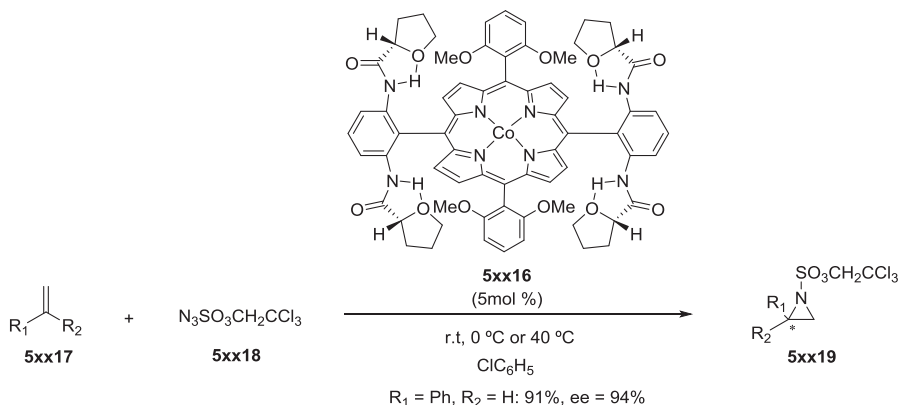
Scheme 5.8. Ariridination of alkenes with trichloroethoxysulfonyl azide **5xx18** catalyzed by cobalt (II) chiral porphyrin **5xx16**.

An important reaction for the synthesis of optically active alcohols from ketones is the reduction of carbonyl compounds.[63] In 1995, the group of Mukaiyama and co-workers reported the first enantioselective borohydride 1,2-reduction of ketones catalyzed by chiral cobalt complexes (Scheme 5.9).[64]

$R_1 = CH_2$, $R_2 = O\text{-}C(Me)_2$, $R_3=R_4 = H$, $R_5 = Me$: > 98%, ee = 93%
$R_1 = n\text{-}Pr$, $R_2=R_3=R_4=R_5 = H$: > 98%, ee = 97%
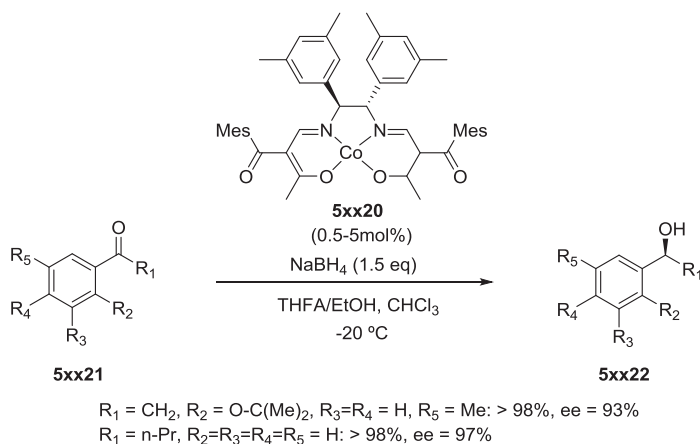
Scheme 5.9. Borohydride reduction of aromatic ketones.

The reduction of various aromatic ketones was achieved using sodium borohydride, tetrahydrofurfuryl alcohol (THFA) and ethanol as solvent in presence of a chiral (β-oxoaldiminato) cobalt(II) complex **5xx20**, which led to the formation of the corresponding alcohols in high yields and enantioselectivities. The use of chloroform in this reaction was proved by Yamada and co-workers to be not only the solvent of the reaction but also the activator for the cobalt complex.[65] The same authors have also reported the borohydride reduction of *ortho*-fluorinated benzhyldrols **5xx24**, which are important frameworks of pharmaceutical compounds, catalyzed by sterically hindered chiral cobalt(II) complex **5xx23**, with high yields and enantioselectivities up to 97% (Scheme 5.10).[66] The authors postulated that the chelation between the fluorine atom and the carbonyl oxygen enhance the differentiation of the two aryl groups of the benzophenones during the enantioselective reduction.

R = Ph, X$_1$=X$_2$=X$_3$=X$_4$=F: 92%, ee = 96%
R = Et, X$_1$=X$_2$=X$_3$=X$_4$=H: 86%, ee = 97%
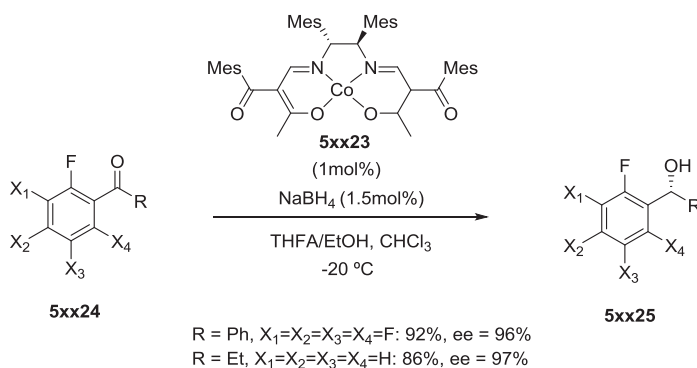
Scheme 5.10. Borohydride reduction of *ortho*-fluorinated benzhyldrols.

In addition to that, the same group also reported the enantioselective borohydride reduction of a range of 1,3-dicarbonyl compounds catalyzed by similar cobalt(II) complex (**5xx26**) providing excellent yields and enantioselectivities (96-99%) along with good diastereoselectivities up to

80% (Scheme 5.11).[67] It is important to highlight that cyclization of these diols allowed a simple route to enantiopure C_2-symmetrical cyclic amines.[68]
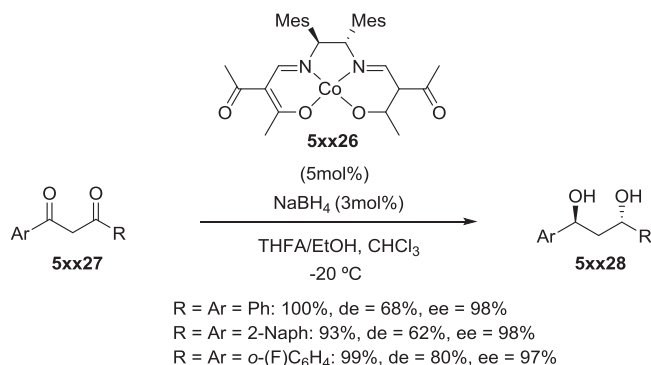
Scheme 5.11. Borohydride reduction of 1,3-diketones catalyzed by (β-oxoaldiminato) cobalt(II) complex **5xx26**.

The enantioselective reduction of aliphatic ketones still remained a challenge. In this regard, the group of Yamada and co-workers develop a cobalt(III) catalyst (**5xx29**) for the enantioselective reduction of a variety of aliphatic ketones with moderate to high yields (16-97%) and enantioselectivities (61-90%) (Scheme 5.12).
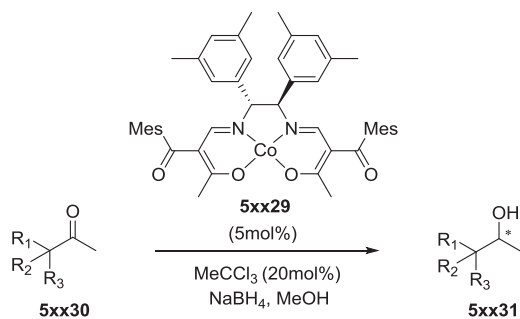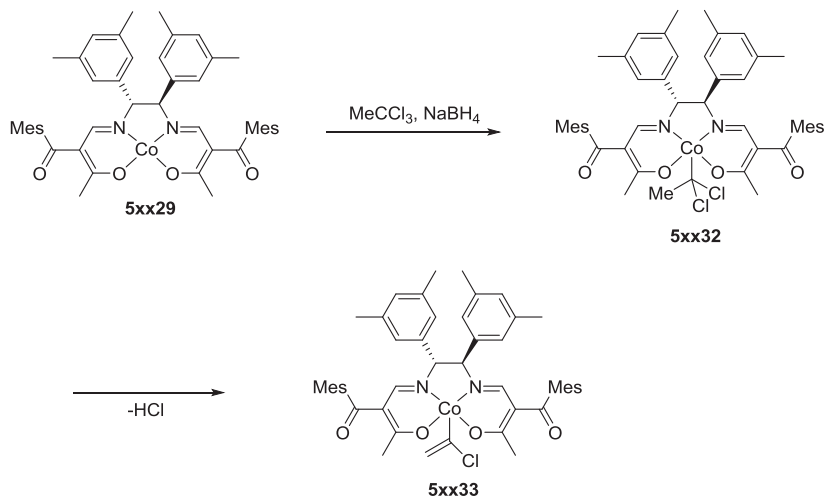
Scheme 5.12. Borohydride reduction of aliphatic ketones catalyzed by **5xx29**.

The authors have demonstrated that the active catalyst is the *in situ* generated cobalt(III) complex **5xx33** which is generated from the cobalt(II) complex **5xx29** upon treatment with 1,1,1-trichloroethane as solvent. Then, the corresponding dichloroethyl-cobalt intermediate (**5xx32**) is further converted into the active cobalt complex **5xx33** via elimination of hydrogen chloride due to the acidity of the terminal methyl group. The active cobalt

complex **5xx33** then underwent the classical mechanism of borohydride reduction of ketones.[69] In 2013, the same authors demonstrated that the corresponding reusable and recyclable cobalt system was also capable to induce chirality in comparable reactions.[70]

Asymmetric hydrosilylation of carbon-heteroatom bonds is a plausible alternative to asymmetric hydrogenation due to the mild conditions and manipulative simplicity.[71] Since the pioneering work developed by Brunner and Amberger in 1991,[72] reasonable attention has been focussed in the asymmetric cobalt-catalyzed hydrosilylation of ketones. In 2010 an important breakthrough was performed by the group of Nishiyama and co-workers who developed a highly efficient cobalt(II) complex of chiral bis(oxazolinylphenyl)amine **5xx34**, that provided enantioselectivities up to 98% (Scheme 5.13).[73]
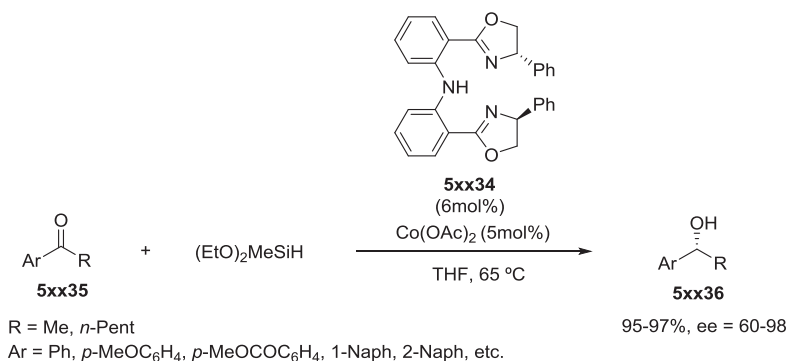
Scheme 5.13. Hydrosililation of alkyl aryl ketones catalyzed by **5xx34**/Co(OAc)$_2$.

Another important reaction is the asymmetric hydrogenation of alkenes for the synthesis of single-enantiomer products. In this field, the group of Ohgo and co-workers reported the use of dimethylglyoximatocobalt(II) compounds in presence of quinine for the asymmetric hydrogenation of alkenes with low to moderate enantiomeric excesses (7-49%).[74] Some years

later, the group of Pfatlz and co-workers reported the hydrogenation of α,β-unsaturated esters using an *in situ* generated cobalt semicorrin complexes with good yield and ee's up to 96%.[75] However, stoichiometric amounts of NaBH$_4$ were needed. In 1992, the group of Iglesias and co-workers reported the use of a 2-aminocarbonylpyrrolide cobalt(I) complex for the asymmetric hydrogenation of ethyl-α-benzoilaminocinnamate with enantioselectivities up to 74%.[76] More recently, in 2012, the group of Chirik and co-workers have reported the use of bis(imino)pyridine cobalt(I) complexes (**5xx37**) for the asymmetric hydrogenation of geminal-disubstituted alkenes with high conversion and enantioselectivities up to 96% (Scheme 5.14).[77]

R$_1$ = Ph, R$_2$ = ^{i}Pr: 87%, ee = 90%
R$_1$ = Ph, R$_2$ = Cy: 70%, ee = 80%
R$_1$ = *p*-NMe$_2$Ph, R$_2$ = ^{i}Pr: 98%, ee = 96%
R$_1$ = *p*-OMePh, R$_2$ = ^{i}Pr: 98%, ee = 94%
R$_1$ = *p*-MePh, R$_2$ = ^{i}Pr: 98%, ee = 90%
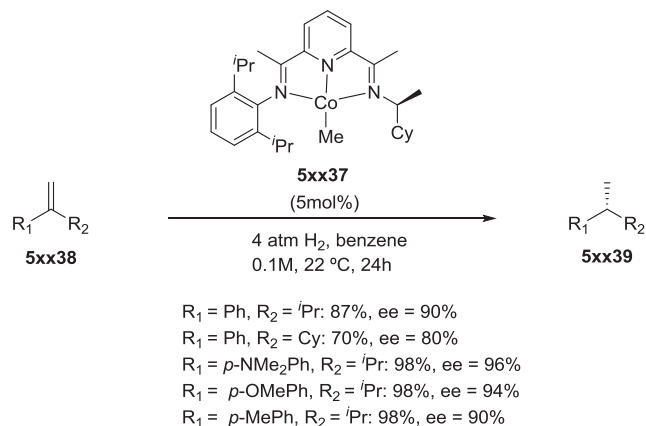
Scheme 5.14. Hydrogenation of geminal-disubstituted alkenes catalyzed by bis(amino)pyridine cobalt (I) complex **5xx37**.

This bis(imino)pyridine cobalt(I) complex **5xx37** has C$_1$-symmetry in which one imine has a large 2,6-diisopropylaryl ring and the other has chiral unit. The authors postulated that the large aryl substituents prevent the formation of the catalytically inactive bis(chelate) metal complexes.[78]

Chiral cobalt catalysts have also been applied to the enantioselective polymerization of monosubstituted epoxides where chiral racemic

monomers are kinetically resolved during polimerization. Two products are obtained with this process: enantiopure epoxides and stereoregular polyethers. In 2008, Coates and co-workers reported a chiral bimetallic cobalt(III) catalyst **5xx40** for the kinetic resolution of monosubstituted epoxides.[79] This enantioselective polymerization catalyst provided high activity and enantioselectivities up to 99% for a range of ring-opened isotactic polyethers **5xx42** (Scheme 5.15).
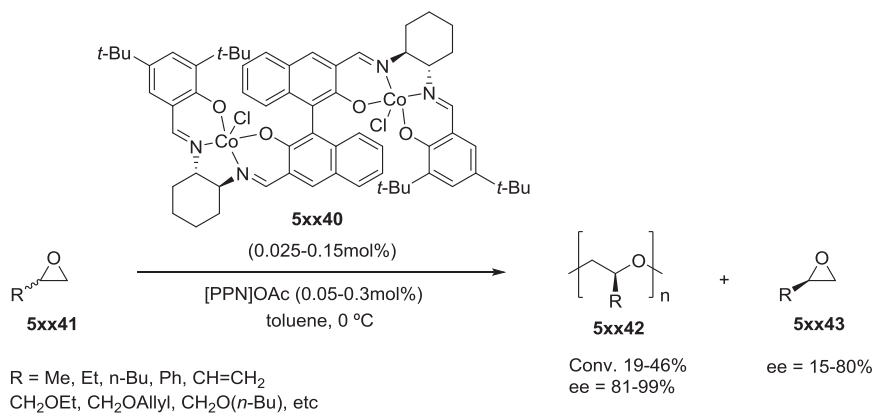
Scheme 5.15. Polymerization of epoxides catalyzed by bimetallic cobalt (III) catalyst **5xx40**.

Like most metal-catalyzed systems, two products can be obtained in the cobalt-catalyzed coupling reaction of carbon dioxide and epoxides: cyclic carbonates and polycarbonate products depending on different parameters.[80] A powerful tool for the synthesis of chiral polycarbonates is the copolymerization of monosubstituted epoxides with CO_2. Recently, Lu and co-workers developed the enantioselective copolymerization of cyclohexene oxide with CO_2 catalyzed by chiral dissymmetrical salen cobalt(III)NO_3 complex **5xx44**. This process yielded the corresponding chiral polycarbonate **5xx46** with enantioselectivities up to 96% (Scheme 5.16). It

has to be highlighted that this highly isotactic poly(cyclohexene carbonate) is the first semicrystaline CO_2-based polycarbonate.
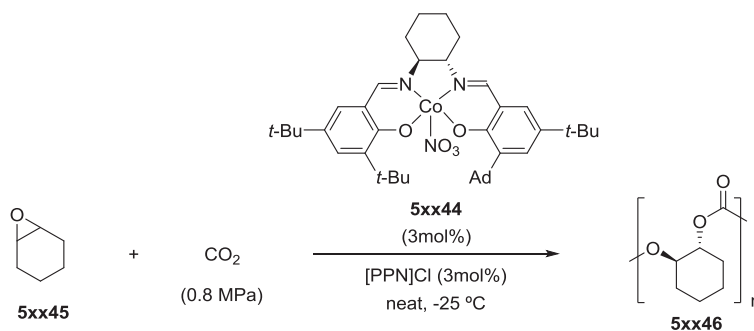
Scheme 5.16. Copolimerization of cyclohexene oxide with CO_2 catalyzed by chiral dissymmetrical salen cobalt(III)NO_3 complex **5xx44**.

5.1.4. COBALT-NHC COMPLEXES IN CATALYSIS

Since the pioneering work of Lappert and co-workers in the late 70s in the synthesis of mono- and bis-carbenes complexes of iron, cobalt, nickel and ruthenium, N-heterocyclic carbenes were employed as ligands for the synthesis of unusual organometallic cobalt species.[81] Major breakthroughs have been achieved in organometallic chemistry rather than in catalysis. Catalytic applications using Co-NHC complexes only appeared recently and are still scarce.[82]

The first application of Co-NHC complexes was reported by Gibson and Loch in 2003.[83] Those authors reported the synthesis of various dinuclear complexes containing NHC ligands (**5xx47**, **5xx48** and **5xx49**) which were tested in the Pauson-Khand reaction (Scheme 5.17). Nevertheless, the [(NHC)Co^0] systems showed lower activity that the $Co_2(CO)_8$ counterpart. It has to be point out though that this served to proof that NHC could be viable ligands for cobalt catalysis.
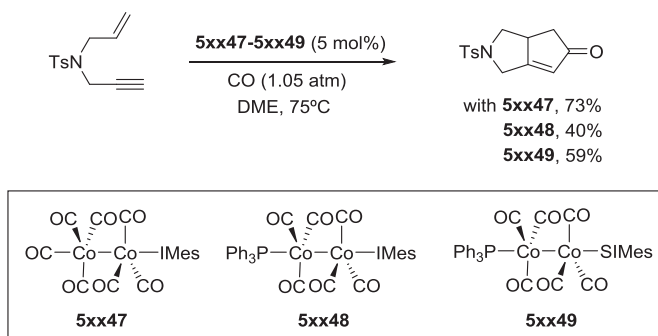
Scheme 5.17. [(NHC)Co]-catalyzed Phauson-Khand reaction.

Some years later, in 2005, Okamoto and co-workers reported the use of **5xx50** in combination with Zn powder and $CoCl_2$ for the efficient intramolecular cyclotrimerization of triynes (Scheme 5.18).[84]
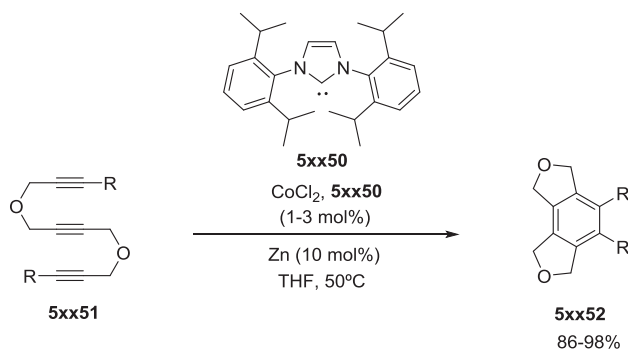
Scheme 5.18. Intramolecular cyclotrimerization of triynes catalyzed by **5xx50**.

More recently, Gandon and Aubert tested the effect of NHC in the cyclization of enediynes for the formation of polycyclic cyclohexadienes.[85] The NHC ligand showed superior activity in this reaction when compared to other well established catalytic systems, such as $[(Cp)Co(CO)_2]/FeCl_3$ and $CoI_2/Mn/PPh_3$. Importantly, NHC **5xx50** could be used catalytically with 1eq of manganese (used as reducing agent), while 2eq. of PPh_3 and 10eq. of Mn were generally required. Furthermore, substrates possessing terminal

substituents on the olefin cyclized in a diastereospecific manner (Scheme 5.19).
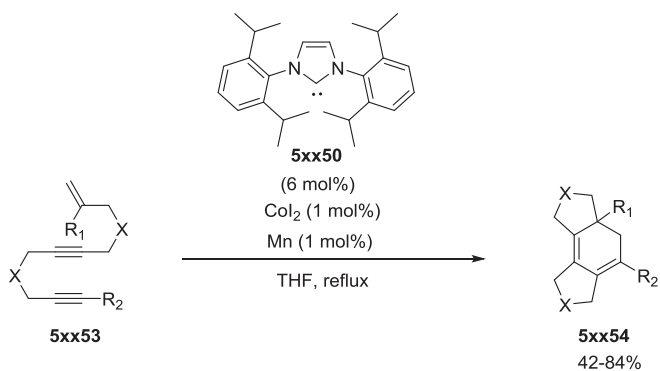
Scheme 5.19. Cyclization of enediynes catalyzed by **5xx50**.

The group of Llewellyn and co-workers obtained promising results in the hydroformilation of 1-octene using the hydrido cobalt complex **5xx55** as catalyst (Scheme 5.20).[86] This catalytic system provided unusual high regioselectivity towards the more substituted 2-methyl-octanal product rather than the linear nonanal. The authors postulated that the [(NHC)Co] complex catalyzes the alkene isomerization prior to the hydroformilation.
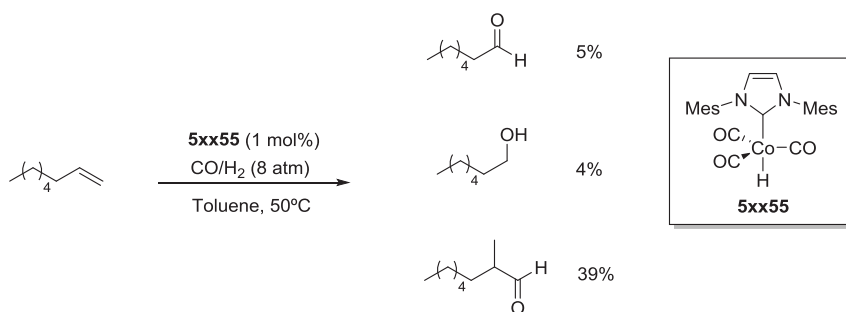
Scheme 5.20. Hydroformilation of 1-octene catalyzed by **5xx55**.

Despite the early interest of organometallic chemists, the successful use of Co-NHC systems in catalysis only dates back to 2003 and nowadays, only few cobalt N-heterocyclic carbenes have been reported.

5.2. OBJECTIVE OF THIS CHAPTER

As previously commented, among the polydentate ligand structure with carbene donors, tripodal and pincer-type systems have attracted much of attention as a result of their high activity, variability and stability. In this regard, NHCs have shown to be alternative ligands to phosphines in several catalytic processes.

There are only two examples in the literature which deal with Cobalt pincer complexes, being all the examples CNC-type ligands. Moreover, the synthesis and application of chiral Cobalt pincer complexes has not been reported to date.

In this context, we decided to prepare a family of chiral CˆNˆC ligands in which a nitrogen atom of the imidazole moiety is substituted by methyl and phenyl groups (Scheme 5.21, **5xx56**), methyl and naphthyl groups (Scheme 5.21, **5xx57**) and methyl and cyclohexyl groups (Scheme 5.21, **5xx58**). Moreover, the synthesis of the corresponding Cobalt related complexes has been attempted and their catalytic performance in the asymmetric hydrogenation of ketones was studied. In addition, experiments in order to determine the species involved in catalysis were carried out.
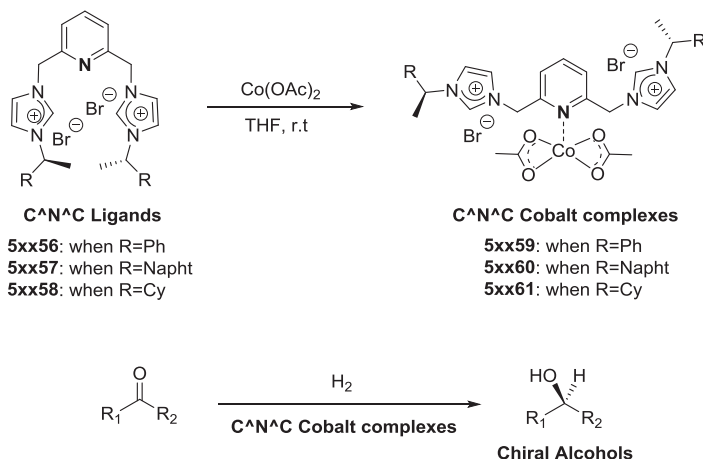
Scheme 5.21. Chiral CˆNˆC Cobalt complexes and their application to the asymmetric hydrogenation of ketones.

5.3. RESULTS AND DISCUSSION

5.3.1. SYNTHESIS OF CHIRAL PYRIDINE-BISCARBENE LIGANDS

The synthesis of the *bis*-imidazolium salts **5xx56-58** can be accomplished in two steps. The strategy used for the preparation of these compounds was previously reported by Herrmann and co-workers (for compounds **5xx56** and **5xx57**).[87] The first step involved the synthesis of the imidazoles **5xx62-64** through a one-pot method starting from glyoxal, formaldehyde and the corresponding amine (Scheme 5.22). The chiral modified imidazoles **5xx62-64** were achieved in moderate yields (25-32%), in agreement with the literature values. To synthesize the pyridine-bridge imidazolium salts **5xx56-58**, the 2,6-bis(bromomethyl)-pyridine was treated with two equivalents of the corresponding chiral modified imidazole (**5xx62-64**) in THF at 80ºC during 24h. After recrystalization (for compound **5xx56** and **5xx57**) or column chromatography (for **5xx58**) the pyridine-bridge

imidzolium salts **5xx56-5xx58** were obtained in moderate to good yields (40-63%) (Scheme 5.22).
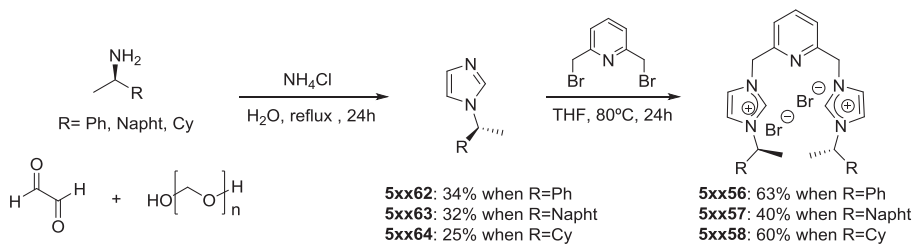
Scheme 5.22. Synthesis of the pyridine-bridge imidazolium salts **5xx56**-**5xx58**.

As proof of concept, we test our pyridine-bridge imidazolium salt **5xx56** in the asymmetric hydrogenation of ketones. For these initial test high catalyst loading (20mol%) and high pressure (40bar) were employed, using Co(OAc)$_2$ as cobalt precursor, KO^{t}Bu as base, T=40 ºC and THF as solvent. The ratio between **5xx56**:Co(OAc)$_2$:base was set at 1:1:3 and cyclohexyl phenyl ketone was chosen as substrate. The results are shown in Table 5.1.

The combination between the pyridine-bridge imidazolium salt **5xx56** with Co(OAc)$_2$ as precursor effectively catalyzed the asymmetric hydrogenation of cyclohexyl phenyl ketone with 80% conversion and moderate enantiomeric excess (33%) (entry 1). Importantly, no conversion was observed using the pyridine-bridge imidazolium salt **5xx56** or the Co(OAc)$_2$ precursor alone (entries 2 & 3).

Table 5.1. Asymmetric hydrogenation of cyclohexyl phenyl ketone catalyzed by **5xx56**:Co(OAc)$_2$, **5xx65** and Co(OAc)$_2$.[a]
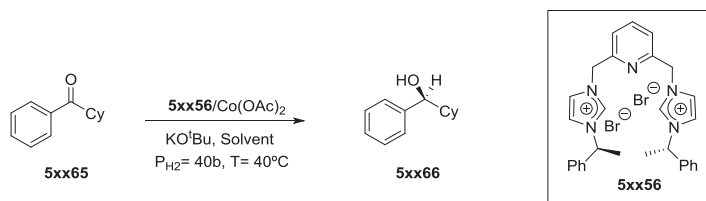
Entry	Catalyst	Conv. (%)[b]	ee (%)[c]
1	**5xx56**/Co(OAc)$_2$	80	33
2	**5xx56**	0	-
3	Co(OAc)$_2$	0	-

[a] General conditions: **5xx56**:Co(OAc)$_2$:KO^{t}Bu= 1:1:3, 0.02mmol of **5xx56**, 0.02mmol of Co(OAc)$_2$, 0.06mmol of KO^{t}Bu, 0.1mmol of ketone, 2.5ml of THF, H$_2$ pressure= 40bar, temperature = 40ºC, time = 16h. [b] Conversion was calculated by ^{1}H NMR. [c] Enantiomeric excess was calculated by GC using a ChirasilDex CB column.

In view of the results obtained, we focus our efforts in the isolation of a Co-Pyridine-Biscarbene complex for its application in the asymmetric hydrogenation of ketones.

5.3.2. SYNTHESIS OF CHIRAL CO-PYRIDINE-BISCARBENE COMPLEXES

As previously outlined in the introduction, promising results have been obtained in the asymmetric hydrogenation of alkenes using cobalt alkyl pincer type complexes.[77] With this results in mind, we envisioned a synthesis for the related Co(I) Pyridine-Biscarbene complexes **5xx67**-**5xx69** from the Co(II) Pyridine-Biscarbene complexes **5xx70**-**5xx72** in two steps (Scheme 5.23).
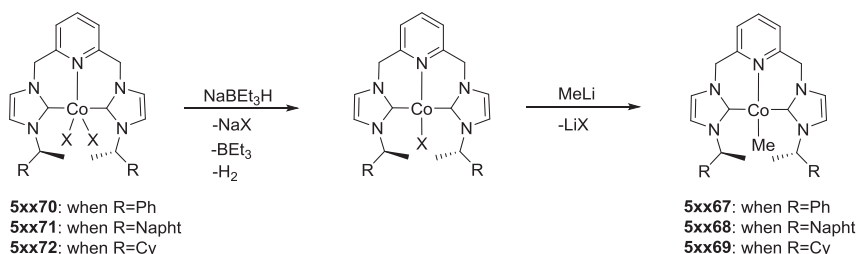
Scheme 5.23. Envisioned synthesis of Co(I) Pyridine-Biscarbene complexes **5xx67**-**5xx69** from complexes **5xx70-5xx72**.

As previously outlined in Seccion 5.2.1.1., two synthetic procedures have been reported in the literature for the synthesis of Co(II) Pyridine-Biscarbene complexes of the type Py-bisc-CoX$_2$. Nevertheless, both methodologies are limited to pyridine-bridged imidazolium salts containing sterically demanding groups (2,6-di*iso*propylphenyl) at the imidazole fragment.[50,51] For this reason, we explored the reaction of the pyridine-bridge imidazolium salts (**5xx56-5xx58**) with Co(OAc)$_2$ extrapolating the common conditions used for the related palladium systems.[87]

The pyridine-bridge imidazolium salts **5xx56** was reacted with Co(OAc)$_2$ in THF for 48h during which time a blue powder precipitated. The ^{1}H NMR spectrum showed the signals corresponding to the initial pyridine-bridge imidazolium salt **5xx56** with the characteristic acidic proton at 9.5ppm. However, the solubility as well as the color of the isolated compound was very distinct from that of the initial ligand.

Compared to the spectra of the Co(OAc)$_2$, the IR spectra of the isolated blue compound showed a shift to lower frequencies of the $v(CO_2)$ band ($v(CoOAc)_2$ 1559, 1419 and 1341; v(blue compound) 1552, 1418 and 1330) as well as the characteristic bands of the pyridine-bridged imidazolium salt **5xx56** (Figure 5.10). This fact suggested that the isolated blue compound incorporate the ligand **5xx56** and the Co(OAc)$_2$ moiety coordinated.

Nevertheless, the acetate signals of the Co(OAc)$_2$ fragment were not detected by NMR-spectroscopy. In this regard, an NMR of the Co(OAc)$_2$ precursor was recorded in which no signals were observed for the acetate moiety. This observation was thus in agreement with the NMR results for the isolated blue solid, in which the acetate signals couldn't be detected.
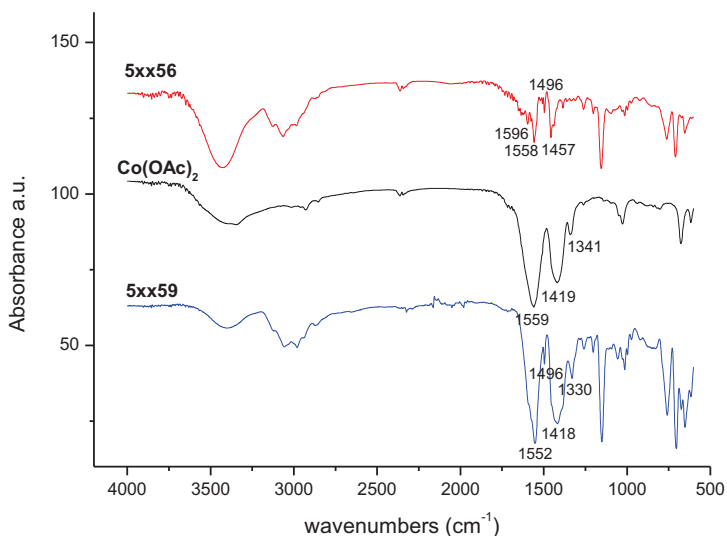
Figure 5.10. IR spectra comparison for pyridine-bridge imidazolium salt **5xx56**, Co(OAc)$_2$ precursor and Co(II)-pyridine biscarbene complex **5xx59**.

In order to gain further information about the oxidation state of our cobalt complex, the magnetic susceptibility was measured and the obtained value (μeff=5.2) indicated a Co^{2+} present in the compound (range for Co^{2+}=4.3-5.2). When the Co(II) complex was analysed by mass spectrometry (HRMS), the detection of the pyridine-bridge imidazolium salt **5xx56** and the Co(OAc)$_2$ moiety were individually identified. This fact can be explained by the facility of the pyridine-Co(OAc)$_2$ to fragment under the mass spectra conditions. In view of this result, it was decided to carry out an

ICP of the Co(II) complex in order to ascertain the percentage of cobalt in our sample. The ICP value obtained ([Co]= 7,62%) was in agreement with the theoretical value ([Co]=7.5%) for the Co(II) complex **5xx59**. In line with that, the determination by Elemental Analysis, also confirmed the formation of **5xx59** (calc. value for $C_{33}H_{37}CoBr_2N_5O_4.CH_2Cl_2$, C, 46.87; H, 4.51; N, 8.04; Found: C, 46.09; H, 4.48; N, 8.19).

With all the collected data, it is proposed that the structure of the isolated blue compound corresponds to the Co(II)-pyridine complex **5xx59** having the Co(OAc)$_2$ fragment coordinated to the pyridine of the ligand instead of the initially expected Co(II)-pyridine biscarbene complex **5xx70** (Scheme 5.24). Complexes **5xx60** and **5xx61** bearing a naphthyl and a cyclohexyl moiety at the imidazole ring respectively were also obtained by reaction of the corresponding pyridine-bridge imidazole salts (**5xx57** and **5xx58**) with Co(OAc)$_2$ in THF at room temperature for 48h (Scheme 5.24).
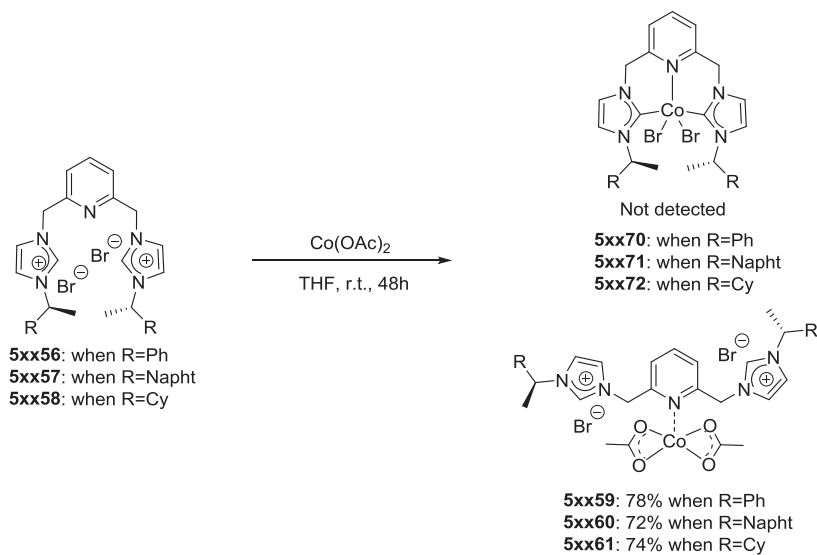
Scheme 5.24. Synthesis of Co(II)-pyridine complexes **5xx59-5xx61**.

At this stage, we investigate two different synthetic procedures in order to isolate a Co(II)-pyridine biscarbene complex as well as to find out the role of the base in our catalytic system. This strategy involved two synthetic pathways: a) reaction of pyridine-brigded imidazolium salt **5xx56** with KO^{t}Bu and then addition of Co(OAc)$_2$ precursor and b) reaction of Co(II)-pyridine complex **5xx59** with KO^{t}Bu as base.

We first explored the pathway involving a first reaction of the pyridine-bridged imidazolium salt **5xx56** with KO^{t}Bu and then addition of the Co(OAc)$_2$ as metal precursor. Initially, the pyridine-brigded imidazolium salt **5xx56** was deprotonated using 3eq of KOtBu (same eq. as used in catalysis) to yield the corresponding carbene **5xx73** (Scheme 5.25). In the ^{1}H NMR spectra, the disappearance of the carbene proton at 10.96ppm confirmed the formation of the carbene **5xx73**, which was isolated in 50% yield.
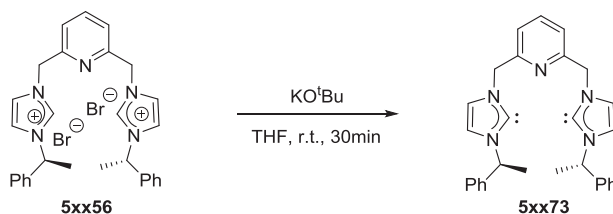
Scheme 5.25. Synthesis of carbene **5xx73**.

In 1960, Wanzlick and Schikora reported a chemical equilibrium between the carbene compound and its dimer.[88] In such case, the disappearance of the imidazole proton could not confirm the formation of the carbene moiety and indeed, the dimer compound is not able to react further. As proof of concept, the formation of the borane compound **5xx74** by reaction with BH$_3$-THF was carried out (Scheme 5.26). The crude product was purified by column chromatography to obtain **5xx74** in 30% yield. In the ^{1}H NMR, a

broad quartet at 2.42ppm (J_{H-B}= 84Hz) was detected and attributed to the BH$_3$ unit with coupling between the protons and the boron nucleus ([11]B, S=3/2). In the ^{11}B{^{1}H} NMR spectra, a single peak was observed at -33.3ppm. Mass spectrometry was also used for the characterization of this compound, detecting the main ion at m/z= 462.2830, attributed to the [M-BH$_3$]$^+$ ion. This assay confirmed the previous formation of the carbene **5xx73** and excludes the formation of its dimer.
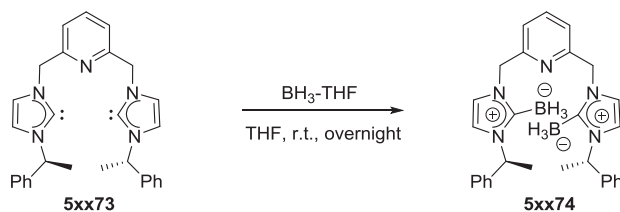
Scheme 5.26. Synthesis of the borane adduct **5xx74**.

Once these preliminary tests were performed, we next carry out the reaction of the pyridine-bridged imidazolium salt **5xx56** with KO^{t}Bu and Co(OAc)$_2$ as metal precursor. It has to be mentioned that in this case, the generated carbene **5xx73** was not isolated in order to mimic the scenario under the catalytic conditions were a 80% conversion and 33% ee was obtained for the asymmetric hydrogenation of cyclohexyl phenyl ketone (Table 5.1, entry 1).

The pyridine-bridged imidazolium salt **5xx56** was reacted with 3eq of KO^{t}Bu for 30min in order to assure the formation of the corresponding carbene ligand. Upon addition of the base, a color change from cream to brown was observed. Then, the Co(OAc)$_2$ precursor was added to the mixture. The reaction was run for overnight at room temperature and after precipitation with a DCM/ether mixture, two products were isolated. The

products were characterized by NMR, IR-spectroscopy and magnetic susceptibility.

After the characterization by NMR and IR-spectroscopy, one of the products was attributed to unreacted $Co(OAc)_2$. On the other hand, the ^1H NMR spectra of the second isolated product showed the disappearance of the imidazole proton which confirmed the successful deprotonation of the initial imidazole **5xx56**. However, no more information could be extracted by ^1H NMR due to the broadness of the peaks.
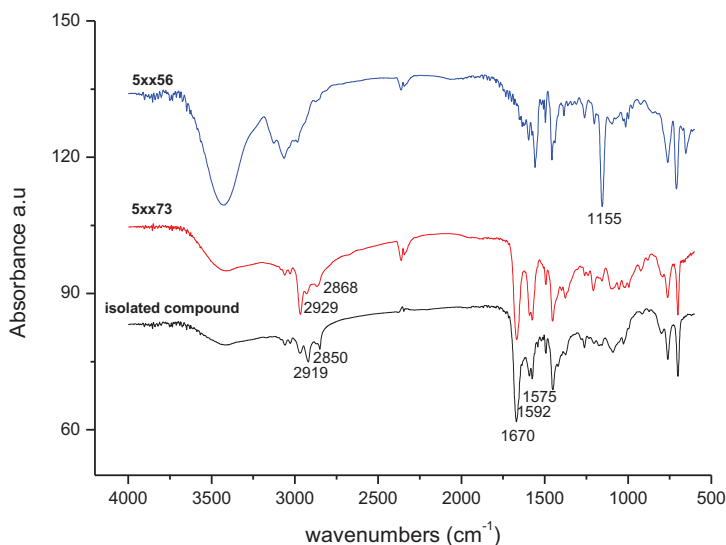
Figure 5.11. IR spectra comparison for pyridine-bridge imidazolium salt **5xx56**, carbene ligand **5xx73** and the isolated compound.

Compared to the spectra of the ligand (**5xx56**), the IR spectra of the second isolated product showed the disappearance of the band at 1155cm^{-1} attributed to the C-N stretching band (Figure 5.11). Moreover, a shift to lower frequencies in the C-H region was detected when compared to the

carbene ligand **5xx73** (Figure 5.11). It has to be highlighted, that the bands corresponding to the acetate moiety were not present in the IR spectra.

In order to gain further information about the oxidation state of our cobalt complex, the magnetic susceptibility was measured and the obtained value (μeff=5.0) indicated a Co^{2+} present in the compound (range for Co^{2+}=4.3-5.2).

With all the collected data, it is proposed that the structure of the isolated compound corresponds to the Co(II)-pyridine biscarbene complex **5xx75** in which the imidazolium fragments are coordinated to the cobalt atom. In this case the cobalt nucleus is coordinated to two bromide atoms which came from the initial imidazolium salt **5xx56** (Scheme 5.27).
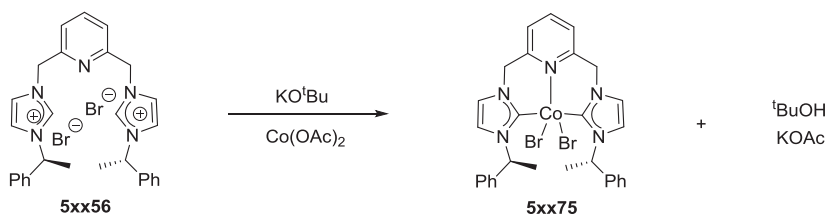
Scheme 5.27. Proposed structure for **5xx75** from reaction of pyridine-bridged imidazolium salt **5xx56**, KO^{t}Bu as base and Co(OAc)$_2$.

The second pathway involved the use of the Co(II)-pyridine complex **5xx59** in combination with KO^{t}Bu as base. In this case, the reaction was carried out with the Co(II)-pyridine complex **5xx59** and 1.8eq of KO^{t}Bu. Upon addition of the base, a color change from blue to brown was observed and the solution became homogeneous (note that the Co(II)-pyridine complex **5xx59** is insoluble in THF). Two products were also isolated after precipitation with a DCM/ether mixture. The characterization of the products was performed using NMR and IR-spectroscopy.

The characterization by ^{1}H NMR and IR-spectroscopy of one product revealed the isolation of unreacted Co(II)-pyridine complex **5xx59**, so as less than 2eq of base were used for this test. To our delight, the second isolated product exhibited the same pattern in the IR spectra as well as in the ^{1}H NMR (with the disappearance of the imidazolium protons) confirming the formation of the previously proposed Co(II)-pyridine biscarbene complex **5xx75** having the Co-Br$_2$ coordinated to the pyridine and iminazolium fragments (Scheme 5.28).
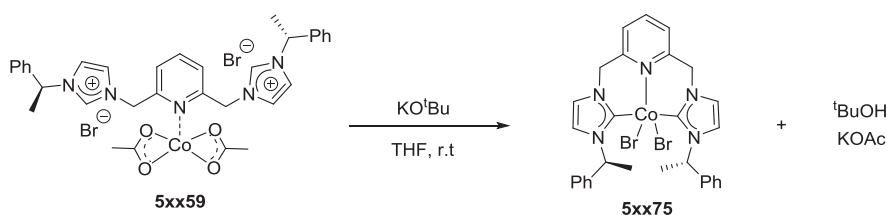
Scheme 5.28. Proposed structure for **5xx75** from reaction of Co(II)-pyridine **5xx59** and KO^{t}Bu as base.

In view of the results obtained, we could conclude that both pathways a) reaction of pyridine-brigded imidazolium salt **5xx56** with KO^{t}Bu and then addition of Co(OAc)$_2$ precursor or b) reaction of Co(II)-pyridine complex **5xx59** with KO^{t}Bu as base, gave the Co(II)-pyridine biscarbene complex **5xx75**. We could extract as well that the role of the base, in both cases, is to deprotonate the imidazolium salt to form the corresponding pyridine biscarbene **5xx73** (pathway a) or to form the Co(II)-pyridine biscarbene complex **5xx75** (pathway b).
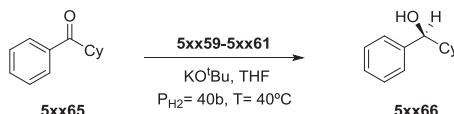
5.3.3. CATALYTIC ASYMMETRIC HYDROGENATION OF KETONES

We decided to test our Co(II)-pyridine complexes **5xx59**, **5xx60** and **5xx61** in the asymmetric hydrogenation of ketones. As there were no previous
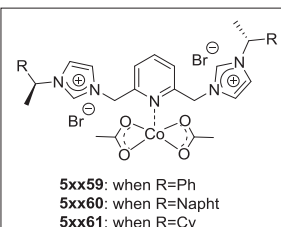
studies using chiral Co-NHCs as catalysts for hydrogenation processes, high catalyst loading (20mol%) (based on the proposed structures of **5xx59-5xx61**) as well as high H_2 pressures (40bar) using KO^tBu as base, T= 40ºC and THF as solvent were first tested. For these initial tests, cyclohexyl phenyl ketone was chosen as a benchmark substrate. The ratio between catalyst:base was 1:3. First results are summarized in Table 5.2.

The chiral Co(II)-pyridine complex **5xx59** effectively catalyzed the asymmetric hydrogenation of cyclohexyl phenyl ketone with 98% conversion and 55% enantioselectivity (entry 1). On the other hand, poor catalytic performance was observed when the chiral Co(II)-pyridine complex **5xx60** and **5xx61** were tested (entry 2 & 3). It has to be highlighted though, that the Co(II)-pyridine complex **5xx61** provided same results in terms of enantioselectivity than the Co(II)-pyridine complex **5xx59**.

Table 5.2. Asymmetric hydrogenation of cyclohexyl phenyl ketone catalyzed by **5xx59**, **5xx60** and **5xx61**.[a]

Entry	Catalyst	Conversion (%)[b]	ee (%)[c]
1	**5xx59**	98	55
2	**5xx60**	10	27
3	**5xx61**	21	56

[a] General conditions: Co(II)-complex/KO^tBu= 1:3, 0.02mmol of Co(II)-complex, 0.06mmol of KO^tBu, 0.1mmol of ketone, 2.5ml of THF, H_2 pressure= 40bar, temperature = 40ºC, time = 16h. [b] Conversion was calculated by ^1H NMR. [c] Enantiomeric excess was calculated by GC using a ChirasilDex CB column.

The study of different solvents was conducted using the Co(II)-pyridine complex **5xx59** (Table 5.3). Using an apolar solvent such as toluene, low conversion and enantioselectivity was obtained (27% conversion, 31% ee) compared to the results in THF (Entry 1 & 2). Using polar aprotic solvents such as CH_3CN also low conversion and enantiomeric ratio were achieved (entry 3). Nonetheless, the use of DMF as solvent achieved full conversion although lower enantioselectivity (43%) was reached. It has to be mentioned that the Co(II)-pyridine complex **5xx59** was only soluble in DMF which could also explained the high conversion obtained with this solvent. In the case of THF, the initial cobalt catalyst is not soluble although after addition of the base an homogeneous brown solution is observed.

Table 5.3. Asymmetric hydrogenation of cyclohexyl phenyl ketone catalyzed by **5xx59** using different solvents.[a]
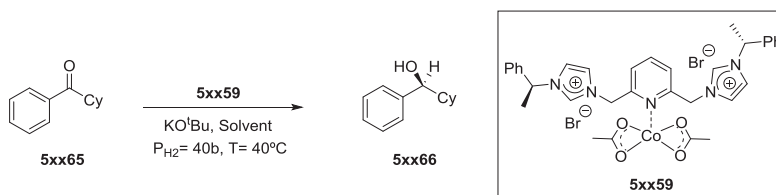
Entry	Solvent	T (°C)	P_{H2} (bar)	Conv. (%)[b]	ee (%)[c]
1	THF	40	40	98	55
2	Toluene	40	40	27	31
3	CH_3CN	40	40	32	20
4	DMF	40	40	100	43

[a] General conditions: Co(II)-complex/KO^{t}Bu= 1:3, 0.02mmol of Co(II)-complex, 0.06mmol of KO^{t}Bu, 0.1mmol of ketone, 2.5ml of solvent, H_2 pressure= 40bar, temperature = 40°C, time = 16h. [b] Conversion was calculated by ^{1}H NMR. [c] Enantiomeric excess was calculated by GC using a ChirasilDex CB column.

Having found THF as the optimal solvent, we next carried out the asymmetric hydrogenation of cyclohexyl phenyl ketone at diverse catalyst

loadings (Table 5.4). A decrease in the catalyst loading from 20mol% to 10mol% practically did not affect to neither the conversion nor the enantioselectivity (entries 1-3). Interestingly, a further decrease up to 5mol% of catalyst loading showed a moderate 60% conversion towards the corresponding chiral alcohol preserving the enantiomeric ratio untouched.

Table 5.4. Asymmetric hydrogenation of cyclohexyl phenyl ketone catalyzed by **5xx59** at different catalyst loadings.[a]
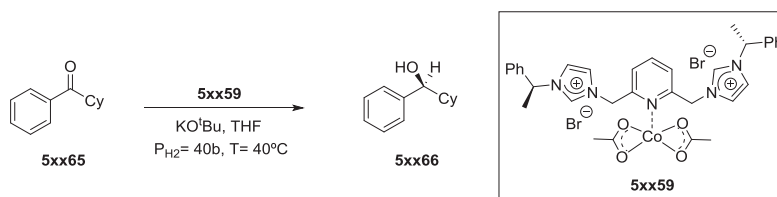
Entry	Cat. loading (mol%)	Conv. (%)[b]	ee(%)[c]
1	20	98	55
2	15	90	54
3	10	90	55
4	5	60	55

[a] General conditions: Co(II)-complex/KO^{t}Bu= 1:3, 2.5ml of THF, H_2 pressure= 40bar, temperature = 40ºC, time = 16h. [b] Conversion was calculated by ^{1}H NMR. [c] Enantiomeric excess was calculated by GC using a ChirasilDex CB column.

The study of the temperature was also conducted at 5mol% of catalyst loading using KO^{t}Bu as base and THF as solvent (Table 5.5). Increasing the temperature from 40ºC to 80ºC had a dramatic impact on the enantiomeric excess whereas the conversion was maintained (entry 1 & 2). On the contrary, at room temperature (entry 3) the reaction was inhibited. In terms of pressure, the best balance between conversion and enantiomeric excess was found at 20bar of H_2 pressure (entry 4).

Table 5.5. Asymmetric hydrogenation of cyclohexyl phenyl ketone catalyzed by **5xx59** at distinct temperatures and pressures.[a]
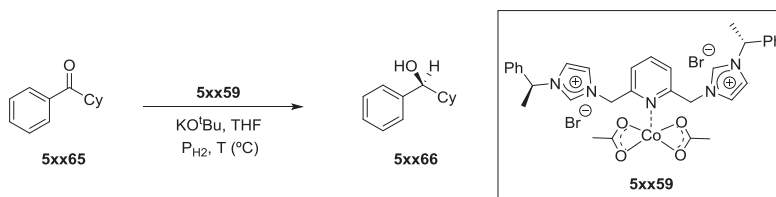
Entry	T (ºC)	P_{H2} (bar)	Conv. (%)[b]	ee(%)[c]
1	40	40	60	55
2	80	40	56	20
3	R.T	40	0	-
4	40	20	40	55
5	40	10	24	55

[a] General conditions: Co(II)-complex/KO^{t}Bu= 1:3, 0.005mmol of Co(II)-complex, 0.015mmol of KO^{t}Bu, 0.1mmol of ketone, 2.5ml of THF, time = 16h. [b] Conversion was calculated by ^{1}H NMR. [c] Enantiomeric excess was calculated by GC using a ChirasilDex CB column.

Next, an optimization of the base was performed (Table 5.6). When DBU, NaO^{i}Pr, and NaOH were used (entries 2-4), no conversions were obtained, indicating that stronger bases were needed. However, the use of stronger bases NaH inhibited the reaction (entry 5). This fact could be attributed to some decomposition of the catalyst under such conditions. The use of potassium bis(trimethylsilyl) amide (KHMDS) (entry 6) gave similar results in terms of conversions (*ca.* 37%) with enantiomeric excess mainly unaffected (*ca.* 54%). The relatively high pKa value required to gather activity could be attributed to the need to deprotonate the pyridine-bridge imidazolium salt **5xx59** to form the catalytically active species as suggested in the previous section.

Table 5.6. Asymmetric hydrogenation of cyclohexyl phenyl ketone catalyzed by **5xx59** using different bases.[a]
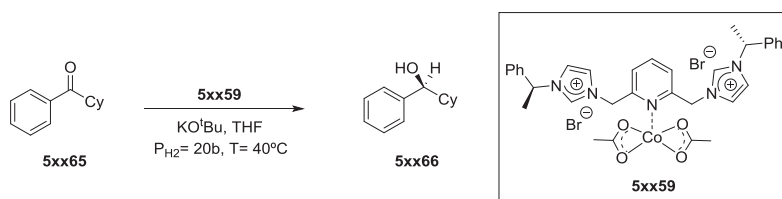
| Entry	Base	pKa	Conv. (%)[b]	ee (%)[c]
1	KO^{t}Bu	17	40	55
2	DBU	12	0	-
3	NaO^{i}Pr	15.5	0	-
4	NaOH	13.8	0	-
5	NaH	35	0	-
6	KHMDS	26	37	54

[a] General conditions: Co(II)-complex/KO^{t}Bu= 1:3, 0.005mmol of Co(II)-complex, 0.015mmol of KO^{t}Bu, 0.1mmol of ketone, 2.5ml of THF, H$_2$ pressure= 20bar, temperature = 40°C, time = 16h. [b] Conversion was calculated by ^{1}H NMR. [c] Enantiomeric excess was calculated by GC using a ChirasilDex CB column.

Finally, the effect of the catalyst:base ratio was investigated (Table 5.7). The reaction did not proceed in absence of the base (entry 1). No conversion was observed with **5xx59**:base ratio below 1:3 (entries 2-3). At ratios of 3, 4 and 6, conversion of 40-49% were obtained with a modest decrease in the enantioselectivity when 6 eq. of base were used (entries 4-6). As a result of this study, we can extract that the base play a fundamental role in the reaction and that the optimal **5xx59**:base ratio of 1:3 indicate that deprotonation of the pyridine-bridge imidazolium salt **5xx59** is mandatory to form the catalytically active species as outlined in the previous section.

Table 5.7. Asymmetric hydrogenation of cyclohexyl phenyl ketone catalyzed by **5xx59** using KOtBu as base at various catalyst:base ratios.[a]
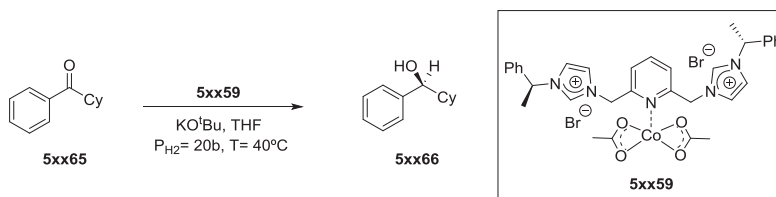
Entry	Catalyst:Base	Conv. (%)[b]	ee (%)[c]
1	No base	0	-
2	1:1	0	-
3	1:2	0	-
4	1:3	40	55
5	1:4	45	50
6	1:6	49	39

[a] General conditions: 0.005mmol of Co(II)-complex, 0.015mmol of KO^{t}Bu, 0.1mmol of ketone, 2.5ml of THF, H$_2$ pressure= 20bar, temperature = 40°C, time = 16h. [b] Conversion was calculated by ^{1}H NMR. [c] Enantiomeric excess was calculated by GC using a ChirasilDex CB column.

Based on these reaction conditions, the scope and limitations of the Co(II)-pyridine complex **5xx59** were looked at. The optimized conditions were 5mol% of catalyst loading, a ratio **5xx59**:base of 1:3, using KO^{t}Bu as base, at P$_{H2}$= 20bar, T= 40°C for 16h. Nevertheless, very low conversions were achieved using these conditions for other substrates than the cyclohexyl phenyl ketone used for the optimization. Although, high pressures were applied (P$_{H2}$= 40bar), still very low conversion (<5%) were obtained in most cases. For this reason, we decided to performed the substrate scope at 20mol% of catalyst loading and P$_{H2}$= 40bar. The results are illustrated in Table 5.8. In order to compare the catalytic activity of the Co(II) pyridine complex **5xx59** with the Co(II) pyridine complex **5xx61**, which gave similar ee's values (Table 5.2, entries 1 & 3) we have performed the asymmetric

hydrogenation of some ketones with both catalytic systems. In brackets are shown the results obtained using the Co(II) pyridine complex **5xx61**.

Table 5.8. Scope of the asymmetric hydrogenation of ketones catalyzed by **5xx59** and **5xx61**.[a]
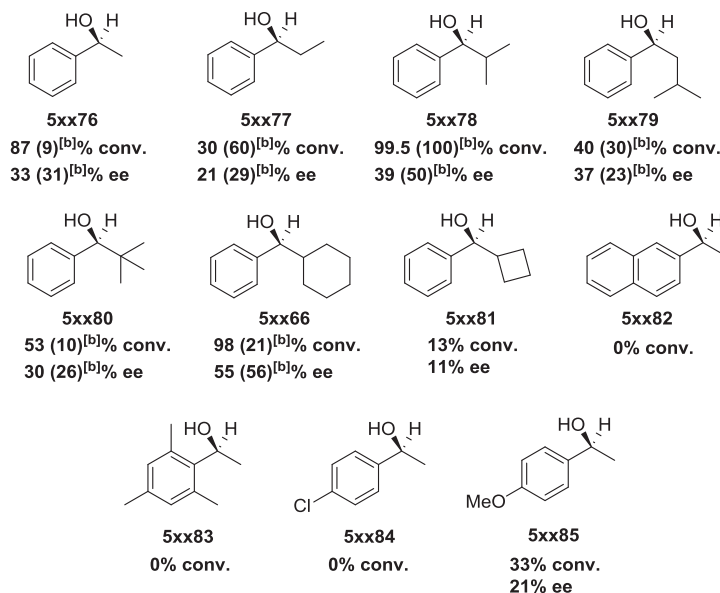
5xx76	**5xx77**	**5xx78**	**5xx79**
87 (9)[b]% conv.	30 (60)[b]% conv.	99.5 (100)[b]% conv.	40 (30)[b]% conv.
33 (31)[b]% ee	21 (29)[b]% ee	39 (50)[b]% ee	37 (23)[b]% ee
5xx80	**5xx66**	**5xx81**	**5xx82**
53 (10)[b]% conv.	98 (21)[b]% conv.	13% conv.	0% conv.
30 (26)[b]% ee	55 (56)[b]% ee	11% ee	
5xx83	**5xx84**	**5xx85**	
0% conv.	0% conv.	33% conv.	
		21% ee	

[a] General conditions: 0.005mmol of Co(II)-complex, 0.015mmol of KO^{t}Bu, 0.1mmol of ketone, 2.5ml of THF, H$_2$ pressure= 40bar, temperature = 40ºC, time = 16h. [b] Using **5xx61** as catalyst. Conversion was calculated by ^{1}H NMR. Enantiomeric excess was calculated by GC using a ChirasilDex CB column.

First of all, acetophenone was converted into the corresponding alcohol in high conversions (87%) whereas low ee's were achieved (33%) using catalyst **5xx59**. Changing the methyl group by an ethyl at the alkyl position had a decrease in both, conversion and enantioselectivity (**5xx77**). Nevertheless, when *iso*-butyrophenone was used as substrate almost complete conversion was achieved accompanied with a moderate ee (99.5% conv., 39% ee). This result might indicate that a certain degree of steric hindrance at the substrate is needed, in particular at the alkyl part in order to achieve high conversions and better enantioinductions. In line with that,

comparable results in terms of enantioselectivity (37%) were obtained when *iso*-valerophenone was employed as substrate (**5xx79**). Similarly, 2,2-dimethylpropiophenone was converted into the corresponding alcohol in moderate conversion and enantioselectivities (**5xx80**). The best results were achieved when cyclohexylphenyl ketone was employed as substrate, with practically full conversion towards the corresponding alcohol and ee's up to 55% (**5xx66**). On the contrary, when more rigid rings were located at the α-position of the ketone, very low conversions and enantioselectivities were achieved (**5xx81**).

Then, replacing the phenyl ring by a naphthalene ring the reaction was inhibited completely (**5xx82**). In a same manner, no conversion was observed when methyl 2,4,6-trimetrylphenyl ketone was employed as substrate (**5xx83**). The introduction of electron-withdrawing groups at the *para*-position of the phenyl ring also inhibited the reaction (**5xx84**). On the contrary, the introduction of electron-donating groups at the *para*-position of the phenyl ring produced moderate conversions to the corresponding alcohol while the enantiomeric excess was quite low (**5xx85**).

When catalyst **5xx61** was employed for the reduction of acetophenone into the corresponding alcohol, very low conversions were achieved in comparison with the ones reached using catalyst **5xx59** although comparable enantiomeric ratios were obtained. Changing the methyl by a ethyl or a *iso*-propyl group, up to complete conversion and up to 50% ee can be obtained, following this trend Me<Ethyl<*iso*-Propyl (**5xx76**, **5xx77** & **7xx78**). On the contrary, lower conversion were achieved using *iso*-valerophenone, 2,2-dimethylpropiophenone or cyclohexylphneyl ketone as substrate, although the latest one provided the best enantiomeric excess of the series (**5xx79**, **5xx80** & **5xx66**).

From these results we could conclude that either using the Co(II) complex **5xx59** or **5xx61**, a certain degree of steric hindrance at the substrate is needed, in particular at the alkyl part in order to achieve high conversions and better enantioinductions.

5.4. CONCLUSIONS

From the study described in this chapter, the following conclusions can be extracted:

i) 1-(R)-(1'phenylethyl)-imidazole (**5xx62**) and 1-(R)-(1'-naphthylethyl)-imidazole (**5xx63**) were synthesized and fully characterized obtaining 34% and 32% yield respectively, as previously reported by Herrmann and co-workers. Additionally, 1-(R)-(1'-cyclohexylethyl)-imidazole (**5xx64**) was also synthesized and fully characterized in a 25% yield, as previously reported by Suzuki and co-workers.

ii) The chiral C^N^C ligands **5xx56** containing a methyl and phenyl groups and the **5xx57** ligand containing a methyl and a naphthyl groups were synthesized and fully characterized obtaining 63% and 40% yield respectively as previously reported by Herrmann and co-workers.

iii) The chiral C^N^C ligands **5xx58** containing a methyl and a cyclohexyl groups was synthesized and fully characterized with a 60% yield.

iv) The chiral Cobalt C^N^C complexes **5xx59**-**5xx61** were synthesized and characterized by NMR, IR, Magnetic Susceptibility, ICP and EA. With all the collected data in hand, it is proposed a coordination of the Co(OAc)$_2$ moiety to the pyridine of the C^N^C ligand.

v) The Cobalt C^N^C complex **5xx59** catalyzes the asymmetric hydrogenation of ketones with moderate to high yields, although low to moderate ee's were obtained.

vi) Initial attempts to obtain a well defined Co(II)-pyridine biscarbene complex having both the carbene and the pyridine coordinated to the metal center were accomplished, although still further investigation need to be performed.

5.5. EXPERIMENTAL PART

<u>GENERAL EXPERIMENTAL CONDITIONS</u>

All preparations and manipulations were carried out under an oxygen-free nitrogen atmosphere using conventional Schlenk techniques or inside a glovebox. Solvents were purified by the system Braun MB SPS-800 and stored under nitrogen atmosphere. Deuterated solvents were degassed via three freeze-pump-thaw cycles and kept in the glovebox over 4Å molecular sieves. Reagents were purchased from Aldrich, Alfa-Aesar and Strem and were used as received.

^{1}H, ^{13}C and ^{11}B-NMR spectra were recorded on a Varian$^®$ Mercury VX 400 (400 MHz, 100.6 MHz, 128 MHz respectively). Chemical shift values for ^{1}H and ^{13}C were referred to internal SiMe$_4$ (0.0 ppm). 2D correlation spectra (gCOSY, gHSQC and gHMBC) were visualized using VNMR program (Varian$^®$). ESI-HMRS were run on an Agilent$^®$ 1100 Series LC/MSD instrument. EA was performed at Serveis Tècnics de Recerca from the Universitat de Girona (Spain).

Reactions were monitored by TLC carried out on 0.25 mm E. Merck$^®$ silica gel 60 F$_{254}$ glass or aluminum plates. Developed TLC plates were visualized under a short-wave UV lamp (254 nm) and by heating plates that were dipped in potassium permanganate. Flash column chromatography was carried out using forced flow of the indicated solvent on Merck$^®$ silica gel 60 (230-400 mesh).

Hydrogenation reactions were carried out in a Berghof 5 x 25mL stainless steel autoclave. Gas chromatography analyses were carried out in a Hewlett-Packard HP 6890 gas chromatograph, using the chiral column CP Chirasil-Dex CB.

Synthesis of 1-(R)-(1'phenylethyl)-imidazole[87] (5xx62)
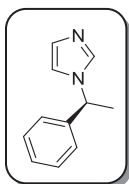
1-(R)-phenylethylamine (15ml, 0.117mol) was dissolved in 120ml H_2O and (ml) phosphoric acid (85%) was added until a pH of approximately 2 was reached. After addition of paraformaldehyde (3.7g, 0.117mol) and glyoxal (13.5ml, 40% in water, 0.117mol), the reaction mixture was heated to 100ºC and saturated ammonium chloride solution (6.3g, 0.117mol, 20ml H_2O) was added drop wise over a period of 45min. Then, the reaction was allowed to stir overnight at 100ºC. The reaction mixture was cooled to 0ºC and NaOH was added until a pH higher than 12 was reached. The product was extracted with dichloromethane (3x100ml) and the combined organic phases were dried over anhydrous $MgSO_4$ and the product evaporated in vacuo. To the crude brown thick liquid was added hexane (100ml) and heated at reflux for 2hours. Then, the yellow liquid was decanted, and leaved it in the fridge to favour the precipitation of the pure product as a pale yellow oil in 34% of yield.

¹H-NMR (CDCl₃, 400 MHz, δ in ppm): δ = 7.58 (s, 1H, N=CH-N), 7.36-7.29 (m, 3H, Ar-), 7.15-7.13 (m, 2H, Ar-), 7.08 (s, 1H, N-HC=CH-N), 6,93 (s, 1H, N-HC=CH-N), 5.34 (q, 1H, *J*= 8Hz, -CH-), 1.85 (d, 3H, *J*= 8Hz, -CH₃). **¹³C{¹H}-NMR** (CDCl₃, 100.6 MHz, δ in ppm): δ = 141.60 (-C-), 136.09 (N=CH-N), 129.43 (Ar-), 128.90 (Ar-), 128.07, (Ar-), 125.99 (N-HC=CH-N), 117.97 (N-HC=CH-N), 56.53 (-CH-), 22.06 (-CH₃). **ESI-HRMS:** Calculated for **C₁₁H₁₂N₂**: Exact: (M: 172.1000; [M+H]⁺: 173.1100); Experimental ([M+H]⁺: 173.1081).

Synthesis of 1-(R)-(1'-napthtylethyl)-imidazole[87] (5xx63)
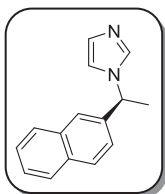
1-(R)-naphthylethylamine (9ml, 0.052mol) was dissolved in 100ml H_2O and phosphoric acid (85%) was added until a pH of approximately 2 was reached. After addition of paraformaldehyde (1.56g, 0.052mol) and glyoxal (5.96ml, 40% in water, 0.052mol), the reaction mixture was heated to 100ºC and saturated ammonium chloride solution (2.78g, 0.052mol, 20ml H_2O) was added drop wise over a period of 45min. Then, the reaction was allowed to stir overnight at 100ºC. The reaction mixture was cooled to 0ºC and NaOH was added until a pH higher than 12 was reached. The product was extracted with dichloromethane (3x100ml), and the combined organic phases were dried over anhydrous $MgSO_4$. The solvent was evaporated in vacuo to give the product as yellow oil in 32% of yield.

^{1}H-NMR (CDCl$_3$, 400 MHz, δ in ppm): δ = 7.84-7.79 (m, 3H, Ar-), 7.66 (s, 1H, N=CH-N), 7.59 (s, 1H, Ar-), 7.53-7.49 (m, 2H, Ar-), 7.25 (dd, 1H, *J*= 4 & 8Hz, Ar-), 7.11 (s, 1H, N-HC=CH-N), 6.97 (s, 1H, N-HC=CH-N), 5.50 (q, 1H, *J*= 8Hz, -CH-), 1.95 (d, 3H, *J*= 4Hz, -CH$_3$). **^{13}C{^{1}H}-NMR** (CDCl$_3$, 100.6 MHz, δ in ppm): δ = 138.97 (-C-), 136.33 (N=CH-N), 133.34 (-C-), 133.07 (-C-), 129.58 (N-HC=CH-N), 129.06 (Ar-), 128.14 (Ar-), 127.84 (Ar-), 126.77 (Ar-), 126.60 (Ar-), 124.94 (Ar-), 124.11 (Ar-), 118.30 (N-HC=CH-N), 56.67 (-CH-), 22.00 (-CH$_3$). **ESI-HRMS:** Calculated for **C$_{15}$H$_{14}$N$_2$**: Exact: (M: 222.1157; [M+H]$^+$: 223.1157); Experimental ([M+H]$^+$: 223.1245).

Synthesis of 1-(R)-(1'-Cyclohexylethyl)-imidazole[89] (5xx64)
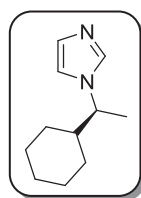
(S)-(+)-1-Cyclohexylethylamine (15ml, 0.10mol) was dissolved in 120ml H_2O and phosphoric acid (85%) was added until a pH of approximately 2 was reached. After addition of paraformaldehyde (3g, 0.10mol) and glyoxal (11.47ml, 40% in

water, 0.10mol), the reaction mixture was heated to 100ºC and saturated ammonium chloride solution (5.34g, 0.10mol, 20ml H_2O) was added drop wise over a period of 45min. Then, the reaction was allowed to stir overnight at 100ºC. The reaction mixture was cooled to 0ºC and NaOH was added until a pH higher than 12 was reached. The product was extracted with dichloromethane (3x100ml) and the combined organic phases were dried over anhydrous $MgSO_4$. The solvent was evavorated in vacuo to give the crude product which was purified by column chromatography (DCM:MeOH 2%) affording the compound as a pale yellow liquid in 25% of yield.

¹H-NMR (CDCl$_3$, 400 MHz, δ in ppm): δ = 7.44 (s, 1H, N=CH-N), 7.00 (s, 1H, N-HC=CH-N), 6.86 (s, 1H, N-HC=CH-N), 3.81(quint, J= 8Hz, 1H, -CH-), 1.76-1.70 (m, 2H, -CH$_2$), 1.65-1.58 (m, 2H, -CH$_2$), 1.53-1.44 (m, 1H, -CH-), 1.41 (d, J= 8Hz, 3H, -CH$_3$), 1.31-1.26 (m, 1H, -CH$_2$), 1.21-1.13 (m, 1H, -CH$_2$), 1.11-1.02 (m, 2H, -CH$_2$), 0.96-0.86 (m, 1H, -CH$_2$), 0.82-0.72 (m, 1H, -CH$_2$).**¹³C{¹H}-NMR** (CDCl$_3$, 100.6 MHz, δ in ppm): δ = 136.30 (N=CH-N), 128.79 (N-HC=CH-N), 117.22 (N-HC=CH-N), 58.90 (-CH-), 44.41 (cy, -CH-), 29.84 (cy, -CH$_2$), 29.41 (cy, -CH$_2$), 26.13 (cy, -CH$_2$), 26.00 (cy, -CH$_2$), 25.87 (cy, -CH$_2$), 19.01 (-CH$_3$). **ESI- HRMS:** Calculated for **C$_{11}$H$_{18}$N$_2$**: Exact: (M: 178.1470; [M+H]$^+$: 179.1470); Experimental ([M+H]$^+$: 179.1595.

Synthesis of 1,1'-Di((R)-1''-phenylethyl)-2,6-lutidinediimidazolium dibromide[87] (5xx56)
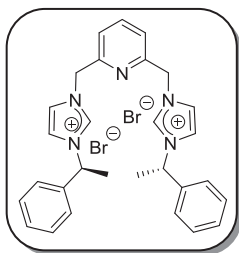
5xx62 (1g, 5.8mmol) was dissolved in 10mL THF in an ACE pressure tube and (0.78g, 2.9mmol) of 2,6-dibromomethyl)pyridine were added. The solution was heated for 24h at 80ºC and a brownish precipitate was obtained. The precipitate was filtered off and

washed three times with 10mL THF. The crude product was recrystalized with dichloromethane/diethyl ether to obtain a yellow oil, which was decanted and dried in high vacuum to obtain a highly hygroscopic beige powder in 63% yield.

^{1}H-NMR (CDCl$_3$, 400 MHz, δ in ppm): δ = 10.81 (t, 2H, *J*= 4Hz, N=CH-N,), 8.13 (t, 2H, *J*= 4Hz, N-HC=CH-N), 7.71 (d, 2H, *J*= 8Hz, *m*-Py), 7.55 (t, 1H, *J*= 8Hz, *p*-Py), 7.45-7.43 (m, 4H, Ar-), 7.37-7.29 (m, 6H, Ar-), 7.23 (t, 2H, *J*= 4Hz, N-HC=CH-N), 6.09 (q, 2H, *J*= 8Hz, -CH-), 5.79 (d, 2H, *J*= 12Hz, -CH$_2$), 5.68 (d, 2H, *J*=12Hz, -CH$_2$), 1.96 (d, 6H, *J*= 8Hz, -CH$_3$). **^{13}C{^{1}H}-NMR** (CDCl$_3$, 100.6 MHz, δ in ppm): δ = 153.19 (Py, -C-), 139.14 (*p*-Py-), 138.26 (-C-), 136.74 (N=CH-N), 129.68 (Ar-), 129.53 (Ar-), 127.11 (Ar-), 124.09 (*m*-Py), 124.07 (-N-HC=CH-N), 120.17 (-N-HC=CH-N), 59.80 (-CH-), 53.59 (-CH$_2$-), 21.46 (-CH$_3$). **ESI-HRMS:** Calculated for **C$_{29}$H$_{31}$Br$_2$N$_5$**: Exact: (M: 607.0946; [M-Br]$^+$: 528.1757); Experimental ([M-Br]$^+$: 528.1752.

Synthesis of 1,1'-Di((R)-1''-naphtylethyl)-2,6-lutidinediimidazolium dibromide[87] (5xx57)
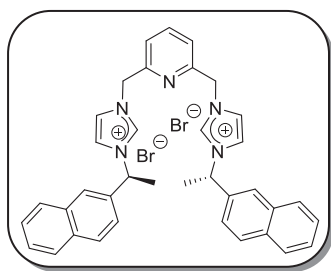
5xx63 (250mg, 1.1mmol) was dissolved in 4mL THF in an ACE pressure tube and (147mg, 0.55mmol) of 2,6-dibromomethyl)pyridine were added. The solution was heated for 24h at 80ºC and a brownish precipitate was obtained. The precipitate was filtered off and washed three times with 5mL THF. The crude product was recrystalized with dichloromethane/diethyl ether to obtain a yellow oil, which was decanted and dried in high vacuum to obtain a highly hygroscopic beige powder in 40% yield.

¹H-NMR (CDCl₃, 400 MHz, δ in ppm): δ = 10.63 (s, 2H, N=CH-N), 7.96 (s, 2H, Ar-), 7.89 (s, 2H, N-HC=CH-N), 7.83-7.72 (m, 6H, Ar-), 7.59 (d, 2H, *J*= 8Hz, *m*-Py), 7.51 (t, 1H, *J*= 8Hz, *p*-Py), 7.45-7.39 (m, 6H, Ar-), 7.16 (s, 2H, N-HC=CH-N), 6.15 (q, 2H, *J*= 8Hz, -CH-), 5.69 (d, 2H, *J*= 12Hz, -CH₂), 5.57 (d, 2H, *J*= 12Hz, -CH₂), 1.98 (d, 3H, *J*= 8Hz, -CH₃). **¹³C{¹H}-NMR** (CDCl₃, 100.6 MHz, δ in ppm): δ = 153.06 (Py, -C-), 139.20 (*p*-Py), 136.69 (N=CH-N), 135.50 (-C-), 133.43 (-C-), 133.18 (-C-), 129.63 (Ar-), 128.41 (Ar-), 127.87 (Ar-), 127.26 (Ar-), 127.09 (Ar-), 126.68 (Ar-), 124.21 (Ar-), 123.99 (*m*-Py), 123.87 (N-HC=CH-N), 120.28 (N-HC=CH-N), 59.97 (-CH-), 53.60 (-CH₂), 21.37 (-CH₃).

ESI-HRMS: Calculated for **C₃₇H₃₅Br₂N₅**: Exact: M: 707.1259 [M-Br]⁺: 628.2070); Experimental ([M-Br]⁺: 628.2066.

**Synthesis of 1,1'-Di((R)-1''-cyclohexylethyl)-2,6-lutidinediimidazolium dibromide (5xx58)**
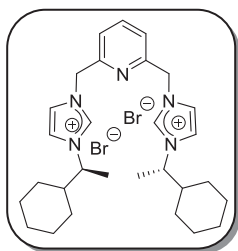
5xx64 (300mg, 1.6mmol) was dissolved in 5mL THF in an ACE pressure tube and (223mg, 0.84mmol) of 2,6-dibromomethyl)pyridine were added. The solution was heated for 24h at 80ºC and a brownish precipitate was obtained. The precipitate was filtered off and washed three times with 5mL THF. The crude product was recrystalized with dichloromethane/diethyl ether to obtain a pale yellow oil, which was decanted and dried in high vacuum to obtain a highly hygroscopic beige powder in 60% yield.

¹H-NMR (CDCl₃, 400 MHz, δ in ppm): δ = 10.60 (s, 2H, N=CH-N), 8.23 (t, 2H, *J*= 4Hz, N-HC=CH-N), 7.76 (d, 2H, *J*= 8Hz, *m*-Py), 7.63 (t, 1H, *J*= 8Hz, *p*-Py), 7.30 (t, 2H, *J*= 4Hz, N-HC=CH-N), 5.77 (d, 2H, *J*= 16Hz), 5.72 (d, 2H, *J*= 16Hz), 4.57 (quint, 2H, *J*= 8Hz, -CH-), 1.78-1.57 (m, 10H, Cy), 1.53 (d, 6H, *J*= 4Hz, -CH₃), 1.27-0.98 (m, 12H, Cy). **¹³C{¹H}-NMR** (CDCl₃,

100.6 MHz, δ in ppm): δ = 153.35 (Py, -C-), 139.21 (*p*-Py), 136.84 (N=CH-N), 124.16 (*m*-Py), 124.00 (N-HC=CH-N), 119.78 (N-HC=CH-N), 62.10 (-CH-), 53.46 (-CH$_2$), 43.57 (Cy, -CH-), 29.12 (Cy, -CH$_2$-), 25.79 (Cy, -CH$_2$-), 25.72 (Cy, -CH$_2$-), 25.66 (Cy, -CH$_2$-), overlapped signals, 18.51 (-CH$_3$).

ESI-HRMS: Calculated for **C$_{29}$H$_{43}$Br$_2$N$_5$**: Exact: M: 619.1885 [M-Br]$^+$: 540.2702); Experimental ([M-Br]$^+$: 540.2694.

Synthesis of 2,6-bis((3-(1-phenylethyl)-2,3-dihydro-1*H*-imidazol-1yl)methyl)pyridine (5xx73)
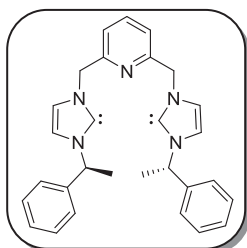
A solution of KO^{t}Bu (110mg, 0.99mmol) in THF (10ml) was added dropwise to a stirred suspension of **5xx56** (0.2g, 0.328mmol) in THF (15ml) at room temperature. After the mixture was stirred for 30 min, the solution was evaporated and the crude orange powder was extracted with diethyl ether to remove the excess of base and evaporated to dryness to give the product as an orange liquid in 48% yield.

^{1}H-NMR (C$_7$D$_8$, 400 MHz, δ in ppm): δ = 7.40-7.38 (m, 4H, Ar-), 7.31-7.26 (m, 5H, Ar-), 7.23-7.19 (m, 4H, Ar-), 7.11 (d, 2H, *J*= 4Hz *m*-Py), 6.78 (d, 1H, *J*= 4Hz, Ar-), 6.56 (d, 1H, *J*= 4Hz, Ar-), 5.62 (q, 2H, *J*= 4Hz, -CH-), 5.53 (s, 4H, -CH$_2$), 1.93 (d, 6H, *J*= 8Hz, -CH$_3$). **^{13}C{^{1}H}-NMR** (C$_7$D$_8$, 100.6 MHz, δ in ppm): δ = 158.39 (Py, -C-), 143.48 (CH-), 137.21 (-C-), 128.38 (CH-), 127.44 (CH-), 126.93 (CH-), 120.62 (CH-), 119.64 (CH-), 118.07 (CH-), 59.53 (-CH-), 56.83 (-CH$_2$), 22.53 (-CH$_3$).

Synthesis of ((R)-1,1'-(pyridine-2,6-diylbis(methylene))bis(3-((R)-1-phenylethyl)-1H-imidazole-3-ium-2,1-diyl))ditrihydroborate (5xx74)
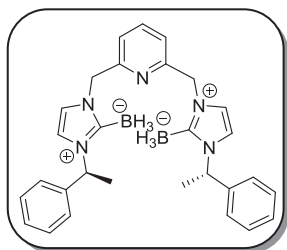
A solution of KO*t*Bu (276mg, 1.2mmol) in THF (10 ml) was added dropwise to a stirred suspension of the **5xx56** (500mg, 0.82mmol) in THF (15ml) at room temperature. The mixture was then stirred for 30 min at room temperature followed by the addition of BH$_3$·THF (1.97ml, 1.97mmol) at the same temperature. The reaction was then stirred overnight. Volatiles were evaporated under vacuum and the mixture was re-dissolved in DCM (2ml) and filtered through a short pad of Celite. The Celite was washed with DCM and the filtrate was concentrated. The crude material was purified on silica using a 5% EtOH in DCM to obtain the product as a white solid in 29% yield.

^{1}H-NMR (C$_6$D$_6$, 400 MHz, δ in ppm): δ = 7.48-7.45 (m, 6H, Ar-), 7.38-7.31 (m, 5H, Ar-), 7.15 (s, 2H, Ar-), 6.75 (q, 2H, *J*= 8Hz, -CH-), 6.63 (d, 2H, J= 8Hz, N-HC=CH-N, -CH-), 6.36 (d, 2H, J= 4Hz, N-HC=CH-N, -CH-), 5.53 (s, 4H, -CH$_2$), 2.42 (q, 6H, J_{B-H}= 84Hz, -BH$_3$), 1.63 (d, 6H, *J*= 8Hz, -CH$_3$). **^{13}C{^{1}H}-NMR** (C$_6$D$_6$, 100.6 MHz, δ in ppm): δ = 155.73 (*o*-Py), 140.59 (Ar, -C-), 137.80 (Ar-), 128.82 (Ar-), 127.98 (Ar-), 127.32 (Ar-), 121.61 (Ar-), 120.01 (N-HC=CH-N), 115.96 (N-HC=CH-N), 55.96 (-CH-), 53.11 (-CH$_2$), 19.55 (-CH$_3$). **^{11}B{^{1}H}-NMR** (C$_6$D$_6$, 128 MHz, δ in ppm): δ = -33.27 (s). **ESI-HRMS:** Calculated for **C$_{29}$H$_{35}$B$_2$N$_5$:** Exact (M: 475.3079; [M-BH$_3$]$^+$: 462.2824); Experimental ([M-BH$_3$]$^+$: 462.2830).

Synthesis of Co(II)-C^N^C complex 5xx59
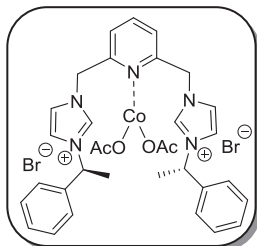
5xx56 (0.5g, 0.82mmol) was dissolved in 15ml of THF and Co(OAc)$_2$ (145.3mg, 0.82mmol) was added to the mixture. After stirring the solution 48h at room temperature, a blue solid precipitated. The solid was filtered and dried in vacuum to obtain the product as a blue powder in 78% yield (based on the proposed structure).

^{1}H-NMR (C$_2$D$_6$SO, 400MHz, δ in ppm): δ = 9.49 (s, 2H, -N=CH-N-), 7.97 (t, 1H, *p*-Py-), 7.83 (s, 2H, N-HC=CH-N), 7.69 (s, 2H, N-HC=CH-N), 7.46-7.37 (m, 12H, Ar-), 5.82 (q, 2H, J= 8 Hz, -CH-), 5.50 (s, 4H, -CH$_2$), 1.86 (d, 6H, J= 8Hz, -CH$_3$). **^{13}C{^{1}H}-NMR** (C$_2$D$_6$SO, 100.6MHz, δ in ppm): δ = 153.47 (Py, -C-), 139.31 (*p*-Py), 138.88 (-C-), 136.02 (N=CH-N), 128.95 (Ar-), 128.67 (Ar-), 126.47 (Ar-), 123.47 (N-HC=CH-N), 122.08 (Ar-), 120.94 (N-HC=CH-N), 58.58 (-CH-), 52.78 (-CH$_2$), 20.41 (-CH$_3$). Elemental Analysis calculated for **C$_{33}$H$_{37}$CoBr$_2$N$_5$O$_4$·CH$_2$Cl$_2$,** C, 46.87; H, 4.51; N, 8.04; Found: C, 46.09; H, 4.48; N, 8.19. **ICP**: [Co]$_{theoretical}$=7.5%; [Co]$_{found}$= 7,62%.

Synthesis of Co(II)-C^N^C complex 5xx60

5xx57 (0.5g, 0.70mmol) was dissolved in 15ml of THF and Co(OAc)$_2$ (125.2mg, 0.70mmol) was added to the mixture. After stirring the solution 48h at room temperature, a blue solid precipitated. The solid was filtered and dried in vacuum to obtain the product as a blue powder in 72% yield (based on the proposed structure).

^{1}H-NMR (C$_2$D$_6$SO, 400MHz, δ in ppm): δ = 9.49 (s, 2H, N=CH-N), 7.98-

7.91 (m, 9H, Ar-), 7.85 (s, 2H, N-HC=CH-N), 6.69 (s, 2H, N-HC=CH-N), 7.58-7.49 (m, 6H, Ar-), 7.44 (d, 2H, J= 8Hz, *m*-Py), 5.96 (q, 2H, J= 8Hz, -CH-), 5.49 (s, 4H, -CH$_2$), 1.94 (d, 6H, J= 4Hz, -CH$_3$). ^{13}C{^{1}H}-NMR (C$_2$D$_6$SO, 100.6MHz, δ in ppm): δ = 153.59 (Py, -C-), 136.55 (-C-), 136.26 (N=CH-N), 132.75 (-C-), 132.64 (-C-), 128.93 (Ar-), 128.02 (Ar-), 127.64 (Ar-), 126.88 (Ar-), 126.85 (Ar-), 125.90 (Ar-), 125.36 (Ar-), 124.21 (Ar-), 123.58 (N-HC=CH-N), 122.19 (*m*-Py), 121.15 (N-HC=CH-N), 58.84 (-CH-), 52.92 (-CH$_2$), 20.41 (-CH$_3$). Elemental Analysis calculated for **C$_{41}$H$_{41}$CoBr$_2$N$_5$O$_4$·CH$_2$Cl$_2$**, C, 51.93; H, 4.46; N, 7.21; Found: C, 50.66; H, 4.47; N, 7.34. **ICP**: [Co]$_{theoretical}$=6.65%; [Co]$_{found}$= 6.79%.
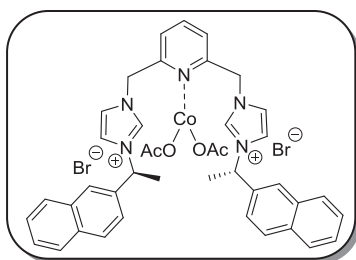
Synthesis of Co(II)-C^N^C complex 5xx61
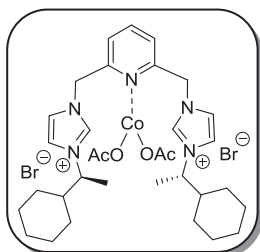
5xx58 (0.45g, 0.73mmol) was dissolved in 13ml of THF and Co(OAc)$_2$ (128.6mg, 0.73mmol) was added to the mixture. After stirring the solution 48h at room temperature, a blue solid precipitated. The solid was filtered and dried in vacuum to obtain the product as a blue powder in 74% yield (based on the proposed structure).

^{1}**H-NMR** (C$_2$D$_6$SO, 400MHz, δ in ppm): δ = 9.31 (bs, 2H, N=CH-N), 7.96-7.42 (m, 7H, Ar-), 5.49 (bs, 4H, -CH$_2$), 4.31 (bs, 2H, -CH-), 1.74-0.86 (m, 28H, Cy & -CH$_3$). ^{13}**C{^{1}H}-NMR** (C$_2$D$_6$SO, 100.6MHz, δ in ppm): δ = 152.3 (Py, -C-), 139.54 (Ar-), 136.50 (N=CH-N), 123.91 (Ar-), 122.62 (Ar-), 121.50 (Ar-), 61.41 (-CH-), 53.39 (-CH$_2$), 42.85 (Cy, -CH-), 29.64 (Cy, -CH$_2$), 28.99 (Cy, -CH$_2$), 28.78 (Cy, -CH$_2$), 25.96 (Cy, -CH$_2$), 25.74 (Cy, -CH$_2$), 18.16 (-CH$_3$). Elemental Analysis calculated for **C$_{33}$H$_{49}$CoBr$_2$N$_5$O$_4$·CH$_2$Cl$_2$**, C, 46.22; H, 5.82; N, 7.93; Found: C, 45.55; H, 6.12; N, 8.01. **ICP**: [Co]$_{theoretical}$=7.38%; [Co]$_{found}$= 7.07%.

5.6. REFERENCES

1. Herrmann, W. A. Angew. Chem. Int. Ed. 2002, 41, 1290-1309.
2. Crabtree, R. H. *The organometallic chemistry of the transition metals*, 5th ed.; John Wiley & Sons: Hoboken, New Jersey, 2009; pp315-319.
3. Wang, F.; Liu, L.; Wang, W.; Li, S. and Shi, M. *Coord. Chem. Rev.* **2012**, *256*, 804-853.
4. Öfele, K. *J. Organomet. Chem.* **1968**, *12*, P42.
5. Wanzlick, H. W. and Schonherr, H. J. *Angew. Chem. Int. Ed. Engl.* **1968**, *7*, 141-142.
6. Arduengo, A. J.; Rasika Dias, H. V.; Harlow, R. L. and Kline, M. *J. Am. Chem. Soc.* **1992**, *114*, 5530-5534.
7. Tolman, C. A. *Chem Rev.* **1977**, *77*, 313-348.
8. Öfele, K.; Herrmann, W. A.; Mihalios, D.; Elison, M.; Herdtweck, E.; Scherer, W. and Mink. J. *J. Organomet. Chem.* **1993**, *459*, 177-184.
9. Huang, J.; Schanz, H-J.; Stevens, E. D. and Nolan, S. P. *Organometallics*, **1999**, *18*, 2370-2375.
10. Perrin, L.; Clot, E.; Eisenstein, O.; Loch, J. and Crabtree, R. H. *Inorg. Chem.* **2001**, *40*, 5806-5811.
11. Denk, K.; Sirsch, P. and Herrmann, W. A. *J. Organomet. Chem.* **2002**, *649*, 219-224.
12. Chianese, A. R.; Li, X.; Janzen, M. C.; Faller, J. W. and Crabtree, R. H. *Organometallics*, **2003**, *22*, 1663-1667.
13. Hillier, A. C.; Sommer, W. J.; Yong, B. S.; Petersen, J. L.; Cavallo, L. and Nolan, S. P. *Organometallics*, **2003**, *22*, 4322-4326.
14. Lee, M-T. and Hu, C-H. *Organometallics*, **2004**, *23*, 976-983.
15. Crabtree, R. H. *J. Organomet. Chem.* **2005**, *690*, 5451-5457.
16. Chianese, A. R.; Kovacevic, A.; Zeglis, B. M.; Faller, J. W. and Crabtree, R. H. *Organometallics*, **2004**, *23*, 2461-2468.
17. Dorta, R.; Stevens, E. D.; Scott, N. M.; Costabile, C.; Cavallo, L.; Hoff, C. D. and Nolan, S. P. *J. Am. Chem. Soc.* **2005**, *127*, 2485-2495.
18. Gusev, D. G. *Organometallics*, **2009**, *28*, 6458-6461.
19. Benhamou, L.; Chardon, E.; Lavigne, G.; Laponnaz, S. B. and César, V. *Chem. Rev.* **2011**, *111*, 2705-2733.
20. Grimmett, M. R. *Imidazole and Benzimidazole Synthesis*, Academic Press, San Diego, **1997**.
21. (a) Martin, T. A.; Ellul, C. E.; Mahon, M. F.; Warren, M. E.; Allan, D. and Whittlesey, M. K. *Organometallics* **2011**, *30*, 2200-2211. (b) Zhang, C. and Wang, Z.-X. *Organometallics* **2009**, *28*, 6507-6514. (c) Kong, Y.; Cheng, M.; Ren, H.; Xu, S.; Song, H.; Yang, M.; Liu, B. and Wang, B. *Organometallics* **2011**, *30*, 1677-1681. (d) Zhing, K.; Conda-Sheridan, M.; Cooke, S. R. and

Louie, J. *Organometallics* **2011**, *30*, 2546-2552. (e) Laskowski, C. A.; Miller, A. J. M.; Hillhouse, G. L. and Cundari, T. R. *J. Am. Chem. Soc.* **2011**, *133*, 771-773.

22. (a) Herrmann, W. A.; Gerstberger, G. and Spiegler, M. *Organometallics* **1997**, *16*, 2209-2212. (b) Enders, D.; Gielen, H.; Raabe, G.; Runsink, J. and Teles, J. H. *Chem. Ber.* **1996**, *129*, 1483-1488. (c) Türkmen, H.; Pape, T.; Hahn, F. E. and Çetinkaya, B. *Organometallics* **2008**, *27*, 571-575. (d) Yuan, D. and Huynh, H. V. *Organometallics* **2010**, *29*, 6020-6027. (e) Winkelmann, O. H.; Riekstins, A.; Nolan, S. P. and Navarro, O. *Organometallics* **2009**, *28*, 5809-5813. (f) Oertel, A. M.; Freudenreich, J.; Gein, J.; Ritleng, V.; Veiros, L. F. and Chetcuti, M. J. *Organometallics* **2011**, *30*, 3400-3411.

23. (a) Liao, C.-Y.; Chan, K.-T.; Zeng, J.-Y.; Hu, C.-H.; Tu, C.-Y. and Lee, H. M. *Organometallics* **2007**, *26*, 1692-1702. (b) Jean-Baptiste dit Dominique, F.; Gornitzka, H. and Hemmert, C. *Organometallics* **2010**, *29*, 2868-2873. (c) Li, K.; Guan, X.; Ma, C.-W.; Lu, W.; Chen, Y. and Che, C.-M. *Chem. Commun.* **2011**, *47*, 9075-9077.

24. Enders, D.; Breuer, K.; Raabe, G.; Runsink, J.; Teles, J. H.; Melder, J.-P.; Ebel, K. and Brode, S. *Angew. Chem., Int. Ed. Engl.* **1995**, *34*, 1021-1023.

25. Nyce, G. W.; Csihony, S.; Waymouth, R. M. and Hedrick, J. L. *Chem. Eur. J.* **2004**, *10*, 4073-4079.

26. (a) Voutchkova, A. M.; Appelhans, L. N.; Chianese, A. R. and Crabtree, R. H. *J. Am. Chem. Soc.* **2005**, *127*, 17624-17625. (b) Delaude, L. *Eur. J. Inorg. Chem.* **2009**, 1681-1699.

27. Bittermann, A.; Baskakov, D. and Herrmann, W. A. *Organometallics* **2009**, *28*, 5107-5111.

28. (a) Blakemore, J. D.; Chalkley, M. J.; Farnaby, J. H.; Guard, L. M.; Hazari, N.; Incarvito, C. D.; Luzik, E. D. Jr. and Suh, H. W. *Organometallics* **2011**, *30*, 1818-1829. (b) Samantaray, M. K.; Dash, C.; Shaikh, M. M.; Pang, K.; Butcher, R. J. and Ghosh, P. *Inorg. Chem.* **2011**, *50*, 1840-1848. (c) Chang, Y.-H.; Liu, Z.-Y.; Liu, Y.-H.; Peng, S.-M.; Chen, J.-T. and Liu, S.-T. *Dalton Trans.* **2011**, *40*, 489-494. (d) Simpson, P. V.; Skelton, B. W.; Brown, D. H. and Baker, M. V. *Eur. J. Inorg. Chem.* **2011**, 1937-1952. (e) Powell, A. B.; Bielawski, C. W. and Cowley, A. H. *J. Am. Chem. Soc.* **2010**, *132*, 10184-10194.

29. Baskakov, D.; Herrmann, W. A.; Herdtweck, E. and Hoffmann, S. D. *Organometallics* **2007**, *26*, 626-632.

30. (a) Liu, S.-T.; Hsieh, T.-Y.; Lee, G.-H. and Peng, S.-M. *Organometallics* **1998**, *17*, 993. (b) Ruiz, J. and Perandones, B. F. *J. Am. Chem. Soc.* **2007**, *129*, 9298-9299. (c) Liu, S.-T.; Lee, C.-I.; Fu, C.-F.; Chen, C.-H.; Liu, Y.-H.; Elsevier, C. J.; Peng, S.-M. and Chen, J.-T. *Organometallics* **2009**, *28*, 6957-6962. (d) Furst, M. R. L. and Cazin, C. S. J. *Chem. Commun.* **2010**, *46*, 6924-

6925. (e) W. N. O. W.; Lough, A. J. and Morris, R. H. *Organometallics* **2011**, *30*, 1236-1252. (f) W. N. O. W.; Lough, A. J. and Morris, R. H. *Organometallics* **2009**, *28*, 6755-6761. (g) Liu, B.; Liu, X.; Chen, C.; Chen, C. and Chen, W. *Organometallics* **2012**, *31*, 282−288.

31. Liu, B.; Xia, Q. and Chen, W. *Angew. Chem., Int. Ed.* **2009**, *48*, 5513-5516.

32. Enders, D.; Breuer, K.; Runsink, J. and Teles, J. H. *Helv. Chim. Acta* **1996**, *79*, 1899-1902.

33. Herrmann, W. A.; Goossen, L. T.; Köcher, C. and Artus, G. R. J. *Angew. Chem. Int. Ed.* **1996**, 35, 2805-2807.

34. Powell, M. T.; Hou, D.-R.; Perry, M. C.; Cui, X. and Burgess, K. *J. Am. Chem. Soc.* **2001**, *123*, 8878-8879.

35. Seiders, T. J.; Ward, D. W. and Grubbs, R. H. *Org. Lett.* **2001**, *3*, 3225-3228.

36. (a) Moulton, C. J. and Shaw, B. L. *J. Chem. Soc., Dalton Trans.* **1976**, 1020-1024. (b) van Koten, G.; Timmer, K.; Noltes, J. G. and Spek, A. L. *J. Chem. Soc., Chem. Commun.* **1978**, 250-252. (c) Creaser, C. S. and Kaska, W. C. *Inorg. Chim. Acta* **1978**, *30*, 325-326.

37. (a) Benito-Garagorri, D.and Kirchner, K. *Acc. Chem. Res.* **2008**, *41*, 201-213. (b) Van der Vlugt, J. I. and Reek, J. N. H. *Angew. Chem. Int. Ed.* **2009**, *48*, 8832-8846. (c) Milstein, D. *Top. Catal.* **2010**, *53*, 915-923. (d) Van Koten, G. *Top. Organomet. Chem.* **2013**, *40*, 1-20. (e) Roddick, D. M. *Top. Organomet. Chem.* **2013**, *40*, 49-88.

38. Peris, E. and Crabtree, R. H. *Coord. Chem. Rev.* **2004**, 2239-2246.

39. Jensen, C. M.; Dalin, S.; Lewandowski, B.; Kumashiro, K. K.; Niemczura, W. P.; Morales-Morales, D. and Whang, Z. *Proccedings of the 2001 U.S DOE Hydrogen Program* **2001**, 500-508.

40. Hu, X.; Castro-Rodriguez, I. and Meyer, K. *Organometallics* **2003**, *22*, 3016-3018.

41. Mas-Marza, E.; Poyatos, M.; Sanau, M. and Peris, E. *Organometallics* **2004**, *23*, 323-325.

42. Peris, E.; Loch, J.A.; Mata, J. and Crabtree, R.H. *Chem. Commun*. **2001**, 201-202.

43 Tulloch, A. A. D.; Danopoulos, A. A.; Tizzard, G. J.; Coles, S. J.; Hursthouse, M. B.; Hay-Motherwell, R. S. and Motherwell, W. B. *Chem. Commun.* **2001**, 1270-1271.

44. Chen, J. C. C. and Lin, I. J. B. *Dalton* **2000**, 839-840.

45. Pugh, D. and Danopoulos, A. A. *Coord. Chem. Rev.* **2007**, *251*, 610-641.

46. Gridnev, A. A. and Mihaltseva, I. M. *Synth. Commun.* **1994**, *24*, 1547-1555.

47. Kiyomori, A.; Marcoux, J.-F. and Buchwald, S. L. *Tetrahedron Lett.* **1999**, *40*, 2657-2660.

48. Johnson, A. L.; Kauer, J. C.; Hsarma, D. C. and Dorfman, R. I. *J. Med. Chem.* **1969**, *12*, 1024-1028.

49. Kida, T.; Kikuzawa, A.; Higashimoto, H.; Nakatsuji, Y. and Akashi, M. *Tetrahedron* **2005**, *61*, 5763-5768.

50. McGuinness, D. S.; Gibson, V. C. and Steed, J. W. *Organometallics* **2004**, *23*, 6288-6292.

51. Danopoulos, A. A.; Wright, J. A.; Motherwell, W. B. and Ellwood, S. *Organometallics* **2004**, *23*, 4807-4810.

52. Pellissier, H. and Clavier, H. *Chem. Rev.* **2014**, *114*, 2775-2823 and references therein.

53. Bertz, S. H. *J. Am. Chem. Soc.* **1981**, *103*, 3599-3601.

54. (a) *Advances in Cycloadditon*; Curran, D. P., Ed.; JAI Press: Greenwich, CT, 1994; Vols. I-III. (b) Trost, B. M. *Angew. Chem. Int. Ed. Engl.* **1995**, *34*, 259-281.

55. (a) Doyle, M. P. and Forbes, D. C. *Chem. Rev.* **1998**, *98*, 911-936. (b) Davies, H. M. L. and Antoulinakis, E. *Org. React*. **2001**, *57*, 1. (c) Pellissier, H. *Tetrahedron*, **2008**, *64*, 7041-7095.

56. (a) Nozaki, H.; Moriuti, S.; Takaya, H. and Noyori, R. *Tetrahedron Lett*. **1966**, *7*, 5239-5244. (b) Nozaki, H.; Takaya, H.; Moriuti, S. and Noyori, R. *Tetrahedron*, **1968**, *24*, 3655-3669.

57. (a) Aratani, T.; Yoneyoshi, Y. and Nagase, T. *Tetrahedron Lett*. **1975**, *16*, 1707-1710. (b) Aratani, T. Yoneyoshi, Y. and Nagase, T. *Tetrahedron Lett.* **1977**, *18*, 2599-2602. (c) Aratani, T.; Yoneyoshi, Y. and Nagase, T. *Tetrahedron Lett.* **1982**, *23*, 685-688. (d) Aratani, T. *Pure Appl. Chem*. **1985**, *57*, 1839-1844.

58. Jomni, G.; Pagliarin, R.; Rizzi, G.; and Sisti, M. *Synlett* **1993**, 833-834.

59. Nakamura, A.; Konishi, A.; Tatsuno, Y. and Otsuka, S. *J. Am. Chem. Soc.* **1978**, *100*, 3443-3448.

60. (a) Fukuda, T. and Katsuki, T. *Synlett* **1995**, 825-826. (b) Katsuki, T. *Res. Dev. Pure Appl. Chem.* **1997**, *1*, 35. (c) Fukuda, T. and Katsuki, T. *Tetrahedron* **1997**, *53*, 7201-7208.

61. (a) Jones, J. R.; Ruppel, J. V.; Gao, G.-Y.; Moore, T. M. and Zhang, X. P. *J. Org. Chem.* **2008**, *73*, 7260-7265. (b) Ruppel, J. V.; Jones, J. E.; Huff, C. A.; Kamble, R. M.; Chen, Y. and Zhang, X. P. *Org. Lett.* **2008**, *10*, 1995-1998.

62. Subbarayan, V.; Ruppel, J. V.; Zhu, S.; Perman, J. A. and Zhang, X. P. *Chem. Commun.* **2009**, 4266-4268.

63. (a) Corey, E. J. and Helal, C. *Angew. Chem. Int. Ed.* **1998**, *37*, 1986-2012. (b) Noyori, R. and Ohkuma, T. *Angew. Chem. Int. Ed.* **2001**, *40*, 40-73. (c) Yamada, T. *Speciaity Chem. Magazine* **2008**, *28*, 44.

64. Nagata, T.; Yorozu, K.; Yamada, T. and Mukaiyama, T. *Angew. Chem. Int. Ed. Engl.* **1995**, *34*, 2145-2149.

65. Kokura, A.; Tanaka, S.; Teraoka, H.; Shibahara, A.; Ikeno, T.; Nagata, T. and Yamada, T. *Chem. Lett.* **2007**, *36*, 26-27.

66. Kokura, A.; Tanaka, S.; Ikeno, T. and Yamada, T. *Org. Lett*. **2006**, *8*, 3025-3027.

67. Ohtsuka, Y.; Kubota, T.; Ikeno, T.; Nagata, T. and Yamada, T. *Synlett* **2000**, 535-537.

68. Sato, M.; Gunji, Y.; Ikeno, T. and Yamada, T. *Synthesis* **2004**, 1434-1438.

69. Iwakura, I.; Hatanaka, M.; Kokura, A.; Teraoka, H.; Ikeno, T.; Nagata, T. and Yamada, T. *Chem. Asian J.* **2006**, *1*, 656-663.

70. Tsubo, T.; Chen, H.-H.; Yokomori, M.; Kikuchi, S. and Yamada, T. *Bull. Chem. Soc. Jpn.* **2013**, *86*, 983-986.

71. (a) Riant, O.; Mostefaï, N. And Courmarcel, J. *Synthesis* **2004**, 2943-2958. (b) Arena, C. G. *Mini-Rev. Org. Chem*. **2009**, *6*, 159-167.

72. Brunner, H. and Amberger, K. *J. Organomet. Chem*. **1991**, *417*, C63.

73. Inagaki, T.; Phong, L. T.; Furuta, A.; Ito, J.I. and Nishiyama, H. *Chem. Eur. J.* **2010**, *16*, 3090-3096.

74. Ohgo, Y.; Takeuchi, S.; Natori, Y. and Yoshimura, J. *Bull. Chem. Soc. Jpn.* **1981**, *54*, 2124-2135.

75. Leutenegger, U.; Madin, A. and Pfaltz, A. *Angew. Chem.* **1989**, *101*, 61-62.

76. Corma, A.; Iglesias, M.; del Pino, C. and Sánchez, F. *J. Organomet. Chem.* **1992**, *31*, 233-246.

77. Monfette, S.; Turner, Z. R.; Semproni, S. P. and Chirik, P. J. *J. Am. Chem. Soc*. **2012**, *134*, 4561-4564.

78. (a) Tondreau, A. M.; Darmon, J. M.; Wile, B. M.; Floyd, S. K.; Lobkovsky, E. and Chirik, P. J. *Organometallics* **2009**, *28*, 3928-3940. (b) Wile, B. M.; Trovitch, R. J.; Bart, S. C.; Tondreau, A. M.; Lobkovsky, E.; Milsmann, C.; Bill, E.; Wieghardt, K. and Chirik, P. J. *Inorg. Chem.* **2009**, *48*, 4190-4200.

79. (a) Hirahata, W.; Thomas, R. M.; Lobkovsky, E. B. and Coates, G. W. *J. Am. Chem. Soc.* **2008**, *120*, 17658-17659. (b) Ajiro, H.; Peretti, K. L.; Lobkovsky, E. B. and Coates, G. W. *Dalton Trans*. **2009**, 8828-8830. (c) Thomas, R. M.; Widger, P. C. B.; Ahmed, S. M.; Jeske, R. C.; Hirahata, W.; Lobkovsky, E. B. and Coates, G. W. *J. Am. Chem. Soc*. **2010**, *132*, 16520-16525. (d) Widger, P. C. B.; Ahmed, S. M. and Coates, G. W. *Macromolecules* **2011**, *44*, 5666-5670.

80. Ren, W. M.; Wu, G. P.; Lin, F.; Jiang, J. Y.; Liu, C.; Luo, Y. and Lu, X. B. *Chem. Sci.* **2012**, *3*, 2094-2102.

81. Lappert, M. F. and Pye, P. L. *J. Chem. Soc. Dalton Trans.* **1977**, 2172-2180.

82. Díez-González, S.; Marion, N. and Nolan, S. P. *Chem. Rev.* **2009**, *109*, 3612-3676.

83. Gibson, S. E.; Johnstone, C.; Loch, J. A.; Steed, J. W. and Stevenazzi, A. *Organometallics*, **2003**, *22*, 5374-5377.

84. Saino, N.; Kogure, D. and Okamoto, S. *Org. Lett.* **2005**, *7*, 3065–3067.

85. Geny, A.; Gaudrel, S.; Slowinski, F.; Amatore, M.; Chouraqui, G.; Malacria, M.; Aubert, C. and Gandon, V. *Adv. Synt. Catal.* **2009**, 351, 271-275.

86. Llewellyn, S. A.; Green, M. L. H. and Cowley, A. R. *Dalton Trans.* **2006**, 4164-4168.

87. Schneider, S. K.; Schwarz, J.; Frey, G. D.; Herdtweck, W. and Herrmann, W. *J. Organomet. Chem.* **2007**, *692*, 4560-4568.

88. Wanzlick, H. W. and Schikora, E. *Angew. Chem.* **1960**, *72*, 494.

89.   Suzuki, Y.; Wakatsuki, J.; Tsubaki, M. and Sato, M. *Tetrahedron* **2013**, *69*, 9690-9700.

CHAPTER 6

GENERAL CONCLUSIONS

From the study of chiral Fe-PNNP-based complexes carried out in <u>Chapter 3</u>, the following conclusions were extracted:

- Two chiral diamine derivatives (**3xx48** and **3xx49**) based on a pyrrolidine moiety have been synthesized and characterized in four steps from L-(+)-Tartaric acid.

- These chiral diamine derivatives (**3xx48** and **3xx49**) were employed in the synthesis of chiral PNNP ligands **3xx46** and **3xx47** and **3xx65**.

- The corresponding PNNP iron(II) complexes (**3xx66**, **3xx67**, **3xx68** and **3xx72**) were synthesized in good yields. The X-Ray structures of complexes **3xx68** and **3xx72** were also elucidated.

- An analogous iron (II) complex bearing a cyclohexyl backbone (**3xx73**) was also synthesized and characterized. The X-Ray structure of this complex was also elucidated.

This novel family of chiral PNNP ligands were applied in combination with $Fe_3(CO)_{12}$ as iron source in the asymmetric transfer hydrogenation of a wide range of substrates.

- Substrates such as *iso*-butyrophenone, *iso*-valerophenone and *tert*-butyl diphenyl ketone having bulky groups at the alkylic position were hydrogenated using the **3xx47**/$Fe_3(CO)_{12}$ catalytic system, obtaining high conversions and enantioselectivities.

- The reduction of cyclic phenyl ketones and ketones containing annulated-rings using the **3xx47**/$Fe_3(CO)_{12}$ catalytic system showed moderate to high conversion whereas high enantiomeric ratios were obtained in all cases.

- Heteroaromatic methyl ketones were also hydrogenated but in this case with low conversions although the enantioselectivity was comparable to that obtained for 1-phenylethanol.

- Asymmetric transfer hydrogenation of imines and alkenes were also explored although no conversion was obtained in both cases. Interestingly, moderate conversion and enantioselectivity was obtained when a diphenylphosphinyl imine was employed as substrate.

- The initial poisoning tests performed using Hg as poisoning agent, suggested that the asymmetric transfer hydrogenation catalyzed by **3xx47**/$Fe_3(CO)_{12}$ is probably heterogeneous, having **3xx47**-modified iron particles acting as active catalyst.

From the study of zinc complexes containing a N_2O_2, N_2NH_2, N_4 and $N_4(NH)$ ligand scaffolds with a pyrrolidine backbone carried out in <u>Chapter 4</u>, the following conclusions can be extracted:

- A new set of ligands containing a pyrrolidine backbone; N_2O_2(pyrrolidine) (**4xx25**), N_2NH_2(pyrrolidine) (**4xx26**), N_4(pyrrolidine) (**4xx27**) and $N_4(NH)$(pyrrolidine) (**4xx28**) were synthesized and fully characterized obtaining moderate to high yields (40-95%).

- The corresponding zinc (II) complexes were also synthesized. The X-Ray structures of complexes **4xx29** and **4xx31** were also obtained.

This novel family of zinc (II) complexes were applied in the synthesis of cyclic carbonates from CO_2 and epoxides and the following conclusions can be drawn:

- The **4xx31**/TBAI catalytic system catalyzes the coupling of CO_2 with a variety of terminal and aromatic epoxides with good to high conversions (61-89%) towards the corresponding cyclic carbonate. Furthermore, internal epoxides such as cyclohexene oxide and 2,3-epoxybutane were efficiently converted to the corresponding cyclic carbonate (Conv.= 66% and 72% respectively). It has to be mentioned that this is the highest conversion obtained for 2,3-epoxybutane using a zinc (II) complex. Methyl epoxioleate that derives from a natural product was also converted in a 46% conversion.

- The **4xx31**/TBAI catalytic system was recycled up to 5 times without appreciable lost of activity for the coupling of CO_2 with propylene oxide which demonstrated the robustness of the catalytic system.

From the study of C^N^C pincer-based cobalt complexes carried out in Chapter 5, the following conclusions can be extracted:

- The chiral C^N^C ligands **5xx56** containing a methyl and phenyl groups and the **5xx57** ligand containing a methyl and a naphthyl groups were synthesized and fully characterized.

- The novel chiral C^N^C ligands **5xx58** containing a methyl and a cyclohexyl groups was synthesized and fully characterized with a 60% yield.

- The chiral Cobalt C^N^C complexes **5xx59-5xx61** were synthesized and fully characterized by NMR, IR, Magnetic Susceptibility, ICP and EA. With all the collected data in hand, it was proposed a coordination of the $Co(OAc)_2$ moiety to the pyridine of the C^N^C ligand maintaining the imidizales uncoordinated.

- The Cobalt C^N^C complex **5xx59** catalyzes the asymmetric hydrogenation of ketones with moderate to high yields, although low to moderate ee's were obtained.
- Initial attempts to obtain a well defined Co(II)-pyridine biscarbene complex having both the carbene and the pyridine coordinated to the metal center were accomplished, although still further investigation need to be performed.

APPENDIX

PUBLICATIONS

"Robust zinc complexes bearing pyrrolidine based ligands as recyclable catalysts for the synthesis of cyclic carbonates from CO_2 and epoxides" Mercade, E.; Zangrando, E.; Claver, C. and Godard, C. *ChemCatChem*, **2015**. *Accepted.*

"Novel chiral PNNP ligands with a pyrrolidine backbone. Synthesis, characterization and application in Fe-catalyzed asymmetric transfer hydrogenation of ketones" Mercade, E.; Zangrando, E.; Clotet, A.; Claver, C. and Godard, *Manuscript to be submitted.*

"A mild route to solid-supported rhodium nanoparticle catalysts and their application to the selective hydrogenation reaction of substituted arenes" Moreno-Marrodan, C.; Liguoni, F.; Mercade, E.; Godard, C.; Claver, C. and Barbaro, P. *Catal. Sci. Tecnhol.* **2015**, *5*, 3762-3772.

"Ligand effect in the Rh-NP catalysed partial hydrogenation of substituted arenes" Llop, J.; Gual, A.; Mercade, E.; Claver, C. and Godard, C. *Catal. Sci. Tecnhol.* **2013**, *3*, 2828-2833.

CONFERENCES AND SCIENTIFIC MEETINGS

Mercade, E.; Godard, C.; Claver, C. ***Synthesis of chiral PNNP ligands bearing a pyrrolidine backbone. Application in ATH of ketones.*** Reunión Grupo Especializado en Química Organometálica. Tarragona, Spain, September **2014**. Poster communication.

Mercade, E.; Krinsky, J. L.; Godard, C.; Claver, C. ***Synthesis of anchorable chiral PNNP ligands. Application in catalysis.*** 20th Conference on

Organometallic Chemistry. St Andrews, England, July **2013**. Poster communication.

Mercade, E.; Castillon, S.; Claver, C.; Godard, C. ***Synthesis of chiral PNNP ligands with a pyrrolidine backbone. Application in asymmetric hydrogenation reactions using heterogenized catalysts.*** 15th International Congress on Catalysis. Munich, Germany, July **2012**. Poster communication.

Mercade, E.; Krinsky, J. L.; Claver, C.; Godard, C. ***Síntesis de ligandos quirales PNNP con esqueleto pirrolidina. Aplicación en reacciones de reducción asimétrica.*** Reunión Grupo Especializado en Química Organometálica. Castellón, Spain, June **2012**. Poster communication.

Mercade, E.; Godard, C.; Claver, C. ***Synthesis of immobilized PNNP ligand for asymmetric hydrogenation reactions in flow systems.*** 19th International Conference on Organometallic Chemistry. Tolouse, France, July **2011**. Poster communication.

Mercade, E.; Castillon, S.; Krinsky, J. L.; Claver, C.; Godard, C. ***Towards the synthesis of immobilized PNNP ligands for asymmetric hydrogenation reactions.*** SYNFLOW Summer School. St. Andrews, England, June **2011**. Oral communication.

2nd China Spain Bilateral Symposium on Catalysis. Institute of Chemical Research of Catalonia (ICIQ). Tarragona, Spain, November **2010**. *Participation.*

Llop, J.; Mercade, E.; Godard, C.; Claver, C.; Castillon, S.; Gebauer, E.; Muller, T. ***Hidrogenación de arenos monocíclicos disubstituidos utilizando nanopartículas de Rh.*** Reunión Grupo Especializado en

Química Organometálica. Punta Umbría, Spain, September **2010**. *Poster communication.*

RESUMEN DE LA TESIS

Esta tesis doctoral aborda la síntesis de nuevos ligandos polidentados, y su posterior coordinación con metales de la primera serie de transición para formar catalizadores efectivos en las reacciones de transferencia de hidrógeno asimétrica, hidrogenación y acoplamiento de CO_2 con epóxidos. En el Capítulo 3 se describe la síntesis de nuevos ligandos quirales tipo PNNP. Los correspondientes complejos de hierro se obtuvieron en buenos rendimientos, y sus estructuras de rayos-X fueron resueltas. La reacción de trasferencia de hidrógeno asimétrica de diversos sustratos cetona se llevó a cabo con un sistema catalítico compuestos por ligandos $PNNP/Fe_3(CO)_{12}$ obteniendo de moderadas a elevadas conversiones y enantioselectividades.

En el capítulo 4 se describe la síntesis de una nueva familia de ligandos tipo N_2O_2, N_2NH_2, N_4 y $N_4(NH)$. Los correspondientes complejos de zinc se obtuvieron en buenos rendimientos y sus estructuras de rayos-X fueron resueltas. Los complejos de zinc resultantes catalizaron la reacción de acoplamiento de CO_2 con epóxidos terminales e internos, siendo el complejo de zinc-N_4 el más activo de la serie. Este mismo complejo se pudo reciclar hasta cinco veces sin pérdida significativa de actividad, lo que probó la robusteza del mismo.

En el Capítulo 5 se describe la síntesis de ligandos C^N^C de tipo pincer. Posteriormente, se coordinaron a cobalto, observando la coordinación del centro de cobalto únicamente a la piridina del ligando, dejando los imidazoles del ligando sin coordinar al centro metálico. Posteriormente se estudió la actividad de estos complejos en la hidrogenación asimétrica de varias cetonas.